Three-Dimensional Analysis of Steel Frames and Subframes in Fire

By

Samer Rida Najjar

A thesis submitted to the Department of Civil and Structural Engineering in

partial fulfilment of the requirements for the

Degree of Doctor of Philosophy

University of Sheffield

March 1994

Summary

The aim of the present work is to develop a sophisticated analytical model for columns within three-dimensional assemblies in fire conditions.

A preliminary investigation into this problem resulted in the development of a simplified approach for the analysis of isolated columns in fire. This model is based on the Perry-Robertson approach to defining critical loads of imperfect columns at ambient temperature. It takes into account uniform and gradient temperature distributions across the section of an isolated pin-ended column. It also accounts for initial out-of-straightness, load eccentricity and equal end-moments.

A three-dimensional finite element model has subsequently been developed for the analysis of frames in fire conditions. This model is based on a beam finite element with a single node at each end of the element. At each node eight degrees of freedom are introduced. The finite element solution of the problem is obtained using an incremental iterative procedure based on the Newton-Raphson method, adapted to account for elevated temperature effects. The developed procedure offers a unique treatment of the thermal effects which allows solutions to be arrived at regardless of the problem's boundary conditions. The finite element formulation takes into consideration geometrical and material nonlinearities, initial out-of-straightness and residual stresses. It allows for virtually any temperature distribution across and along the structural members, and the analysis can handle any three-dimensional skeletal steel structure. The developed model allows the material mechanical properties to be expressed either as trilinear or continuous functions which vary with temperature.

A computer program, 3DFIRE, has been developed based on the above-mentioned formulation and validated extensively against a wide range of previous analytical and experimental work. This program has then been used to perform parametric studies to establish the most prominent features of column behaviour in fire whether as isolated members or as part of structural assemblies. These studies have yielded a large amount of data from which generalised conclusions have been made.

The analysis has been extended recently to include composite beams within the structural assembly. This development was undertaken to enable analytical studies on the test building at Cardington, in which fire tests are planned to take place in the near future.

Contents

List of figures

List of tables

Notations

Special Symbols

$\{\ \}$	Denotes a column vector.
$<\ >$	Denotes a row vector.
$[\ ]$	Denotes a matrix.
$[\ ]^T$	Denotes a matrix transpose.
$[\ ]^{-1}$	Denotes a matrix inverse.
Σ	Denotes a summation.
Δ	Prefixed to other term denotes an increment.
δ	Prefixed to other term denotes a virtual variation.
∂	Denotes partial differentiation.
d	Denotes ordinary differentiation.
$'$	Denotes differentiation with respect to single argument.
$''$	Denotes second derivative with respect to single argument.

Roman Symbols

A_T, B_T, n_T	Parameters of Ramberg-Osgood Equation at temperature $T^\circ C$.
$a_1, a_2, ..., a_7$	Values defined in Eq. 3.27.
$b_{1j}, b_{2j}, ..., b_{7j}$	Values defined in Eq. 3.59.
$e_{1j}, e_{2j}, ..., e_{7j}$	Values defined in Eq. 3.36.
e_i	Initial load eccentricity.
e_θ	Thermally-induced load eccentricity.
E_{20}, E_θ	Young's modulus at temperatures $20^\circ C$ and $\theta^\circ C$ respectively.
E_t	Tangent modulus.
G	Shear modulus.
$I_y, I_y^2, ...etc$	Cross-sectional properties defined in Eq. 3.62.
J	Torsional index.
$[\ K_1\ ], [\ K_2\ ] to [\ K_7\ ]$	Submatrices of the tangent stiffness matrix.
$[\ K_T\ ]$	Tangent stiffness matrix.
l, A, V	Length, cross-sectional area and volume of the finite element respectively.
$n, m_x, m_x^2, m_y, m_y^2, m_\omega, m_z, T_{sv}$	Internal stress resultants defined in Eq. 3.25.

P, M	Applied load and moment respectively.
Q	Applied load in local system of coordinates.
Q_R	Resisting forces.
q	Displacement in local system of coordinates.
R	Applied load in local system of coordinates.
r	Displacement in global system of coordinates.
$[\,T\,]$	Transformation matrix.
u, v, w	Displacements of an arbitrary point in the direction of z, y, x respectively.
u_o, v_o, w_o	Displacements of the origin point in the direction of z, y, x respectively.
W	Virtual work.
X, Y, Z	Global coordinates.
x, y, z	Local coordinates.
y	Rise in lateral defection of Perry column.
y_i	Initial out-of-straightness.
y_θ	Out-of straightness due to thermal gradient.

Greek Symbols

α, β, γ	Angles of an element in space defined in Fig. 3.6.
α_i	Weighting factor in Gaussian integration.
α_i	Weighting factor in Gaussian integration.
$\epsilon_m, \epsilon_r, \epsilon_\theta$	Mechanical, residual and thermal strains respectively.
ϵ_z	Axial strain in the local z-direction.
$\sigma_{y20}, \sigma_{y\theta}$	Yield stress at temperature $20^\circ C$ and θ respectively.
σ_z	Axial strain in the local z-direction.
θ_x	Rotation angle in y-axis direction.
θ_y	Rotation angle in x-axis direction.
θ_z	Twist angle about z-axis.
ω	Sectorial coordinate defined in Fig. 3.2.
ϕ	Cubic shape function defined in Fig. 3.5.
ψ_i	Unbalanced forces of Eq. 3.28.

Acknowledgement

The author would like to express his gratitude to Dr. I. W. Burgess for his distinguished supervision throughout this project.

The author wishes to thank Professor P. Waldron and all other members of staff in the Civil Engineering Department for making provision to write this thesis during the author's work as a teaching assistant.

The financial support by a Frank Greaves Simpson award from University of Sheffield for this research project was gratefully received.

Declaration

Except where specific reference has been made to the work of others, this thesis is the result of my own work. No part of it has been submitted to any University for a degree, diploma or other qualification.

S. R. Najjar.

CHAPTER 1

Introduction

1.1 General

The safe use of any structure is a primary criterion for designers, analysts and legislators. Fire is one of the main threats to this safe use in terms of its immediate danger to the inhabitants, and the feasibility of re-using the structure. Statutory regulations are enforced in many countries to ensure this aspect of safety along with other aspects. For example, the Department of the Environment and the Welsh office (1985a; 1985b) issue Building Regulations which specify appropriate periods of fire resistance for different buildings. These periods vary depending on the following main factors:

- Height of the building.

- Floor area of each storey.

- Cubic capacity of the building or the compartment.

- The building's use.

Based on the above considerations it is clear that fire resistance periods are not only concerned with the structural fire resistance of the building. These periods are concerned with allowing enough time for both property protection and life safety. Malhotra (1986) studied fire resistance periods in an attempt to separate the provisions for life safety and property protection in the current regulations.

The role of structural analysis in fire safety is to provide numerical tools to aid understanding of the structural behaviour in fire conditions. Such tools can then be used to give insights into the structural fire resistance, allowing the appropriate design decisions to be made.

1.2   Steel in Fire

Structural steelwork is a popular construction material due to its advantages as a relatively cheap material, its fast erection and light weight.

However, the greatest disadvantage of steel as a structural material is its vulnerability to elevated temperatures. Under fire conditions steel loses a considerable amount of its strength and stiffness, forcing designers to protect the main load-carrying members at a high cost. Latter (1985) reported in a British Steel Corporation survey on multi-storey steel frame buildings that fire protection can contribute as much as 30% to the construction cost of the structural frame.

Amongst the main load-carrying members are the columns which are most vulnerable to the fire effects. In the following section a brief review of previous analytical work on columns in fire is presented.

1.3   Previous Analytical Work on Columns in Fire

Fire research dates back to the late nineteenth century, when the great loss resulting from the structural failure of buildings during accidental fires was first realised. Uddin and Culver (1975) compiled a comprehensive literature review about fire research, containing 219 references, up to 1971-1972. This extensive amount of research has been carried out mainly to study the effects of fire on structural endurance, material properties and protective materials, along with the nature and development of fires. Most of the research up to that point was based

on studying the effects of actual fires and collecting experimental observations. Apparently the complexity of the fire problem from the analytical point of view deterred any sophisticated analytical work from being undertaken.

One of the earlier analytical studies on steel columns subject to fire was carried out by Culver (1972). The problem considered was that of an isolated column with uniform temperature across its section and a variation of temperature along its height. An eigenvalue solution was obtained by using finite differences over 16 nodal points along the height of the column. Bilinear stress-strain characteristics proposed by Brockenbrough (1970) were used to establish the flexural rigidity at each point along the column. The same stress-strain characteristics were used by Ossenbruggen et al (1973) to obtain solutions for isolated columns under thermal gradients along the height and across the section. An iterative procedure was used, making an initial guess of the thermal bowing and updating it until equilibrium was attained.

Cheng and Mak (1975) developed a finite element program for the analysis of planar steel frames in fire. Thermal gradients and creep effects were included in their formulation. Cheng (1983) used this formulation to investigate the effects of creep in fire.

Witteveen and Twilt (1975) and Witteveen et al (1976; 1977) presented comparisons between test and analytical results for reduced-scale columns and plane frames using a computer program. The theoretical background and solution procedure were not presented in their publications.

Furumura and Shinohara (1978) developed a finite element inelastic analysis of plane steel frames in fire. The creep effect and material unloading were considered in the analysis. A thermal analysis was used to predict the protected steel tem-

peratures under standard fire conditions.

Kruppa (1979) suggested a simplified analysis for beams and beam-columns under uniform temperature profile. The analysis was based on the assumption that stress-strain characteristics remain elastic-perfectly plastic at elevated temperatures. The method is based on comparing the ultimate stress at ambient temperature with the stress at an assumed temperature under a given load. The failure condition is reached when both stresses become equal.

Jain and Rao (1983) developed a numerical technique for the analysis for plane frames in fire. Incremental and iterative procedures were used to obtain solutions. Creep and large deformations were also accounted for.

Baba and Nagura (1985) used a one-dimensional finite element method to study the effect of time-dependent material properties on the behaviour of single-storey single-bay frames. In this study strain hardening and creep were considered and a comparison was made between small and finite deformations using a bilinear model for material properties.

Giżejowski (1986) developed a finite element model for the analysis of in-plane behaviour of frame-type structures using a bilinear stress-strain model. Geometrical imperfections, residual stresses and thermal gradients were included in the analysis.

Aribert and Abdel Aziz (1987) developed a numerical model for the buckling analysis of members in bending and compression. This model takes into account imperfections of the columns (out-of-straightness, residual stresses), non-uniformity of temperature (in both longitudinal and transverse directions of the member), variability of temperature over a time span, and creep.

Cooke (1987) performed an experimental programme including model columns heated along one flange. A simplified calculation method was used to compare experimental and theoretical deformations based on separation of the thermal bowing deformations from the P-Δ effect.

Franssen (1987) developed a finite element model for plane composite frames and used the finite difference method to predict temperatures within the material. The developed program CEFICOSS has been described and used for a large number of studies (Schleich et al 1985; Dotreppe 1986; Schleich 1988; Franssen 1989).

Olawale (1988) developed a finite strip formulation for the analysis of perfect isolated columns in fire. The small-deflection formulation took account of residual stresses, load eccentricity and local buckling. Burgess et al (1992) used the developed program to obtain solutions for a wide range of perfect columns in fire.

El-Rimawi (1989) used a secant stiffness approach for the analysis of flexural members in fire. This analysis was later extended (El-Rimawi et al 1993) for the analysis of plane frames in fire. The developed computer program has been used to study the behaviour of steel frames and subframes with semi-rigid connections in fire.

Saab (1990), and Saab and Nethercot (1991) developed a non-linear finite element analysis of plane frames in fire. The developed analysis was used to study the behaviour of non-sway and sway frames in fire conditions assuming various heating and protection schemes.

Kouhia et al (1988) developed a geometrically non-linear finite element analysis for steel frames in fire. An elastic-plastic material model was used in the analysis. Only plane multi-storey frames were reported, though the developed model is applicable to three-dimensional beams and frames.

Up to this point, the last-mentioned analysis is the only three-dimensional model which has been reported on for the analysis of steel frames in fire. The need for more sophisticated analytical tools that can model column behaviour in fire has been realised by various research groups. A column's position in relation to the superstructure is an important factor in deciding its bearing capacity. Simplified rules have been drawn up to find this capacity at ambient temperature by using subassemblies or specifying a value for the effective length. It is also noticeable that at ambient temperature plane frame analysis can provide good correlation of the actual behaviour of a three-dimensional assembly provided that intuition suggests the axis about which the column is expected to fail. Such simplified approaches may be acceptable for ambient temperature analysis but are not necessarily valid at elevated temperatures. In the presence of the many non-uniformities caused by fire, such as thermal gradients along the height and across the section of the column, concepts such as the weak axis can become irrelevant. The influence of the superstructure on the column's bearing capacity in fire is a complex phenomenon. Unlike ambient temperature situations, the fire is likely to influence the stiffnesses of the column and adjacent structural members to different extents. In order to study the fire effect on columns in three-dimensional assemblies it is worth while using a three-dimensional analysis. Another aspect of the problem is the mechanical behaviour of steel at elevated temperatures. While it is quite acceptable to assume an elastic-perfectly-plastic characteristic at ambient temperature this is much less justifiable at elevated temperatures. Most of the previous research has used bilinear models in the fire context without considering the effect of the highly non-linear characteristics at elevated temperatures. Hence it is both important and desirable to develop numerical tools that are capable of tackling the above problems along with the traditionally important features of column behaviour such

as the geometric and imperfection-sensitivity effects. Recently three-dimensional models have been developed in Europe.

At City University, London, Jeyarupalingam and Virdi (1991) developed a three-dimensional frame analysis for fire conditions. The developed analysis was an extended and generalised version of the numerical method developed by Virdi and Dowling (1973; 1976) and Virdi (1981) for inelastic analysis of columns at ambient temperature. The method is based on finding an equilibrium deflected shape which satisfies static equilibrium conditions for each increment of load, time or temperature. These equilibrium conditions are checked at a number of stations at regular intervals.

At the Building Research Establishment, Watford, Wang and Moore (1991) have developed a finite element program for the analysis of framed structures in fire. The program was developed in the first instance for two-dimensional steel/composite frames, and its capability was then extended to three-dimensional frames. The model is based on a beam element with two nodes, each of which has six degrees of freedom. The principle of virtual work is used to generate stiffness matrices and solutions are obtained by a Newton-Raphson procedure.

At the Université de Liège, Franssen has recently extended his analysis to three-dimensions. At the time of writing no published material has referred to this extension.

At the University of Sheffield, the present project started in 1990 to develop a three-dimensional analysis of steel frames in fire conditions. This development was intended to take account of geometrical and material non-linearities and to enable the modelling of any thermal non-uniformity within the structure. It also allows the analysis of the full skeletal structure without any need to restrict the analysis

to a reduced model. However, the major initial objective was to use the analysis to study three-dimensional column subframes in fire conditions.

1.4 Steel's Mechanical Properties in Fire

When steel is heated it expands in a more or less linear fashion with temperature. It also progressively loses strength and stiffness with temperature rise. Elevated temperature tests (Kirby and Preston 1988) on structural steels show that the stress-strain characteristics very rapidly lose their ambient-temperature bilinear nature (the normal engineer's assumption) and become distinctly curvilinear at higher temperatures.

In order to investigate the structural behaviour of steel in fire it is necessary to obtain a reliable description of its mechanical properties at elevated temperatures. The required properties include thermal expansion and stress-strain characteristics. The obvious route to obtain such properties is by performing tensile tests on steel subject to elevated temperature. The results from such tests can then be incorporated into mathematical models that can be used in the analysis of steel structures in fire.

1.4.1 Material Properties Tests

Stress-strain characteristics of steel at elevated temperatures are obtained from tensile tests. Different types of test are inherently expected to show some variation in stress-strain characteristics due to variable rates of loading and heating. There are two main testing procedures for steel at elevated temperature.

The first type of test consists of loading the steel specimen under uniform temperature conditions. In these tests the steel specimen is first heated to a specified temperature, a procedure that allows the rise of strain due to free thermal expansion to be measured separately. Loads can then be applied and the additional strain can be measured along with the applied stress. By repeating the test for different levels of temperature a family of stress-strain curves can be obtained.

The second type of test loads the steel specimen under transient heating conditions. In this method of testing the specimen is heated at a specified rate of temperature increase for different, constant loads. This method obviously implies that total strains, including mechanical and thermal expansion strains, must be measured as one quantity. Consequently, another set of similar specimens must be tested at the same rate of heating but without loading, in order to determine the thermal expansion separately. Stress-strain data acquired from tests can then be rearranged to produce a family of stress-strain curves at constant temperature.

It is clearly much easier to obtain the mechanical properties of steel at elevated temperature by using the first method. Nevertheless, Kirby and Preston (1988) have concluded that predictions of the structural behaviour at small strains from data derived under steady-state heating conditions are optimistic, and information should preferably be used from transient tests.

1.4.2   Stress-Strain Models

In the context of structural analysis, the stress-strain characteristics constitute important parameters which are bound to influence analytical predictions. The natural approach to incorporating the stress-strain characteristics in any analysis

is by representing them by a mathematical model. Hence it is of great importance to adopt a satisfactory mathematical model that describes accurately the stress-strain-temperature relationship of steel in fire. Various elevated-temperature models are available, some of which have attempted to maintain the bilinear ambient-temperature nature of steel characteristics, while the others have attempted to model the real curvilinear nature of these characteristics in mathematical form. Some of the more well-known models are presented in the following sections.

1.4.2.1 ECCS Model

The European Convention for Constructional Steelwork (1983) suggested a mathematical model for stress-strain characteristics of steel in fire based on data obtained in the Netherlands and elsewhere. In the ECCS document it is pointed out that using different stress-strain relationships will have an effect on the critical temperatures of beams, and in particular of columns. The ECCS model defines the elastic modulus and the yield stress at different temperatures. This effectively implies a bilinear representation of the steel stress-strain characteristics.

The elastic modulus E_θ is given as:

For $\quad \theta \leq 600\ ^\circ C$

$$E_\theta = E_{20}\left[1.0 - 17.2 \times 10^{-2}\ \theta^4\ 11.8 \times 10^{-9}\ \theta^3 - 34.5 \times 10^{-7}\theta^2 + 15.9 \times 10^{-5}\theta\right]$$

and for $\quad \theta > 600\ ^\circ C$

E_θ is undefined.

The yield stress $\sigma_{y\theta}$ is given as:

For $\quad \theta \leq 600\ ^\circ C$

$$\sigma_{y\theta} = \sigma_{y20} \left[1.0 + \frac{\theta}{767 \; ln\left(\frac{\theta}{1750}\right)} \right]$$

and for $\quad 600 < \theta \leq 1000 \; ^\circ C$

$$\sigma_{y\theta} = \sigma_{y20} \left[\frac{108 \left(1 - \frac{\theta}{1000}\right)}{\theta - 440} \right]$$

The absence of a definition for the elastic modulus beyond the temperature of $600^\circ C$ was justified by the ECCS (1983) as a result of the lack of knowledge about steel properties beyond this temperature and the usual attainment of critical conditions below this temperature level.

1.4.2.2 Modified ECCS Model

In order to overcome the limitation of the ECCS model, Franssen (1987) suggested a modification to account for temperatures greater than $600^\circ C$. The modified model is given in the following equations.

The elastic modulus E_θ and the yield stress σ_θ are given as:

For $\quad \theta \leq 100 \; ^\circ C \quad$ and $X = \frac{\theta}{100}$ in the following equations.

$$E_\theta = E_{20},$$

$$\sigma_{y\theta} = \sigma_{y20}$$

for $\quad 100 < \theta \leq 500 \; ^\circ C$

$$E_\theta = E_{20} \left[-0.018 \; X^2 + 0.036 \; X + 0.982 \right]$$

$$\sigma_{y\theta} = \sigma_{y20} \left[0.00295 \; X^3 - 0.0488 \; X^2 + 0.0887 \; X + 0.957 \right]$$

for $\quad 500 < \theta \leq 600 \; ^\circ C$

$$E_\theta = E_{20} \left[-0.018 \; X^2 + 0.036 \; X + 0.982 \right]$$

$$\sigma_{y\theta} = \sigma_{y20} \left[-0.000421\ X^3 + 0.02344\ X^2 - 0.3806\ X + 1.919 \right]$$

for $\theta > 600\ ^\circ C$

$$E_\theta = E_{20} \left[0.0000925926\ X^3 + 0.125\ X^2 - 0.34\ X + 2.12 \right]$$

$$\sigma_{y\theta} = \sigma_{y20} \left[-0.000421\ X^3 + 0.02344\ X^2 - 0.3806\ X + 1.919 \right]$$

This modified model is worth considering for analytical purposes. Although the ECCS argument about critical temperatures not exceeding 600°C may be valid for structural members subject to their full service load, in reality most of those members bear a fraction of that load. This is the case, for example, in multi-storey columns.

1.4.2.3   CTICM Model

Centre Technique Industriel de la Construction Métallique (1982) suggested another bilinear model for steel stress-strain characteristics in fire.

The elastic modulus E_θ is given as:

For $0 < \theta \leq 600\ ^\circ C$

$$E_\theta = E_{20} \left[1.0 + \frac{\theta}{2000\ ln\left(\frac{\theta}{1100}\right)} \right]$$

and for $600 < \theta \leq 1000\ ^\circ C$

$$E_\theta = E_{20} \left[\frac{690 - 0.69\ \theta}{\theta - 53.5} \right]$$

The yield stress $\sigma_{y\theta}$ is given as:

For $20 < \theta \leq 600\ ^\circ C$

$$\sigma_{y\theta} = \sigma_{y20} \left[1.0 + \frac{\theta}{900\ ln\left(\frac{\theta}{1750}\right)} \right]$$

and for $\quad 600 < \theta \leq 1000\ ^{\circ}C$

$$\sigma_{y\theta} = \sigma_{y20} \left[\frac{340 - 0.34\ \theta}{\theta - 240} \right]$$

Fig. 1.1 shows the variation of yield stress at elevated temperatures normalised with respect to the ambient temperature yield stress for the three previous bilinear models. The elastic modulus variation for the same models is shown on Fig. 1.2.

1.4.2.4 Ramberg-Osgood Model

The high temperature stress-strain tests carried out by Kirby and Preston (1988) produced data that has been adopted by BS5950 Pt. 8 (1990) and subsequently by EC3 Pt. 10 (1990). This data has been reported to provide better correlation with large scale beam and column tests (Lawson and Newman 1990) than the earlier models.

El-Rimawi (1989) suggested a mathematical model to fit the test data, based on Ramberg-Osgood equations (Ramberg and Osgood 1942), which describes stress-strain curves by three parameters. The relationship between the strain and stress at any temperature T is given in this model as:

$$\epsilon_T = \frac{\sigma_T}{a_T \cdot A_T} + 0.01 \left(\frac{\sigma_T}{b_T \cdot B_T} \right)^{n_T}$$

in which:

$$A_T = 180 \times 10^3$$

$$B_T = 0.00134T^2 - 0.26T + 254.67 10^3$$

$$n_T = 237 - 1.58T \qquad\qquad \text{For} \quad 20 \leq T \leq 100$$
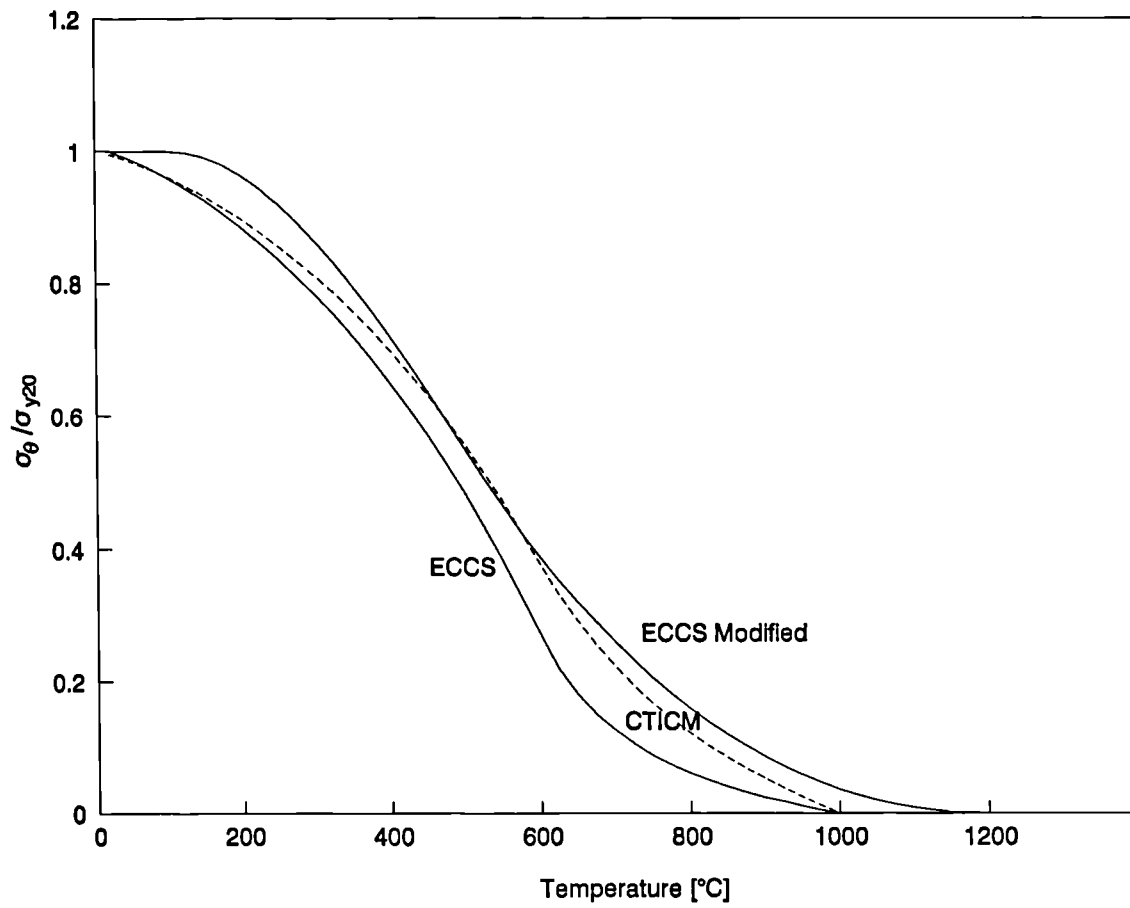
Fig. 1.1 Yield Stress at Elevated Temperatures

(Different Bilinear Models)
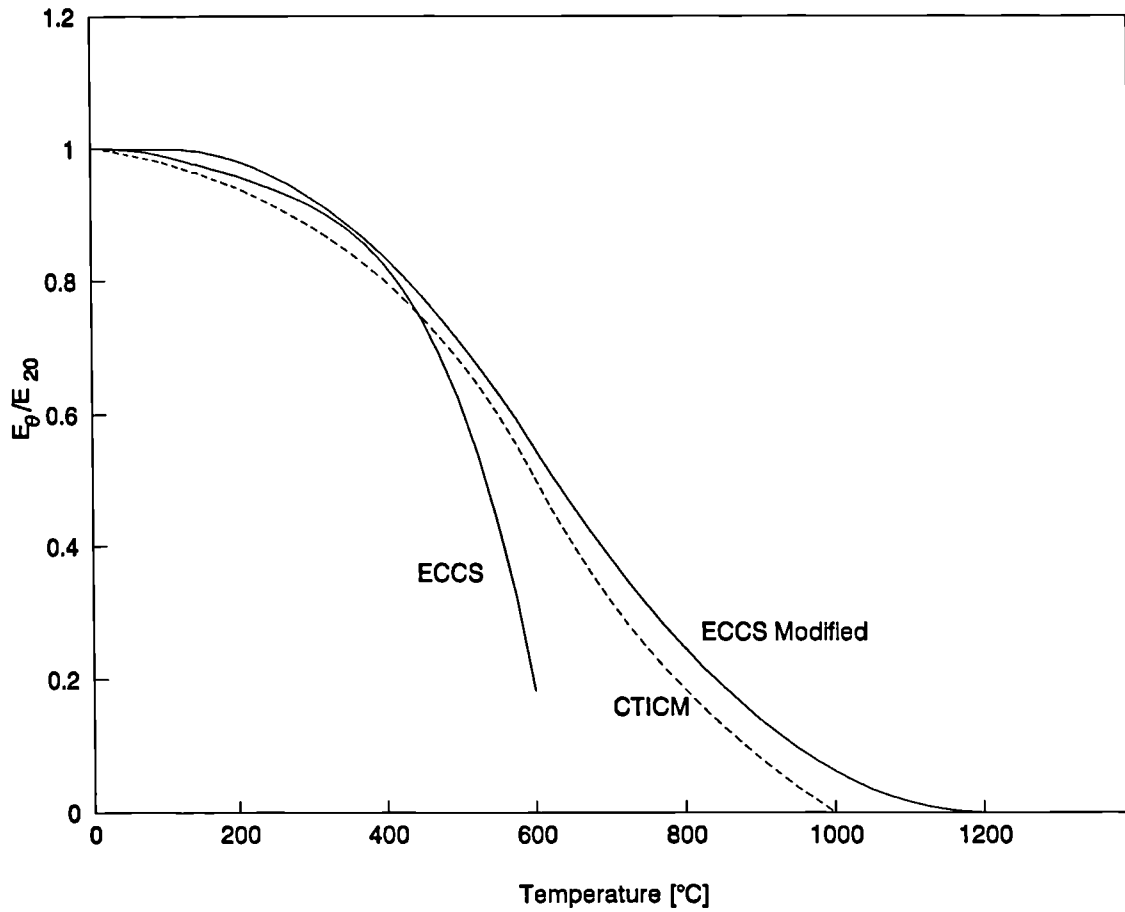
Fig. 1.2 Elastic Modulus at Elevated Temperatures

(Different Bilinear Models)

$$A_T = (194 - 0.14T) \times 10^3$$

$$B_T = 242$$

$$n_T = 15.3 \times 10^{-7} (400 - T)^{3.1} + 6 \qquad \text{For} \quad 100 < T \le 400$$

$$A_T = (295.333 - 0.39333T) \times 10^3$$

$$B_T = 492.667 - 0.6266T$$

$$n_T = 6 \qquad \text{For} \quad 400 < T \le 700$$

$$A_T = (30.5 - 0.015T) \times 10^3$$

$$B_T = 306 - 0.36T$$

$$n_T = 0.04T - 22 \qquad \text{For} \quad 700 < T \le 800$$

and

$$a_T = \frac{E_2 0}{180 \times 10^3}$$

$$b_T = \frac{\sigma_y 20}{250}$$

1.4.2.5 EC3 Model

EC3 Pt. 10 (1990) suggests a mathematical model based on the same test data (Kirby and Preston 1988), which describes the stress-strain relationships with a linear-elliptical shape, as is shown on Fig. 1.3 and compared with the Ramberg-Osgood model.

The stress-strain relationship at any temperature is defined in the three ranges of Fig. 1.3 as:

Range I (linear):
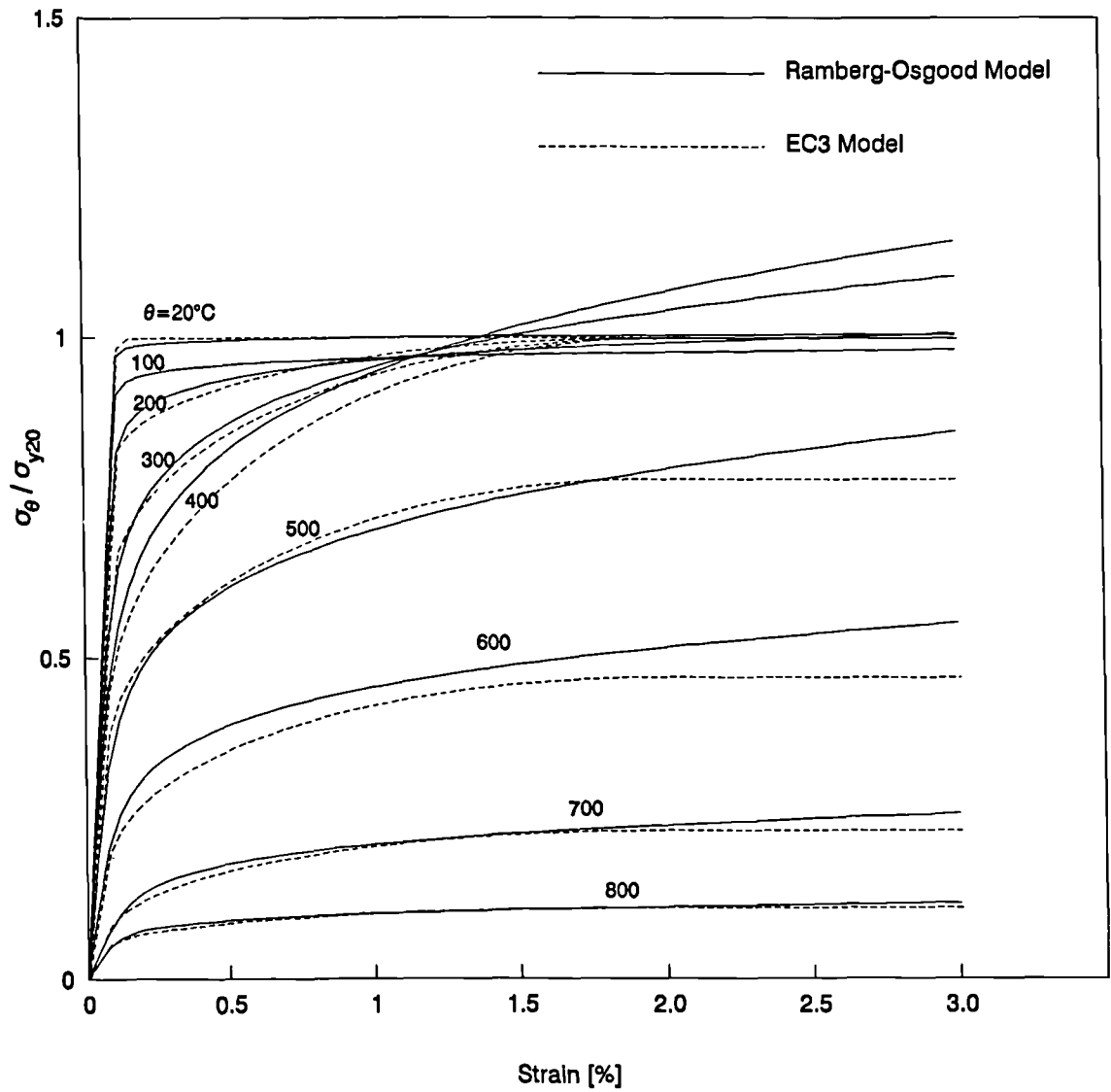
Fig. 1.3 Elevated Temperature Stress-Strain Characteristics for Steel Continuous Models

$$\sigma(\epsilon, \theta_a) = E_{a,f}.\epsilon$$

$$E(\epsilon, \theta_a) = E_{a,f}$$

Range II (elliptical):

$$\sigma(\epsilon, \theta_a) = \frac{b}{a}.\sqrt{(a^2 - (\epsilon_{y,f} - \epsilon)^2)} + f_{b,f}$$

$$E(\epsilon, \theta_a) = \frac{b.(\epsilon_{y,f} - \epsilon)}{a.\sqrt{a^2 - (\epsilon - \epsilon_{p,f})^2}}$$

with:

$$a^2 = \frac{E_{a,f}.(\epsilon_{y,f} - \epsilon_{p,f})^2 + c(\epsilon_{y,f} - \epsilon_{p,f})}{E_{a,f}}$$

$$b^2 = E_{a,f}.(\epsilon_{y,f} - \epsilon_{p,f}).c + c^2$$

$$c^2 = \frac{f_{y,f} - f_{p,f})}{2.((f_{p,f} - f_{y,f}) + E_{a,f}.(\epsilon_{y,f} - \epsilon_{p,f}))}$$

Range III (linear):

$$\sigma(\epsilon, \theta_a) = f_{y,f}$$

$$E(\epsilon, \theta_a) = 0$$

in which:

$$\epsilon_{p,f} = \frac{f_{p,f}}{E_{a,f}}$$

$$\epsilon_{y,f} = 2\%$$

$$\epsilon_{u,f} = 20\%$$

The parameters of the stress-strain curves ($E_{a,f}$, $f_{p,f}$ and $f_{y,f}$) are given in Table 1.1.

Temperature $^\circ C$	Parameters related to ambient temperature values		
	Effective yield Stress $\frac{f_{y,f}}{f_d}$	Slope elastic range $\frac{E_{a,f}}{E_a}$	Proportional limit $\frac{f_{p,f}}{f}$
20	1.00	1.00	1.00
100	1.00	1.00	1.00
200	1.00	0.90	0.80
300	1.00	0.80	0.60
400	1.00	0.70	0.42
500	0.78	0.60	0.36
600	0.47	0.31	0.18
700	0.23	0.13	0.075
800	0.11	0.09	0.05
900	0.06	0.0675	0.0375
1000	0.04	0.045	0.025
1100	0.02	0.0225	0.0125
1200	0.00	0.000	0.000

Table 1.1: EC3 stress-strain parameters at elevated temperatures.

All the material models illustrated in this section will be considered later in this study to assess their reliability in representing the mechanical properties of steel in fire analysis.

1.4.3 Creep

The phenomenon of creep can be defined as the strain which occurs with the passage of time under a constant stress state. At ambient temperature creep has an effect on steel when high loads are applied for a very long time. At elevated temperatures the phenomenon of creep is associated with the temperature and rate of heating. Although heating rates can vary infinitely, in real fire situations the range is reasonably well controlled.

Previous research has shown that at elevated temperatures any significant effect of creep, for structures subjected to normal fire growth and periods, starts beyond the temperature range $450^{\circ}C - 500^{\circ}C$. Furumura and Shinohara (1978) concluded that any change in structural temperature/deflection characteristics can only be noticed at temperatures higher than $450^{\circ}C$. Aribert and Abdel Aziz (1987) reported that the creep effect becomes significant at temperatures in excess of $545^{\circ}C$. Cheng (1983) noticed a rapid increase of a heated beam deflection at temperatures beyond $550^{\circ}C$. Knight (1975), using a creep analysis, arrived at the conclusion that temperature history has little bearing on the deformation and critical temperatures for beams.

Witteveen et al (1977) used experimental results from earlier work (Witteveen and Twilt 1975; Witteveen et al 1976) to conclude that a time-independent approach to the fire is possible within certain limits of heating rate. These limits were designed to range between $5^{\circ}C - 50^{\circ}C per minute$ in order to simulate the range of rates at which unprotected members and heavily protected members are heated. Within such a range and at temperatures not exceeding $600^{\circ}C$ no significant effect of creep has been reported. This work has shown clearly that effect of creep is

insignificant within the practical limits of actual fires.

Furthermore, experimentally-based models of steel mechanical properties often include the effect of creep implicitly, especially when experimental results are obtained under transient heating conditions. The BS5950 Pt. 8 and EC3 Pt. 10 stress-strain data was obtained using a wide range of heating rates (Kirby and Preston 1988).

1.5 Scope and Layout of the Research

The main objective of this research project is to develop a three-dimensional analysis of steel columns in fire conditions.

In this chapter various stress-strain models for steel at elevated temperatures have been presented. The availability of different stress-strain models, some of which adopt a bilinear representation while others adopt a curvilinear representation, illustrates the complexity of the problem of modelling structural behaviour under such conditions.

In Chapter 2 an investigation is presented which was carried out to assess the feasibility of establishing a simplified model for pin-ended isolated columns in fire and to develop the reduced modulus concepts used later. This investigation resulted in a promising simplified model for the problem under consideration.

In Chapter 3 a three-dimensional finite element formulation is developed for a beam element. This formulation is highly non-linear in terms of the high order terms included. It accounts for moderately large deformations, material non-linearities and instability. A coordinate transformation in space has been developed to allow

the analysis of full three-dimensional frames.

In Chapter 4 the treatment of fire within the developed software based on the proposed formulation is illustrated. The developed program 3DFIRE is extensively validated against available analytical and experimental data.

In Chapter 5 the program is used to carry out a parametric study. Results from this study have shown interesting trends in the structural behaviour of columns in fire conditions. Columns are considered first as isolated structural elements, then as a part of structural assemblies.

In Chapter 6 generalised conclusions drawn from the parametric studies are set out. Recommendations for further work are proposed at the end of this chapter.

A recent development to extend the capability of the present analysis to composite frames is briefly presented in Appendix A. Results from various analyses concerning the proposed fire tests at Cardington are also presented.

CHAPTER 2

Perry Elastic Analysis for Isolated Columns in Fire

2.1   Introduction

The structural behaviour of columns is a very complex phenomenon whether at ambient or elevated temperatures. This behaviour is far removed from the classical 'Euler-load-and-squash' idealisation for pin-ended struts. The presence of many initial imperfections such as initial out-of-straightness, eccentricity of the axial thrust line and residual stress patterns produced by hot rolling results in a considerable reduction in the buckling loads as predicted for perfect columns. Furthermore, the connections between columns and beams in real structures, which are frequently regarded as simple, normally exhibit a considerable rotational stiffness depending on the connection details. Given these behavioural complexities it is hardly surprising that failure prediction procedures for design have always been based on lower-bound rationalisations of results from large numbers of tests on columns in isolation and in subassemblages. In some cases the formulas used have been simple curve-fitting exercises, with no pretence of a basis in structural mechanics, while others have been based on simplified treatment of the behaviour of imperfect columns. One of the simplest and most successful approaches taken from the latter group has been that known in Britain as Perry-Robertson analysis.

Ayrton and Perry (1886) suggested a process for elastic analysis of practical isolated columns with initial imperfections. This process is based on regarding all imperfections in a column as a single initial out-of-straightness of a half sine-wave form. Failure for the purposes of this method is defined by the first occurrence of material yield. Robertson (1925) was able, on the basis of test results on as-rolled sections, to postulate a workable relationship between the required out-of-straightness for a given strut and its slenderness ratio. With minor amendment, based on subsequent testing, this original relationship survived the era of

permissible-stress design codes in UK. With the advent of limit-state codes such as BS5950 (1985) much fresh testing and analytical work was carried out, with the result that Perry rationalisation again survived but imperfection-slenderness relationships were redefined in terms of four different section classes and buckling axes. An almost identical approach has now been used in the European code EC3 (1988).

As an initial step in the present work, an investigation has been carried out to assess the feasibility of developing Perry analysis to include the effects of fire.

2.2 Assumptions

To retain Perry's definition of 'failure' by the material reaching a 'first yield', a bilinear stress-strain idealisation must be used for steel at elevated temperatures. A transformed section concept has been introduced to Perry's formula to represent the non-uniform deterioration of material stiffness with temperature. The elastic transformed section concept which is commonly used in composite section analysis has been found adequately capable of dealing with this non-uniformity. The centroid of a cross-section under thermal gradient is relocated within the transformed section, which introduces a load eccentricity to the column. The following assumptions were made throughout this study:

1. The column is isolated and simply supported.

2. 'Failure' is defined by the first occurrence of yield at any part of the column.

3. Any curvature due to non-uniform distribution of temperature was assumed to be an initial out-of-straightness of half sine-wave form.

4. Initial load eccentricity and equal end moments can be applied to the column.

5. A constant thermal expansion coefficient was assumed.

6. Temperature distribution over the column length is uniform.

7. Thermal gradients are assumed to vary linearly across the cross-section.

To support the last assumption, a thermal analysis was performed for a shelf-angle beam using the program FIRES-T2 developed by Bresler et al (1977). In the thermal context this case is similar to that of a column embedded in a wall. Fig. 2.1 shows temperature profiles across the steel section which illustrate clearly that assuming a linear distribution of temperatures is an acceptable assumption. Results from experiments carried out by British Steel Corporation (1987) show similar temperature distribution to that predicted by FIRES-T2 and support the linear-distribution assumption.

2.3   Problem Model

The problem of an isolated column under thermal gradient was idealised as illustrated in Fig. 2.2. The main concept of this model is to find an ambient-temperature elastic section which is equivalent to the heated one. This equivalent section can be obtained by reducing the thicknesses of all plates of the steel cross-section using the modular ratio E_T/E_{20}. In performing this transformation, it is important to keep the original mid-surface contour intact, or in other words to reduce the thickness of each plate but not its length. The purpose of this provision is to allow for a correct calculation of the other plane sectional properties. The need to calculate the second moment of area about both principal axes may arise,

Temperature Distribution Within The Web

Distance up web (mm)

Temperature (centigrade)
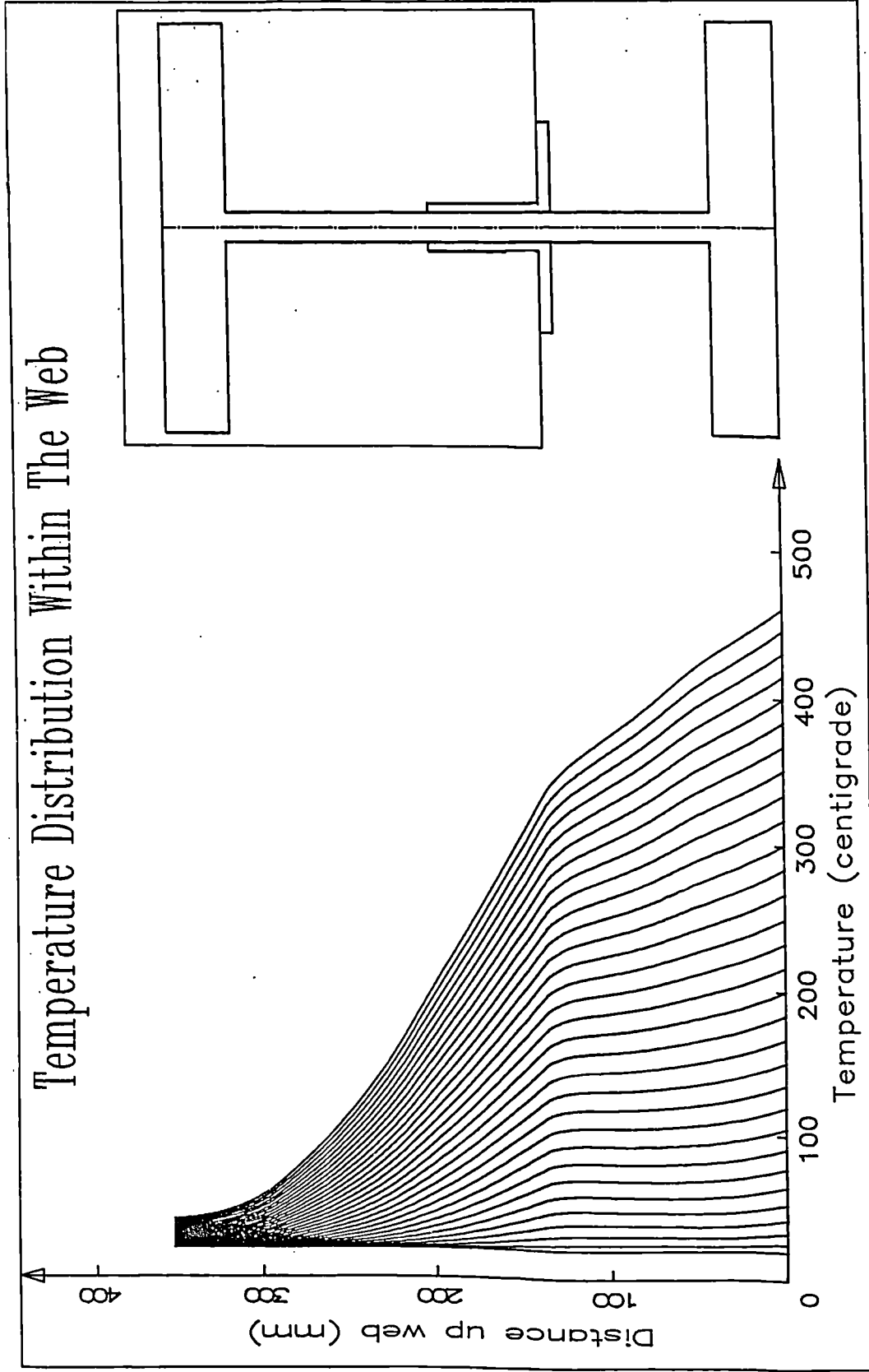
Fig. 2.1 Illustration of Temperature Distribution in a Shelf-Angle Beam, from Thermal Analysis
Case is similar to column embedded in a wall

P

P

TEMP1 TEMP2

P

TEMP1 TEMP2

-------- Original Section

———— Equivalent Section

e_θ : Shift in Centroid's Postion
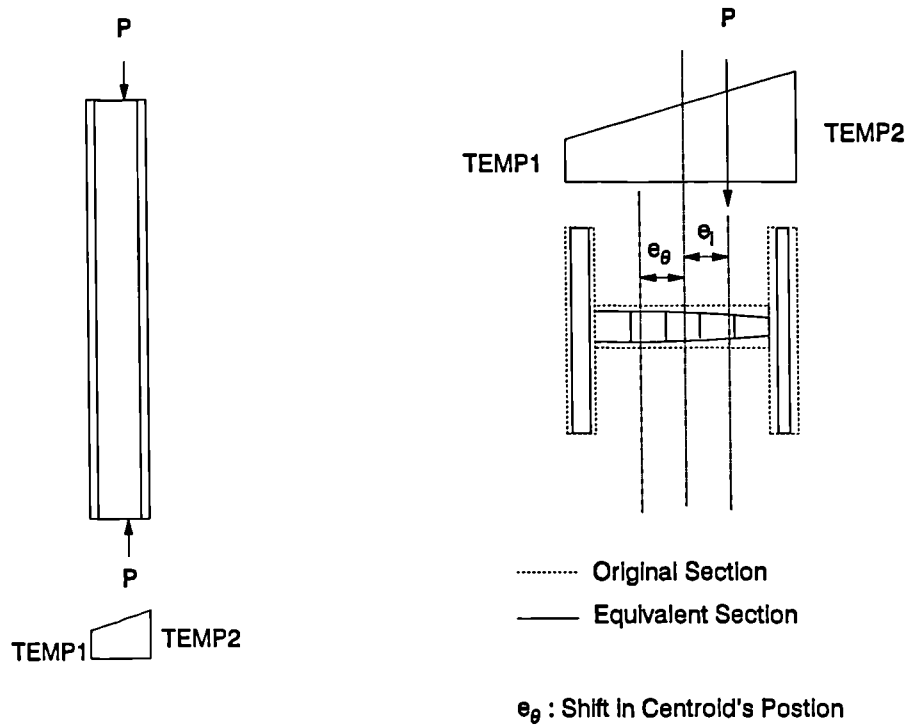
YI = Initial Out-Of-Straightness

Y_θ = Thermal Gradient Curvature

Y = Lateral Disp. Due to Load

e_I = Initial Load Eccentricity

e_θ = Load Eccentricity Due to Centroid Shift

$e = e_\theta + e_I$

P

e

y_θ

y_I y

a

δ_θ y_c

e

P
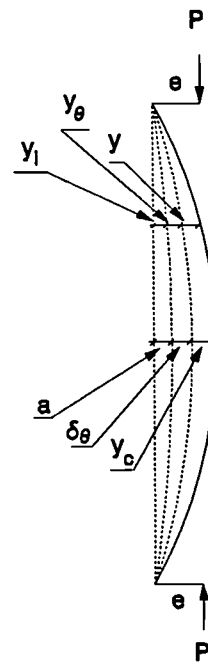
Fig. 2.2 Perry Model of Pinned-Ended Column at Elevated Temperature

for example, if the column is heated non-uniformly about its major axis while it is not restrained from buckling about its minor axis.

This model implies the introduction of four possible imperfections to the column:

1. The initial imperfection (out-of-straightness) that exists before any rise in temperature.

2. The initial load eccentricity.

3. The thermal bowing imperfection due to the non-uniform temperature distribution across the section.

4. The load eccentricity due to the shift of the section's centroid towards the cooler fibre.

Once this 'equivalent section' at ambient temperature is arrived at, elastic analysis can be performed as described by elementary structural mechanics. Basic mechanics principles allow the computation of deformations and stresses for the same problem at ambient temperature.

The non-uniform decline in material stiffness due to elevated temperatures in parts of the cross-section is accounted for by dividing the steel section into a number of segments, each of which has different stiffness. By calculating the stiffness of each segment according to the average temperature of that segment an even simpler model is established.

It was found that as little as five segments are enough to represent adequately any thermal gradient across the section. To test this a column with a thermal gradient about its major axis with one flange at 500° C and the other flange at 20° C was

loaded to failure. Different numbers of segments were used, to assess their effect on the failure load.

No. of Segments	σ_{cr} / σ_y
5	0.2263
10	0.2249
20	0.2246
40	0.2243
80	0.2243
160	0.2243

Table 2.1: Effect of segment number.

Results from this analysis show a 1 % difference in 'failure' load between five segments and forty segments, while no effect is evident from increasing the number of segments beyond the latter number.

According to Timoshenko and Gere (1978) the moment at any point along a column with initial out-of-straightness and initial load eccentricity (Fig. 2.2) can be expressed as:.

$$M = P\left(y + y_i + y_\theta - e_\theta - e_i\right) \qquad (2.1)$$

where:

y is the rise in deflection,

y_i initial out-of-straightness,

y_θ deflection due to thermal gradient,

e_i initial load eccentricity from the original centroid of the section,

e_θ load eccentricity from the new centroid of the transformed section.

$$M = -EI \frac{d^2y}{dx^2} \tag{2.2}$$

Apply Eq. 2.2 in Eq. 2.1 to get:

$$EI\frac{d^2y}{dx^2} + P\left(y + y_o - e_o\right) = 0 \tag{2.3}$$

where:

$$y_o = y_i + y_\theta$$

and $\quad e_o = e_i + e_\theta$ added algebraically.

Eq. 2.2 is the basic equation of a column with initial out-of-straightness and subject to a load with eccentricity. This equation applies to ambient temperature and elevated temperatures provided that all thermally induced imperfections are included in y_o and e_o and the decline in material stiffness is included in the term EI.

let $\quad k^2 = \frac{P}{EI} \qquad$ then Eq. 2.3 can be rewritten as:

$$\frac{d^2y}{dx^2} + k^2y = -k^2y_o + k^2e_o \tag{2.4}$$

At the mid-height of the column:

$$y_{oc} = a + \delta\theta \tag{2.5}$$

in which:

a is the initial out-of-straightness at the column mid-height,

and $\delta\theta$ is the amplitude of the sine wave due to thermal bowing.

and by assuming the initial shape of the column to have a half sine-wave form; the initial curvature at any point of the column is:

$$y_o = (a + \delta\theta)\, sin(\frac{\pi x}{L}) \tag{2.6}$$

Then Eq. 2.3 becomes:

$$\frac{d^2y}{dx^2} + k^2 y = -k^2(a + \delta\theta).sin(\pi x/L) + k^2 e_o \tag{2.7}$$

solving for y:

$$y = A\, cos(kx) + B\, sin(kx) + k^2(a + \delta\theta)\frac{sin(\pi x/L)}{\frac{\pi^2}{L^2} - k^2} + e_o \tag{2.8}$$

Apply end conditions:

where:

$$y = 0 \quad at \quad x = 0 \quad and \quad x = L, \qquad then:$$

$$y = -e_o.cos\ kx + e_o.(cos\ kL - 1).\frac{sin\ kx}{sin\ kL + e_o} + k^2(a + \delta\theta).\frac{sin\ \pi}{\frac{\pi^2}{L} - k^2}$$

at $x = \frac{1}{2}L$

$$y = -e_o.sec\left(\frac{1}{2}kL - 1\right) + \frac{(a+\delta\theta)}{\frac{P}{P_{cr}}-1}$$

Once the rise in deflection is known, the moments and stresses can be evaluated at any point along the column using the relationship:

$$\sigma = \frac{M.y}{I_t} \tag{2.9}$$

Resulting in:

$$\sigma_1 = \left(\frac{P}{A_t} + \frac{P.c\frac{(a+\delta\theta)}{I_t}}{\frac{P}{P_{cr}-1}} - \frac{P.e_o.c}{I_t}(sec\frac{1}{2}kL - 1)\right)\frac{E_{20}}{E_{Temp1}} \tag{2.10}$$

$$\sigma_2 = \left(\frac{P}{A_t} - \frac{P(d-c)\frac{(a+\delta\theta)}{I_t}}{\frac{P}{P_{cr}} - 1} + P.e_o(d - c)\right)\frac{E_{20}}{E_{Temp2}} \tag{2.11}$$

in which the subscript t refers to sectional properties calculated for the transformed section.

A column in fire experiences four separate imperfections y_i, y_θ, e_i and e_θ. The first two y_i and y_θ act in their own natural directions, but are most critical when they act in the same direction. The thermally-induced load eccentricity acts always in the opposite direction to the thermal bowing. While the thermal bowing is expected to introduce higher bending at the column mid-height, and the load eccentricity due to the centroid shift is expected to produce a counter-moment, it is not obvious which of the two effects is going to be dominant. This point will be investigated later in this chapter.

2.4 Computer Program

Although hand calculation of the governing equations as stated in the previous section is feasible, the fact that the section is divided into segments makes it more

sensible to obtain solutions by computer. To this effect, a computer program was written in QBASIC to perform Perry analysis on columns under uniform temperatures or thermal gradient. The program defines the transformed cross-section by dividing it into the required number of segments and allocating a thickness to each segment in proportion to its modular ratio E_T/E_{20}. Once the transformed section is defined, the new position of the centroid is calculated and load/temperature increments are applied until first yield is reached at any point on the column length.

2.5 Comparison with Other Work

To validate the solution procedure suggested in this study, comparisons with other work were carried out. Fig. 2.3 represents a case previously studied by Corradi et al (1990) using non-linear elasto-plastic finite element analysis. A beam-column subject to a linear thermal gradient of $300^{\circ} - 500^{\circ}C$ and a combination of axial load and end moments was analysed. The 'collapse' loads predicted by elastic Perry analysis are plotted in broken lines on the figure. The results obtained by this analysis may be regarded as lower bounds to the limiting loads of the case under consideration, while the curves of the more complex study constitute a nearly exact representation of the failure loads. It can be noticed from these curves that failure loads are remarkably similar for both analyses when the element is a column (i.e. when no end-moments exist). On the other hand the difference between failure loads when the axial applied load is minimal reflects the difference between the elastic and plastic moment capacities of the element under consideration. The major axis form factor of most H-sections tends to lie in the range 1.10 to 1.20, and for the HE200M section used in the analysis it is actually 1.17. It is obvious that Perry analysis will under-predict failure loads in this region, although the
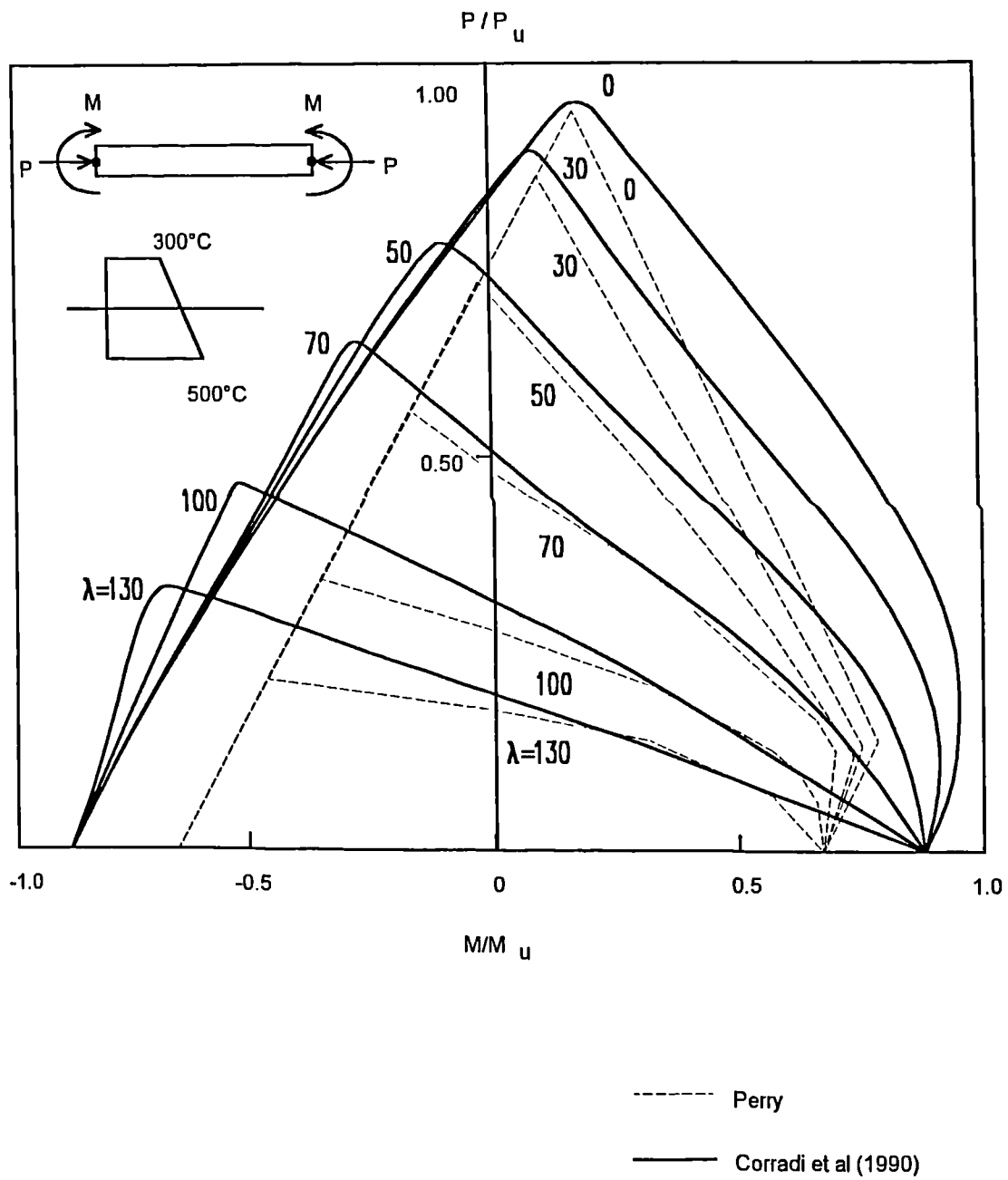
**Fig. 2.3   Comparison between Perry Analysis and
The Finite Element Method**

non-uniform material stiffness across the section dictates that the amount of this shortfall is not exactly in line with the form factor.

Cooke (1987) performed at City University a series of very carefully controlled tests on model-scale II-section columns under thermal gradient, monitoring temperatures and deflections as the tests progressed. Fig. 2.4 shows the experimental deflection about the major axis against time for one of Cooke's tests, compared with the deflection predicted by the Perry analysis. It is notable that the deflection behaviour compares very well, including a demonstration of the tendency in later stages of the heating process for centroid movement to become a more dominant effect, as is shown by the reversal of deflection. In this comparison measured temperature gradients have been used in the analysis.

2.6   Study Cases

Several cases of columns with temperature gradient were studied. A typical case is illustrated in Fig. 2.5. The temperature of one flange of an isolated column was kept cool, at ambient temperature, while the temperature of the flange was increased progressively to $600°C$. For each temperature distribution, the failure load was found for several slenderness ratios. When one flange of the column is kept cool and the other flange is heated, first yield usually occurs at the cooler fibre in compression. This situation is valid until the strength of the hot fibre has considerably declined at about $500°C$, after which first yield starts to take place at the hot fibre in tension. This is true for all slenderness ratios studied except for the lowest one (50) for which failure occurs at the hot fibre in compression. This is due to the fact that the effect of load eccentricity is dominant in this case, while
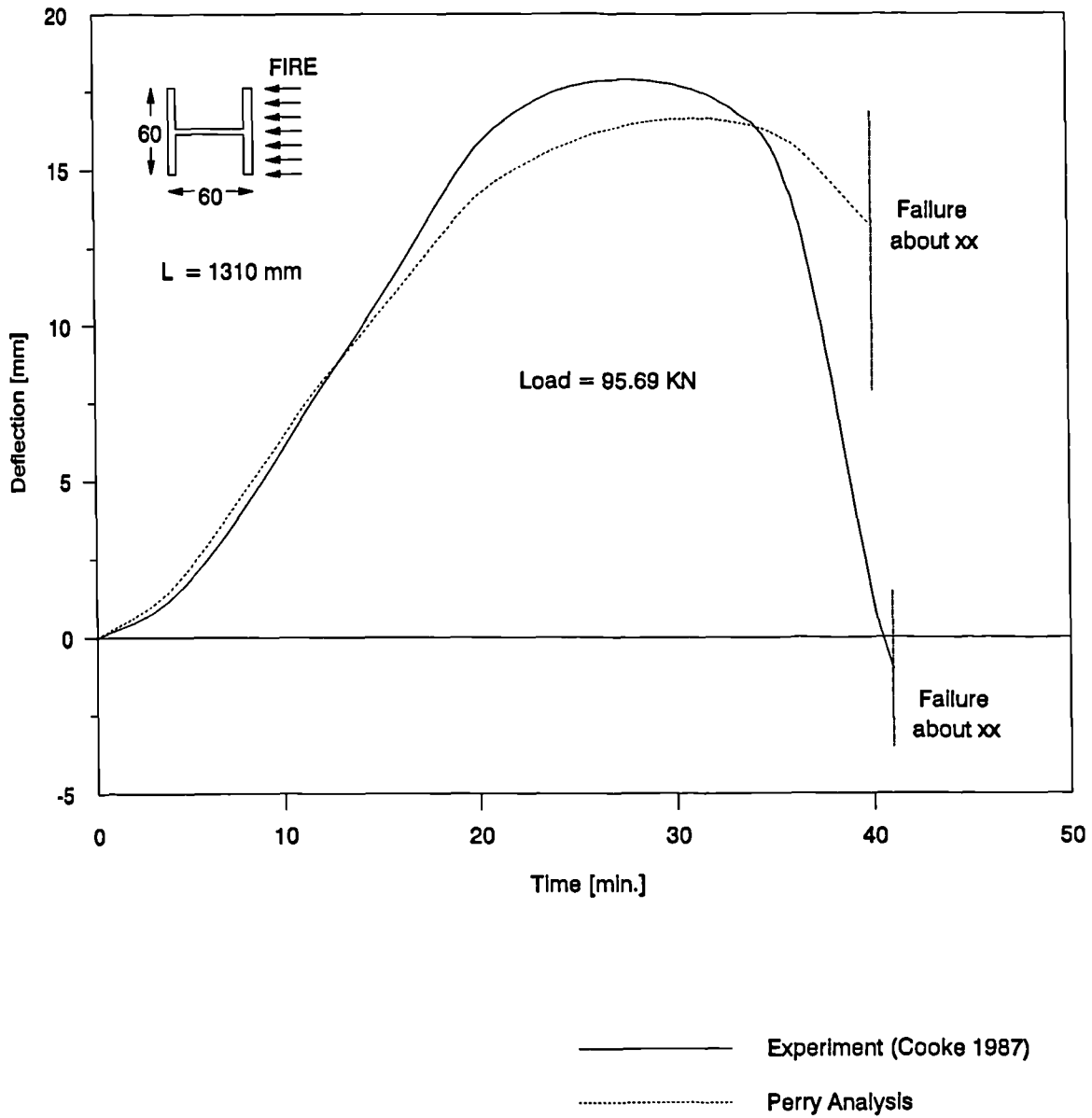
Fig. 2.4 Comparison of Experimental Deflection with Perry Analysis Prediction
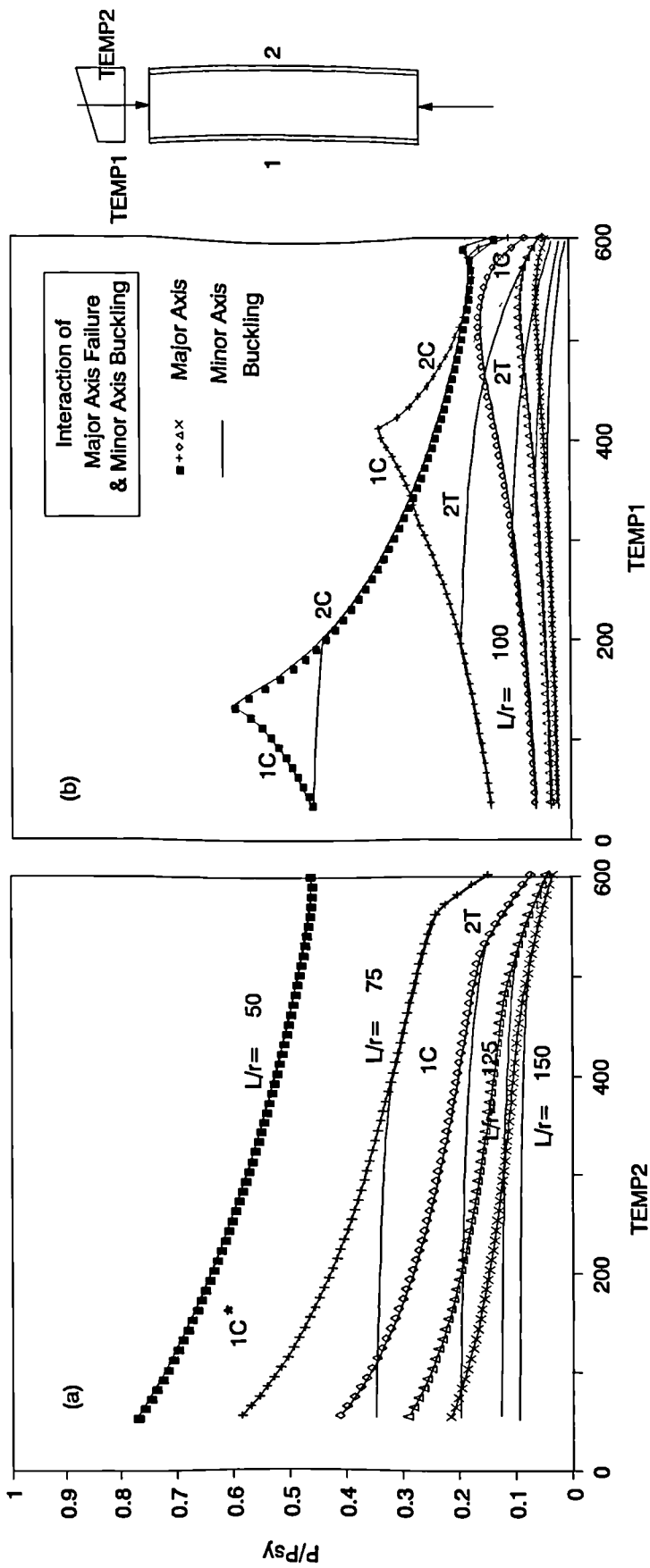
Fig. 2.5

Failure Loads For Columns at Different Slenderness Ratios:

a: when one flange is heated to 600°C with the other cool.

b: when the cool flange is then allowed to heat to 600°C.

* Denotes mode of failure (Major Axis)

the effect of thermal curvature is the dominant one in all other cases. It seems that the effect of the thermally-induced load eccentricity is dominant at low slenderness ratios. This conclusion is also supported by later studies using the finite element method. The bilinear stress-strain model suggested by ECCS was used in this case.

2.7   Conclusions

It should be emphasised that the Perry analysis presented here is not being recommended as a substitute for non-linear finite element analysis but as a complement to it. The Perry model uses only simple concepts of elastic structural mechanics and, at minimal computational effort, provides a lower-bound benchmark for failure temperatures which is unlikely to be highly out of line with finite element results. This fact allows this model to be used as a means to provide engineers with a simplified understanding of the many interacting effects influencing steel columns in fire. Such an understanding can be based on simple structural mechanics calculations rather than having to rely on empirical formulas.

It is also very useful as a model for demonstrating the major structural effects and their qualitative relevance in particular cases. The values of the various imperfection components can be traced as heating progresses and can be linked directly with the deflection behaviour. Given that the analysis is essentially computational, with a section divided into segments, it is easy to include the effect of self-equilibrating residual stress patterns, so a very complete elastic model of the buckling can be produced. Such elastic models are known to provide very good approximations to buckling limits at ambient temperature.

It may also be the case that design guidelines are eventually more conveniently

framed in the general context of this approach than simply based on curve-fitting

to a combination of test and finite element results.

CHAPTER 3

3-D Finite Element Formulation for Space Frames in Fire

3.1 Introduction

The problem of analysing structural behaviour under fire conditions is a considerably complex one. Whether in a real fire or in a furnace, the structural element is expected to undergo a non-uniform distribution of temperature across its section and along its length. This complexity means that failure might occur by any combination of factors. In the past various researchers have suggested different approaches to address structural behaviour in fire. Most, if not all of the previous work adopted an in-plane analysis approach. Under non-uniform temperature profiles both the centre of gravity and the shear centre lose their significance. Furthermore, in columns, the usual pattern of failure about the weak axis of unrestrained columns is not necessarily valid. With the differential deterioration of the stiffness and strength of different parts of the cross section, failure may occur about the strong axis by torsional buckling or by lateral-torsional buckling. All these considerations mean that a three-dimensional approach is necessary and desirable. Using the finite element method would solve the problem of variation in temperature along the structural member, apart from its advantage in solving the governing equations for complex systems in a very effective way (Zienkiewicz, 1971).

3.2 Formulation

The following formulation which is highly non-linear, was chosen to obtain more accurate solutions. This formulation is based on a beam element with one node at each end. It is based on displacement fields rather than stress fields due to the

advantage in ease of programming for digital computers (Chen and Atsuta, 1977).

3.2.1 Assumptions

The following assumptions were made in order to formulate the governing equations for the beam element:

- The element is straight, prismatic and symmetric about both principal axes

- The reference axis of the element coincides with the centroidal axis of the cross-section.

- Apart from warping deformations plane sections remain plane after deformation. This assumption effectively reduces the usual assumption of "plane sections remain plane" after deformation into "plane plates remain plane" after deformation.

- Sections consist of thin plates, so that shearing deformations are neglected.

- Strain reversal is not accounted for.

- Certain assumptions about displacements will be stated in the next section when the need for such assumptions arises.

3.2.2 Displacement Derivation

Based on the above assumptions the displacements u, v and w of an arbitrary point A (Fig. 3.1) on the midsurface contour of a beam element with an I cross-section can be derived from geometry and expressed in terms of the displacements of the reference axis of the beam-column as:

$$u = u_o - (y. \sin\theta_y + x. \sin\theta_x) \tag{3.1}$$

$$v = v_o - y + (y. \cos\theta_y \cos\theta_z + x. \cos\theta_x \sin\theta_z) \tag{3.2}$$

$$w = w_o - x + (x. \cos\theta_x \cos\theta_z - y. \cos\theta_y \sin\theta_z) \tag{3.3}$$

in which x and y are the coordinates of point A, and all other displacements are shown in Fig. 3.1.

By choosing the undeformed axis of the element as a reference for displacements, the following formulation becomes a Lagrangian formulation rather than an Eulerian formulation in which the reference deformations are those of the deflected element.

If the following assumptions are made :

1. The slope of the deflected element in the y-direction is:

$$v'_o = \sin\theta_y \tag{3.4}$$

and the slope in the x-direction:

$$w'_o = \sin\theta_x \tag{3.5}$$

2. The twist angle θ_z is "reasonably small" so that:

$$\sin\theta_z = \theta_z \qquad and, \tag{3.6}$$

$$\cos\theta_z = 1 \tag{3.7}$$

Front View

u_o

Δz

O

y A

u

Δz

Δv_o

θy

O

A

y

z

v_o

v

Top View

u_o

Δz

O

x A

u

Δz

Δw_o

θx

O A

x

z

w_o

w

Side View

w_o

X

x

O

y

A

w

v_o

v

θz

O

A

Y

$y.\cos \theta y$

$x.\cos \theta x$
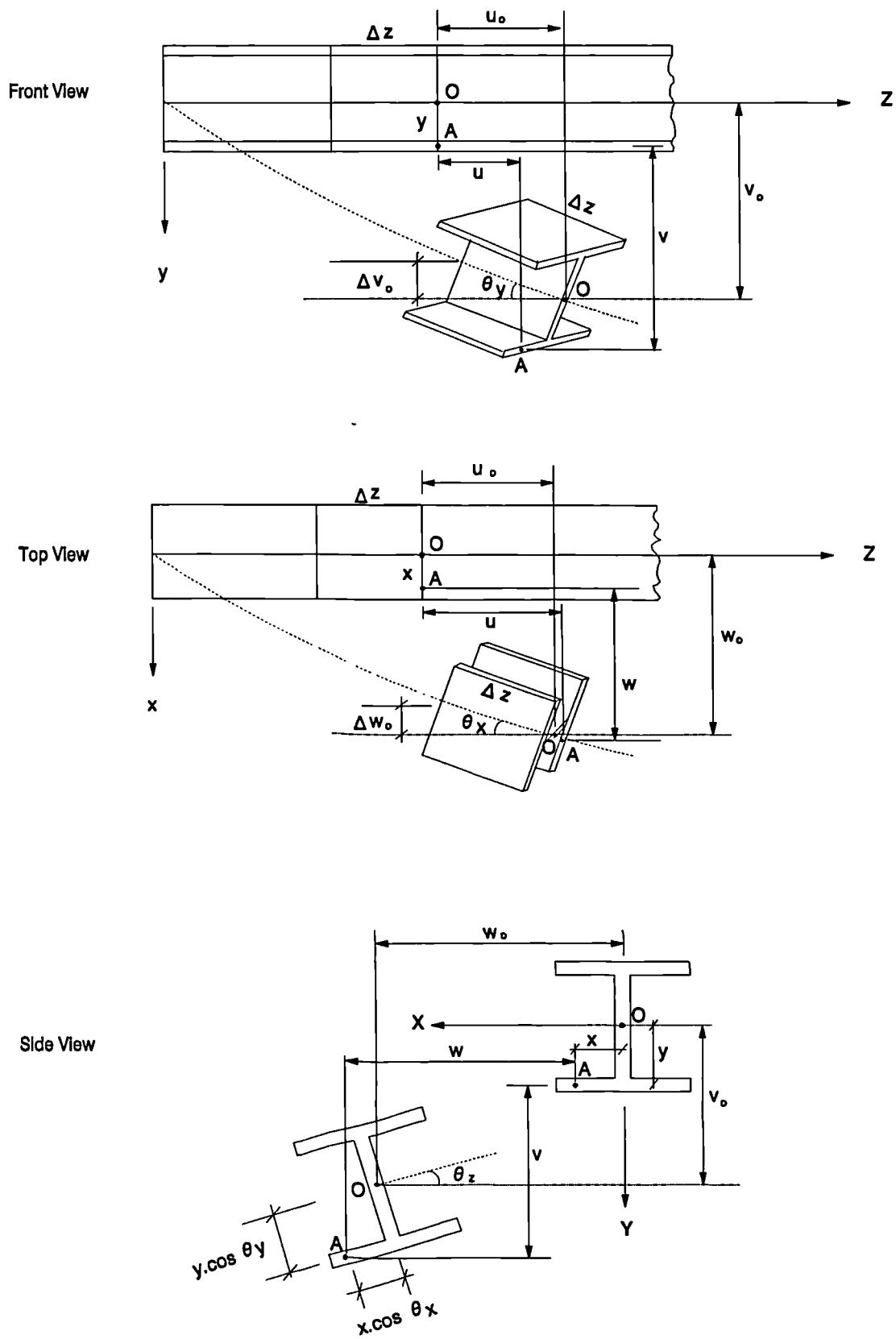
Fig. 3.1 Deformations of Infinitesimal Segment z

then Eqs. 3.1-3.3 can be rewritten as:

$$u = u_o - (y\, v_o' + x\, w_o') \tag{3.8}$$

$$v = v_o - y + (y\, cos\theta_y + x\, \theta_z\, cos\theta_x) \tag{3.9}$$

$$w = w_o - x + (x\, cos\theta_x - y\, \theta_z\, cos\theta_y) \tag{3.10}$$

Eq. 3.8 is a Bernoulli-Navier equation, which neglects the effect of warping due to the assumption that plane sections remain plane after deformation. However, the effect of warping which was introduced by Vlasov (1961) is significant in the case of thin-walled open cross sections, which is the case for most of the standard I and H structural sections. Adding the term for warping, Eq. 3.8 becomes:

$$u = u_o - y\, v_o' - x\, w_o' + \omega\, \theta_z' \tag{3.11}$$

where ω is the sectorial coordinate of the point A defined in Fig. 3.2.

3.2.3   Strain-Displacement Relationship

The axial strain at the arbitrary point A may be obtained from the large displacement equation given by Saada (1974) as:

$$\epsilon_z = u' + \frac{1}{2} [(u')^2 + (v')^2 + (w')^2] \tag{3.12}$$

In small displacement formulations the first quadratic term is normally discarded. This is due to the assumption that displacements are small and consequently the second order term is very small compared to the first order one. The last two

$\omega = 2 *$ Shaded Area

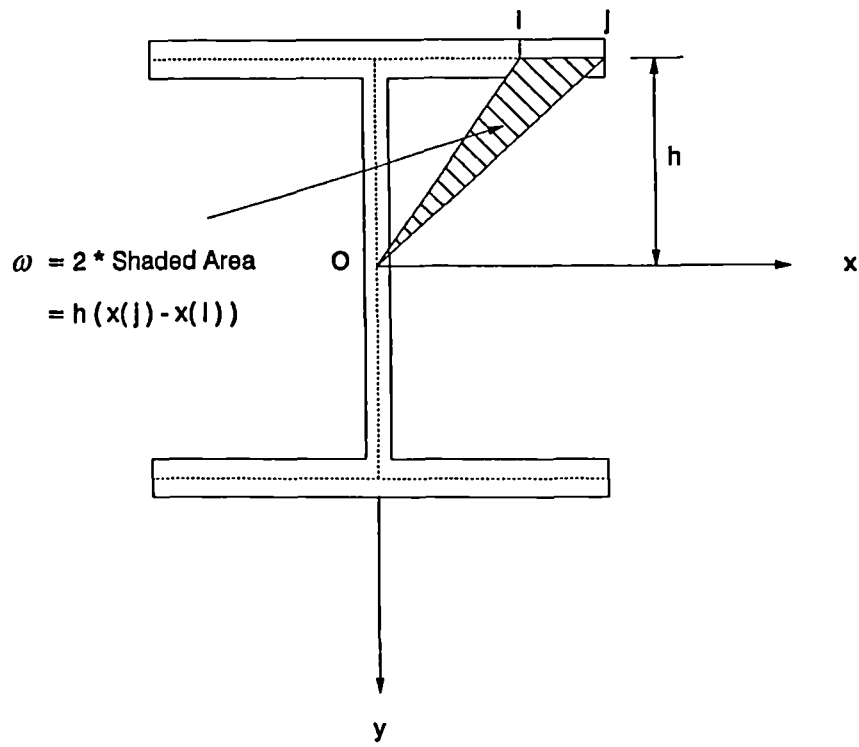$= h \left(x(J) - x(I) \right)$

Fig. 3.2   Definition of Sectorial Coordinate of Segment IJ

quadratic terms must be kept in any formulation that accounts for bending, as they represent the only contribution of bending displacements to the axial strain of any point on the cross-section. A nonlinear formulation may be obtained by differentiating Eqs 3.9-3.11 with respect to z to produce:

$$u' = u'_o - y\,v''_o - x\,w''_o + \omega\,\theta''_z \tag{3.13}$$

$$v' = v'_o - y\,sin\theta_y\,\frac{d\theta_y}{dz} - x\,\theta_z\,sin\theta_x\,\frac{d\theta_x}{dz} + x\,\theta'_z\,cos\theta_x \tag{3.14}$$

$$w' = w'_o - x\,sin\theta_x\,\frac{d\theta_x}{dz} + y\,\theta_z\,sin\theta_y\,\frac{d\theta_y}{dz} - y\,\theta'_z\,cos\theta_y \tag{3.15}$$

From Fig. 3.3 the physical interpretation of $cos\theta_y$ and $cos\theta_x$ allows them to be approximated as:

$$cos\theta_y = \sqrt{1 - (v'_o)^2}$$

$$cos\theta_x = \sqrt{1 - (w'_o)^2} \tag{3.16}$$

To find the values of $\frac{d\theta_y}{dz}$ and $\frac{d\theta_x}{dz}$, v'_o and w'_o of Eqs. 3.4 and 3.5 are differentiated to produce:

$$v''_o = cos\theta_y\,\frac{d\theta_y}{dz}$$

$$w''_o = cos\theta_x\,\frac{d\theta_x}{dz} \tag{3.17}$$

resulting in:

$$\frac{d\theta_y}{dz} = \frac{v''_o}{cos\theta_y}$$

$$\frac{d\theta_x}{dz} = \frac{w''_o}{cos\theta_x} \tag{3.18}$$

$$\Delta z \sqrt{1-v_o^2}$$

z

$$\theta_y$$

$$\Delta v_o$$

$$\Delta z$$

y

$$\sin \theta_y = \Delta v_o / \Delta z = v_o^{'}$$

$$\cos \theta_y = \sqrt{1-v_o^{'2}}$$

$$\Delta z \sqrt{1-w_o^2}$$

z

$$\theta_x$$

$$\Delta w_o$$

$$\Delta z$$

x

$$\sin \theta_x = \Delta w_o / \Delta z = w_o^{'}$$
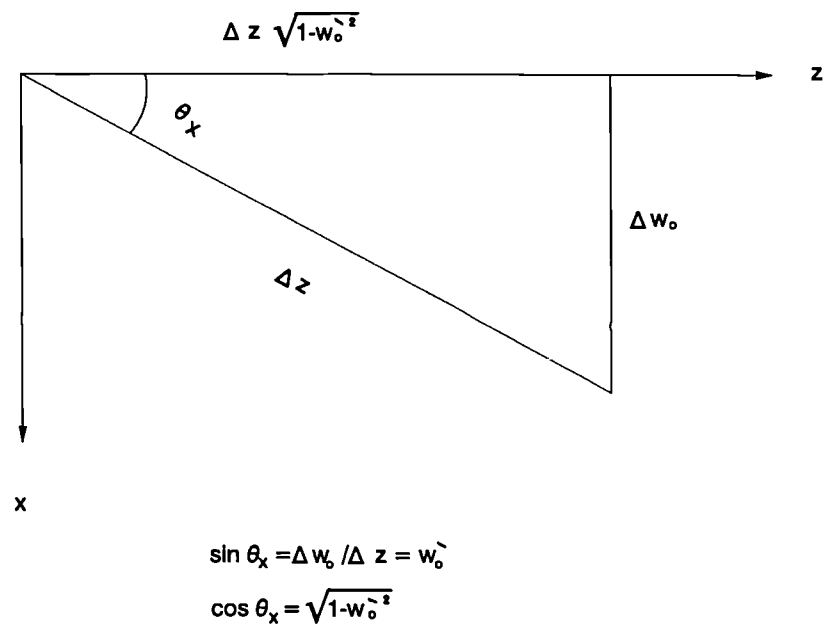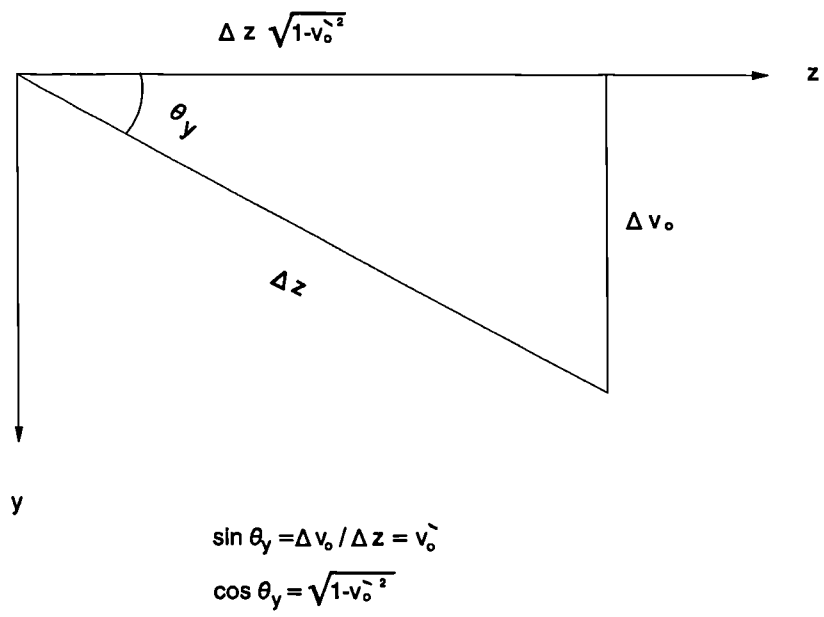
$$\cos \theta_x = \sqrt{1-w_o^{'2}}$$

Fig. 3.3   Physical Interpretation of cos θ_y and cos θ_x

Apply Eq. 3.16 to Eq. 3.18 to get:

$$\frac{d\theta_y}{dz} = \frac{v_o''}{\sqrt{1 - (v_o')^2}}$$

$$\frac{d\theta_x}{dz} = \frac{w_o''}{\sqrt{1 - (w_o')^2}} \tag{3.19}$$

Substituting Eqs. 3.19 and 3.16 into Eqs. 3.14 and 3.15, discarding "small terms" containing $\theta_z \sin\theta_y$ and $\theta_z \sin\theta_x$, and using Eqs. 3.4 and 3.5 produces:

$$v' = v_o' - y \frac{v_o' v_o''}{\sqrt{1 - (v_o')^2}} + x \ \theta_z' \sqrt{1 - (w_o')^2} \tag{3.20}$$

$$w' = w_o' - x \frac{w_o' w_o''}{\sqrt{1 - (w_o')^2}} - y \ \theta_z' \sqrt{1 - (v_o')^2} \tag{3.21}$$

The nonlinearity in the above equations is ensured by retaining terms containing $\cos\theta_x$ and $\cos\theta_y$.

Apply Eqs. 3.13, 3.20 and 3.21 to Eq. 3.12 to get:

$$
\begin{aligned}
\epsilon_z \ = \ & u_o' - y \ v_o'' - x \ w_o'' + \omega \ \theta_z'' + \frac{1}{2} \ (u_o')^2 - y \ u_o' v_o'' \\[2mm]
& - \ x \ u_o' w_o'' + \omega \ u_o' \theta_z'' + \frac{1}{2} \ y^2 \ (v_o'')^2 + \frac{1}{2} \ x^2 \ (w_o'')^2 \\[2mm]
& + \ \frac{1}{2} \ (w_o')^2 - x \ \frac{(w_o')^2 w_o''}{\sqrt{1 - (w_o')^2}} - y \ \theta_z' w_o' \sqrt{1 - (v_o')^2} \\[2mm]
& + \ \frac{1}{2} \ x^2 \ \frac{(w_o' w_o'')^2}{1 - (w_o')^2} + \frac{1}{2} \ y^2 \ (\theta_z')^2 (1 - (v_o')^2) \\[2mm]
& + \ \frac{1}{2} \ (v_o')^2 - y \ \frac{(v_o')^2 v_o''}{\sqrt{1 - (v_o')^2}} + x \ \theta_z' v_o' \sqrt{1 - (w_o')^2} \\[2mm]
& + \ \frac{1}{2} \ y^2 \ \frac{(v_o' v_o'')^2}{1 - (v_o')^2} + \frac{1}{2} \ x^2 \ (\theta_z')^2 \ (1 - (w_o')^2)
\end{aligned} \tag{3.22}
$$

In arriving at Eq. 3.22 high order terms related to warping have been neglected.

Eq. 3.22 is the strain-displacement equation that expresses the axial strain at any point on the cross section in terms of the displacements of the reference axis. This can be done simply by substituting values for x, y and ω into the equation.

3.2.4 Total Equilibrium

Once the strain-displacement relationship is established, the principle of virtual work can be used to arrive at the equilibrium equation for the beam-column element. The principle of virtual work may be written over the length of the beam-column, as:

$$\delta W = \int_V \sigma_z \, \delta \epsilon_z \, dV \; - \; <Q> \; \{\delta q\} \; = \; 0 \tag{3.23}$$

In this virtual work equation it is clear that the strain is assumed to be essentially uniaxial and the effect of any other strain is ignored.

The variation in strain $\delta \epsilon_z$ can be obtained from Eq. 3.22 noting that u'_o, v'_o, v''_o, w'_o, w''_o, θ'_z and θ''_z may vary independently. Eq. 3.23 becomes:

$$
\begin{aligned}
\delta W = & \left(\int_l \int_A \sigma_z \left[\left\{ (1 + u'_o) \; - \; y\, v''_o \; - \; x\, w''_o \; + \; \omega \theta''_z \right\} \delta u'_o \right. \right. \\[2mm]
& + \left\{ v'_o + y \left(\frac{\theta'_z v'_o w'_o}{\sqrt{1 - (v'_o)^2}} - 2 \frac{v'_o v''_o}{\sqrt{1 - (v'_o)^2}} - \frac{(v'_o)^3 v''_o}{(1 - (v'_o)^2)^{3/2}} \right) \right. \\[2mm]
& + \; y^2 \left(\frac{v'_o (v''_o)^2}{1 - (v'_o)^2} + \frac{(v'_o)^3 (v''_o)^2}{(1 - (v'_o)^2)^2} - (\theta'_z)^2 v'_o \right) \\[2mm]
& + \; x \left(\theta'_z \sqrt{1 - (w'_o)^2} \right) \Big\} \delta v'_o
\end{aligned}
$$

$$
+ \left\{ w'_o - x \left(\frac{\theta'_z v'_o w'_o}{\sqrt{1 - (w'_o)^2}} + 2 \frac{w'_o w''_o}{\sqrt{1 - (w'_o)^2}} + \frac{(w'_o)^3 w''_o}{(1 - (w'_o)^2)^{3/2}} \right) \right.
$$

$$
+ \ x^2 \left(\frac{w'_o (w''_o)^2}{1 - (w'_o)^2} + \frac{(w'_o)^3 (w''_o)^2}{(1 - (w'_o)^2)^2} - (\theta'_z)^2 w'_o \right)
$$

$$
- \ y \left(\theta'_z \sqrt{1 - (v'_o)^2} \right) \right\} \delta w'_o
$$

$$
- \ \left\{ y \left(1 + u'_o + \frac{(v'_o)^2}{\sqrt{1 - (v'_o)^2}} \right) - y^2 \left(v''_o + \frac{(v'_o)^2 v''_o}{1 - (v'_o)^2} \right) \right\} \delta v''_o
$$

$$
- \ \left\{ x \left(1 + u'_o + \frac{(w'_o)^2}{\sqrt{1 - (w'_o)^2}} \right) - x^2 \left(w''_o + \frac{(w'_o)^2 w''_o}{1 - (w'_o)^2} \right) \right\} \delta w''_o
$$

$$
+ \ \left\{ x \, v'_o \sqrt{1 - (w'_o)^2} - y \, w'_o \sqrt{1 - (v'_o)^2} \right.
$$

$$
+ \ y^2 \, \theta'_z (1 - (v'_o)^2) + x^2 \, \theta'_z (1 - (w'_o)^2) \right\} \delta \theta'_z
$$

$$
+ \ \left. \{ \omega \, (1 + u'_o) \} \, \delta \theta''_z \right] \, dA \, dz \right) - \ <Q> \{ \delta q \ \} = 0 \tag{3.24}
$$

The stress resultants are defined as:

$$
n = \int_A \sigma_z . dA
$$

$$
m_x = \int_A \sigma_z . y . dA
$$

$$
m_x^2 = \int_A \sigma_z . y^2 . dA
$$

$$
m_y = \int_A \sigma_z . x . dA
$$

$$
m_y^2 = \int_A \sigma_z . x^2 . dA
$$

$$
m_\omega = \int_A \sigma_z . \omega . dA
$$

$$m_z = \int_A \sigma_z.(x^2 + y^2) \cdot \theta'_z \cdot dA$$

$$T_{sv} = G \, J \, \theta'_z \tag{3.25}$$

where:

n	is the internal normal force
$m_x, \, m_y$	internal moments about the respective axes
$m_x^2, \, m_y^2$	second moments of the normal stress about respective axes
m_ω	bimoment
m_z	torsional moment due to warping deformations
T_{sv}	twisting moment due to St. Venant shear stress
$J = \frac{1}{3}\sum b \, t^3,$	in which b is the plate length, and t is the thickness
G	the elastic shear modulus.

Using the definitions in Eq. 3.25, Eq. 3.24 can be rewritten as:

$$\int_l (a_1 \, \delta u'_o \; + \; a_2 \, \delta v'_o + a_3 \, \delta v''_o + a_4 \, \delta w'_o + a_5 \, \delta w''_o$$

$$+ \; a_6 \, \delta\theta'_z + a_7 \, \delta\theta''_z \;) \; dz - \, < Q > \{q\} = 0 \tag{3.26}$$

where:

$$a_1 \;\; = \;\; n \, (1 + u'_o) - m_x \, (v''_o) - m_y \, (w''_o) + m_\omega \, (\theta''_z)$$

$$a_2 \;\; = \;\; n(v'_o) + m_x \left[\frac{v'_o}{\sqrt{1 - (v'_o)^2}}(\theta'_z w'_o - 2v''_o - \frac{(v'_o)^2 v''_o}{1 - (v'_o)^2}) \right]$$

$$+ \; m_y(\theta'_z\sqrt{1 - (w'_o)^2}) + m_x^2 \left[v'_o(\frac{(v'_o)^2(v''_o)^2}{(1 - (v'_o)^2)^2} + \frac{(v''_o)^2}{1 - (v'_o)^2} - (\theta'_z)^2) \right]$$

$$a_3 \;\; = \;\; -m_x \left[(1 + u'_o) + \frac{(v'_o)^2}{\sqrt{1 - (v'_o)^2}} \right] + m_x^2 \left[v''_o(1 + \frac{(v'_o)^2}{1 - (v'_o)^2}) \right]$$

$$a_4 = n(w_o') - m_y \left[\frac{w_o'}{\sqrt{1 - (w_o')^2}} (\theta_z' v_o' + 2w_o'' + \frac{(w_o')^2 w_o''}{1 - (w_o')^2}) \right]$$

$$- m_x(\theta_z' \sqrt{1 - (v_o')^2}) + m_y^2 \left[w_o'(\frac{(w_o' w_o'')^2}{(1 - (w_o')^2)^2} + \frac{(w_o'')^2}{1 - (w_o')^2} - (\theta_z')^2) \right]$$

$$a_5 = -m_y \left[(1 + u_o') + \frac{(w_o')^2}{\sqrt{1 - (w_o')^2}} \right] + m_y^2 \left[w_o''(1 + \frac{(w_o')^2}{1 - (w_o')^2}) \right]$$

$$a_6 = -m_x(w_o' \sqrt{1 - (v_o')^2}) + m_y(v_o' \sqrt{1 - (w_o')^2}) + m_x^2 \theta_z'(1 - (v_o')^2)$$

$$+ m_y^2 \theta_z'(1 - (w_o')^2) + T_{sv} + 0.5 M_z \theta_z'^2$$

$$a_7 = m_\omega (1 + u_o') \tag{3.27}$$

The integration of terms between addition signs in Eq. 3.26 represents the virtual work due to internal forces in the direction of the virtual displacement attached to each term. The final term in Eq. 3.26 is the virtual work due to an arbitrary displacement $\{q\}$ in the direction of the applied forces $< Q >$.

3.2.5 Incremental Equilibrium

If displacements u_o, v_o, w_o, θ_z are functions of a discrete set of displacement coordinates, q_i, Eq. 3.26 may be written as:

$$\psi_i = 0 \tag{3.28}$$

in which:

$$\psi_i = \int_l (a_1 \frac{\partial u_o'}{\partial q_i} + a_2 \frac{\partial v_o'}{\partial q_i} + a_3 \frac{\partial v_o''}{\partial q_i} + a_4 \frac{\partial w_o'}{\partial q_i} + a_5 \frac{\partial w_o''}{\partial q_i}$$

$$+ a_6 \frac{\partial \theta_z'}{\partial q_i} + a_7 \frac{\partial \theta_z''}{\partial q_i}) dz - Q_i \tag{3.29}$$

In other words the difference between the internal forces and the external loads must equal zero, which is the target for attaining total equilibrium.

It should be noticed that the internal forces of Eq. 3.29 were arrived at by differentiating the virtual work terms of Eq. 3.26 with respect to the virtual displacement q_i.

The non-linearity of Eq. 3.29 discounts the possibility of direct solution. Consequently recourse to an iterative approach to the solution is necessary.

The Newton-Raphson method offers a first order approximation to Eq. 3.28 which can be rewritten according to Zienkiewicz and Taylor (1991) as:

$$\psi_i^{n+1} = \psi_i^n + \left(\frac{\partial \psi_i}{\partial q_j}\right)^n \Delta q_j^n = 0 \tag{3.30}$$

in which n is the iteration counter and q_j is also a set of displacement coordinates. Fig. 3.4 shows a schematic illustration of Newton-Raphson solution between successive increments j and i.

If Eq. 3.29 is not satisfied ($\psi_i \neq 0$), corrections to q_i may be obtained by rearranging Eq. 3.30 to produce:

$$\Delta \psi_i = \left(\frac{\partial \psi_i}{\partial q_j}\right)^n \Delta q_j^n = -\psi_i^n \tag{3.31}$$

Total equilibrium can be attained by substituting Eq. 3.29 into Eq. 3.30 for repeated indices j and i, to result in:

$$\left(\int_l \left(\frac{\partial a_1}{\partial q_j}\frac{\partial u_o'}{\partial q_i} + \frac{\partial a_2}{\partial q_j}\frac{\partial v_o'}{\partial q_i} + \frac{\partial a_3}{\partial q_j}\frac{\partial v_o''}{\partial q_i} + \frac{\partial a_4}{\partial q_j}\frac{\partial w_o'}{\partial q_i} + \frac{\partial a_5}{\partial q_j}\frac{\partial w_o''}{\partial q_i}\right.\right.$$
$$\left.\left. + \frac{\partial a_6}{\partial q_j}\frac{\partial \theta_z'}{\partial q_i} + \frac{\partial a_7}{\partial q_j}\frac{\partial \theta_z''}{\partial q_i}\right)dz\right) \Delta q_j = Q_i - \int_l \left(a_1\frac{\partial u_o'}{\partial q_i} + a_2\frac{\partial v_o'}{\partial q_i}\right.$$
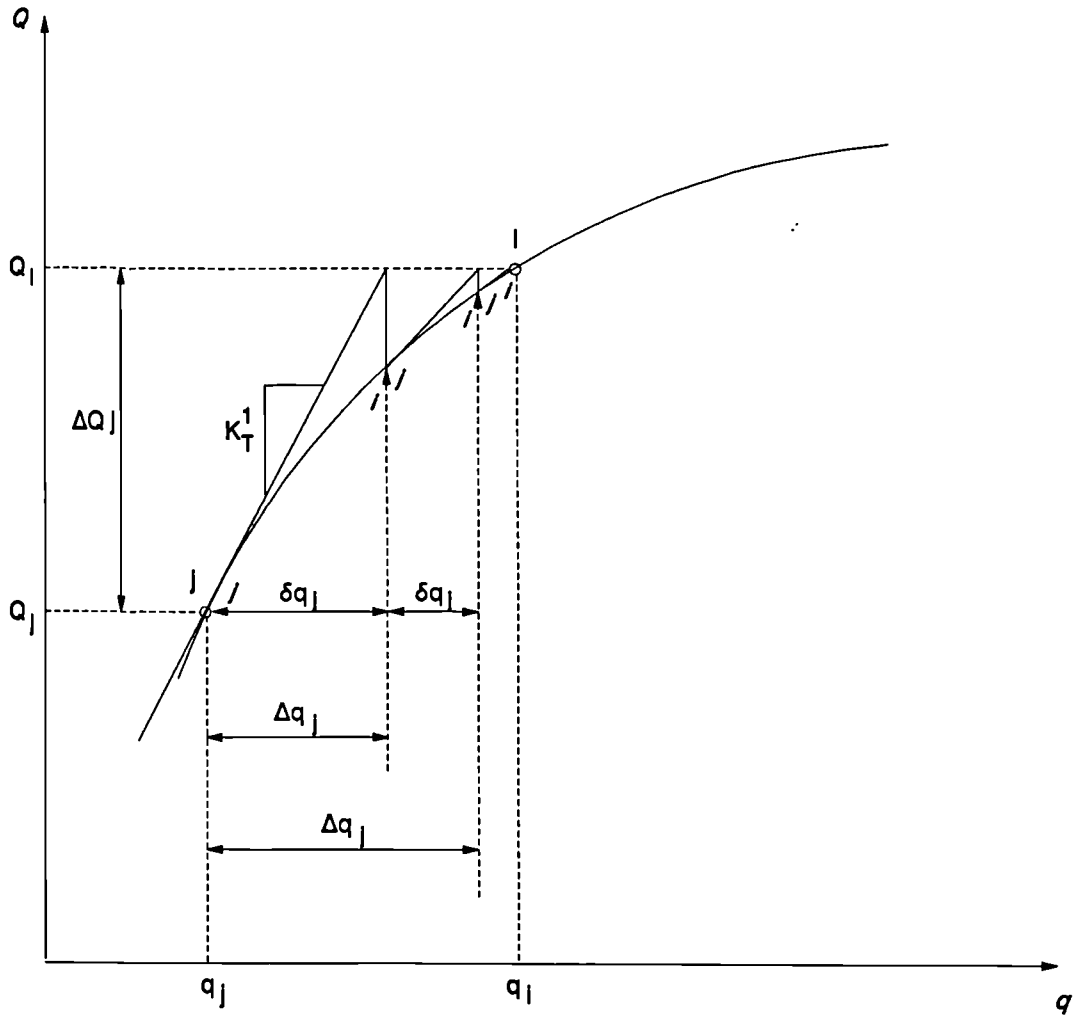
Fig. 3.4   Newton-Raphson Procedure

$$+a_3 \frac{\partial v_o^{''}}{\partial q_i} + a_4 \frac{\partial w_o'}{\partial q_i} + a_5 \frac{\partial w_o^{''}}{\partial q_i} + a_6 \frac{\partial \theta_z'}{\partial q_i} + a_7 \frac{\partial \theta_z^{''}}{\partial q_i}) dz \qquad (3.32)$$

Once the expressions for u_o, v_o, w_o, θ_z are defined in terms of $q's$, all terms of Eq. 3.32 may be evaluated by numerical integration. Eq. 3.32 is the basic Newton-Raphson equation that represents incremental equilibrium and can be written symbolically as:

$$[K_T]\{\Delta q\} = \{\Delta Q\} \qquad (3.33)$$

in which $[K_T]$ is the Jacobian in mathematical terms, or the element tangent stiffness matrix in structural terms, and is a function of geometric and material nonlinearities, $\{\Delta Q\}$ is the load vector of incremental (unbalanced) forces and $\{\Delta q\}$ is the vector of incremental displacements.

The great advantage of the virtual work method compared with other energy theorems such as minimisation principles is the fact that it is applicable to both elastic and inelastic material response. The use of minimum principles such as minimum potential energy requires special treatment to account for inelasticity.

The influence coefficient $(K_T)_{ij}$ in Eq. 3.33 is evaluated as:

$$(K_T)_{ij} = \int_l (\frac{\partial a_1}{\partial q_j} \frac{\partial u_o'}{\partial q_i} + \frac{\partial a_2}{\partial q_j} \frac{\partial v_o'}{\partial q_i} + \frac{\partial a_3}{\partial q_j} \frac{\partial v_o^{''}}{\partial q_i} + \frac{\partial a_4}{\partial q_j} \frac{\partial w_o'}{\partial q_i}$$

$$+ \frac{\partial a_5}{\partial q_j} \frac{\partial w_o^{''}}{\partial q_i} + \frac{\partial a_6}{\partial q_j} \frac{\partial \theta_z'}{\partial q_i} + \frac{\partial a_7}{\partial q_j} \frac{\partial \theta_z^{''}}{\partial q_i}) dz \qquad (3.34)$$

Eq. 3.34 can be rewritten as:

$$(K_T)_{ij} = \int_l (e_{1j} \frac{\partial u_o'}{\partial q_i} + e_{2j} \frac{\partial v_o'}{\partial q_i} + e_{3j} \frac{\partial v_o^{''}}{\partial q_i} + e_{4j} \frac{\partial w_o'}{\partial q_i} + e_{5j} \frac{\partial w_o^{''}}{\partial q_i}$$

$$+ e_{6j} \frac{\partial \theta_z'}{\partial q_i} + e_{7j} \frac{\partial \theta_z^{''}}{\partial q_i}) dz \qquad (3.35)$$

in which the values of e_{1j}, e_{2j}...etc. can be obtained by differentiating the values of a_1 to a_7 with respect to q_j to get :

$$e_{1j} = \frac{\partial n}{\partial q_j}(1 + u'_o) + n\frac{\partial u'_o}{\partial q_j} - \frac{\partial m_x}{\partial q_j}(v''_o) - m_x\frac{\partial v''_o}{\partial q_j} - \frac{\partial m_y}{\partial q_j}(w''_o)$$

$$- m_y\frac{\partial w''_o}{\partial q_j} + \frac{\partial m_\omega}{\partial q_j}(\theta''_z) + m_\omega\frac{\partial \theta''_z}{\partial q_j}$$

$$e_{2j} = \frac{\partial n}{\partial q_j}(v'_o) + n\frac{\partial v'_o}{\partial q_j} + \frac{\partial m_x}{\partial q_j}\left[\frac{v'_o}{\sqrt{1 - (v'_o)^2}}(\theta'_z w'_o - 2v''_o - \frac{(v'_o)^2 v''_o}{1 - (v'_o)^2})\right]$$

$$+ m_x\left[\frac{1}{\sqrt{1 - (v'_o)^2}}(\theta'_z w'_o - 2v''_o + \frac{(v'_o)^2 w'_o \theta'_z}{1 - (v'_o)^2} - \frac{5(v'_o)^2 v''_o}{1 - (v'_o)^2} - \frac{3(v'_o)^4 v''_o}{(1 - (v'_o)^2)^2})\frac{\partial v'_o}{\partial q_j}\right.$$

$$\left. - \frac{v'_o}{\sqrt{1 - (v'_o)^2}}(2 + \frac{(v'_o)^2}{1 - (v'_o)^2})\frac{\partial v''_o}{\partial q_j} + \frac{\theta'_z v'_o}{\sqrt{1 - (v'_o)^2}}\frac{\partial w'_o}{\partial q_j} + \frac{v'_o w'_o}{\sqrt{1 - (v'_o)^2}}\frac{\partial \theta'_z}{\partial q_j}\right]$$

$$+ \frac{\partial m_y}{\partial q_j}(\theta'_z\sqrt{1 - (w'_o)^2}) + m_y\left[\sqrt{1 - (w'_o)^2}\frac{\partial \theta'_z}{\partial q_j} - \frac{\theta'_z w'_o}{\sqrt{1 - (w'_o)^2}}\frac{\partial w'_o}{\partial q_j}\right]$$

$$+ \frac{\partial m_x^2}{\partial q_j}\left[v'_o(\frac{(v'_o)^2(v''_o)^2}{(1 - (v'_o)^2)^2} + \frac{(v''_o)^2}{1 - (v'_o)^2} - (\theta'_z)^2)\right]$$

$$+ m_x^2\left[\left(\frac{(v''_o)^2}{1 - (v'_o)^2}(1 + \frac{4(v'_o)^4}{(1 - (v'_o)^2)^2} + \frac{5(v'_o)^2}{1 - (v'_o)^2}) - (\theta'_z)^2\right)\frac{\partial v'_o}{\partial q_j}\right.$$

$$\left. + \left(\frac{2v'_o v''_o}{1 - (v'_o)^2}(1 + \frac{(v'_o)^2}{1 - (v'_o)^2})\right)\frac{\partial v''_o}{\partial q_j} - 2v'_o\theta'_z\frac{\partial \theta'_z}{\partial q_j}\right]$$

$$e_{3j} = -\frac{\partial m_x}{\partial q_j}(1 + u'_o) - m_x\frac{\partial u'_o}{\partial q_j} - \frac{\partial m_x}{\partial q_j}(\frac{(v'_o)^2}{\sqrt{1 - (v'_o)^2}})$$

$$- m_x\left[\frac{v'_o}{\sqrt{1 - (v'_o)^2}}(2 + \frac{(v'_o)^2}{1 - (v'_o)^2})\frac{\partial v'_o}{\partial q_j}\right] + \frac{\partial m_x^2}{\partial q_j}\left[v''_o(1 + \frac{(v'_o)^2}{1 - (v'_o)^2})\right]$$

$$+ m_x^2\left[(\frac{2v'_o v''_o}{1 - (v'_o)^2}(1 + \frac{(v'_o)^2}{1 - (v'_o)^2}))\frac{\partial v'_o}{\partial q_j} + (1 + \frac{(v'_o)^2}{1 - (v'_o)^2})\frac{\partial v''_o}{\partial q_j}\right]$$

$$e_{4j} = \frac{\partial n}{\partial q_j}(w'_o) + n\frac{\partial w'_o}{\partial q_j} - \frac{\partial m_x}{\partial q_j}(\theta'_z\sqrt{1 - (v'_o)^2})$$

$$- m_x \left[\sqrt{1-(v_o')^2} \frac{\partial \theta_z'}{\partial q_j} - \frac{\theta_z' v_o'}{\sqrt{1-(v_o')^2}} \frac{\partial v_o'}{\partial q_j} \right]$$

$$- \frac{\partial m_y}{\partial q_j} \left[\frac{w_o'}{\sqrt{1-(w_o')^2}} (\theta_z' v_o' + 2w_o'' + \frac{(w_o')^2 w_o''}{1-(w_o')^2}) \right]$$

$$- m_y \left[(\frac{1}{\sqrt{1-(w_o')^2}} (\theta_z' v_o' + 2w_o'' + \frac{(w_o')^2 v_o' \theta_z'}{1-(w_o')^2} + \frac{5(w_o')^2 w_o''}{1-(w_o')^2} - \frac{3(w_o')^4 w_o''}{(1-(w_o')^2)^2}) \frac{\partial w_o'}{\partial q_j} \right.$$

$$\left. + \frac{w_o'}{\sqrt{1-(w_o')^2}} (2 + \frac{(w_o')^2}{1-(w_o')^2}) \frac{\partial w_o''}{\partial q_j} + \frac{\theta_z' w_o'}{\sqrt{1-(w_o')^2}} \frac{\partial v_o'}{\partial q_j} + \frac{v_o' w_o'}{\sqrt{1-(w_o')^2}} \frac{\partial \theta_z'}{\partial q_j} \right]$$

$$+ \frac{\partial m_y^2}{\partial q_j} \left[w_o' (\frac{(w_o')^2 (w_o'')^2}{(1-(w_o')^2)^2} + \frac{(w_o'')^2}{1-(w_o')^2} - (\theta_z')^2) \right]$$

$$+ m_y^2 \left[\left(\frac{(w_o'')^2}{1-(w_o')^2} (1 + \frac{4(w_o')^4}{(1-(w_o')^2)^2} + \frac{5(w_o')^2}{1-(w_o')^2}) - (\theta_z')^2 \right) \frac{\partial w_o'}{\partial q_j} \right.$$

$$\left. + \left(\frac{2w_o' w_o''}{1-(w_o')^2} (1 + \frac{(w_o')^2}{1-(w_o')^2}) \right) \frac{\partial w_o''}{\partial q_j} - 2w_o' \theta_z' \frac{\partial \theta_z'}{\partial q_j} \right]$$

$$e_{5j} = -\frac{\partial m_y}{\partial q_j} (1 + u_o') - m_y \frac{\partial u_o'}{\partial q_j} - \frac{\partial m_y}{\partial q_j} (\frac{(w_o')^2}{\sqrt{1-(w_o')^2}})$$

$$- m_y \left[\frac{w_o'}{\sqrt{1-(w_o')^2}} (2 + \frac{(w_o')^2}{1-(w_o')^2}) \frac{\partial w_o'}{\partial q_j} \right] + \frac{\partial m_y^2}{\partial q_j} \left[w_o'' (1 + \frac{(w_o')^2}{1-(w_o')^2}) \right]$$

$$+ m_y^2 \left[(\frac{2w_o' w_o''}{1-(w_o')^2} (1 + \frac{(w_o')^2}{1-(w_o')^2})) \frac{\partial w_o'}{\partial q_j} + (1 + \frac{(w_o')^2}{1-(w_o')^2}) \frac{\partial w_o''}{\partial q_j} \right]$$

$$e_{6j} = -\frac{\partial m_x}{\partial q_j} (w_o' \sqrt{1-(v_o')^2}) + m_x \left[\frac{v_o' w_o'}{\sqrt{1-(v_o')^2}} \frac{\partial v_o'}{\partial q_j} - \sqrt{1-(v_o')^2} \frac{\partial w_o'}{\partial q_j} \right]$$

$$+ \frac{\partial m_y}{\partial q_j} (v_o' \sqrt{1-(w_o')^2}) + m_y \left[\sqrt{1-(w_o')^2} \frac{\partial v_o'}{\partial q_j} - \frac{v_o' w_o'}{\sqrt{1-(w_o')^2}} \frac{\partial w_o'}{\partial q_j} \right]$$

$$+ \frac{\partial m_x^2}{\partial q_j} \theta_z' (1 - (v_o')^2) + m_x^2 \left[(1 - (v_o')^2) \frac{\partial \theta_z'}{\partial q_j} - 2v_o' \theta_z' \frac{\partial v_o'}{\partial q_j} \right]$$

$$+ \ \frac{\partial m_y^2}{\partial q_j}\theta_z'(1-(w_o')^2) + m_y^2\left[(1-(w_o')^2)\frac{\partial \theta_z'}{\partial q_j} - 2w_o'\theta_z'\frac{\partial w_o'}{\partial q_j}\right] + GJ\frac{\partial \theta_z'}{\partial q_j}$$

$$e_{7j} \ = \ \frac{\partial m_\omega}{\partial q_j}(1+u_o') + m_\omega\frac{\partial u_o'}{\partial q_j} \qquad\qquad (3.36)$$

and the unbalanced load vector ΔQ_i is evaluated as:

$$\Delta Q_i = Q_i - \int_l (a_1\frac{\partial u_o'}{\partial q_i} + a_2\frac{\partial v_o'}{\partial q_i} + a_3\frac{\partial v_o''}{\partial q_i} \ + \ a_4\frac{\partial w_o'}{\partial q_i} + a_5\frac{\partial w_o''}{\partial q_i}$$

$$+ \ a_6\frac{\partial \theta_z'}{\partial q_i} + a_7\frac{\partial \theta_z''}{\partial q_i})dz \qquad (3.37)$$

To evaluate the vector of incremental forces $\{\Delta Q\}$ in Eq. 3.37 it is necessary to evaluate the stress resultants defined in Eq. 3.25 at any section.

3.3 Finite Element Model

In any stiffness approach, the solution is reached by solving the set of equilibrium equations for the unknown displacements. In standard stiffness analysis the number of unknowns is finite and confined to the nodal displacements. By deleting unknowns corresponding to the boundary conditions the equilibrium equation is readily solved. On the other hand, the finite element method requires the solution of integrals over the volume of each finite element. This implies the introduction of an infinite number of unknown displacements over that volume rendering the problem insoluble. The standard solution for this problem is to reduce the infinite number of unknown displacements to a finite number of unknown nodal displacements by using "shape functions". The role of these shape functions is to define the displacement state at any point over the volume of the finite element in terms of its nodal displacements. By assuming that displacements at any point are known if the nodal displacements are known, integrals over the volume of each element can
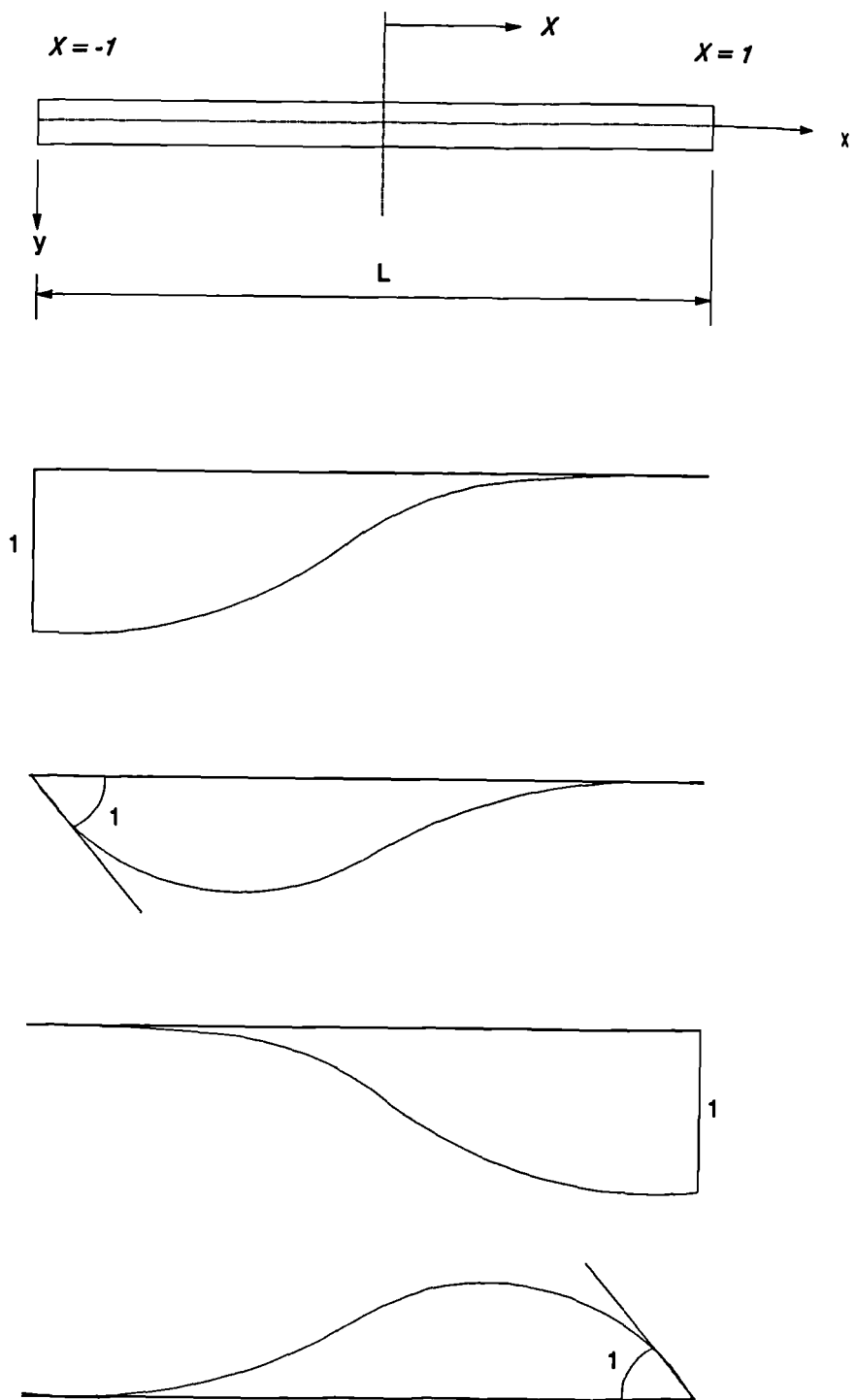
$$< \phi > = < 1/4\,(X + 2)\,(X - 1)^2, \quad L/8\,(X + 1)\,(X - 1)^2,$$
$$1/4\,(2 - X)\,(X + 1)^2, \quad L/8\,(X - 1)\,(X + 1)^2 >$$

Fig. 3.5   Cubic Shape Function

be solved in terms of the unknown nodal displacements. As a result the number of unknowns becomes equal to the number of equations and the problem becomes soluble. The finite element model used was based on an approximation of all the displacements by cubic shape functions. This allows the displacement vector to be calculated in the first instance, and then updated until equilibrium is satisfactorily reached.

In the following sections incremental displacements and forces will be calculated along with the tangent stiffness matrix. Incremental stress resultants arising in the stiffness matrix will also be calculated along with section properties.

3.3.1 Evaluation of Incremental Displacements

The displacements u_o, v_o, w_o, θ_z may be approximated in terms of the displacement coordinates $< q >$ of the incremental equilibrium equation (Eq. 3.33) as:

$$u_o = < \phi > \{\overline{u}\}$$

$$v_o = < \phi > \{\overline{v}\}$$

$$w_o = < \phi > \{\overline{w}\}$$

$$\theta_z = < \phi > \{\overline{\theta}_z\} \tag{3.38}$$

in which $\overline{u}$, $\overline{v}$, $\overline{w}$, $\overline{\theta}_z$ are the vectors of nodal displacements and ϕ is a standard cubic shape function (Fig.3.5). Vectors of nodal displacements are:

$$< \overline{u} > = < u_i, \quad (\frac{\partial u}{\partial z})_i, \quad u_j, \quad (\frac{\partial u}{\partial z})_j >$$

$$< \overline{v} > = < v_i, \quad (\theta_y)_i, \quad v_j, \quad (\theta_y)_j >$$

$$< \overline{w} > = < w_i, \quad (\theta_x)_i, \quad w_j, \quad (\theta_x)_j >$$

$$< \bar{\theta}_z > \quad = \quad < (\theta_z)_i, \quad (\theta_z')_i, \quad (\theta_z)_j, \quad (\theta_z')_j > \tag{3.39}$$

where i, j refer to node numbers at each element.

Differentiating Eq. 3.38:

$$u_o' \quad = \quad < \phi' > \quad \{\, \bar{u}\,\}$$

$$v_o' \quad = \quad < \phi' > \quad \{\, \bar{v}\,\}$$

$$v_o'' \quad = \quad < \phi'' > \quad \{\, \bar{v}\,\}$$

$$w_o' \quad = \quad < \phi' > \quad \{\, \bar{w}\,\}$$

$$w_o'' \quad = \quad < \phi'' > \quad \{\, \bar{w}\,\}$$

$$\theta_z' \quad = \quad < \phi' > \quad \{\, \bar{\theta}_z\,\}$$

$$\theta_z'' \quad = \quad < \phi'' > \quad \{\, \bar{\theta}_z\,\} \tag{3.40}$$

Differentiating Eq. 3.40 with respect to q_i results in:

$$\frac{\partial u_o'}{\partial q_i} \quad = \quad \phi_{qi}'$$

$$\frac{\partial v_o'}{\partial q_i} \quad = \quad \phi_{qi}'$$

$$\frac{\partial v_o''}{\partial q_i} \quad = \quad \phi_{qi}''$$

$$\frac{\partial w_o'}{\partial q_i} \quad = \quad \phi_{qi}'$$

$$\frac{\partial w_o''}{\partial q_i} \quad = \quad \phi_{qi}''$$

$$\frac{\partial \theta_z'}{\partial q_i} \quad = \quad \phi_{qi}'$$

$$\frac{\partial \theta_z''}{\partial q_i} \quad = \quad \phi_{qi}'' \tag{3.41}$$

$\{ Q_R \}$ can be evaluated by Gaussian integration as:

$$\left\{ Q_R \right\} = \sum_{i=1}^{n} \alpha_i \cdot \left\{ \begin{array}{c} a_1 \left\{ \phi' \right\} \\[2mm] a_2 \left\{ \phi' \right\} + a_3 \left\{ \phi'' \right\} \\[2mm] a_4 \left\{ \phi' \right\} + a_5 \left\{ \phi'' \right\} \\[2mm] a_6 \left\{ \phi' \right\} + a_7 \left\{ \phi'' \right\} \end{array} \right\}_i \tag{3.46}$$

where n is the total number of sampling points along the element, α_i is the weight-ing factor for the ith sampling point and a_1 to a_7 are calculated at the ith sampling point.

3.3.3 Evaluation of Element Stiffness Matrix [K_T]

The element stiffness matrix [K_T] is a (16 × 16) matrix.

Substitute Eq. 3.41 into Eq. 3.36 to get:

(a) *for* $i = 1$ *to* 4

$$(K_T)_{ij} = \int_l (e_{1j} \cdot \phi'_{qi}) \, dz$$

(b) *for* $i = 5$ *to* 8

$$(K_T)_{ij} = \int_l (e_{2j} \cdot \phi'_{qi} + e_{3j} \cdot \phi''_{qi}) \, dz$$

(c) *for* $i = 9$ *to* 12

$$(K_T)_{ij} = \int_l (e_{4j} \cdot \phi'_{qi} + e_{5j} \cdot \phi''_{qi}) \, dz$$

(d) *for* $i = 13$ *to* 16

$$(K_T)_{ij} = \int_l (e_{6j} \cdot \phi'_{qi} + e_{7j} \cdot \phi''_{qi}) \, dz \tag{3.47}$$

where e_{1j} *to* e_{7j} are defined in Eq. 3.36. Thus the j_{th} column of the stiffness matrix can be written as:

$$\{K_T\}_j = \int_l \left\{ \begin{array}{c} e_1 \; \{\phi'\} \\ e_2 \; \{\phi'\} \; + \; e_3 \; \{\phi''\} \\ e_4 \; \{\phi'\} \; + \; e_5 \; \{\phi''\} \\ e_6 \; \{\phi'\} \; + \; e_7 \; \{\phi''\} \end{array} \right\} \cdot dz \qquad (3.48)$$

and the full element stiffness matrix [K] as:

$$[K_T] = \int_l \left\{ \begin{array}{c} \{\phi'\} \; < e_1 > \\ \{\phi'\} \; < e_2 > \; + \; \{\phi''\} \; < e_3 > \\ \{\phi'\} \; < e_4 > \; + \; \{\phi''\} \; < e_5 > \\ \{\phi'\} \; < e_6 > \; + \; \{\phi''\} \; < e_7 > \end{array} \right\} \cdot dz \qquad (3.49)$$

or:

$$[K_T] = \left[\begin{array}{c} [K_1] \\ [K_2] \; + \; [K_3] \\ [K_4] \; + \; [K_5] \\ [K_6] \; + \; [K_7] \end{array} \right] \qquad (3.50)$$

in which [K_1] *to* [K_7] are (4 × 16) matrices and their values are:

$$[K_1] = \int_l (e_{1j} \; \phi'_{qi}) \; dz$$

$$= \int \phi' \left[(1 + u'_o) < \frac{\partial n}{\partial q} > -v''_o < \frac{\partial m_x}{\partial q} > -w''_o < \frac{\partial m_y}{\partial q} > +\theta''_z < \frac{\partial m_\omega}{\partial q} > \right.$$

$$\left. + \; n < \phi'_1 > -m_x < \phi''_2 > -m_y < \phi''_3 > +m_\omega < \phi''_4 > \right] \; dz$$

$$[K_2] = \int_l (e_{2j} \; \phi'_{qi}) \; dz$$

$$= \int \phi' \left[v'_o < \frac{\partial n}{\partial q} > + \left(\frac{v'_o}{\sqrt{1 - (v'_o)^2}} (\theta'_z w'_o - 2v''_o - \frac{(v'_o)^2 v''_o}{1 - (v'_o)^2}) \right) < \frac{\partial m_x}{\partial q} > \right.$$

$$+ \left(v_o'(\frac{(v_o'v_o'')^2}{(1-(v_o')^2)^2} + \frac{(v_o'')^2}{1-(v_o')^2} - (\theta_z')^2) \right) < \frac{\partial m_x^2}{\partial q} >$$

$$+ (\theta_z'\sqrt{1-(w_o')^2}) < \frac{\partial m_y}{\partial q} > +n < \phi_2' >$$

$$+ m_x \left(\frac{1}{\sqrt{1-(v_o')^2}}(\theta_z'w_o' - 2v_o'' + \frac{(v_o')^2 w_o'\theta_z'}{1-(v_o')^2} - \frac{5(v_o')^2 v_o''}{1-(v_o')^2} - \frac{3(v_o')^4 v_o''}{(1-(v_o')^2)^2}) < \phi_2' > \right.$$

$$- \frac{v_o'}{\sqrt{1-(v_o')^2}}(2 + \frac{(v_o')^2}{1-(v_o')^2}) < \phi_2'' > + \frac{v_o'\theta_z'}{\sqrt{1-(v_o')^2}} < \phi_3' >$$

$$\left. + \frac{v_o'w_o'}{\sqrt{1-(v_o')^2}} < \phi_4' > \right)$$

$$+ m_x^2 \left((\frac{(v_o'')^2}{1-(v_o')^2}(1 + \frac{4(v_o')^4}{(1-(v_o')^2)^2} + \frac{5(v_o')^2}{1-(v_o')^2}) - (\theta_z')^2) < \phi_2' > \right.$$

$$\left. + \left(\frac{2v_o'v_o''}{1-(v_o')^2}(1 + \frac{(v_o')^2}{1-(v_o')^2}) \right) < \phi_2'' > -2v_o'\theta_z' < \phi_4' > \right)$$

$$+ m_y \left. \left(\sqrt{1-(w_o')^2} < \phi_4' > -(\frac{w_o'\theta_z'}{\sqrt{1-(w_o')^2}}) < \phi_3' > \right) \right] dz$$

$$[K_3] = \int_l (e_{3j} \; \phi_{qi}') \; dz$$

$$= \int_l \phi'' \left[-\left((1 + u_o') + \frac{(v_o')^2}{\sqrt{1-(v_o')^2}} \right) < \frac{\partial m_x}{\partial q} > \right.$$

$$+ \left(v_o''(1 + \frac{(v_o')^2}{1-(v_o')^2}) \right) < \frac{\partial m_x^2}{\partial q} >$$

$$- m_x \left(< \phi_1' > + \left(\frac{v_o'}{\sqrt{1-(v_o')^2}}(2 + \frac{(v_o')^2}{1-(v_o')^2}) \right) < \phi_2' > \right)$$

$$+ m_x^2 \left. \left(\frac{2v_o'v_o''}{1-(v_o')^2}(1 + \frac{(v_o')^2}{1-(v_o')^2}) < \phi_2' > +(1 + \frac{(v_o')^2}{1-(v_o')^2}) < \phi_2'' > \right) \right] dz$$

$$[K_4] = \int_l (e_{4j} \; \phi_{qi}') \; dz$$

$$= \int_l \phi' \left[w'_o < \frac{\partial n}{\partial q} > - \left(\frac{w'_o}{\sqrt{1-(w'_o)^2}} (\theta'_z v'_o + 2w''_o + \frac{(w'_o)^2 w''_o}{1-(w'_o)^2}) \right) < \frac{\partial m_y}{\partial q} > \right.$$

$$+ \left(w'_o (\frac{(w'_o w''_o)^2}{(1-(w'_o)^2)^2} + \frac{(w''_o)^2}{1-(w'_o)^2} - (\theta'_z)^2) \right) < \frac{\partial m_y^2}{\partial q} >$$

$$- (\theta'_z \sqrt{1-(v'_o)^2}) < \frac{\partial m_x}{\partial q} >$$

$$+ n < \phi'_3 > -m_x \left(\sqrt{1-(v'_o)^2} < \phi'_4 > -(\frac{v'_o \theta'_z}{\sqrt{1-(v'_o)^2}}) < \phi'_2 > \right)$$

$$- m_y \left(\frac{1}{\sqrt{1-(w'_o)^2}} (\theta'_z v'_o + 2w''_o + \frac{(w'_o)^2 v'_o \theta'_z}{1-(w'_o)^2} + \frac{5(w'_o)^2 w''_o}{1-(w'_o)^2} + \frac{3(w'_o)^4 w''_o}{(1-(w'_o)^2)^2}) < \phi'_3 > \right.$$

$$+ \frac{w'_o}{\sqrt{1-(w'_o)^2}} (2 + \frac{(w'_o)^2}{1-(w'_o)^2}) < \phi''_3 > + \frac{w'_o \theta'_z}{\sqrt{1-(w'_o)^2}} < \phi'_2 >$$

$$+ \left. \frac{w'_o v'_o}{\sqrt{1-(w'_o)^2}} < \phi'_4 > \right)$$

$$+ m_y^2 \left((\frac{(w''_o)^2}{1-(w'_o)^2} (1 + \frac{4(w'_o)^4}{(1-(w'_o)^2)^2} + \frac{5(w'_o)^2}{1-(w'_o)^2}) - (\theta'_z)^2) < \phi'_3 > \right.$$

$$+ \left. \left. \frac{2w'_o w''_o}{1-(w'_o)^2} (1 + \frac{(w'_o)^2}{1-(w'_o)^2}) < \phi''_3 > -2w'_o \theta'_z < \phi'_4 > \right) \right] \, dz$$

$$[K_5] = \int_l (e_{5j} \, \phi'_{qi}) \, dz$$

$$= \int_l \phi'' \left[- \left((1+u'_o) + \frac{(w'_o)^2}{\sqrt{1-(w'_o)^2}} \right) < \frac{\partial m_y}{\partial q} > \right.$$

$$+ \left(w''_o (1 + \frac{(w'_o)^2}{1-(w'_o)^2}) \right) < \frac{\partial m_y^2}{\partial q} >$$

$$- m_y \left(< \phi'_1 > + \left(\frac{w'_o}{\sqrt{1-(w'_o)^2}} (2 + \frac{(w'_o)^2}{1-(w'_o)^2}) \right) < \phi'_3 > \right)$$

$$+ \left. m_y^2 \left(\frac{2w'_o w''_o}{1-(w'_o)^2} (1 + \frac{(w'_o)^2}{1-(w'_o)^2}) < \phi'_3 > +(1 + \frac{(w'_o)^2}{1-(w'_o)^2}) < \phi''_3 > \right) \right] \, dz$$

$$[K_6] \;=\; \int_l (e_{6j}\;\phi'_{qi})\;dz$$

$$= \int_l \phi'_{qi}\left[-w'_o\sqrt{1-(v'_o)^2} < \frac{\partial m_x}{\partial q} > +\theta'_z(1-(v'_o)^2) < \frac{\partial m_x^2}{\partial q} >\right.$$

$$+\; v'_o\sqrt{1-(w'_o)^2} < \frac{\partial m_y}{\partial q} > +\theta'_z(1-(w'_o)^2) < \frac{\partial m_y^2}{\partial q} >$$

$$+\; m_x\left(\frac{v'_o w'_o}{\sqrt{1-(v'_o)^2}} < \phi'_2 > -\sqrt{1-(v'_o)^2} < \phi'_3 >\right)$$

$$+\; m_y\left(\sqrt{1-(w'_o)^2} < \phi'_2 > -\frac{v'_o w'_o}{\sqrt{1-(w'_o)^2}} < \phi'_3 >\right)$$

$$+\; m_x^2\left((1-(v'_o)^2) < \phi'_4 > -2v'_o\theta'_z < \phi'_2 >\right)$$

$$+\; \left. m_y^2\left((1-(w'_o)^2) < \phi'_4 > -2w'_o\theta'_z < \phi'_3 >\right) + \theta'_z\frac{\partial GJ}{\partial q} + GJ < \phi'_3 >\right]\;dz$$

$$[K_7] \;=\; \int_l (e_{7j}\;\phi'_{qi})\;dz$$

$$= \int_l \phi''\left[(1+u'_o) < \frac{\partial m_\omega}{\partial q} > +m_\omega < \phi'_1 >\right]\;dz$$

$$(3.51)$$

The terms $< \phi'_1 >$, $< \phi'_2 >$, $< \phi''_2 >$, $< \phi'_3 >$, $< \phi''_3 >$, $< \phi'_4 >$, $< \phi''_4 >$ are 1×16 row vectors defined as:

$$< \phi'_1 > \;=\; << \phi' > : < 0 > : < 0 > : < 0 >>$$

$$< \phi'_2 > \;=\; << 0 > : < \phi' > : < 0 > : < 0 >>$$

$$< \phi''_2 > \;=\; << 0 > : < \phi'' > : < 0 > : < 0 >>$$

$$< \phi'_3 > \;=\; << 0 > : < 0 > : < \phi' > : < 0 >>$$

$$< \phi''_3 > \;=\; << 0 > : < 0 > : < \phi'' > : < 0 >>$$

$$' < \phi_4' > \; = \; << \; 0 \; > \; : \; < \; 0 \; > \; : \; < \; 0 \; > : \; < \phi' > >$$

$$< \phi_4'' > \; = \; << \; 0 \; > \; : \; < \; 0 \; > \; : \; < \; 0 \; > : \; < \phi'' > > \tag{3.52}$$

in which $< \phi' >$ and $< \phi'' >$ are the derivatives of the cubic shape function

vector. In the above equation the cubic shape function vectors are enlarged from

1 x 4 to 1 x 16 by adding extra zeros to facilitate matrix multiplication.

3.3.4 Evaluation of Stress Resultants

Using the relationship $\sigma_z = E_t \, \epsilon_z$, Eq. 3.26 can be rewritten in matrix form as:

$$
\begin{bmatrix} n \\ m_x \\ m_x^2 \\ m_y \\ m_y^2 \\ m_\omega \end{bmatrix}
=
\begin{bmatrix}
A & I_y & I_{y2} & I_x & I_{x2} & I_\omega \\
I_y & I_{y2} & I_{y3} & I_{xy} & I_{x2y} & I_{\omega y} \\
I_{y2} & I_{y3} & I_{y4} & I_{xy2} & I_{x2y2} & I_{\omega y2} \\
I_x & I_{xy} & I_{xy2} & I_{x2} & I_{x3} & I_{\omega x} \\
I_{x2} & I_{x2y} & I_{x2y2} & I_{x3} & I_{x4} & I_{\omega x2} \\
I_\omega & I_{\omega y} & I_{\omega y2} & I_{\omega x} & I_{\omega x2} & I_{\omega2}
\end{bmatrix}
\cdot
\begin{bmatrix} ED_1 \\ -ED_2 \\ \frac{E}{2}D_3 \\ -ED_4 \\ \frac{E}{2}D_5 \\ ED_6 \end{bmatrix}
\tag{3.53}
$$

in which the values D_1, D_2, .., D_7 can be found by rearranging Eq. 3.26 to get:

$$
\epsilon_z = \left[u_o' + \frac{1}{2}\left((u_o')^2 + (v_o')^2 + (w_o')^2 \right) \right]
$$

$$
- \; y \left[v_o'' + u_o' v_o'' + \theta_z' w_o' \sqrt{1 - (v_o')^2} + \frac{(v_o')^2 v_o''}{\sqrt{1 - (v_o')^2}} \right]
$$

$$
+ \; \frac{1}{2} y^2 \left[(v_o'')^2 + (\theta_z')^2 (1 - (v_o')^2) + \frac{(v_o' v_o'')^2}{1 - (v_o')^2} \right]
$$

$$
- \; x \left[w_o'' + u_o' w_o'' - \theta_z' v_o' \sqrt{1 - (w_o')^2} + \frac{(w_o')^2 w_o''}{\sqrt{1 - (w_o')^2}} \right]
$$

$$
+ \; \frac{1}{2} x^2 \left[(w_o'')^2 + \frac{(w_o' w_o'')^2}{1 - (w_o')^2} + (\theta_z')^2 (1 - (w_o')^2) \right]
$$

$$+ \quad \omega \left[\theta_z''(1 + u_o') \right] \qquad (3.54)$$

The values of D_1, D_2, ... D_7 are the terms in brackets in Eq. 3.54 in the order in which they appear in the equation, and section properties of Eq. 3.53 are defined in the next section.

Once the axial mechanical strain (ϵ_m) is calculated from Eq. 3.60, residual and thermal strains $(\epsilon_r$ and ϵ_θ respectively) are added algebraically to constitute the total strain ϵ:

$$\epsilon = \epsilon_m + \epsilon_r + \epsilon_\theta \qquad (3.55)$$

The incremental stress resultants in the terms e_{1j} to e_{7j} of Eq. 3.36 are evaluated by taking the variations of the stress resultants as follows:

$$\partial n = \int_A E_t \, \delta\epsilon \, dA$$

$$\partial m_x = \int_A E_t \, \delta\epsilon \, y \, dA$$

$$\partial m_x^2 = \int_A E_t \, \delta\epsilon \, y^2 \, dA$$

$$\partial m_y = \int_A E_t \, \delta\epsilon \, x \, dA$$

$$\partial m_y^2 = \int_A E_t \, \delta\epsilon \, x^2 \, dA$$

$$\partial m_\omega = \int_A E_t \, \delta\epsilon \, \omega \, dA \qquad (3.56)$$

using the relation $E_t.A = E.A_t$, "the transformed-section concept", Eq. 3.56 can be rewritten:

$$\frac{\partial n}{\partial q_j} = \int_{At} E \frac{\partial \epsilon}{\partial q_j} \, dA_t$$

$$\frac{\partial m_x}{\partial q_j} = \int_{At} E \frac{\partial \epsilon}{\partial q_j} \, y \, dA_t$$

$$\frac{\partial m_x^2}{\partial q_j} = \int_{At} E \frac{\partial \epsilon}{\partial q_j} \, y^2 \, dA_t$$

$$\frac{\partial m_y}{\partial q_j} = \int_{At} E \frac{\partial \epsilon}{\partial q_j} x \, dA_t$$

$$\frac{\partial m_y^2}{\partial q_j} = \int_{At} E \frac{\partial \epsilon}{\partial q_j} x^2 \, dA_t$$

$$\frac{\partial m_\omega}{\partial q_j} = \int_{At} E \frac{\partial \epsilon}{\partial q_j} \omega \, dA_t \tag{3.57}$$

The incremental stress resultants can be evaluated using Eq. 3.53 as:

$$\frac{\partial n}{\partial q_j} = E \, A \, b_{1j} - E \, I_y \, b_{2j} + \frac{E}{2} I_{y2} b_{3j} - E I_x b_{4j} + \frac{E}{2} I_{x2} b_{5j} + E I_\omega b_{6j}$$

$$\frac{\partial m_x}{\partial q_j} = E \, I_y \, b_{1j} - E \, I_{y2} \, b_{2j} + \frac{E}{2} I_{y3} b_{3j} - E I_{xy} b_{4j} + \frac{E}{2} I_{x2y} b_{5j} + E I_{\omega y} b_{6j}$$

$$\frac{\partial m_x^2}{\partial q_j} = E \, I_{y2} \, b_{1j} - E \, I_{y3} \, b_{2j} + \frac{E}{2} I_{y4} b_{3j} - E I_{xy2} b_{4j} + \frac{E}{2} I_{x2y2} b_{5j} + E I_{\omega y2} b_{6j}$$

$$\frac{\partial m_y}{\partial q_j} = E \, I_x \, b_{1j} - E \, I_{xy} \, b_{2j} + \frac{E}{2} I_{xy2} b_{3j} - E I_{x2} b_{4j} + \frac{E}{2} I_{x3} b_{5j} + E I_{\omega x} b_{6j}$$

$$\frac{\partial m_y^2}{\partial q_j} = E \, I_{x2} \, b_{1j} - E \, I_{x2y} \, b_{2j} + \frac{E}{2} I_{x2y2} b_{3j} - E I_{x3} b_{4j} + \frac{E}{2} I_{x4} b_{5j} + E I_{\omega x2} b_{6j}$$

$$\frac{\partial m_\omega}{\partial q_j} = E \, I_\omega \, b_{1j} - E \, I_{\omega y} \, b_{2j} + \frac{E}{2} I_{\omega y2} b_{3j} - E I_{\omega x} b_{4j} + \frac{E}{2} I_{\omega x2} b_{5j} + E I_{\omega 2} b_{6j}$$

$$\tag{3.58}$$

in which b_{1j} to b_{6j} are the derivatives of the terms D_1 to D_7 of Eq. 3.53 with respect to q_j, and all section properties are taken for the transformed section.

The values of the terms b_{1j} to b_{6j} are evaluated as:

$$b_{1j} = (1 + u_o') \frac{\partial u_o'}{\partial q_j} + v_o' \frac{\partial v_o'}{\partial q_j} + w_o' \frac{\partial w_o'}{\partial q_j}$$

$$b_{2j} = v_o'' \frac{\partial u_o'}{\partial q_j} + \left[\frac{v_o'}{\sqrt{1 - (v_o')^2}} (2v_o'' + \frac{(v_o')^2 v_o''}{1 - (v_o')^2} - \theta_z' w_o') \right] \frac{\partial v_o'}{\partial q_j}$$

$$+ \left[(1 + u_o') + \frac{(v_o')^2}{1 - (v_o')^2} \right] \frac{\partial v_o''}{\partial q_j} + \left[\theta_z' \sqrt{1 - (v_o')^2} \right] \frac{\partial w_o'}{\partial q_j}$$

$$+ \left[w_o' \sqrt{1 - (v_o')^2} \right] \frac{\partial \theta_z'}{\partial q_j}$$

$$b_{3j} = \left[2v_o'\left(\frac{(v_o'')^2}{1-(v_o')^2}(1+\frac{(v_o')^2}{1-(v_o')^2}) - (\theta_z')^2\right)\right]\frac{\partial v_o'}{\partial q_j}$$

$$+ \left[2v_o''(1+\frac{(v_o')^2}{1-(v_o')^2})\right]\frac{\partial v_o''}{\partial q_j} + \left[2\theta_z'(1-(v_o')^2)\right]\frac{\partial \theta_z'}{\partial q_j}$$

$$b_{4j} = w_o''\frac{\partial u_o'}{\partial q_j} + \left[\frac{w_o'}{\sqrt{1-(w_o')^2}}(2w_o'' + \frac{(w_o')^2 w_o''}{1-(v_o')^2} + \theta_z'v_o')\right]\frac{\partial w_o'}{\partial q_j}$$

$$+ \left[(1+u_o') + \frac{(w_o')^2}{1-(w_o')^2}\right]\frac{\partial w_o''}{\partial q_j} - \left[\theta_z'\sqrt{1-(w_o')^2}\right]\frac{\partial v_o'}{\partial q_j}$$

$$- \left[v_o'\sqrt{1-(w_o')^2}\right]\frac{\partial \theta_z'}{\partial q_j}$$

$$b_{5j} = \left[2w_o'\left(\frac{(w_o'')^2}{1-(w_o')^2}(1+\frac{(w_o')^2}{1-(w_o')^2}) - (\theta_z')^2\right)\right]\frac{\partial w_o'}{\partial q_j}$$

$$+ \left[2w_o''(1+\frac{(w_o')^2}{1-(w_o')^2})\right]\frac{\partial w_o''}{\partial q_j} + \left[2\theta_z'(1-(w_o')^2)\right]\frac{\partial \theta_z'}{\partial q_j}$$

$$b_{6j} = \theta_z''\frac{\partial u_o'}{\partial q_j} + [(1+u_o')]\frac{\partial \theta_z''}{\partial q_j} \tag{3.59}$$

For each Gauss point on the element u_o', v_o', v_o'', w_o', w_o'', θ_z', θ_z'' are evaluated from Eq. 3.38.

Substitute Eq. 3.59 into Eq. 3.58:

For j $=$ 1 *to* 4

$$\frac{\partial n}{\partial q_j} = \left[EA(1+u_o') - EI_y v_o'' - EI_x w_o'' + EI_\omega \theta_z''\right]\phi_{qj}'$$

$$\frac{\partial m_x}{\partial q_j} = \left[EI_y(1+u_o') - EI_{y2}v_o'' - EI_{xy}w_o'' + EI_{\omega y}\theta_z''\right]\phi_{qj}'$$

$$\frac{\partial m_x^2}{\partial q_j} = \left[EI_{y2}(1+u_o') - EI_{y3}v_o'' - EI_{xy2}w_o'' + EI_{\omega y2}\theta_z''\right]\phi_{qj}'$$

$$\frac{\partial m_y}{\partial q_j} = \left[EI_x(1+u_o') - EI_{xy}v_o'' - EI_{x2}w_o'' + EI_{\omega x}\theta_z''\right]\phi_{qj}'$$

$$\frac{\partial m_y^2}{\partial q_j} = \left[EI_{x2}(1+u_o') - EI_{x2y}v_o'' - EI_{x3}w_o'' + EI_{\omega x2}\theta_z''\right]\phi_{qj}'$$

$$\frac{\partial m_\omega}{\partial q_j} = \left[EI_\omega(1 + u_o') - EI_{\omega y}v_o'' - EI_{\omega x}w_o'' + EI_{\omega 2}\theta_z'' \right] \phi_{qj}'$$

For $j = 5$ to 8

$$\frac{\partial n}{\partial q_j} = \left[EA\, v_o' - EI_y \left[\frac{v_o'}{\sqrt{1 - (v_o')^2}}(2v_o'' + \frac{(v_o')^2 v_o''}{1 - (v_o')^2} - \theta_z'w_o') \right] \right.$$

$$+ \left. EI_{y2}\left\{ v_o' \left(\frac{(v_o'')^2}{1 - (v_o')^2}(1 + \frac{(v_o')^2}{1 - (v_o')^2}) - (\theta_z')^2 \right) \right\} + EI_x(\theta_z'\sqrt{1 - (w_o')^2} \right] \phi_{qj}'$$

$$+ \left[\frac{1}{2}EI_{y2}\left(2v_o''(1 + \frac{(v_o')^2}{1 - (v_o')^2}) \right) - EI_y \left((1 + u_o') + \frac{(v_o')^2}{\sqrt{1 - (v_o')^2}}) \right) \right] \phi_{qj}''$$

$$\frac{\partial m_x}{\partial q_j} = \left[EI_y\, v_o' - EI_{y2} \left[\frac{v_o'}{\sqrt{1 - (v_o')^2}}(2v_o'' + \frac{(v_o')^2 v_o''}{1 - (v_o')^2} - \theta_z'w_o') \right] \right.$$

$$+ \left. EI_{y3}\left\{ v_o' \left(\frac{(v_o'')^2}{1 - (v_o')^2}(1 + \frac{(v_o')^2}{1 - (v_o')^2}) - (\theta_z')^2 \right) \right\} + EI_{xy}(\theta_z'\sqrt{1 - (w_o')^2} \right] \phi_{qj}'$$

$$+ \left[\frac{1}{2}EI_{y3}\left(2v_o''(1 + \frac{(v_o')^2}{1 - (v_o')^2}) \right) - EI_{y2} \left((1 + u_o') + \frac{(v_o')^2}{\sqrt{1 - (v_o')^2}}) \right) \right] \phi_{qj}''$$

$$\frac{\partial m_x^2}{\partial q_j} = \left[EI_{y2}\, v_o' - EI_{y3} \left[\frac{v_o'}{\sqrt{1 - (v_o')^2}}(2v_o'' + \frac{(v_o')^2 v_o''}{1 - (v_o')^2} - \theta_z'w_o') \right] \right.$$

$$+ \left. EI_{y4}\left\{ v_o' \left(\frac{(v_o'')^2}{1 - (v_o')^2}(1 + \frac{(v_o')^2}{1 - (v_o')^2}) - (\theta_z')^2 \right) \right\} + EI_{xy2}(\theta_z'\sqrt{1 - (w_o')^2} \right] \phi_{qj}'$$

$$+ \left[\frac{1}{2}EI_{y4}\left(2v_o''(1 + \frac{(v_o')^2}{1 - (v_o')^2}) \right) - EI_{y3} \left((1 + u_o') + \frac{(v_o')^2}{\sqrt{1 - (v_o')^2}}) \right) \right] \phi_{qj}''$$

$$\frac{\partial m_y}{\partial q_j} = \left[EI_x\, v_o' - EI_{xy} \left[\frac{v_o'}{\sqrt{1 - (v_o')^2}}(2v_o'' + \frac{(v_o')^2 v_o''}{1 - (v_o')^2} - \theta_z'w_o') \right] \right.$$

$$+ \left. EI_{xy2}\left\{ v_o' \left(\frac{(v_o'')^2}{1 - (v_o')^2}(1 + \frac{(v_o')^2}{1 - (v_o')^2}) - (\theta_z')^2 \right) \right\} + EI_{x2}(\theta_z'\sqrt{1 - (w_o')^2} \right] \phi_{qj}'$$

$$+ \left[\frac{1}{2}EI_{xy2}\left(2v_o''(1 + \frac{(v_o')^2}{1 - (v_o')^2}) \right) - EI_{xy} \left((1 + u_o') + \frac{(v_o')^2}{\sqrt{1 - (v_o')^2}}) \right) \right] \phi_{qj}''$$

$$\frac{\partial m_y^2}{\partial q_j} = \left[EI_{x2}\, v_o' - EI_{x2y} \left[\frac{v_o'}{\sqrt{1-(v_o')^2}}(2v_o'' + \frac{(v_o')^2 v_o''}{1-(v_o')^2} - \theta_z' w_o') \right] \right.$$

$$+ \left. EI_{x2y2}\left\{ v_o'\left(\frac{(v_o'')^2}{1-(v_o')^2}(1 + \frac{(v_o')^2}{1-(v_o')^2}) - (\theta_z')^2 \right) \right\} + EI_{x3}(\theta_z'\sqrt{1-(w_o')^2} \right] \phi_{qj}'$$

$$+ \left[\frac{1}{2}EI_{x2y2}\left(2v_o''(1 + \frac{(v_o')^2}{1-(v_o')^2}) \right) - EI_{x2y}\left((1+u_o') + \frac{(v_o')^2}{\sqrt{1-(v_o')^2}} \right) \right] \phi_{qj}''$$

$$\frac{\partial m_\omega}{\partial q_j} = \left[EI_\omega\, v_o' - EI_{\omega y}\left[\frac{v_o'}{\sqrt{1-(v_o')^2}}(2v_o'' + \frac{(v_o')^2 v_o''}{1-(v_o')^2} - \theta_z' w_o') \right] \right.$$

$$+ \left. EI_{\omega y2}\left\{ v_o'\left(\frac{(v_o'')^2}{1-(v_o')^2}(1 + \frac{(v_o')^2}{1-(v_o')^2}) - (\theta_z')^2 \right) \right\} + EI_{\omega x}(\theta_z'\sqrt{1-(w_o')^2} \right] \phi_{qj}'$$

$$+ \left[\frac{1}{2}EI_{\omega y2}\left(2v_o''(1 + \frac{(v_o')^2}{1-(v_o')^2}) \right) - EI_{\omega y}\left((1+u_o') + \frac{(v_o')^2}{\sqrt{1-(v_o')^2}} \right) \right] \phi_{qj}''$$

For $j = 9$ to 12

$$\frac{\partial n}{\partial q_j} = \left[EAw_o' - EI_y(\theta_z'\sqrt{1-(v_o')^2}) - EI_x\frac{w_o'}{\sqrt{1-(w_o')^2}}(2w_o'' + \theta_z'v_o' + \frac{(w_o')^2 w_o''}{1-(w_o')^2}) \right.$$

$$+ \left. EI_{x2}\left(w_o'(\frac{(w_o'')^2}{1-(w_o')^2}(1 + \frac{(w_o')^2}{1-(w_o')^2}) - (\theta_z')^2) \right) \right] \phi_{qj}'$$

$$+ \left[EI_{x2}\left(w_o''(1 + \frac{(w_o')^2}{1-(w_o')^2}) \right) - EI_x\left((1+u_o') + \frac{(w_o')^2}{\sqrt{1-(w_o')^2}} \right) \right] \phi_{qj}''$$

$$\frac{\partial m_x}{\partial q_j} = \left[EI_y w_o' - EI_{y2}(\theta_z'\sqrt{1-(v_o')^2}) - EI_{xy}\frac{w_o'}{\sqrt{1-(w_o')^2}}(2w_o'' + \theta_z'v_o' + \frac{(w_o')^2 w_o''}{1-(w_o')^2}) \right.$$

$$+ \left. EI_{x2y}\left(w_o'(\frac{(w_o'')^2}{1-(w_o')^2}(1 + \frac{(w_o')^2}{1-(w_o')^2}) - (\theta_z')^2) \right) \right] \phi_{qj}'$$

$$+ \left[EI_{x2y}\left(w_o''(1 + \frac{(w_o')^2}{1-(w_o')^2}) \right) - EI_{xy}\left((1+u_o') + \frac{(w_o')^2}{\sqrt{1-(w_o')^2}} \right) \right] \phi_{qj}''$$

$$\frac{\partial m_x^2}{\partial q_j} = \left[EI_{y2}w_o' - EI_{y3}(\theta_z'\sqrt{1-(v_o')^2}) - EI_{xy2}\frac{w_o'}{\sqrt{1-(w_o')^2}}(2w_o'' + \theta_z'v_o' + \frac{(w_o')^2 w_o''}{1-(w_o')^2}) \right.$$

$$+ \quad EI_{x2y2}\left(w_o'(\frac{(w_o'')^2}{1-(w_o')^2}(1+\frac{(w_o')^2}{1-(w_o')^2})-(\theta_z')^2)\right)\Big]\phi_{qj}'$$

$$+ \quad \left[EI_{x2y2}\left(w_o''(1+\frac{(w_o')^2}{1-(w_o')^2})\right) - EI_{xy2}\left((1+u_o')+\frac{(w_o')^2}{\sqrt{1-(w_o')^2}}\right)\right]\phi_{qj}''$$

$$\frac{\partial m_y}{\partial q_j} = \left[EI_x w_o' - EI_{xy}(\theta_z'\sqrt{1-(v_o')^2}) - EI_{x3}\frac{w_o'}{\sqrt{1-(w_o')^2}}(2w_o''+\theta_z'v_o'+\frac{(w_o')^2 w_o''}{1-(w_o')^2})\right.$$

$$+ \quad EI_{x3}\left(w_o'(\frac{(w_o'')^2}{1-(w_o')^2}(1+\frac{(w_o')^2}{1-(w_o')^2})-(\theta_z')^2)\right)\Big]\phi_{qj}'$$

$$+ \quad \left[EI_{x3}\left(w_o''(1+\frac{(w_o')^2}{1-(w_o')^2})\right) - EI_{x2}\left((1+u_o')+\frac{(w_o')^2}{\sqrt{1-(w_o')^2}}\right)\right]\phi_{qj}''$$

$$\frac{\partial m_y^2}{\partial q_j} = \left[EI_{x2}w_o' - EI_{x2y}(\theta_z'\sqrt{1-(v_o')^2}) - EI_{x3}\frac{w_o'}{\sqrt{1-(w_o')^2}}(2w_o''+\theta_z'v_o'+\frac{(w_o')^2 w_o''}{1-(w_o')^2})\right.$$

$$+ \quad EI_{x4}\left(w_o'(\frac{(w_o'')^2}{1-(w_o')^2}(1+\frac{(w_o')^2}{1-(w_o')^2})-(\theta_z')^2)\right)\Big]\phi_{qj}'$$

$$+ \quad \left[EI_{x4}\left(w_o''(1+\frac{(w_o')^2}{1-(w_o')^2})\right) - EI_{x3}\left((1+u_o')+\frac{(w_o')^2}{\sqrt{1-(w_o')^2}}\right)\right]\phi_{qj}''$$

$$\frac{\partial m_\omega}{\partial q_j} = \left[EI_\omega w_o' - EI_{\omega y}(\theta_z'\sqrt{1-(v_o')^2}) - EI_{\omega x}\frac{w_o'}{\sqrt{1-(w_o')^2}}(2w_o''+\theta_z'v_o'+\frac{(w_o')^2 w_o''}{1-(w_o')^2})\right.$$

$$+ \quad EI_{\omega x2}\left(w_o'(\frac{(w_o'')^2}{1-(w_o')^2}(1+\frac{(w_o')^2}{1-(w_o')^2})-(\theta_z')^2)\right)\Big]\phi_{qj}'$$

$$+ \quad \left[EI_{\omega x2}\left(w_o''(1+\frac{(w_o')^2}{1-(w_o')^2})\right) - EI_{\omega x}\left((1+u_o')+\frac{(w_o')^2}{\sqrt{1-(w_o')^2}}\right)\right]\phi_{qj}''$$

For $j = 13$ to 16

$$\frac{\partial n}{\partial q_j} = \left[-EI_y w_o'\sqrt{1-(v_o')^2} + EI_{y2}\,\theta_z'(1-(v_o')^2) + EI_x v_o'\sqrt{1-(w_o')^2}\right.$$

$$+ \quad EI_{x2}\,\theta_z'(1-(w_o')^2)\Big]\phi_{qj}' + [EI_\omega(1+u_o')]\phi_{qj}''$$

$$\frac{\partial m_x}{\partial q_j} = \left[-EI_{y2}w_o'\sqrt{1-(v_o')^2} + EI_{y3}\,\theta_z'(1-(v_o')^2) + EI_{xy}v_o'\sqrt{1-(w_o')^2}\right.$$

$$\left. + \; EI_{x2y}\,\theta_z'(1-(w_o')^2)\right]\phi_{qj}' + [EI_{\omega y}(1+u_o')]\,\phi_{qj}''$$

$$\frac{\partial m_x^2}{\partial q_j} = \left[-EI_{y3}w_o'\sqrt{1-(v_o')^2} + EI_{y4}\,\theta_z'(1-(v_o')^2) + EI_{xy2}v_o'\sqrt{1-(w_o')^2}\right.$$

$$\left. + \; EI_{x2y2}\,\theta_z'(1-(w_o')^2)\right]\phi_{qj}' + [EI_{\omega y2}(1+u_o')]\,\phi_{qj}''$$

$$\frac{\partial m_y^2}{\partial q_j} = \left[-EI_{x2y}w_o'\sqrt{1-(v_o')^2} + EI_{x2y2}\,\theta_z'(1-(v_o')^2) + EI_{x3}v_o'\sqrt{1-(w_o')^2}\right.$$

$$\left. + \; EI_{x4}\,\theta_z'(1-(w_o')^2)\right]\phi_{qj}' + [EI_{\omega x2}(1+u_o')]\,\phi_{qj}''$$

$$\frac{\partial m_y}{\partial q_j} = \left[-EI_{xy}w_o'\sqrt{1-(v_o')^2} + EI_{xy2}\,\theta_z'(1-(v_o')^2) + EI_{x2}v_o'\sqrt{1-(w_o')^2}\right.$$

$$\left. + \; EI_{x3}\,\theta_z'(1-(w_o')^2)\right]\phi_{qj}' + [EI_{\omega x}(1+u_o')]\,\phi_{qj}''$$

$$\frac{\partial m_\omega}{\partial q_j} = \left[-EI_{\omega y}w_o'\sqrt{1-(v_o')^2} + EI_{\omega y2}\,\theta_z'(1-(v_o')^2) + EI_{\omega x}v_o'\sqrt{1-(w_o')^2}\right.$$

$$\left. + \; EI_{\omega x2}\,\theta_z'(1-(w_o')^2)\right]\phi_{qj}' + [EI_{\omega 2}(1+u_o')]\,\phi_{qj}'' \tag{3.60}$$

3.3.5 Evaluation of Section Properties

If a section undergoes biaxial loading, the equivalent section can be determined according to the strain distribution over each plate of that section. Section properties are defined as:

$$A = \int_A dA$$

$$I_y = \int_A y \,.dA$$

$$I_{y2} = \int_A y^2 \,.dA$$

$$I_{y3} = \int_A y^3 \,.dA$$

$$I_{y4} = \int_A y^4 \,.dA$$

$$I_x = \int_A x \,.dA$$

$$I_{x2} = \int_A x^2 \,.dA$$

$$I_{x3} = \int_A x^3 \,.dA$$

$$I_{x4} = \int_A x^4 \,.dA$$

$$I_{xy} = \int_A x \,.\, y \,.dA$$

$$I_{x2y} = \int_A x^2 \,.\, y \,.dA$$

$$I_{xy2} = \int_A x \,.\, y^2 \,.dA$$

$$I_{x2y2} = \int_A x^2 \,.\, y^2 \,.dA$$

$$I_{x3y} = \int_A x^3 \,.\, y \,.dA$$

$$I_{xy3} = \int_A x \,.\, y^3 \,.dA$$

$$I_\omega = \int_A \omega \,.dA$$

$$I_{\omega x} = \int_A \omega \,.\, x \,.dA$$

$$I_{\omega y} = \int_A \omega \,.\, y \,.dA$$

$$I_{\omega x2} = \int_A \omega \,.\, x^2 \,.dA$$

$$I_{\omega y2} = \int_A \omega \,.\, y^2 \,.dA$$

$$I_{\omega 2} = \int_A \omega^2 \,.dA \tag{3.61}$$

If the thickness of each segment of the plate is transformed according to the relation $E_t \, A = E_{20} \, A_t$, the section becomes an equivalent elastic section at ambient temperature.

$$A = \int dA = \sum_{k=1}^{n} A_k$$

$$I_y = \int Y \,.\, dA = \int (y + D_y) \,.\, dA$$

$$= \sum_{k=1}^{n} A_k \,.\, D_y$$

$$I_y^2 = \int Y^2 \cdot dA = \int (y + D_y)^2 \cdot dA$$

$$= \sum_{k=1}^{n} I_{xx} + \sum_{k=1}^{n} A_k \cdot D_y^2$$

$$I_y^3 = \int Y^3 \cdot dA = \int (y + D_y)^3 \cdot dA$$

$$= \int y^3 . dA + 3D_y \int y^2 . dA + 3D_y^2 \int y . dA + \int D_y^3 . dA$$

$$= \sum_{k=1}^{n} 3 I_{xx} \cdot D_y + \sum_{k=1}^{n} A_k \cdot D_y^3$$

$$I_y^4 = \int Y^4 \cdot dA = \int (y + D_y)^4 \cdot dA$$

$$= \int y^4 . dA + 4D_y \int y^3 . dA + 6D_y^2 \int y^2 . dA + 4D_y^3 \int y . dA + \int D_y^4 . dA$$

$$= \sum_{k=1}^{n} I_{4xx} + \sum_{k=1}^{n} 6 I_{xx} \cdot D_y^2 + \sum_{k=1}^{n} A_k \cdot D_y^4$$

where $I_{4xx} = \frac{bh^5}{80}$ for each segment.

In the same way:

$$I_x = \sum_{k=1}^{n} A_k \cdot D_x$$

$$I_x^2 = \sum_{k=1}^{n} I_{yy} + \sum_{k=1}^{n} A_k \cdot D_x^2$$

$$I_x^3 = \sum_{k=1}^{n} 3 I_{yy} \cdot D_x + \sum_{k=1}^{n} A_k \cdot D_x^3$$

$$I_x^4 = \sum_{k=1}^{n} I_{4yy} + \sum_{k=1}^{n} 6 I_{yy} \cdot D_x^2 + \sum_{k=1}^{n} A_k \cdot D_x^4$$

$$I_{xy} = \int X.Y.dA = \int (x + D_x)(y + D_y) \cdot dA$$

$$= \int x.y.dA + D_x.D_y \int dA + D_x \int y.dA + D_y \int x.dA$$

$$= \sum_{k=1}^{n} D_x \cdot D_y \cdot A_k$$

$$I_{x2y} = \int X^2.Y.dA = \int (x + D_x)^2 (y + D_y) \, . \, dA$$

$$= \int x^2.y.dA + 2D_x \int x.y.dA + D_x^2 \int y.dA + 2D_x D_y \int x.dA$$

$$+ D_y \int x^2 + D_x^2 D_y \int dA$$

$$= \sum_{k=1}^{n} I_{yy} \, . \, D_y + \sum_{k=1}^{n} D_x^2 \, . \, D_y \, . \, A_k$$

$$I_{xy2} = \int X.Y^2.dA = \int (x + D_x)(y + D_y)^2 \, . \, dA$$

$$= \int x.y^2.dA + 2D_y \int x.y.dA + D_y^2 \int x.dA + 2D_x D_y \int y.dA$$

$$+ D_x \int y^2 + D_x D_y^2 \int dA$$

$$= \sum_{k=1}^{n} I_{xx} \, . \, D_x + \sum_{k=1}^{n} D_x \, . \, D_y^2 \, . \, A_k$$

$$I_{x2y2} = \int X^2.Y^2.dA = \int (x + D_x)^2 (y + D_y)^2 \, . \, dA$$

$$= \int x^2.y^2.dA + 2D_x \int x.y^2.dA + 2D_y \int x^2.y.dA + D_x^2 \int y^2.dA$$

$$+ D_y^2 \int x^2.dA + 4D_x D_y \int x.y.dA + 2D_x D_y^2 \int x.dA$$

$$+ D_x^2 D_y^2 \int dA + D_x^2 D_y^2 \int dA$$

$$= \sum_{k=1}^{n} I_{xx} \, . \, D_x^2 + \sum_{k=1}^{n} I_{yy} \, . \, D_y^2 + \sum_{k=1}^{n} D_x^2 \, . \, D_y^2 \, . \, A_k + \sum_{k=1}^{n} \frac{t^3 l^3}{144}$$

$$I_\omega = \int \omega.dA$$

$$= \sum_{k=1}^{n} \sum_{r=1}^{5} \frac{bt}{2} (\omega_{ir} + \omega_{jr})$$

$$I_{\omega y} = \int \omega.Y.dA$$

$$= \sum_{k=1}^{n} \sum_{r=1}^{5} \frac{bt}{6} \left[\omega_{ir}(y_{jr} + 2y_{ir}) + \omega_{jr}(y_{ir} + 2y_{jr}) \right]$$

$$I_{\omega y2} = \int \omega . Y^2 . dA$$

$$= \sum_{k=1}^{n} \sum_{r=1}^{5} \frac{bt}{12} \left[\omega_{ir}(4y_{ir}^2 + 2y_{jr}^2 - l^2) + \omega_{jr}(4y_{jr}^2 + 2y_{ir}^2 - l^2) \right]$$

$$I_{\omega x} = \int \omega . X . dA$$

$$= \sum_{k=1}^{n} \sum_{r=1}^{5} \frac{bt}{6} \left[\omega_{ir}(x_{jr} + 2x_{ir}) + \omega_{jr}(x_{ir} + 2x_{jr}) \right]$$

$$I_{\omega x2} = \int \omega . X^2 . dA$$

$$= \sum_{k=1}^{n} \sum_{r=1}^{5} \frac{bt}{12} \left[\omega_{ir}(4x_{ir}^2 + 2x_{jr}^2 - l^2) + \omega_{jr}(4x_{jr}^2 + 2x_{ir}^2 - l^2) \right]$$

$$I_{\omega2} = \int \omega^2 . dA$$

$$= \sum_{k=1}^{n} \sum_{r=1}^{5} \frac{bt}{3} \left[\omega_{ir}^2 + \omega_{jr}\omega_{ir} + \omega_{jr}^2 \right]$$

$$(3.62)$$

where all calculations are based on the transformed section.

3.4 Transformation and Assembly

Once the equilibrium equation $[K_T] \{ q \} = \{ Q \}$ is derived for a finite element in its local coordinate system, it is a matter of using the concept of transformation from local to global coordinates to allow solution for three-dimensional framed structures. The local displacements $\{ q \}$ can be related to the displacements in the global coordinate system $\{ r \}$ by the transformation:

$$\{ q \}_L = [T] \{ r \}_G \qquad\qquad (3.63)$$

in which $[T]$ is the transformation matrix. Eq. 3.63 can be rearranged as:

$$< q >_L = < r >_G [T]^T \qquad\qquad (3.64)$$

If $\{ R \}_G$ is the vector of nodal forces in the global system associated with $\{ r \}_G$, then it can be shown that:

$$< q >_L \{ Q \}_L = < r >_G \{ R \}_G \qquad\qquad (3.65)$$

Substituting Eq. 3.64 into Eq. 3.65 results in:

$$< r >_G [T]^T \{ Q \}_L = < r >_G \{ R \}_G \qquad\qquad (3.66)$$

Or:

$$< r >_G \{ [T]^T \{ Q \}_L - \{ R \}_G \} = 0 \qquad\qquad (3.67)$$

which implies:

$$\{ R \}_G = [T]^T \{ Q \}_L \qquad\qquad (3.68)$$

Multiply the equilibrium equation $[K_T]_L \{ q \}_L = \{ Q \}_L$ by $[T]^T$ to get:

$$[T]^T [K_T]_L \{ q \}_L = [T]^T \{ Q \}_L \qquad\qquad (3.69)$$

Subtitute Eqs. 3.63 and 3.68 into Eq. 3.69 to get:

$$[T]^T [K_T]_L [T] \{ r \}_G = \{ R \}_G \qquad\qquad (3.70)$$

Or:

$$[K_T]_G \; \{ r \}_G \; = \; \{ R \}_G \tag{3.71}$$

in which:

$$[K_T]_G \; = \; [T]^T \; [K] \; [T] \tag{3.72}$$

in which $[K_T]_G$ is the stiffness matrix in the global system, and $\{ r \}_G$ and $\{ R \}_G$ are respectively displacements and forces also in the global system.

Once Eq. 3.71 is reached, which is the equilibrium equation for a finite element in the global system of coordinates, the structure's equilibrium equation:

$$[K_T]_{st} \; \{ r \}_{st} \; = \; \{ R \}_{st} \tag{3.73}$$

can be assembled directly and solved for the structure's unknown displacements.

3.4.0.1   Large Deformation Transformation

An element located in space needs to be catered for in order to make the *program* capable of space frame analysis. Each element positioned in space is defined by seven parameters. These parameters are the x, y, and z coordinates for both nodes of the finite element, along with the local rotation angle γ of the principal axes of the section about the local reference axis. This arrangement allows derivation for a section with a fixed orientation yet allowing the user to input any initial rotation of the section's principal axes.

Referring to Fig. 3.6, the relationship between the reference axes in local and
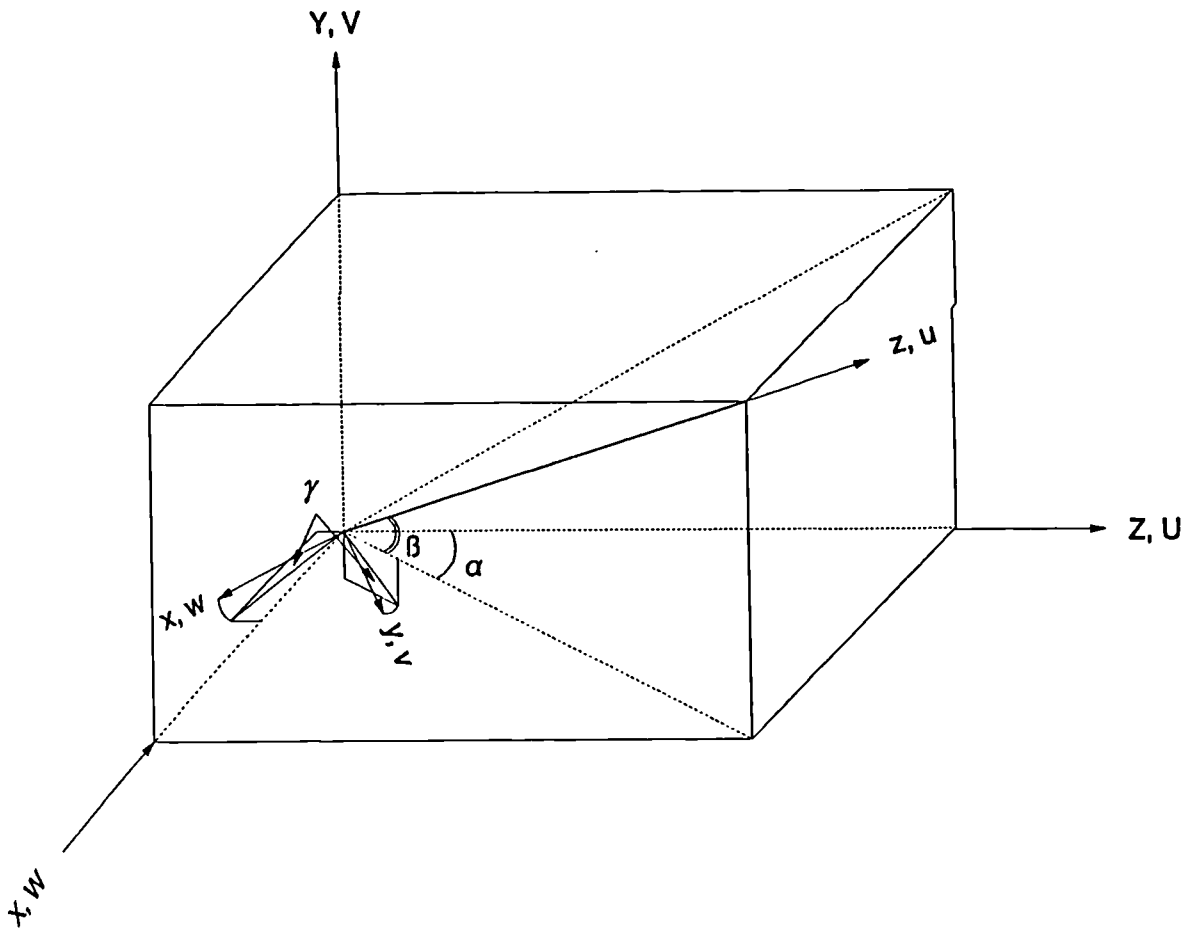
Fig. 3.6   Coordinate Transformation of an Element in Space

global coordinate systems can be expressed as:

$$Z = z.cos\beta.cos\alpha + y(cos\gamma.sin\beta.cos\alpha - sin\gamma.sin\alpha)$$

$$-x(cos\gamma.sin\alpha + sin\gamma.sin\beta.cos\alpha)$$

$$Y = z.sin\beta - y.cos\gamma.cos\beta + x.sin\gamma.cos\beta)$$

$$X = -z.cos\beta.sin\alpha - y(cos\gamma.sin\beta.sin\alpha + sin\gamma.cos\alpha)$$

$$-x(cos\gamma.cos\alpha - sin\gamma.sin\beta.sin\alpha)$$

$$(3.74)$$

While the relationship between the local displacements u, v, w and the global displacements U, V, W are:

$$u = U.cos\alpha.cos\beta + V.sin\beta - W.sin\alpha.cos\beta$$

$$v = U(cos\alpha.sin\beta.cos\gamma - sin\alpha.sin\gamma) - V.cos\beta.cos\gamma$$

$$-W(sin\alpha.sin\beta.cos\gamma + cos\alpha.sin\gamma)$$

$$w = -U(sin\alpha.cos\gamma + cos\alpha.sin\beta.sin\gamma) + V.cos\beta.sin\gamma$$

$$-W(cos\alpha.cos\gamma - sin\alpha.sin\beta.sin\gamma)$$

$$(3.75)$$

in which u, v, and w are functions of z, y and x.

If Eq. 3.75 is differentiated with respect to z then:

$$\frac{\partial u}{\partial z} = \frac{\partial U}{\partial Z}\frac{\partial Z}{\partial z}cos\alpha.cos\beta + \frac{\partial V}{\partial Z}\frac{\partial Z}{\partial z}.sin\beta - \frac{\partial W}{\partial Z}\frac{\partial Z}{\partial z}.sin\alpha.cos\beta$$

$$+ \frac{\partial U}{\partial Y}\frac{\partial Y}{\partial z}cos\alpha.cos\beta + \frac{\partial V}{\partial Y}\frac{\partial Y}{\partial z}.sin\beta - \frac{\partial W}{\partial Y}\frac{\partial Y}{\partial z}.sin\alpha.cos\beta$$

$$+ \frac{\partial U}{\partial X}\frac{\partial X}{\partial z}cos\alpha.cos\beta + \frac{\partial V}{\partial X}\frac{\partial X}{\partial z}.sin\beta - \frac{\partial W}{\partial X}\frac{\partial X}{\partial z}.sin\alpha.cos\beta$$

$$\frac{\partial v}{\partial z} = \frac{\partial U}{\partial Z}\frac{\partial Z}{\partial z}A - \frac{\partial V}{\partial Z}\frac{\partial Z}{\partial z}.cos\beta.cos\gamma - \frac{\partial W}{\partial Z}\frac{\partial Z}{\partial z}.B$$

$$+ \frac{\partial U}{\partial Y}\frac{\partial Y}{\partial z}A - \frac{\partial V}{\partial Y}\frac{\partial Y}{\partial z}.cos\beta.cos\gamma - \frac{\partial W}{\partial Y}\frac{\partial Y}{\partial z}.B$$

$$\frac{\partial w}{\partial z} = \begin{aligned} & + \frac{\partial U}{\partial X}\frac{\partial X}{\partial z}A - \frac{\partial V}{\partial X}\frac{\partial X}{\partial z}.cos\beta.cos\gamma - \frac{\partial W}{\partial X}\frac{\partial X}{\partial z}.B \\ & -\frac{\partial U}{\partial Z}\frac{\partial Z}{\partial z}C + \frac{\partial V}{\partial Z}\frac{\partial Z}{\partial z}.cos\beta.sin\gamma - \frac{\partial W}{\partial Z}\frac{\partial Z}{\partial z}.D \\ & -\frac{\partial U}{\partial Y}\frac{\partial Y}{\partial z}C + \frac{\partial V}{\partial Y}\frac{\partial Y}{\partial z}.cos\beta.sin\gamma - \frac{\partial W}{\partial Y}\frac{\partial Y}{\partial z}.D \\ & -\frac{\partial U}{\partial X}\frac{\partial X}{\partial z}C + \frac{\partial V}{\partial X}\frac{\partial X}{\partial z}.cos\beta.sin\gamma - \frac{\partial W}{\partial X}\frac{\partial X}{\partial z}.D \end{aligned} \qquad (3.76)$$

Differentiate Eq. 3.74 to get:

$$\frac{\partial Z}{\partial z} = cos\alpha.cos\beta$$

$$\frac{\partial Y}{\partial z} = sin\beta$$

$$\frac{\partial X}{\partial z} = -sin\alpha.cos\beta \qquad (3.77)$$

Substitute Eq. 3.77 into Eq. 3.76 to get:

$$\frac{\partial u}{\partial z} = \begin{aligned} & \frac{\partial U}{\partial Z}cos^2\alpha.cos^2\beta + \frac{\partial V}{\partial Z}cos\beta.cos\alpha.sin\beta - \frac{\partial W}{\partial Z}sin\alpha.cos\alpha.cos^2\beta \\ & + \frac{\partial U}{\partial Y}cos\alpha.cos\beta.sin\beta + \frac{\partial V}{\partial Y}sin^2\beta - \frac{\partial W}{\partial Y}.sin\alpha.cos\beta.sin\beta \\ & - \frac{\partial U}{\partial X}cos\alpha.sin\alpha.cos^2\beta - \frac{\partial V}{\partial X}sin\beta.sin\alpha.cos\beta + \frac{\partial W}{\partial X}.sin^2\alpha.cos^2\beta \end{aligned}$$

$$\frac{\partial v}{\partial z} = \begin{aligned} & \frac{\partial U}{\partial Z}cos\alpha.cos\beta.A - \frac{\partial V}{\partial Z}cos^2\beta.cos\alpha.cos\gamma - \frac{\partial W}{\partial Z}cos\alpha.cos\beta.B \\ & + \frac{\partial U}{\partial Y}sin\beta.A - \frac{\partial V}{\partial Y}sin\beta.cos\beta.cos\gamma - \frac{\partial W}{\partial Y}sin\beta.B \\ & - \frac{\partial U}{\partial X}sin\alpha.cos\beta.A + \frac{\partial V}{\partial X}sin\alpha.cos^2\beta.cos\gamma + \frac{\partial W}{\partial X}sin\alpha.cos\beta.B \end{aligned}$$

$$\frac{\partial w}{\partial z} = \begin{aligned} & -\frac{\partial U}{\partial Z}cos\alpha.cos\beta.C + \frac{\partial V}{\partial Z}cos\alpha.cos^2\beta.sin\gamma - \frac{\partial W}{\partial Z}cos\alpha.cos\beta.D \\ & - \frac{\partial U}{\partial Y}sin\beta.C + \frac{\partial V}{\partial Y}sin\beta.cos\beta.sin\gamma - \frac{\partial W}{\partial Y}sin\beta.D \\ & + \frac{\partial U}{\partial X}sin\alpha.cos\beta.C - \frac{\partial V}{\partial X}sin\alpha.cos^2\beta.sin\gamma + \frac{\partial W}{\partial X}sin\alpha.cos\beta.D \end{aligned} \qquad (3.78)$$

Defining:

$$\frac{\partial V}{\partial Z} = \theta_y \ , \qquad \frac{\partial W}{\partial Z} = \theta_x \qquad\qquad (3.79)$$

and as there is no change in the angle between axes after deformation, this can be approximated by the conditions:

$$\frac{\partial U}{\partial Y} = -\frac{\partial V}{\partial Z} \ , \quad \frac{\partial U}{\partial X} = -\frac{\partial W}{\partial Z} \ , \quad \frac{\partial V}{\partial X} = -\frac{\partial W}{\partial Y} \qquad (3.80)$$

Substitute Eqs. 3.79 and 3.80 into Eq. 3.78 to get:

$$\frac{\partial u}{\partial z} = \frac{\partial U}{\partial Z}cos^2\alpha.cos^2\beta + \frac{\partial V}{\partial Y}.sin^2\beta + \frac{\partial W}{\partial X}.sin^2\alpha.cos^2\beta$$

$$\frac{\partial v}{\partial z} = \frac{\partial U}{\partial Z}(cos^2\alpha.cos\beta.sin\beta.cos\gamma - sin\alpha.cos\alpha.cos\beta.sin\gamma)$$

$$- \frac{\partial V}{\partial Z}(cos\alpha.cos\gamma - sin\alpha.sin\beta.sin\gamma) - \frac{\partial W}{\partial Z}cos\beta.sin\gamma$$

$$- \frac{\partial V}{\partial Y}sin\beta.cos\beta.cos\gamma - \frac{\partial W}{\partial Y}(sin\alpha.cos\gamma + cos\alpha.sin\beta.sin\gamma)$$

$$+ \frac{\partial W}{\partial X}(sin^2\alpha.sin\beta.cos\beta.cos\gamma + sin\alpha.cos\alpha.cos\beta.sin\gamma)$$

$$\frac{\partial w}{\partial z} = -\frac{\partial U}{\partial Z}(cos\alpha.sin\alpha.cos\beta.cos\gamma + cos^2\alpha.sin\beta.cos\beta.sin\gamma)$$

$$- \frac{\partial V}{\partial Z}(cos\alpha.sin\gamma + sin\alpha.sin\beta.cos\gamma) - \frac{\partial W}{\partial Z}cos\beta.cos\gamma$$

$$+ \frac{\partial V}{\partial Y}sin\beta.cos\beta.sin\gamma - \frac{\partial W}{\partial Y}(cos\alpha.sin\beta.cos\gamma - sin\alpha.sin\gamma)$$

$$+ \frac{\partial W}{\partial X}(sin\alpha.cos\alpha.cos\beta.cos\gamma - sin^2\alpha.sin\beta.cos\beta.sin\gamma) \qquad (3.81)$$

or:

$$u' = U'\ cos^2\alpha.cos^2\beta + V'\ sin^2\beta + W'\ sin^2\alpha.cos^2\beta$$

$$v' = U'\ (cos^2\alpha.cos\beta.sin\beta.cos\gamma - sin\alpha.cos\alpha.cos\beta.sin\gamma)$$

$$- \theta_y\ (cos\alpha.cos\gamma - sin\alpha.sin\beta.sin\gamma) - \theta_x\ cos\beta.sin\gamma$$

$$- \; V' \; sin\beta.cos\beta.cos\gamma - W'_{,Y} \; (sin\alpha.cos\gamma + cos\alpha.sin\beta.sin\gamma)$$

$$+ \; W' \; (sin^2\alpha.sin\beta.cos\beta.cos\gamma + sin\alpha.cos\alpha.cos\beta.sin\gamma)$$

$$w' \; = \; -U' \; (cos\alpha.sin\alpha.cos\beta.cos\gamma + cos^2\alpha.sin\beta.cos\beta.sin\gamma)$$

$$- \; \theta_y \; (cos\alpha.sin\gamma + sin\alpha.sin\beta.cos\gamma) - \theta_x \; cos\beta.cos\gamma$$

$$+ \; V' \; sin\beta.cos\beta.sin\gamma - W'_{,Y} \; (cos\alpha.sin\beta.cos\gamma - sin\alpha.sin\gamma)$$

$$+ \; W' \; (sin\alpha.cos\alpha.cos\beta.cos\gamma - sin^2\alpha.sin\beta.cos\beta.sin\gamma) \qquad (3.82)$$

The explicit form of the transformation matrix is shown in Fig. 3.7, in which:

$$A = cos\alpha.sin\beta.cos\gamma - sin\alpha.sin\gamma$$

$$B = sin\alpha.sin\beta.cos\gamma + cos\alpha.sin\gamma$$

$$C = sin\alpha.cos\gamma + cos\alpha.sin\beta.sin\gamma$$

$$D = cos\alpha.cos\gamma - sin\alpha.sin\beta.sin\gamma$$

$$E = cos^2\alpha.cos\beta.sin\beta.cos\gamma - sin\alpha.cos\alpha.cos\beta.sin\gamma$$

$$F = cos\alpha.cos\gamma - sin\alpha.sin\beta.sin\gamma$$

$$G = sin\alpha.cos\gamma + cos\alpha.sin\beta.sin\gamma$$

$$H = sin^2\alpha.sin\beta.cos\beta.cos\gamma + sin\alpha.cos\alpha.cos\beta.sin\gamma$$

$$I = cos\alpha.sin\alpha.cos\beta.cos\gamma + cos^2\alpha.sin\beta.cos\beta.sin\gamma$$

$$J = cos\alpha.sin\gamma + sin\alpha.sin\beta.cos\gamma$$

$$K = cos\alpha.sin\beta.cos\gamma - sin\alpha.sin\gamma$$

$$L = sin\alpha.cos\alpha.cos\beta.cos\gamma - sin^2\alpha.sin\beta.cos\beta.sin\gamma$$

and i and j are node numbers.

$$
\begin{bmatrix} u \\ u' \\ v \\ v' \\ w \\ w' \\ \theta_z \\ \theta_z' \\ \hline u \\ u' \\ v \\ v' \\ w \\ w' \\ \theta_z \\ \theta_z' \end{bmatrix}
=
\begin{bmatrix}
C\alpha C\beta & S\beta & -S\alpha C\beta & & C^2\alpha C^2\beta & S^2\beta & S^2\alpha C^2\beta & & & & & & & \\
A & -C\beta C\gamma & -B & & -F & -C\beta S\gamma & E & -S\beta C\beta C\gamma & H & -G & & & & \\
-C & C\beta S\gamma & -D & & J & -C\beta C\gamma & -I & S\beta C\beta S\gamma & L & -K & & & & \\
 & & & & & & & & & & 1 & & & \\
 & & & & & & & & & & & 1 & & \\
\hline
 & & & C\alpha C\beta & S\beta & -S\alpha C\beta & & C^2\alpha C^2\beta & S^2\beta & S^2\alpha C^2\beta & & & & \\
 & & & A & -C\beta C\gamma & -B & & -F & -C\beta S\gamma & E & -S\beta C\beta C\gamma & H & -G & \\
 & & & -C & C\beta S\gamma & -D & & J & -C\beta C\gamma & -I & S\beta C\beta S\gamma & L & -K & \\
 & & & & & & & & & & & & 1 & \\
 & & & & & & & & & & & & & 1
\end{bmatrix}
\begin{bmatrix} U \\ V \\ W \\ \theta_y \\ \theta_z \\ U' \\ V' \\ W' \\ W'_y \\ \theta_z \\ \theta_z' \\ \hline U \\ V \\ W \\ \theta_y \\ \theta_z \\ U' \\ V' \\ W' \\ W'_y \\ \theta_z \\ \theta_z' \end{bmatrix}
$$

Fig 3.7   Transformation Matrix

3.5 Conclusions

A finite element formulation has been developed for a beam element with eight degrees of freedom at each end-node. This formulation takes account of geometric and material non-linearities and can handle large deformations. Transformation of local coordinate displacements to the global system allows the proposed formulation to represent three-dimensional frames. Newton-Raphson solution for the incremental equilibrium equations implies that the solution is based on a tangent-stiffness concept. The fact that residual and thermal strains are added to the total strain vector allows this formulation to handle situations where residual and thermal effects exist. The transformed section concept used in the formulation, along with the ability to divide the section's plates into subsegments, makes this formulation capable of solution for elevated-temperature situations. The last statements may not be an obvious conclusion from the above formulation; nevertheless, details of the solution for fire cases, along with two schemes for using the transformed section concept, will be illustrated clearly in the next chapter with programming details.

CHAPTER 4

3DFIRE

Computer Program Validation

4.1 Introduction

An existing program INSTAF, developed originally at the University of Alberta by El-Zanaty and Murray (1983) for inelastic analysis of plane frames, was used as a basis for the current analysis. INSTAF accounts for material and geometric non-linearities and traces penetration of plasticity through the cross-section. INSTAF uses the tangent stiffness approach and implements a Newton-Raphson procedure to solve the non-linear equilibrium equations for the structure.

The frame solution procedure used in INSTAF can be summarised as follows:

- Read input data.

- Initialise arrays for total displacements, applied forces and incremental displacements.

- From the given nodal connectivity data, calculate the size of the structure's stiffness matrix and prepare a scheme for storing stiffness coefficients under a skyline. This scheme uses one-dimensional arrays to describe the structure of the stiffness matrix, which is stored in turn in another one-dimensional array. The former of these two arrays is used to store the height of each column of the stiffness matrix which contains possible non-zero values above and including the diagonal element. In other words a pointer is stored for each column of the stiffness matrix to identify the number of the diagonal element in the latter array which contains all stiffness coefficients above and including the diagonal of the stiffness matrix. This scheme allows the stiffness matrix to be stored in a single column array and to be retrieved at any time for further calculations. Its other advantage is the apparent contrast to band-

width solution schemes, in which nodal numbering is critical to the memory requirement.

- Each finite element is divided into three sub-elements and their stiffness matrices are formed and condensed into one element stiffness matrix using a static condensation scheme. This procedure was devised to include the effect of plasticity, starting near to the given nodes, in the element stiffness characteristics.

- The difference between the applied and internal forces is calculated and stored in the unbalanced force vector.

- The equilibrium equations are solved for the incremental displacements corresponding to the unbalanced forces.

- Incremental displacements are added to the total displacement vector.

- Internal forces are calculated from internal stresses found from strains derived from the last total displacement update.

- The process of finding unbalanced forces and incremental displacements is repeated, updating total displacements in each iteration, until both incremental displacements and forces are small enough to satisfy a specified accuracy criterion.

The capability of INSTAF to account for geometric and material non-linearities along with its ability to handle large deformations, made it suitable to use as a basis for the program developed in this work. The developed program 3DFIRE also makes use of the valuable routines of INSTAF which handle equation solution and storage schemes.

4.2 Problem Idealisation

Thirteen sampling points are taken on an I-section, dividing each plate into four equal segments. At each sampling point mechanical strains due to the applied loads are calculated from the approximate deformations at the reference axis using cubic shape functions. At each sampling point residual strains and temperatures are introduced. Thermal strains can be calculated at each sampling point using either a constant thermal coefficient or any equation (Fig. 4.1) such as that suggested by the European code EC3-Part 10 (1990). The sampling points divide the cross-section into twelve segments, each of which is considered to have uniform material stiffness corresponding to the average temperature and strain of the segment. Stresses at the edges of each segment are calculated according to the temperatures of the edges' sampling points using the appropriate stress-strain curve. Thermal strains are expected to expand the section if the structural element is not restrained. This expansion will introduce all kinds of deformations on the member according to the temperature distribution across the section. On the other hand, if the structural element is restrained fully or partially, deformations corresponding to the restrained degrees of freedom transform into mechanical compressive stresses. However, this section subdividision into twelve segments is only the basic one; an option to divide each of the twelve segments into any desired number of subsegments is catered for. In this case strains and temperatures at the edges of each subsegment are calculated by linear interpolation.
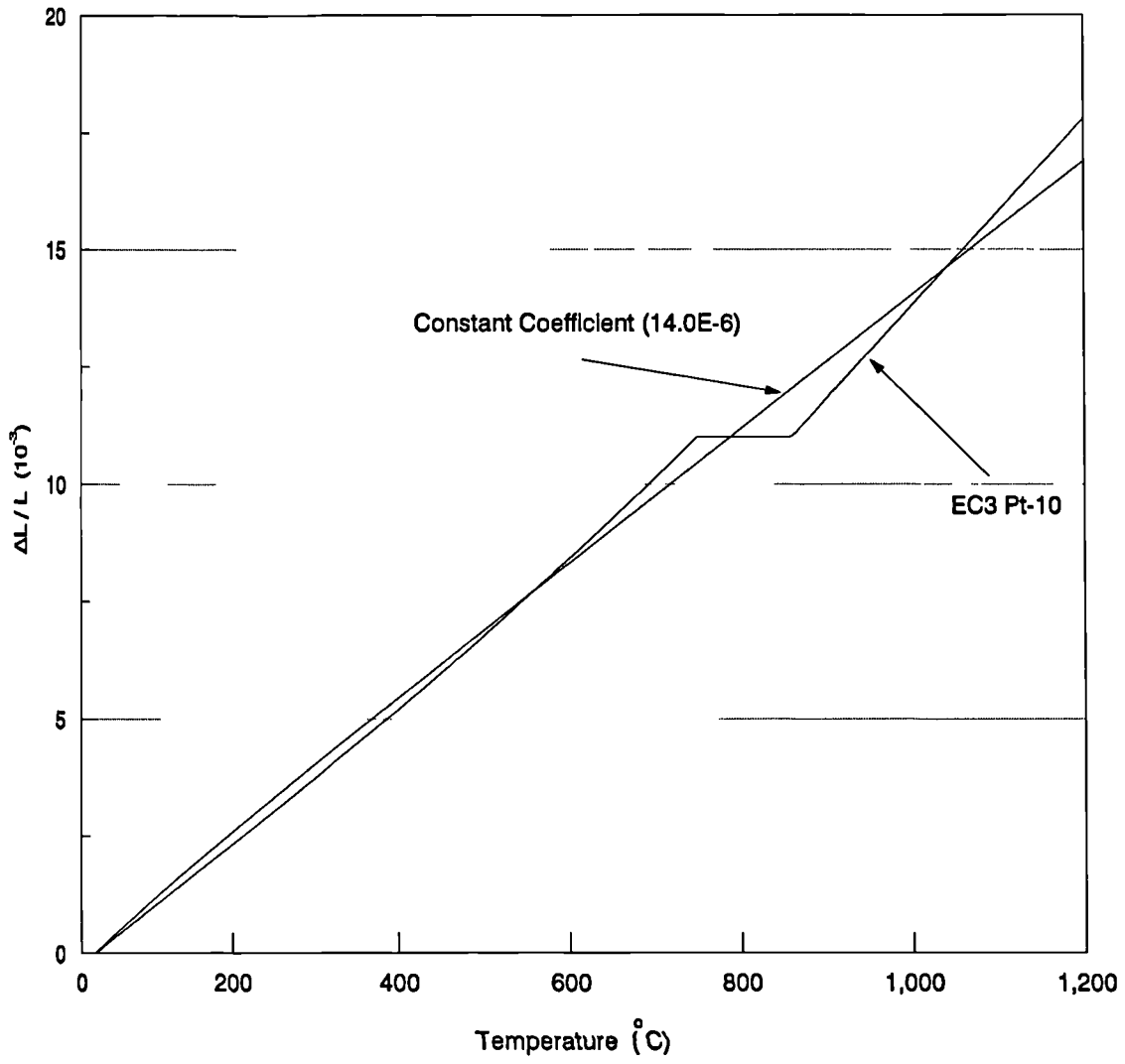
Fig. 4.1   Thermal Expansion Coefficient

4.3   Solution for Fire

Structural analysis at elevated temperatures has to deal with two main aspects.

The first is the influence of thermal expansion, and the second is the decline of material stiffness and strength at high temperatures. Another aspect which has been considered by other researchers is the creep effect at high temperatures. This aspect is not considered in this work.

4.3.1   Thermal Expansion

Unlike residual stresses, thermal stresses are not self-equilibrating. Thermal strains are calculated using either a constant or variable thermal expansion coefficient. By adding thermal expansion strains as compressive mechanical strains, thermally induced deformations/internal forces are added to the displacement/load vectors.

The procedure for incorporating the effects of thermal expansion is illustrated on Figs. 4.2 and 4.3 for both unrestrained and restrained cases. The selected example is very simple for the sake of clarity. Assuming that the strain profile due to the applied load is known (Fig. 4.2), thermal strains are calculated from the given temperature profile and are added as compressive mechanical strains. The total strain includes superimposed bending and axial strains. In this particular example it can be observed that the resultant bending strain is less than that caused by the applied load acting alone. Solving the equilibrium equations for the incremental displacements yields values for the unknown thermally induced displacements. The sign of the axial displacement, for example, changes to the correct one (expansion) due to the negative sign of the unbalanced thermal forces. These incremental dis-

P

Temp.
Distribution

1st Iteration:

$$\{\Delta F\} = \{P_{applied} - P_{internal} - P_{thermal}\} = [K]\,\{\Delta D\}$$

$$\{\Delta D\} = \quad$$

Final Iteration:

$$\{D\} - \{D_{thermal}\} = $$

$$\{\Delta F\} = \{P_{applied} - P_{internal}\} = [K]\,\{\Delta D\}$$

$$\{\Delta D\} = \{\,0\,\}$$

Fig. 4.2   Thermal Expansion (Unrestrained Case)
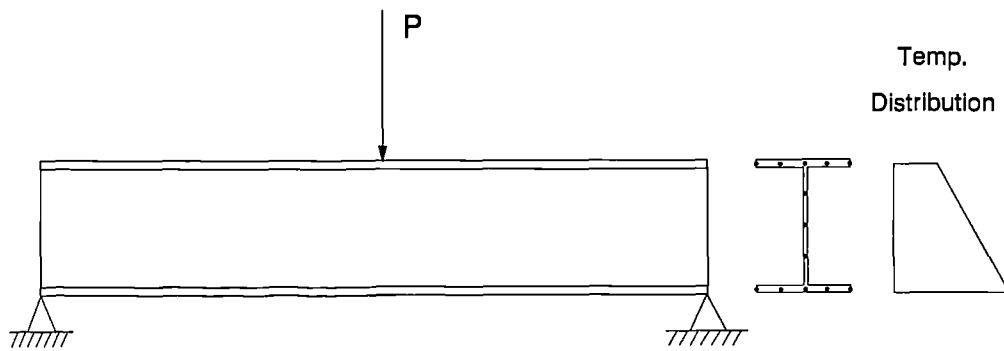
P

1st Iteration:

$$\{\Delta F\} = \{P_{applied} - P_{internal} - P_{thermal}\} = [K]\ \{\Delta D\}$$

$\{\Delta D\} =$

Prevented
displacement
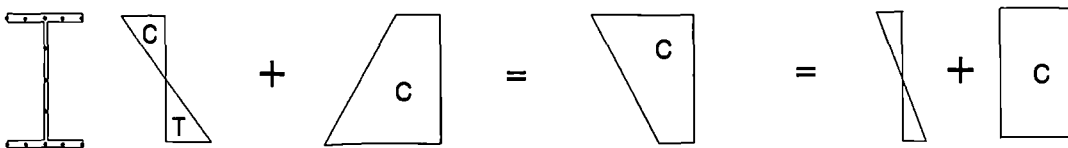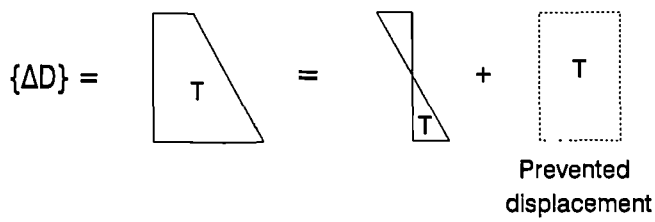
Final Iteration:
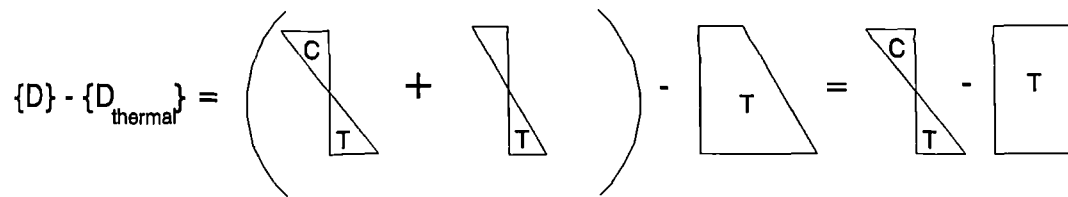
$\{D\} - \{D_{thermal}\} =$

$$\{\Delta F\} = \{P_{applied} - P_{internal} - P_{thermal}\} = \{-P_{axial\ thermal}\ \}$$

$$\{\Delta D\} = \{\ 0\ \}$$

Fig. 4.3   Thermal Expansion (Restrained Case)

placements are added to the total displacement vector which will be used in later iterations to calculate the state of strain across all sections. This implies that all thermal strains that were added in the first iteration must be subtracted in successive iterations in order to ensure that equilibrium conditions are maintained.

In the second case (Fig. 4.3) axial displacement is prevented. The procedure of solution for thermal strains remains exactly the same while the boundary conditions take care of the difference. When incremental displacements are calculated, both the axial displacement and the unbalanced forces at the boundary are set to zero. In this case only the bending displacement is added to the total displacements. In later iterations the total thermal strains are subtracted from total strains, causing a permanent axial compressive strain.

4.3.2 Stiffness and Strength

The availability of many constitutive models for stress-strain characteristics at elevated temperatures means that it is desirable that the present analysis should be capable of accommodating all of them. Two schemes were developed to calculate stresses and material properties, so that any trilinear or continuous (functional) representation of material stress-strain characteristics can be implemented in the analysis.

In the first scheme a trilinear idealisation of the stress-strain relationships under various temperatures was assumed. The temperature of each segment or subsegment is assumed to be uniform for the purpose of calculating its stiffness. Using the relevant stress-strain curve the segment is divided into a maximum of five different zones with different thicknesses, depending on the local strain distributions.

This transformation is conducted according to the modular ratio $(E/E_{T_{av}})_{elastic}$. A second transformation according to the ratio of elastic modulus at the average temperature of the segment to the elastic modulus at $20^\circ C$, E_T/E_{20} is carried out. The stress distribution at each segment is directly obtained from the appropriate curve as illustrated in Fig. 4.4.

The second scheme assumes continuous stress-strain curves. Each segment is divided into the required number of subsegments and the section is transformed using the average strain of each subsegment. Using the average temperature of each subsegment, the appropriate curve can be used to transform the section using the modular ratio of the tangent modulus to the elastic modulus at $20^\circ C$, $E_{tan}/E_{20elastic}$. The stress distribution is determined form the appropriate curves as illustrated in Fig. 4.5 using the actual temperatures and strains at both ends of the segment. Although it is easier to use the average strains and temperatures, this arrangement produced considerably the faster convergence to the solution.

In both schemes sectional transformation allows solution of all the governing equations using Young's modulus at ambient temperature, provided that section properties are calculated for the transformed section. This procedure allows solution of all integrations for the whole cross-section rather than performing the integration for each individual segment.
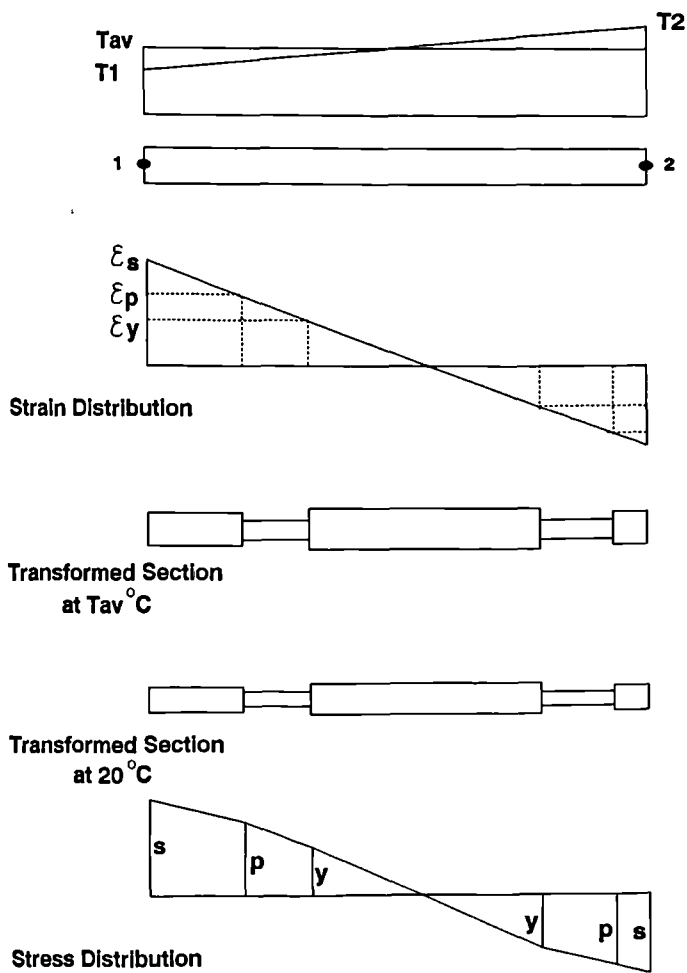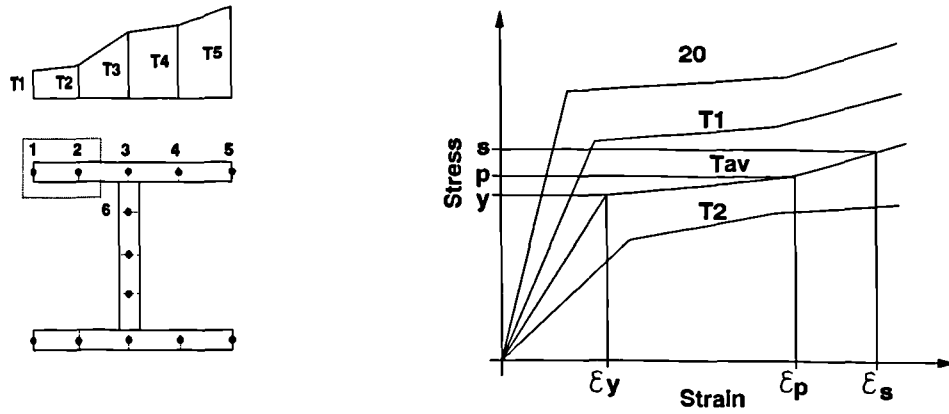
Fig. 4.4 Stiffness and Stresses For a Heated Segment
(Scheme 1 - Trilinear Stress-Strain Models)
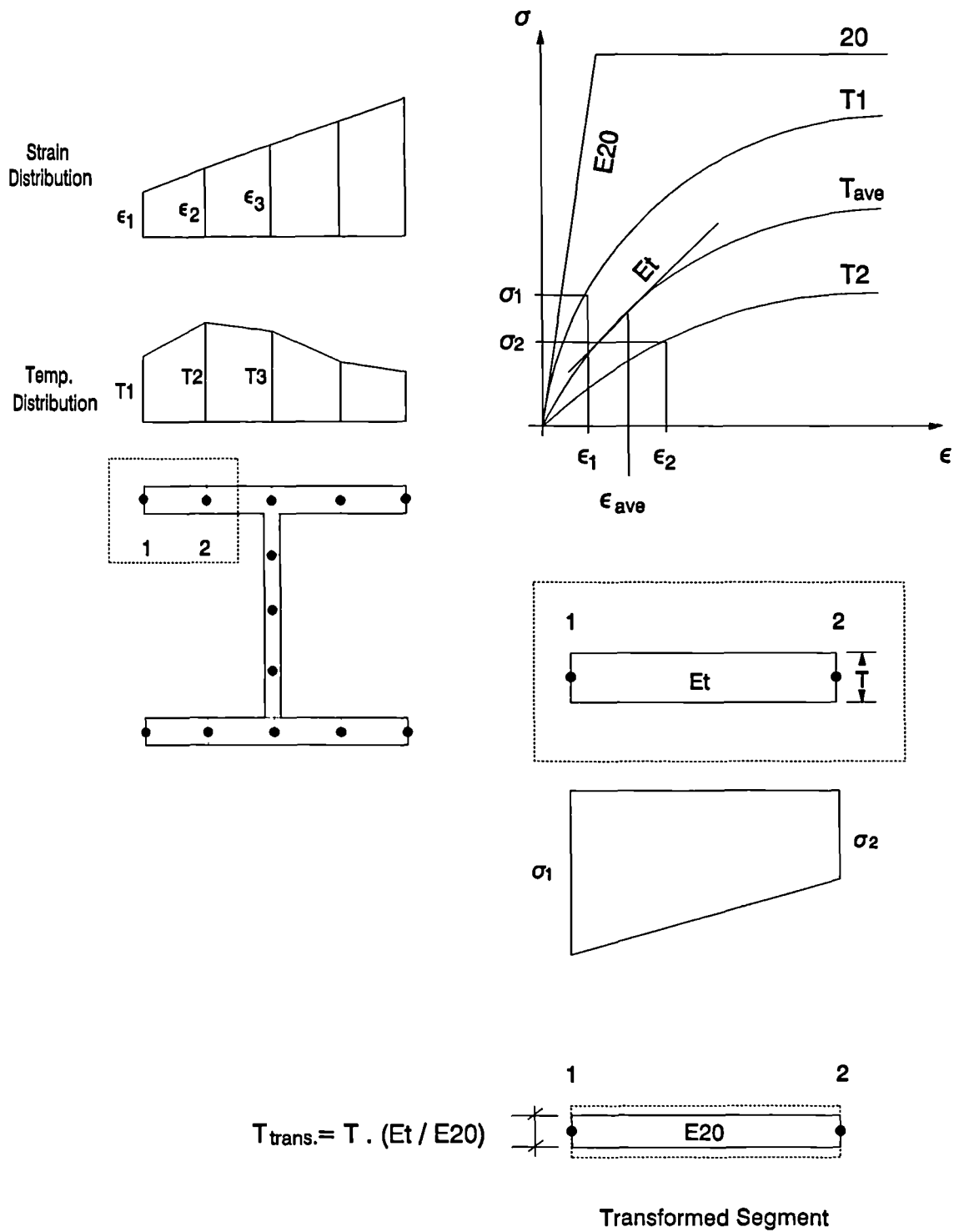
Fig. 4.5 Stiffness and Stresses For a Heated Segment

(Scheme 2 - Continuous Stress-Strain Models)

4.4 Program Flow

4.4.1 The Solution Process

After initialising the required arrays, the flexural part of the tangent stiffness matrix is used to estimate an approximate value of the displacement vector using:

$$[K_F] \{q\} \; = \; \{Q\} \tag{4.1}$$

in which $[K_F]$ is the flexural stiffness matrix, $\{Q\}$ is the vector of applied forces and $\{q\}$ is the vector of unknown displacements. The flexural stiffness matrix $[K_F]$ is exactly the same as the tangent stiffness matrix $[K_T]$ derived in Chapter 3 apart from the fact that it does not include any geometrical effects as all deformations are assumed to equal zero initially.

From the first estimate of deformations stress resultants are calculated. The structure is compressed using the thermal strains and the 'displacements' due to the thermal expansion are evaluated and added to the displacement vector $\{D\}$. Once the boundary conditions of the structure are imposed these thermally induced displacements either remain if the corresponding degree of freedom is unrestrained or are transformed into internal stresses if not. Gaussian integration is used to formulate the governing equations with four Gauss points over the length of each finite element. In subsequent iterations the tangent stiffness matrix $[K_T] \; = \; [K_F] + [K_G]$ is calculated and updated in following way:

- At each Gauss point total strains are evaluated using the total displacements from the previous iteration and approximated using cubic shape functions.

- Thermal strains are subtracted from the total strains.

- Stress resultants are calculated and the geometric part of the tangent stiffness matrix $[K_G]$ is evaluated.

- The tangent stiffness matrix $[K_T]$ is updated.

- The unbalanced load vector needed to balance the internal forces with the external loads is calculated.

- The incremental displacements corresponding to the unbalanced load vector are found.

- This process is repeated until the incremental displacements are small enough for the required accuracy.

4.4.2 The Major Subroutines Used

Program 3DFIRE consists of several subroutines, each of which performs a specific task. In the following the titles of these subroutines are listed and their function explained.

- Subroutine MAIN

  Opens input, output and temporary files.

  Calls subroutine MANAGER to solve for each load/temperature increment.

  Calculates CPU time needed for running the program.

  Closes files at the end of each problem.

- Subroutine MANAGER

Calls various subroutines which read input data and solve the structure's equilibrium equations for each iteration, until convergence/failure is reached.

- Subroutines INPUT1, INPUT2 and BOUND1

These subroutines read input data (problem definition, geometry, material properties, connectivity, loading and boundary conditions data).

- Subroutines COLHT and ADDRESS

The first subroutine calculates the height of each column in the structure's stiffness matrix that contains possible non-zero values, while the second calculates the index of the beginning of each of these columns once the stiffness matrix is stored in a one-dimensional array.

- Subroutine TEMPREAD

Reads temperatures from the input file. In cases where reduced input temperature profiles are defined, it calculates the full profile by means of linear interpolation.

- Subroutine SHAPE

Evaluates the shape function derivatives for each Gauss point on a finite element.

- Subroutine STIFF

Calculates the tangent stiffness matrix for each finite element. Each finite element defined by the user is discretely divided into three sub-elements and their stiffness matrices are condensed back to a single element stiffness matrix. The element stiffness matrix in the local coordinate system is

then transformed to the global system and the structure's stiffness matrix is formed.

- Subroutine TR1

Transforms the force vector from the global to the local system of coordinates.

- Subroutine TR2

Transforms the displacement vector from the local to the global system of coordinates.

- Subroutine ASSEMB

Assembles the element stiffness matrix into the structure's stiffness matrix in the global system of coordinates.

- Subroutines BKSB1, BKSB2, EQFT and EQKBB

These routines perform the task of stiffness matrix condensation.

- Subroutine EQSBST

This subroutine along with BKSB1 performs the equilibrium equation solution by back-substitution and produces the vector of incremental displacements.

- Subroutine BOUND2

Performs the process of adding the boundary conditions to the stiffness matrix.

- Subroutine STRAIN

Divides each plate of the cross-section according to the strain distribution for trilinear stress-strain models.

- Subroutine STEP

Calculates the transformed section properties and stress resultants at each Gauss point for trilinear stress-strain models.

- Subroutine STEPC

Calculates the transformed section properties and stress resultants at each Gauss point for continuous stress-strain models.

- Subroutines ECCS, ECCSM, CTICM, ECCODET, RAMOSB, FURA

These routines define the stress state on any point of the cross-section for a given strain and temperature using ambient-temperature material properties for bilinear or trilinear models.

- Subroutines ECCEQ and RAMOS

These routines define the stress state at any point of the cross-section for a given strain and temperature using ambient temperature material properties for continuous models.

- Subroutines CONVER and DINCR

These routines check convergence in displacements and loads.

4.5 Program Validation

The lack of any comparable three-dimensional previous work has meant that most of the validation of 3DFIRE was performed using ambient temperature analytical and experimental comparisons to check the three-dimensional integrity of the program. Nevertheless, it was possible to carry out fire validations by using some in-plane examples, restraining all out-of-plane degrees of freedom.

4.5.1 Program Sensitivity

To check the reliability of Program 3DFIRE two analytical tests were carried out.

In the first test the influence of the number of the finite elements on the accuracy of solutions was considered. This convergence test is a standard one, since the finite element method produces approximate results due to the assumption that a structure is divided into a finite number of discrete elements which are interconnected at a finite number of nodes. In theory if the number of elements is increased to infinity the finite element method should produce "exact" answers. However, experience shows that dividing the structure into a reasonably small number of finite elements can often produce remarkably accurate solutions. In practical terms any attempt to increase this number is wasteful due to the fact that the extra accuracy becomes practically negligible.

A perfect column with high slenderness ratio, loaded axially, was analysed up to failure. Several division schemes were attempted, starting from assuming the column to be one finite element and then successively subdividing it into twice the

previous number of elements. Although this is inherently an eigenvalue problem not suited to incremental analysis, nevertheless the program produced a remarkably accurate estimate of the Euler load. This was achieved by successive refinement of the load increment after each failure, so that the program retreats after failure to the previous increment and adds to it a fraction of the increment that caused failure. By repeating this process several times the difference between the load level at which a solution was attained and the next load where failure occurred becomes very small. Results from these analyses are shown in Fig. 4.6a, which illustrates the speed of convergence thanks to the high degree of non-linearity of the formulation.

A second case was considered to the same effect, whereby a biaxially loaded column was analysed up to failure using the same procedure. The load was applied with eccentricities about both principal axes, causing applied moments about both principal axes along with an axial force. The column was divided into increasing numbers of finite elements and failure loads were obtained by refining the load increment, following the same procedure performed in the previous case. On the same figure results of this set of analyses are illustrated and the previous conclusions concerning the perfect column are clearly still valid. Although no exact solution is known to this problem, it is clear that failure loads are converging to some solution, as denoted by the broken line on Fig. 4.6b. It is clear from Fig. 4.6 that the difference between failure loads for four finite elements and that for eight elements is very small, leading to the conclusion that no realistic benefit can be obtained from increasing the number of finite elements any more. It can also be noticed that the speed of convergence is still remarkably fast.

In the second test the influence of number of segments in a cross-section at el-
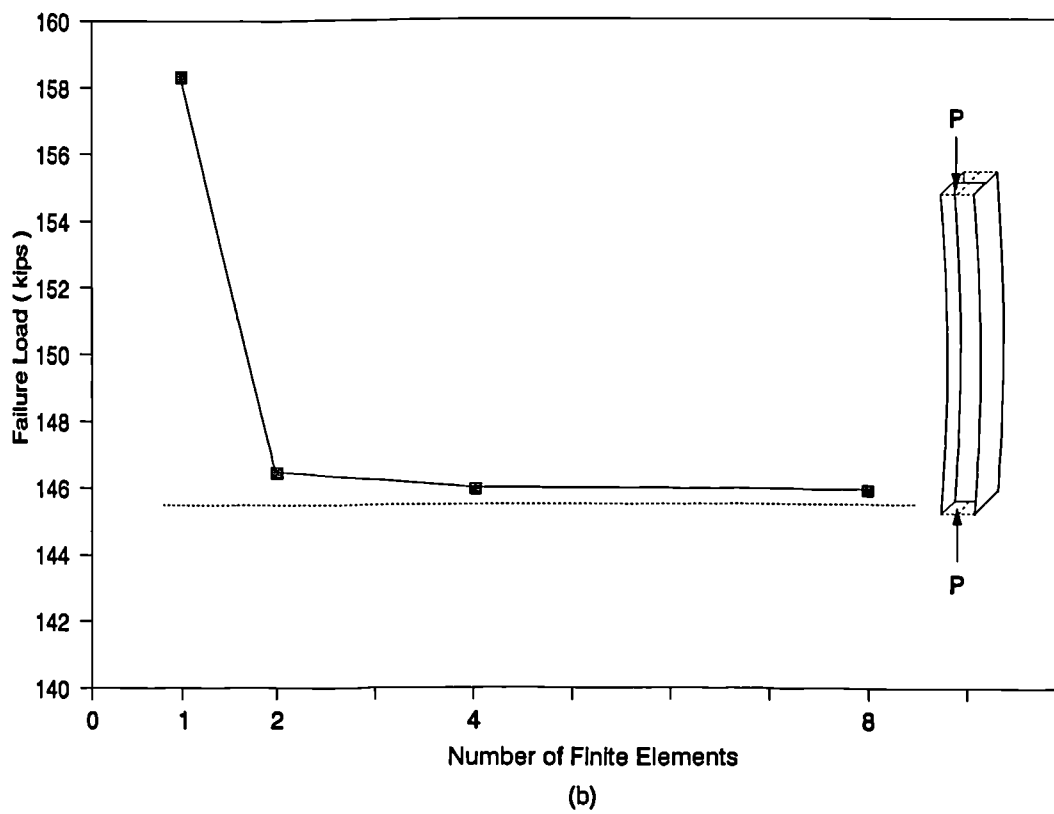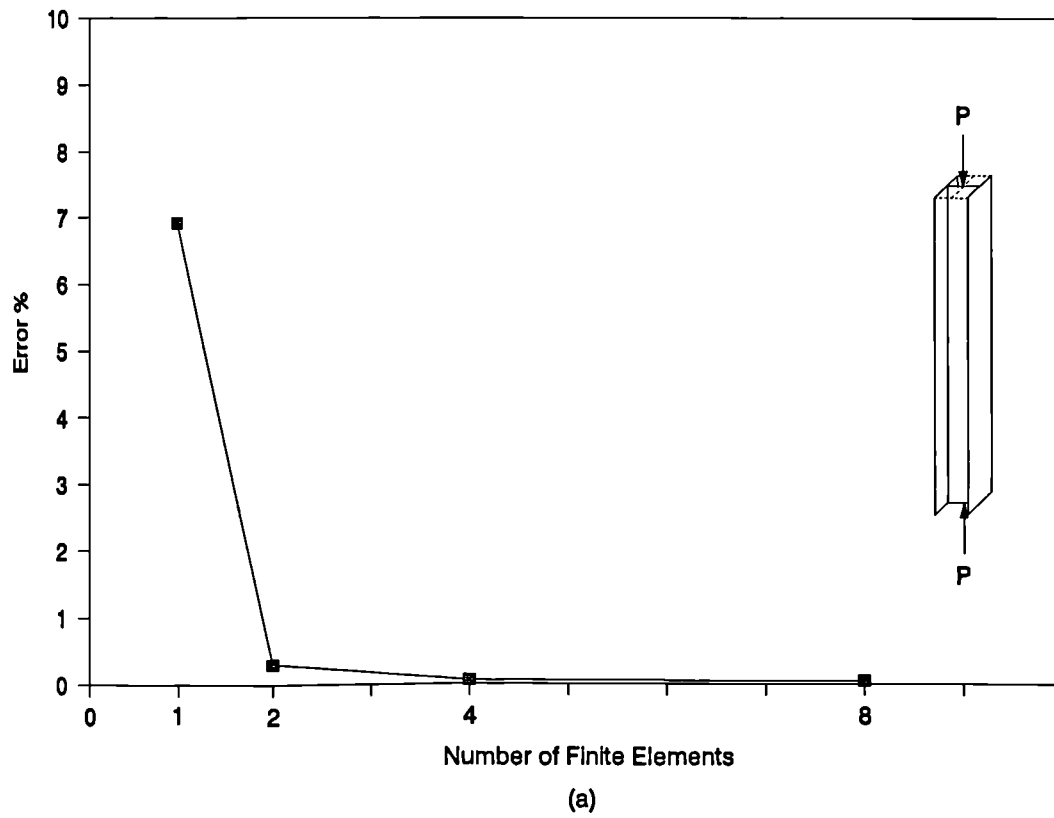
Fig. 4.6   Convergence Test for Program 3DFIRE

evated temperatures was studied. A Universal Beam section was analysed with different numbers of segments across its section. The design load to BS5950 assuming full lateral, restraint was applied and a uniform temperature distribution was increased up to failure. This test ensures that the section is subject to different stains across its depth, yet the same stress-strain curve applies to the whole section because of the uniform temperature profile. Results obtained from this set of analyses (Fig. 4.7) show that the temperature-deflection characteristics of the beam are visually almost indistinguishable regardless of the number of segments. Nevertheless, failure temperatures as obtained to an accuracy of 0.2° C show a tendency to approach the failure temperature of the maximum number of segments from alternate sides.

Another case was considered for a column loaded to 60% of its ultimate load with thermal gradient across its major axis (Fig. 4.8). This column was heated up to failure under a constant load. This case provides a contrast to the previous case, in that now the strain distribution across the section is almost constant while the temperature profile means that a different stress-strain curve applies to each segment. Apart from the fact that solutions are converging from one side, the same high accuracy with a low number of segments is observed.

It is apparent that the basic division of the cross-section into twelve segments is usually quite reasonable. It might however be sensible to exercise caution by increasing the number of segments in abnormal cases where temperature profiles assume very irregular non-uniformity.

(UB 533 X 210 X 101, P = Design Load and Beam Uniformly Heated)
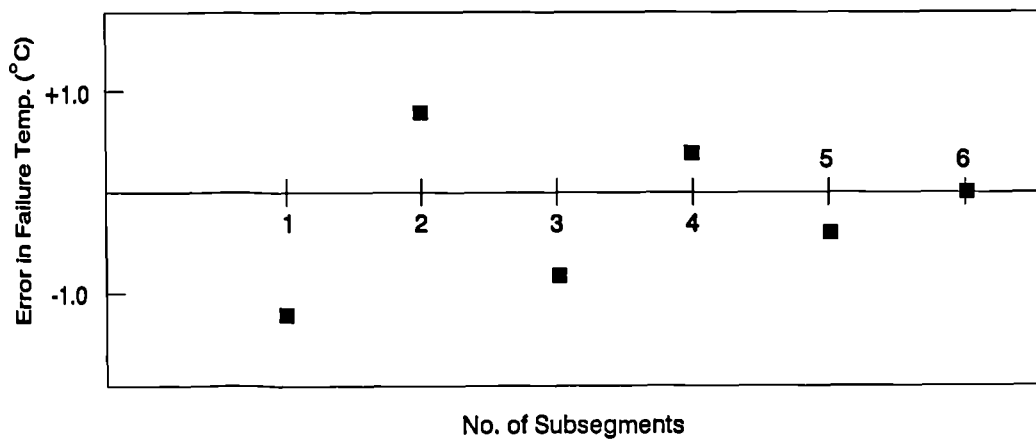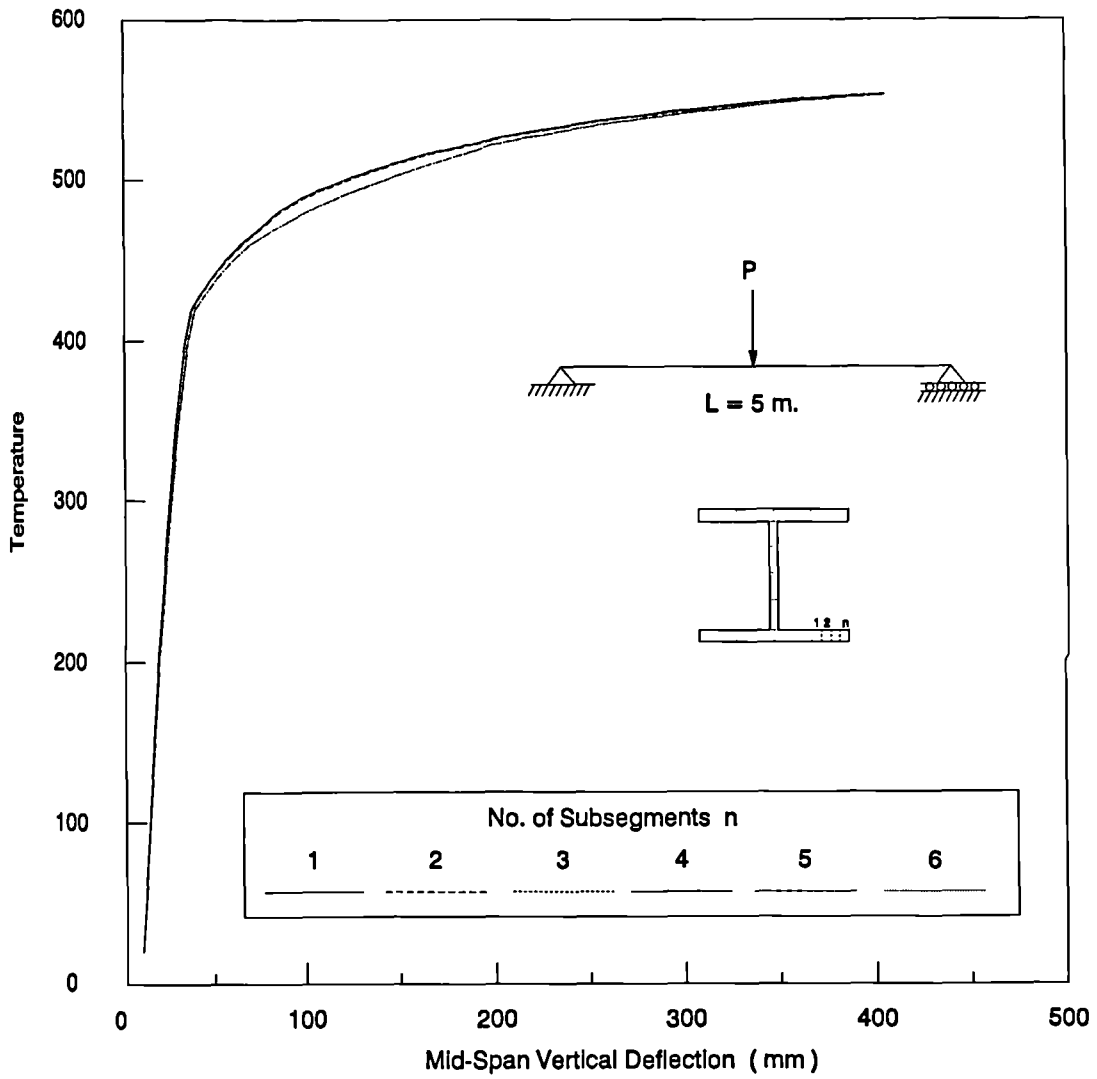
Fig. 4.7   Effect of Section Division (Beam Case)

(UC 203 X 203 X 52, P = 60% of Ultimate Load)
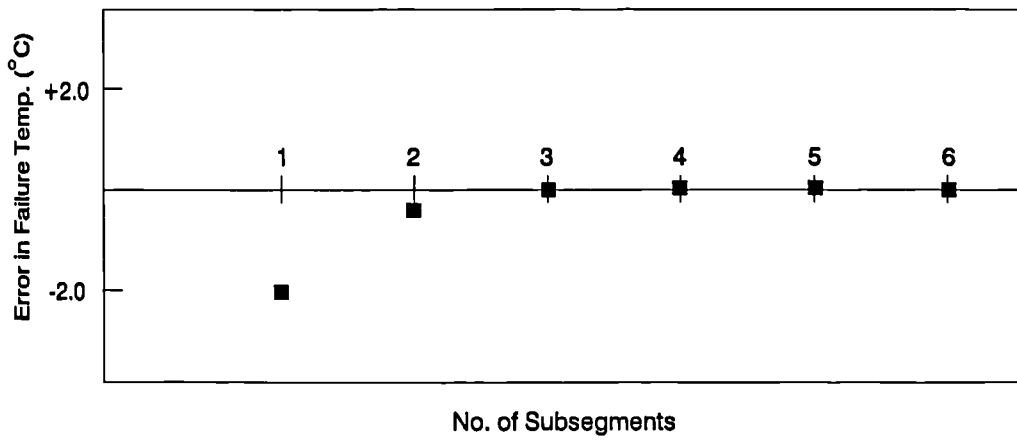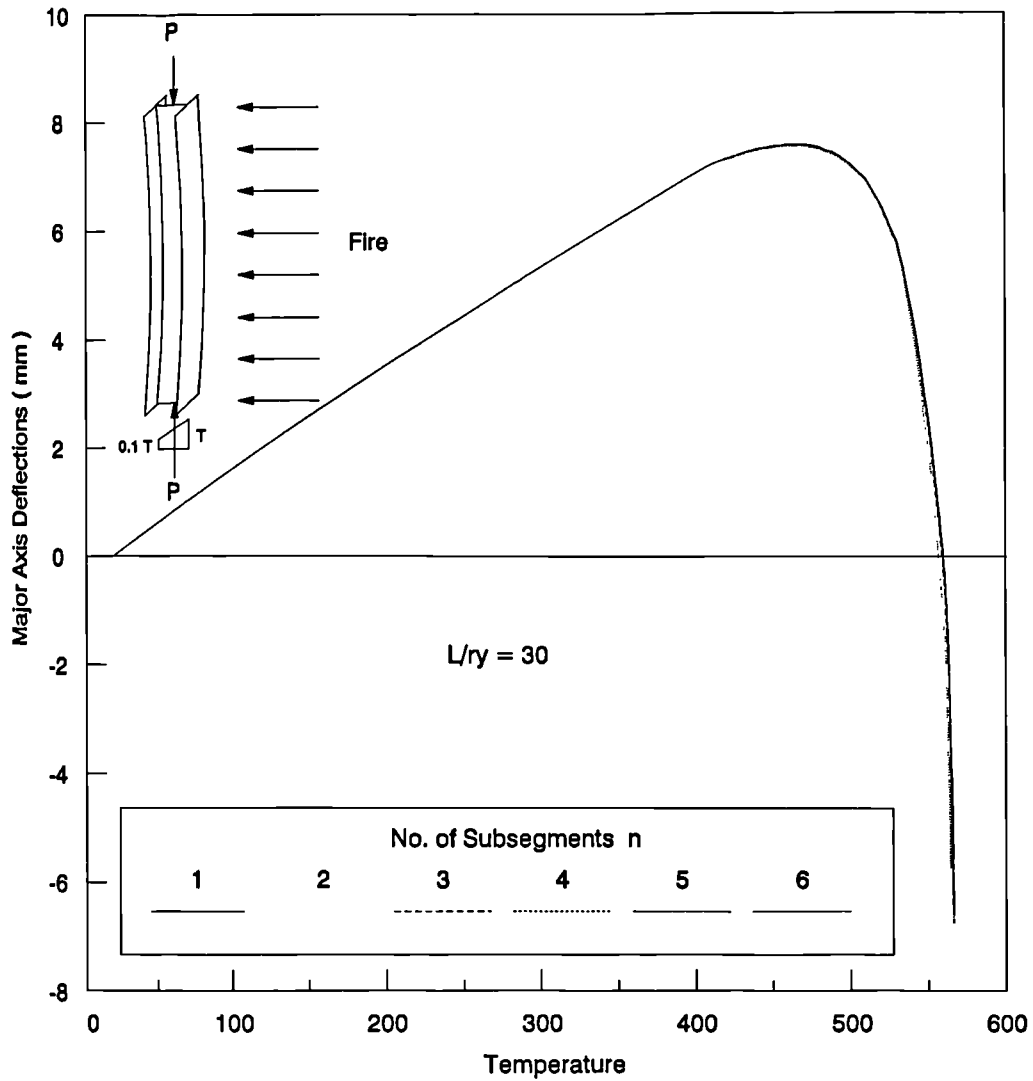
Fig. 4.8   Effect of Section Division (Column Case)

4.5.2 Ambient Temperature Validation

As a part of the validation of the program it is necessary to compare it with other analyses in terms of formulation non-linearity and capability for handling large deformations:

4.5.2.1 Effect of Formulation

Almost all high-order terms have been kept in this formulation. This results in a more accurate prediction of deformations, comparing more favourably with third-order analysis than normal second-order analysis, in which most of the high-order terms are discarded. Fig. 4.9 shows a comparison between a second-order analysis with most high order terms discarded (Vinnakota 1976), a third-order analysis (Soltis and Christiano 1972) and the current analysis. The case analysed is of an elastic biaxially-loaded column at ambient temperature. In this example the data used in the program was identical to that of the previous work and the yield stress was assumed to be infinite. It can be seen that all analyses agree almost exactly on deformation values for most of the load-deflection history. Only at a high load level before failure does the influence of high-order terms become significant, resulting in considerably different prediction of deflections.

4.5.2.2 Deflection Check

A preliminary check of the program was carried out using a cantilever beam ($UB406 \times 178 \times 54$). The cantilever was tested by applying several individual force components at the free end (Figs. 4.10 and 4.11). Results obtained from the program were compared with classical small-deflection analytical solutions for

Elastic Analysis of Biaxially Loaded Column
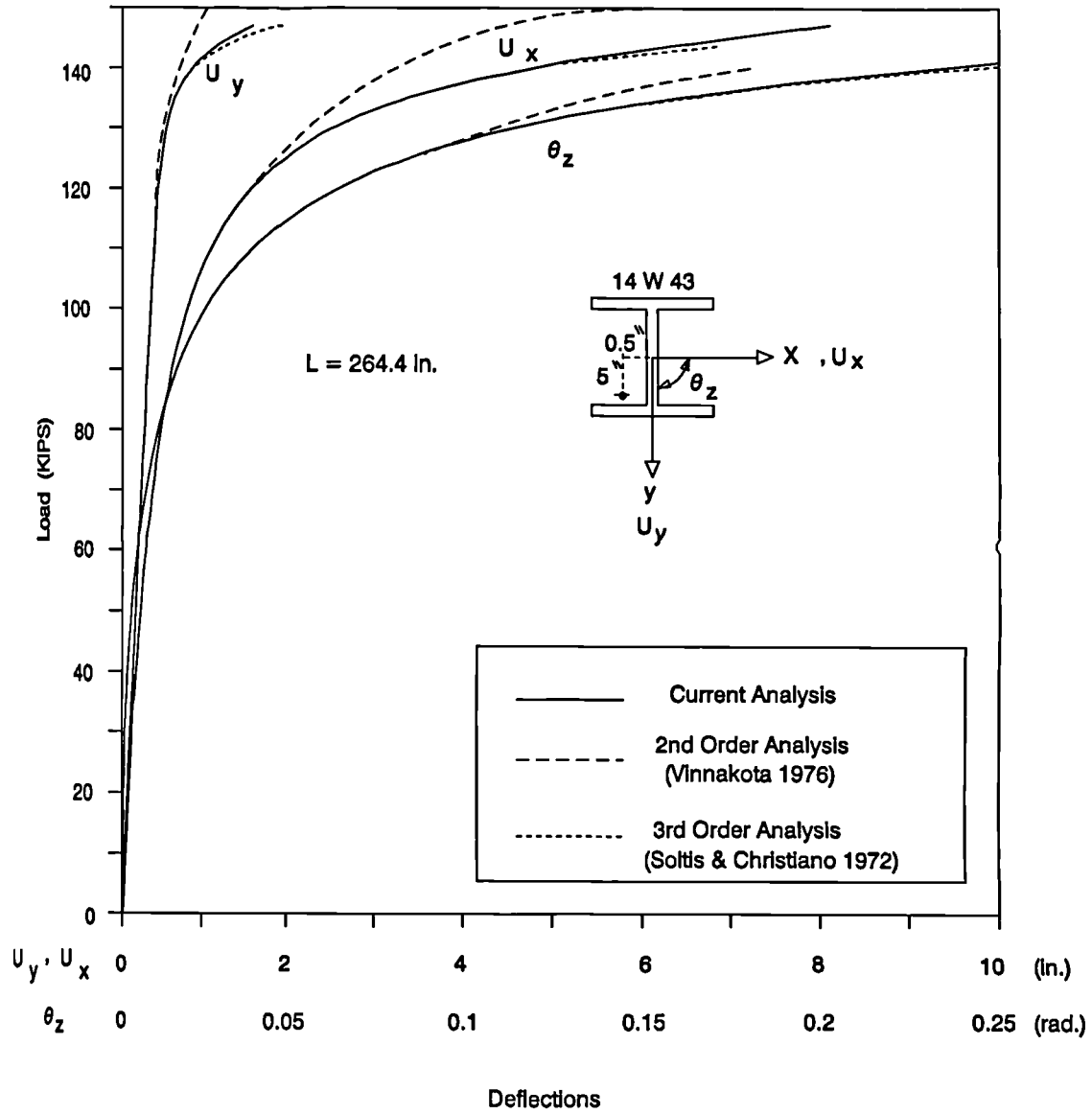
Fig. 4.9 Influence of Analysis Order
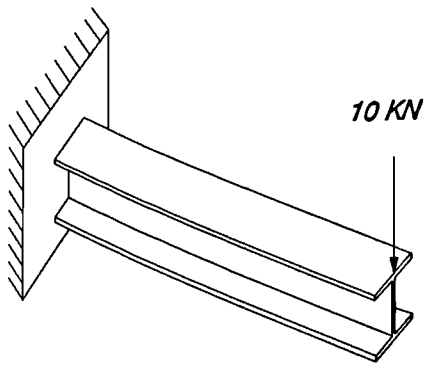
Location		Fixed End	Middle	Free End
Moment (N.mm)	Analytical	0.5E8	0.25E8	
	F.E.A	0.49913E8	0.25E8	
Deflection (mm)	Analytical		3.41	10.93
	F.E.A		3.4	10.89
Rotation (Rad.)	Analytical		0.002459	0.003278
	F.E.A		0.002451	0.003286
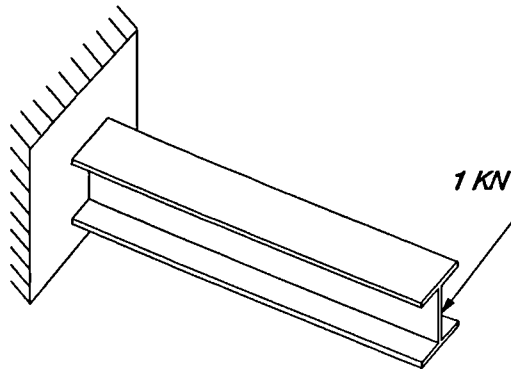
Location		Fixed End	Middle	Free End
Moment (N.mm)	Analytical	0.5E7	0.25E7	
	F.E.A	0.49913E7	0.25E7	
Deflection (mm)	Analytical		6.23	19.95
	F.E.A		6.24	19.97
Rotation (Rad.)	Analytical		0.0044835	0.005978
	F.E.A		0.004494	0.005992
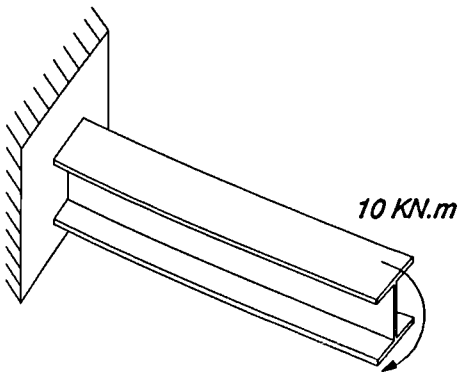
Location		Fixed End	Middle	Free End
Moment (N.mm)	Analytical	1.0E7	1.0E7	1.0E7
	F.E.A	1.0E7	1.0E7	1.0E7
Deflection (mm)	Analytical		0.8196	3.278
	F.E.A		0.8171	3.268
Rotation (Rad.)	Analytical		0.0006556	0.0013113
	F.E.A		0.0006536	0.001307
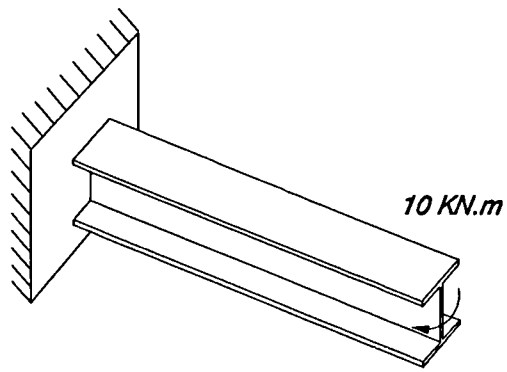
Location		Fixed End	Middle	Free End
Moment (N.mm)	Analytical	1.0E7	1.0E7	1.0E7
	F.E.A	1.0E7	1.0E7	1.0E7
Deflection (mm)	Analytical		14.96	59.84
	F.E.A		14.97	59.9
Rotation (Rad.)	Analytical		0.01196	0.02391
	F.E.A		0.01198	0.02396

Fig. 4.10 Single D. O. F. Assessment (Bending Deflections)

1 KN.m

+B_z

Internal Bimoment
Diagram
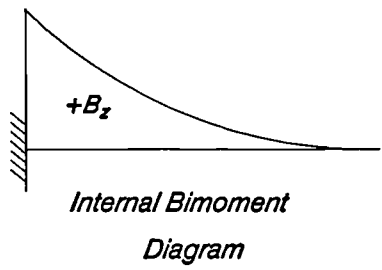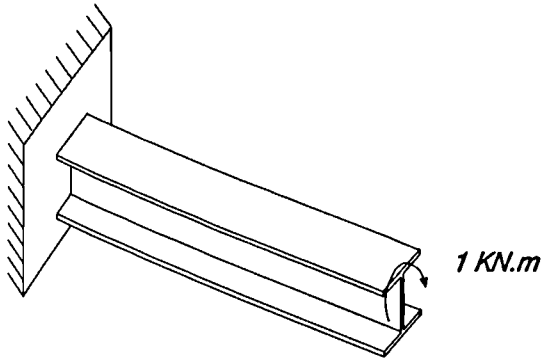
Location		Fixed End	Middle	Free End
St. Venant Torsion (N.mm)	Analytical	0.0	0.6468E6	0.7933E6
	F.E.A.	0.3842E4	0.6440E6	0.7871E6
Warping Torsion (N.mm)	Analytical	1.0E6	0.3531E6	0.2067E6
	F.E.A.	0.9728E6	0.3472E6	0.1969E6
Bimoment (N.mm^2)	Analytical	0.217E10	0.6338E9	0.0
	F.E.A.	0.213E10	0.6120E9	0.170E7

−T_{sv}

−$T_{\omega z}$

Internal Torsion
Diagram

1 KN.m^2

+B_z

Internal Bimoment
Diagram
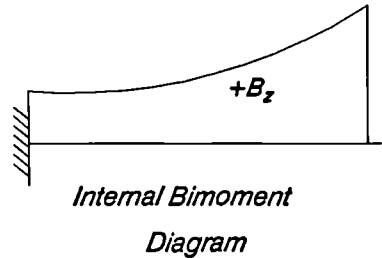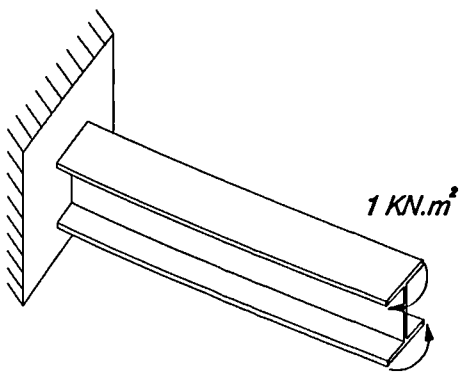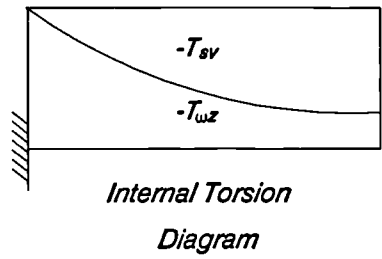
Location		Fixed End	Middle	Free End
St. Venant Torsion (N.mm)	Analytical	0.0	-0.129E6	-0.442E6
	F.E.A.	-0.365E3	-0.129E6	-0.444E6
Warping Torsion (N.mm)	Analytical	0.0	0.1294E6	0.4420E6
	F.E.A.	0.2626E4	0.1290E6	0.4353E6
Bimoment (N.mm^2)	Analytical	0.2067E9	0.3531E9	1.0E9
	F.E.A.	0.2024E9	0.3485E9	1.0E9

$T_{\omega z} = -T_{sv}$

Internal Torsion
Diagram
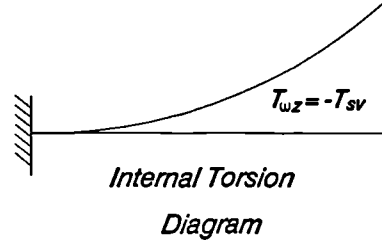
Fig. 4.11   Single D. O. F. Assessment (Torsion and Warping)

deflections and reactions. To minimise the effect of non-linear terms, applied loads were kept to a reasonable minimum.

The well known formulae (Timoshenko and Gere 1978) for flexural deflections due to an applied vertical load P and end moment M,

$$V = \frac{-PL^3}{3EI} = \frac{ML^2}{2EI} \tag{4.2}$$

$$and \quad \theta = \frac{PL^2}{2EI} = \frac{ML}{2EI} \tag{4.3}$$

were used in this instance for end deflections.

With respect to torsion and warping comparison, Zbirohowski-Koścìa (1967) has derived the following equations which were used for comparison.

For a cantilever with an end torque T:

The internal warping torsion:

$$T_\omega(z) = -T\frac{cosh\ k(L-z)}{cosh\ kL} \tag{4.4}$$

and the internal St. Venant torsion:

$$T_{SV}(z) = T - T_\omega(z) \tag{4.5}$$

while the internal bimoment

$$B(z) = \frac{T}{k}\left[\frac{sinh\ k(L-z)}{cosh\ kL}\right] \tag{4.6}$$

For a cantilever with end external bimoment B:

The internal warping torsion

$$T_\omega(z) = Bk\frac{sinh\ kz}{cosh\ kL} \tag{4.7}$$

and the internal St. Venant torsion:

$$T_{SV}(z) = T_\omega(z) \tag{4.8}$$

while the internal bimoment:

$$B(z) = B\ \frac{cosh\ kz}{cosh\ kL} \tag{4.9}$$

Where $k = \sqrt{\frac{GJ}{E_1 I_\omega}}$ and $E_1 = \frac{E}{1-\mu^2}$

Tabulated results on Figs. 4.10 and 4.11 show very good agreement between the classical solutions for deflections and the present analysis.

4.5.2.3 Large Deformation Check

To ensure that any analysis can handle large deformations, no assumptions can be made regarding deflections in the formulation. In this analysis, although certain assumptions have been made regarding deflections (Eqs. 3.4 and 3.5), they are not assumed to be small. It is necessary to validate this approach with other work.

A comparison was carried out with analytical results of a classical example reported by Timoshenko and Gere (1978). This problem, of an elastic cantilever beam loaded with a vertical end load, was solved by Rojahn (1968). Rojahn solved the deflection equations up to a load $P = \frac{10EI}{L^2}$. The current program was used to solve the same problem using an I cross-section. The cantilever beam was divided into eight finite elements and all out-of-plane degrees of freedom were restrained at all nodes. The program continued the analysis up to a load of $P = \frac{19EI}{L^2}$, after

which convergence could not be attained. Results from both solutions are plotted on Fig. 4.12. Vertical and horizontal deflections of the free end compare very well with Rojahn's solution up to the end of his tabulated results. The rotation of the free end compares very well with Rojahn's solution up to the level of $0.3L$ vertical displacement, and compares with reasonable error up to $0.5L$. After the latter level a considerable difference can be noticed. It is clear that the cause of this difference is the assumption related to the rotations in Eq. 3.4. In any circumstances, it is difficult to imagine a realistic situation where stable deformations might reach anywhere near to the deflection-level considered in this example if inelasticity is to be included in the analysis. Hence, the current analysis can be claimed to be a large-deformation analysis.

4.5.2.4 Biaxially Loaded Column Case

Another comparison was carried out with an almost exact solution for a biaxially loaded column. Harstead et al (1968) analysed an isolated column using a numerical procedure that was restricted to single columns with elastic-perfectly plastic material. The numerical procedure consisted of dividing the cross-section into a large number of small areas. By using a computer to solve the governing equations for each of the small areas at a number of stations over the length of half the column, deflections were calculated. They presented two analyses for a biaxially loaded column, with the ends restrained and unrestrained against warping. The results of both analyses are presented on Figs. 4.13 and 4.14. The current analysis compares very well with the reported deflections at the column's mid-span. The small but observable reduction in the ultimate load for both cases, as predicted by the current analysis, can be explained by the respective degrees of non-linearity in
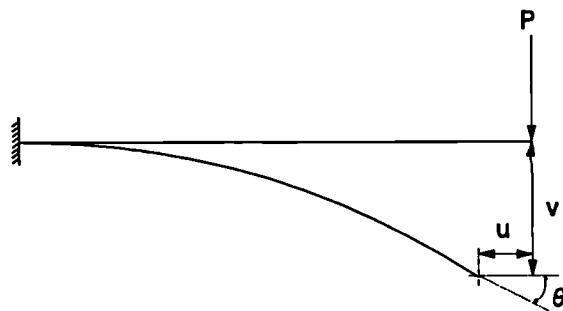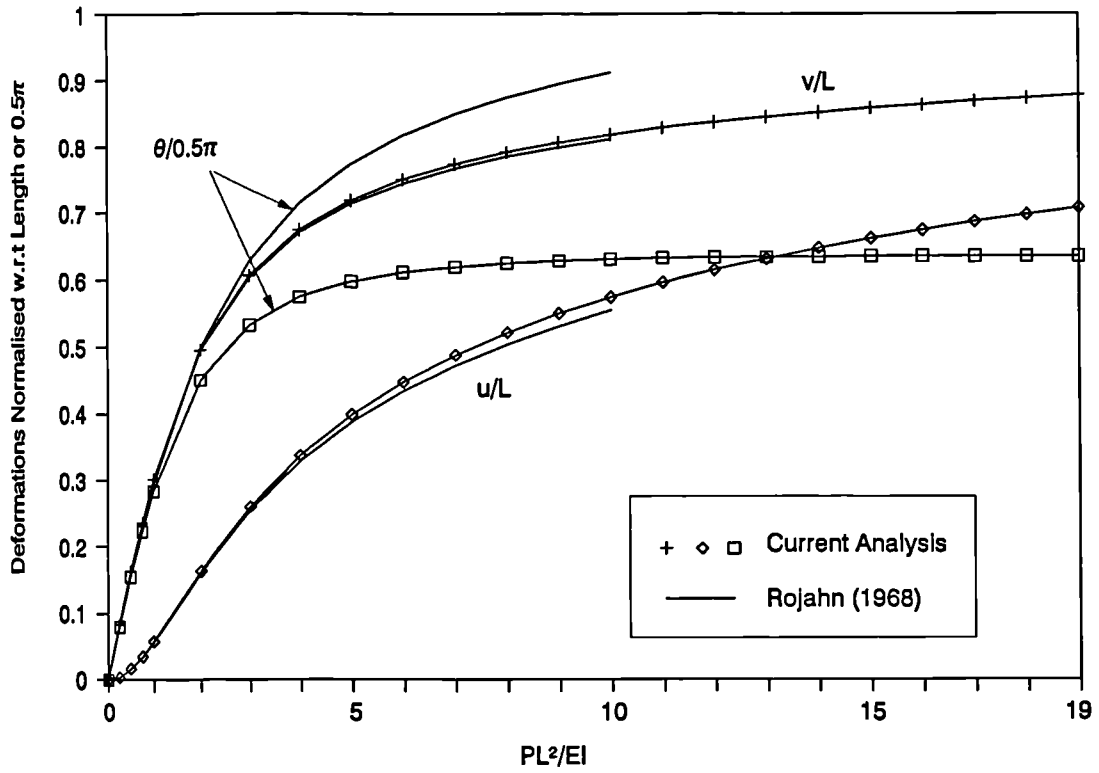
Fig. 4.12   Large Deformation for an Elastic Cantilever Beam
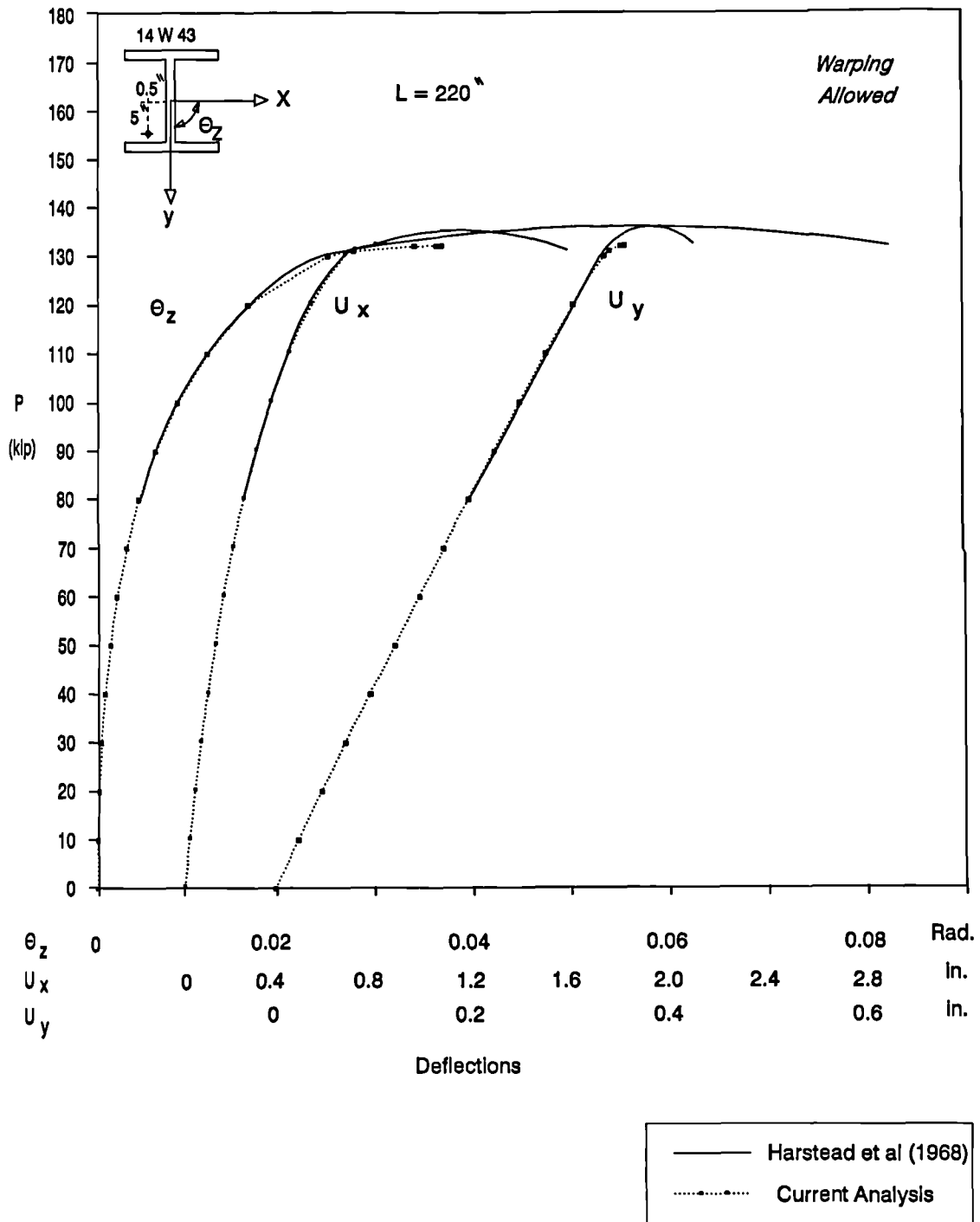
Fig. 4.13 Biaxially Loaded Column (Warping Allowed)
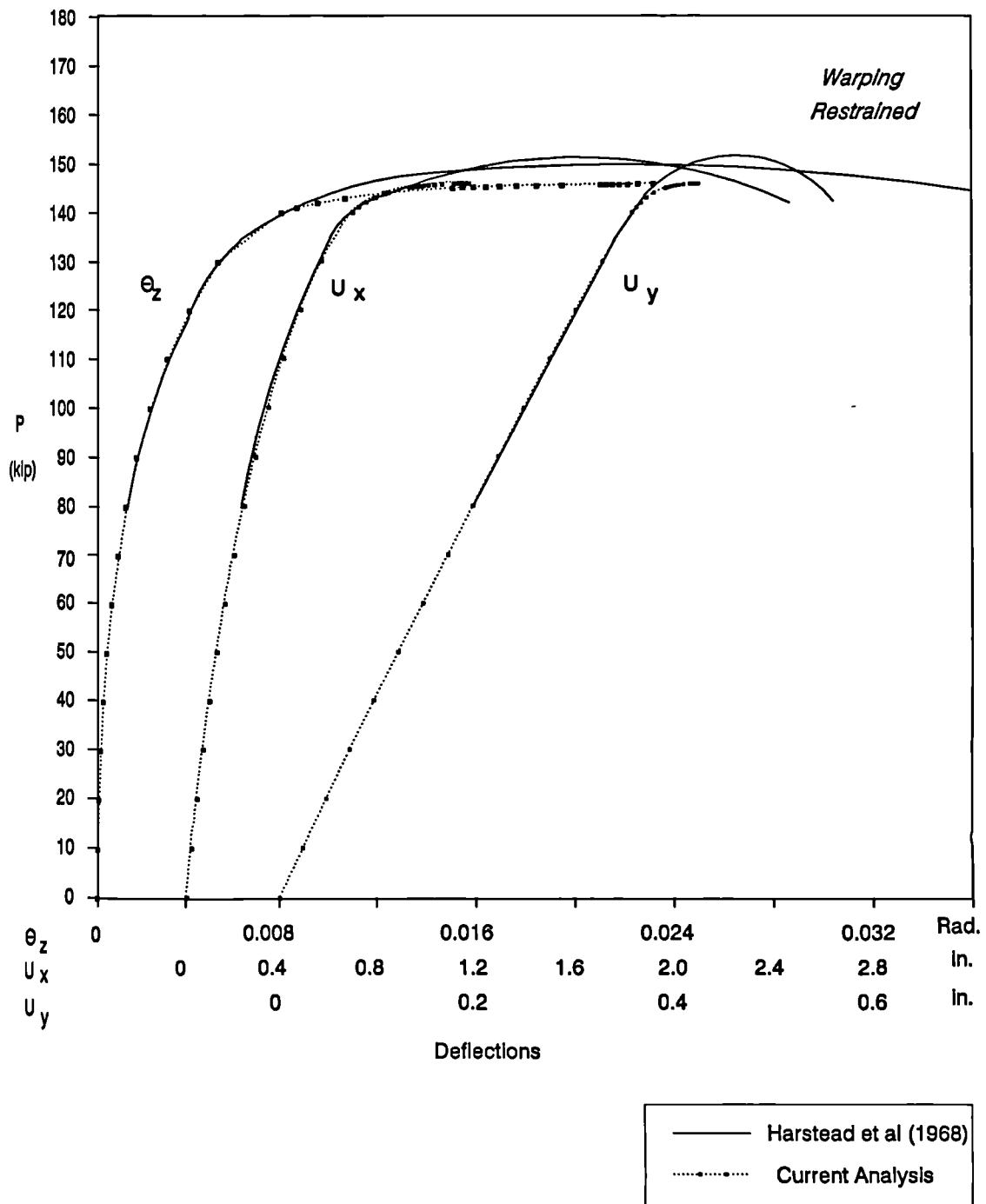
Fig. 4.14 Biaxially Loaded Column (Warping Restrained)

both analyses. It is useful to recall the results of comparing the current analysis with both second-order and third-order analyses for this purpose (Fig. 4.9). It is likely that the mentioned reduction in the predicted ultimate load is due to the inclusion of high order terms in this formulation.

4.5.2.5 Experimental Validation

Several experiments on biaxially loaded columns were carried out by Birnstiel (1968) at New York University. Results for the ultimate loads of twelve experiments were reported in his paper, along with the full observations for two columns out of the twelve. All columns were reported to have extended end-plate connections, hence restraining warping at both ends. Axial load was applied in each case with eccentricities in the directions of both principal axes. Eccentricities as reported in these experiments were not necessarily the same at both ends. Initial out-of-straightness data was measured for all columns and implemented in the analysis. The current program was used to analyse the twelve columns. The ultimate loads obtained from experiments and analyses are given in Table 4.1.

Specimen No.	*Nominal Size*	*YielStress Kip/in²*	*Top*		*Bottom*		*Load(Exp.) Kip*	*Load(Anal.) Kip*	*Error %*
			e_x	e_y	e_x	e_y			
1	$6 \times 6\ H$	29.1	1.62	2.78	1.61	2.78	92.8	94.4	+1.7
2	$5WF18.5$	35.7	1.61	3.28	1.58	3.15	54.1	54.1	+0.0
3	$5WF18.5$	35.7	0.75	2.62	0.86	2.63	62.7	60.4	-3.7
4	$6WF25$	36.0	1.67	2.95	1.66	2.95	86.3	85.2	-1.3
5	$5 \times 5\ H$	37.5	2.36	3.24	2.36	3.10	49.6	53.8	+8.4
6	$5 \times 5\ H$	37.5	2.39	2.51	2.38	2.50	47.9	51.4	+7.3
7	$5 \times 6\ H$	38.0	-0.92	2.78	-0.85	2.87	76.6	84.8	+10.7
8	$5 \times 6\ H$	38.0	0.35	1.85	0.34	1.89	109.4	118.0	+7.9
10	$4 \times 8\ I$	33.3	0.20	2.60	0.18	2.61	85.0	78.8	-7.3
12	$5WF18.5$	34.2	-0.81	2.82	-0.74	2.75	51.0	57.2	+12.1
13	$4WF13$	62.1	0.50	2.67	0.34	2.77	46.1	44.75	-2.9
14	$4WF13$	63.0	0.82	2.36	0.84	2.34	38.7	41.1	+6.2

Table 4.1: Comparison between experimental and theoritical failure loads

The analytical failure loads compare very well with the experimental results for most of the columns, taking into account that residual stresses for columns, although measured, were not reported. Consequently, no residual stresses were considered in the analysis. The full load-deflection history from analysis for specimens 7 and 13 is shown on Figs. 4.15 and 4.16 along with the reported experimental observations. Analytical load-deflection curves compare well with experimental data for both specimens. Strains were measured at several locations of the tested columns. Mid-height experimental and analytical strains at the four corners of
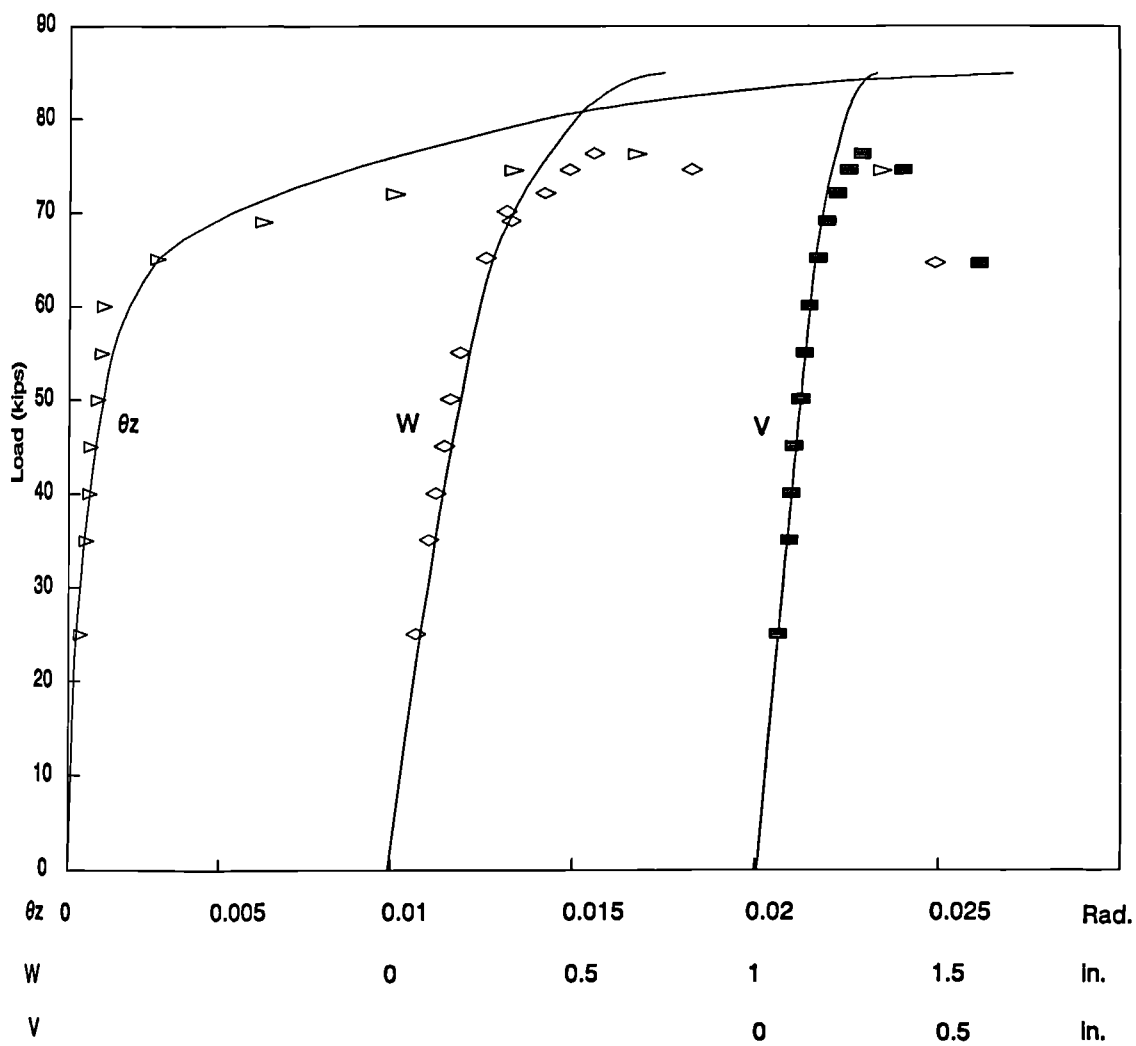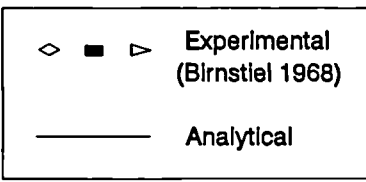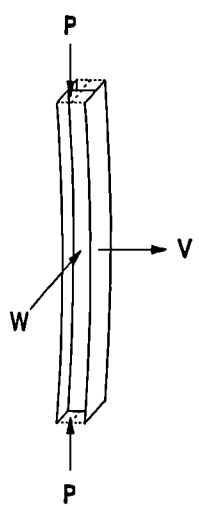
Fig. 4.15 Biaxially Loaded Column - Specimen 7 (Mid-Height Deflections)
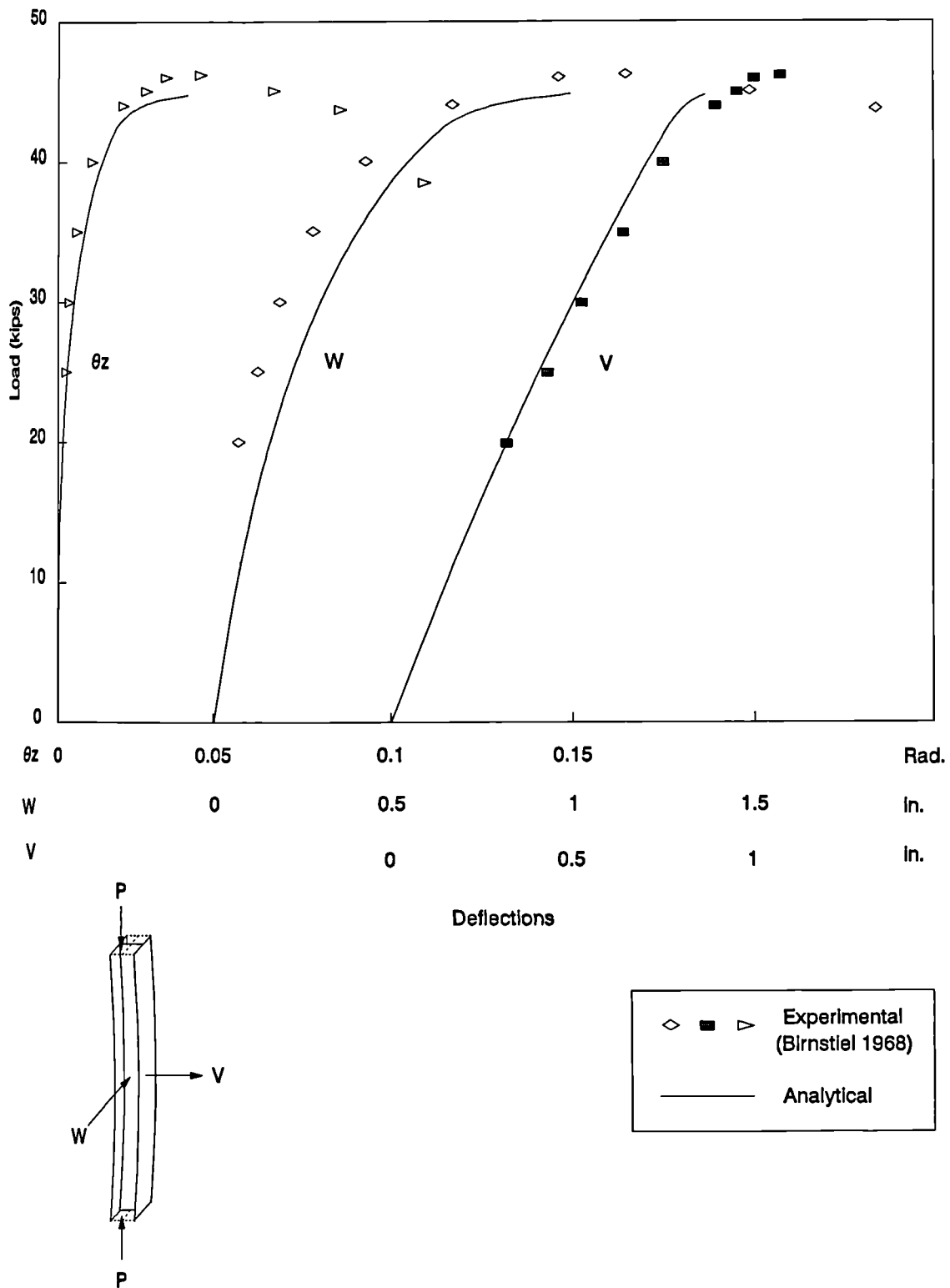
Fig. 4.16 Biaxially Loaded Column - Specimen 13 (Mid-Height Deflections)

the H cross-section are shown on Figs. 4.17 and 4.18. Again the analytical results correlate very well with the experimental measurements.

4.5.2.6 Framed Structures Validation

After assessing the current program's ability to analyse single structural members, it is necessary to do the same for framed structures. Morino and Lu (1971) have carried out several analyses on rigid space frames using a second-order elastic-plastic analysis. Two three-dimensional frames, one with a single storey and the other of two storeys, were selected to compare the current analysis with the previous one. Figs. 4.19 and 4.20 show both frames' geometry and the load-deflection curves for one location on each frame. Numbers on Morino's curves show the sequence of plastic hinge formation along with their locations on the frame as reported in the elastic-plastic analysis.

Results of both analyses compare very well up to the point where plasticity starts to penetrate the cross-section of the first predicted plastic hinge. Differences beyond this point are natural, due to the different approaches adopted by the analyses. The current analysis takes into account the spread of plasticity across the cross-sections of structural elements up to the point at which certain parts of the structure lose their stiffness producing singularity in the stiffness matrix. On the other hand, the previous analysis assumes elastic behaviour up to the point of instantaneous formation of a full plastic hinge, after which the analysis imposes a real mechanical hinge on the structure and continues assuming elastic response of the modified structure.
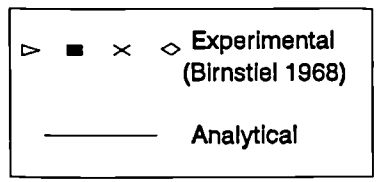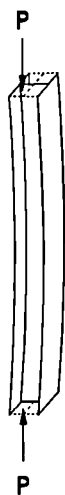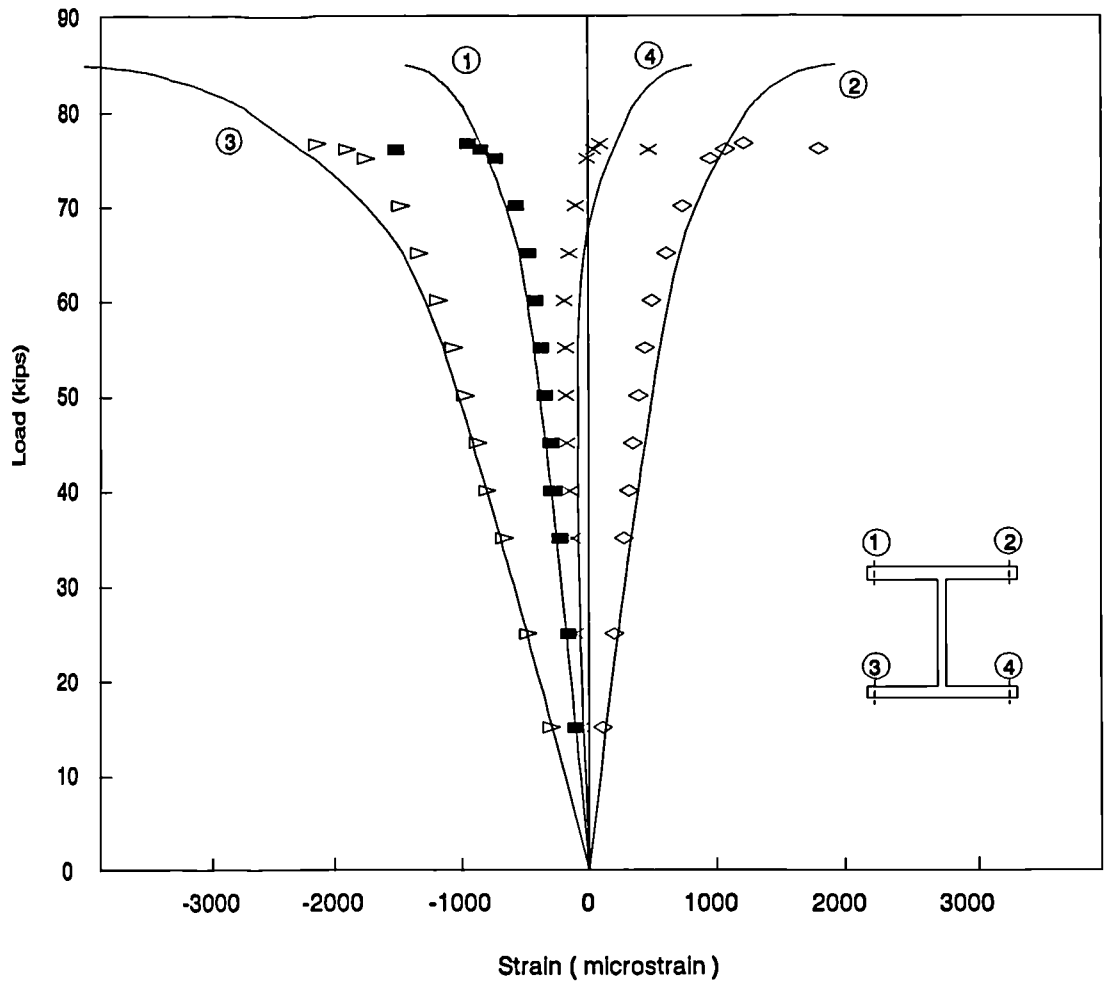
Fig. 4.17 Biaxially Loaded Column - Specimen 7 (Mid-Height Strains)
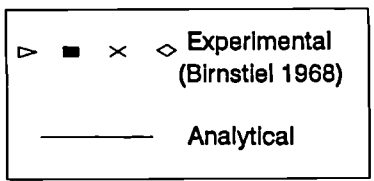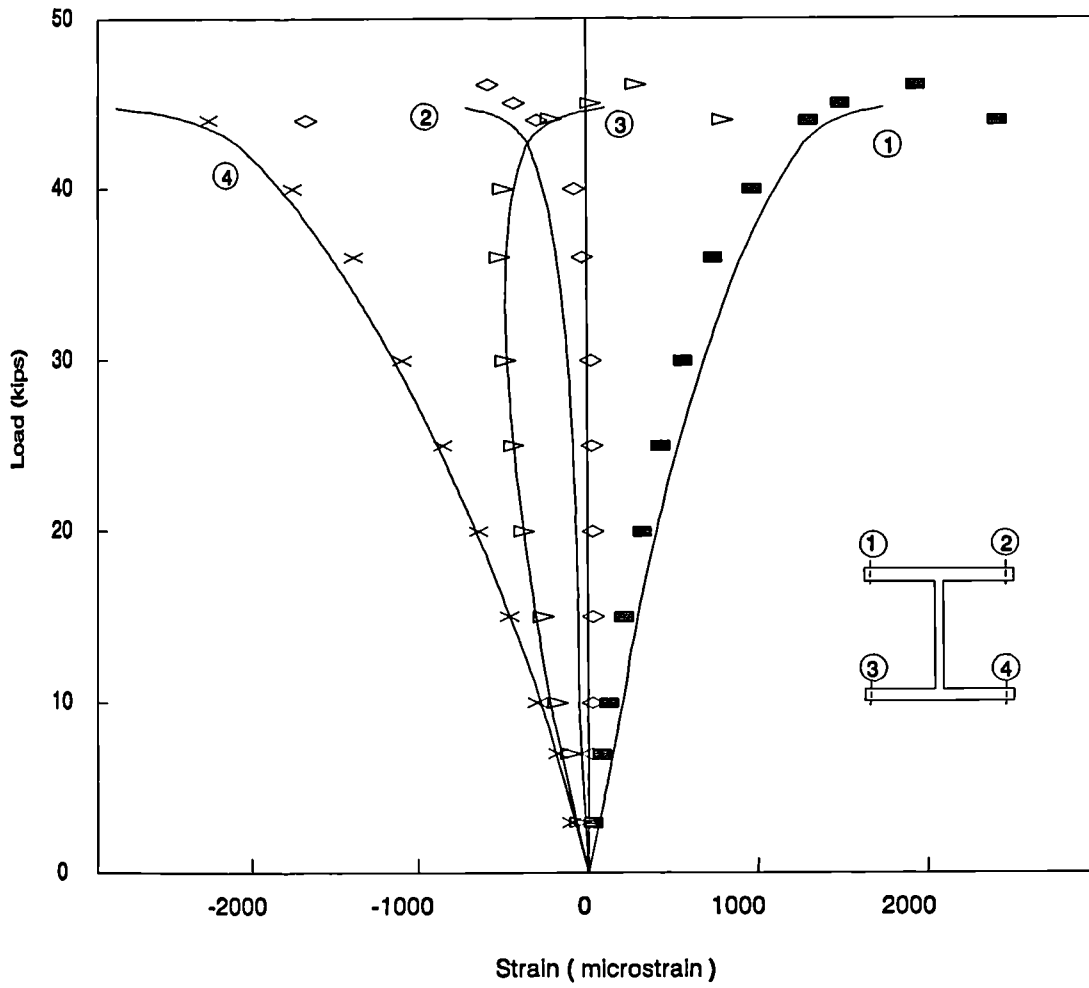
Fig. 4.18 Biaxially Loaded Column - Specimen 13 (Mid-Height Strains)
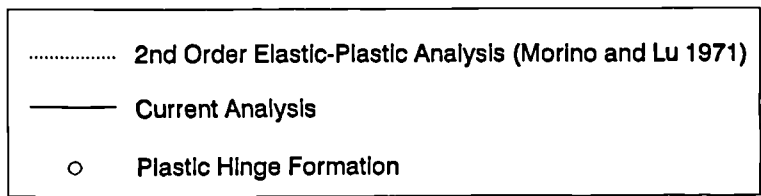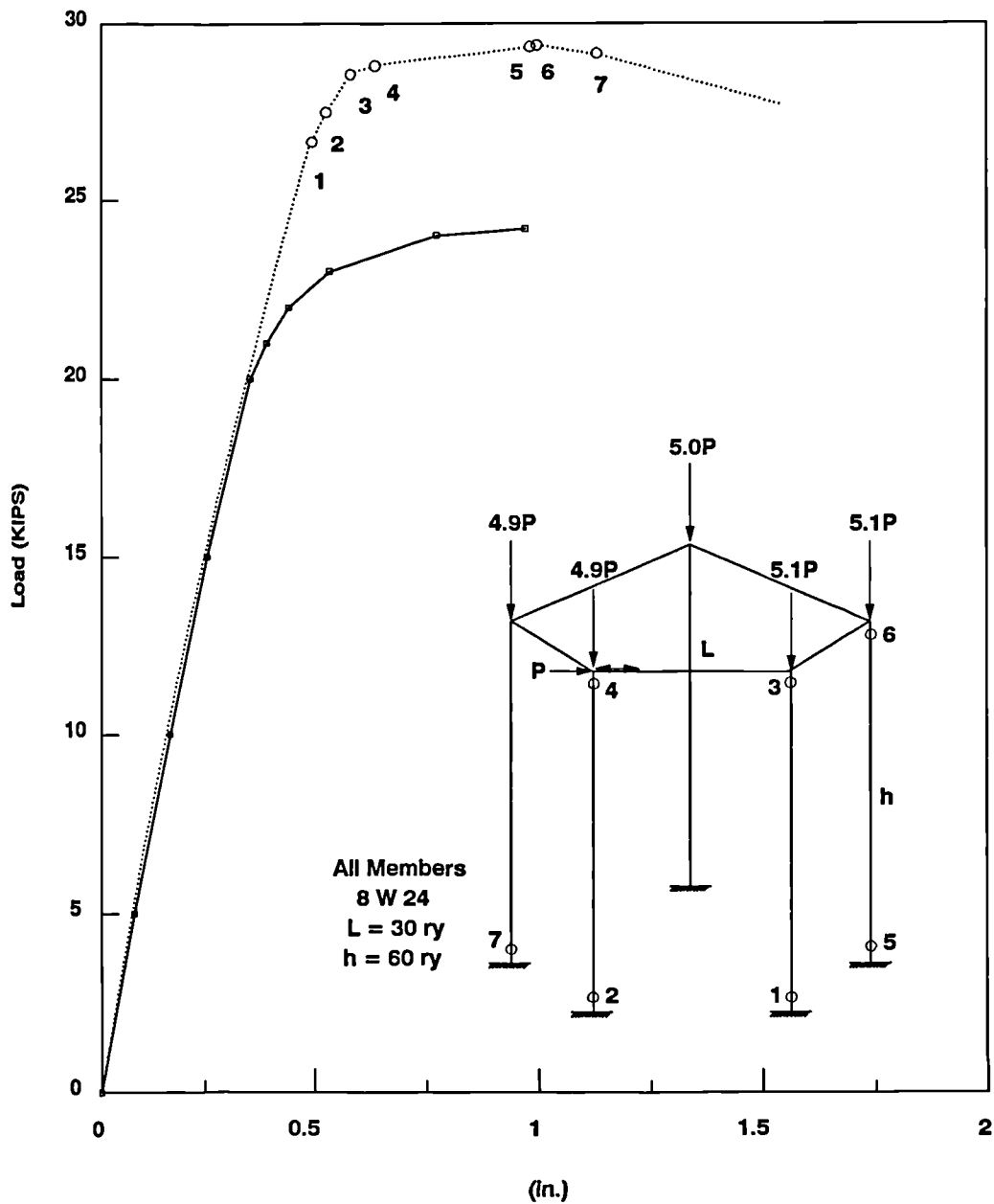
Fig. 4.19 One-Storey Space Frame
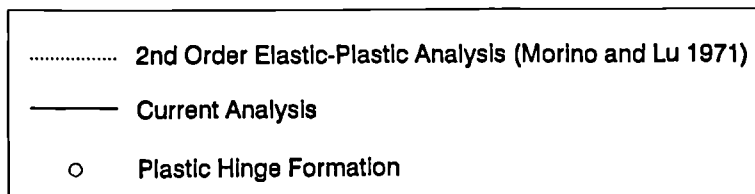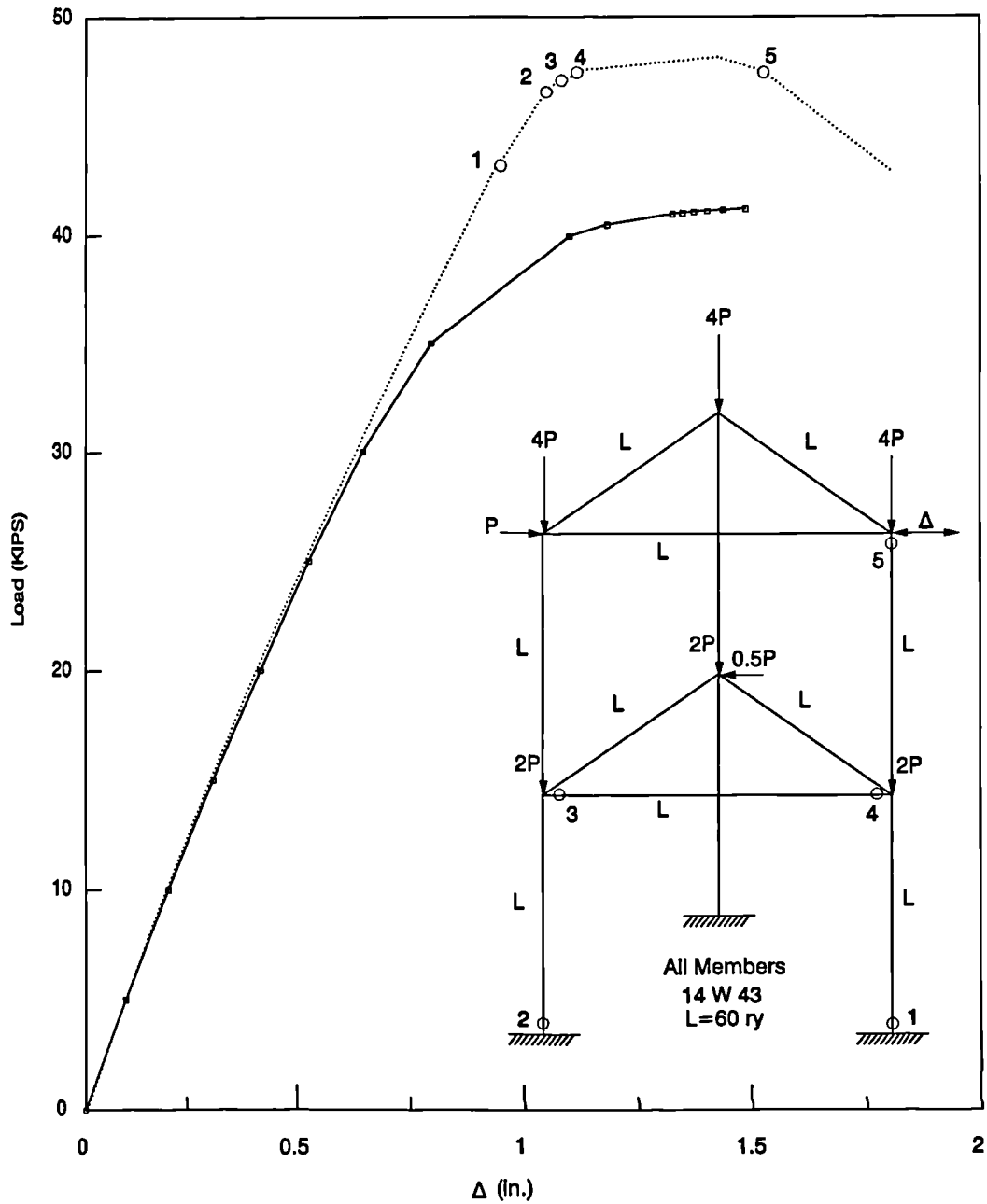
Fig. 4.20 Two-Storey Space Frame

4.5.3 Elevated Temperature Validation

The current program has been validated against previous analytical work and experiments for structures at elevated temperatures.

4.5.3.1 Analytical Validation:

Furumura (1978) developed a F. E. elastic-plastic-creep analysis for in-plane steel frames in fire. The temperature distribution assumed in this reference is illustrated in Fig. 4.21. Temperature distributions across the beam and column sections were obtained assuming structural elements to be fully protected. Three beam-columns were analysed with different end conditions, to compare the Furumura analysis with the present analysis. Figs. 4.22, 4.23 and 4.24 show the three cases and compare results obtained from both analyses. Very good agreement with the previous F.E. analysis is apparent. In this comparison out-of-plane behaviour of the beam-columns was ignored by restraining all degrees of freedom corresponding to out-of-plane deflections at all nodes. Four finite elements were used to model each of the three beams.

In the same reference, the author analysed one portal frame and two subframes. Geometry and loadings of these frames are given in Fig. 4.25. On Figs. 4.26, 4.27 and 4.28 deflections and internal forces as predicted by both analyses are shown. In all comparisons with Furumura's analysis, his assumed stress-strain characteristics for steel at elevated temperatures were used. Furumura also developed a formula for thermal expansion within which he added terms for thermal creep. The three beam examples were solved using both analyses, ignoring the effect of creep, hence the pin-point agreement between both of them. The three frames were solved by
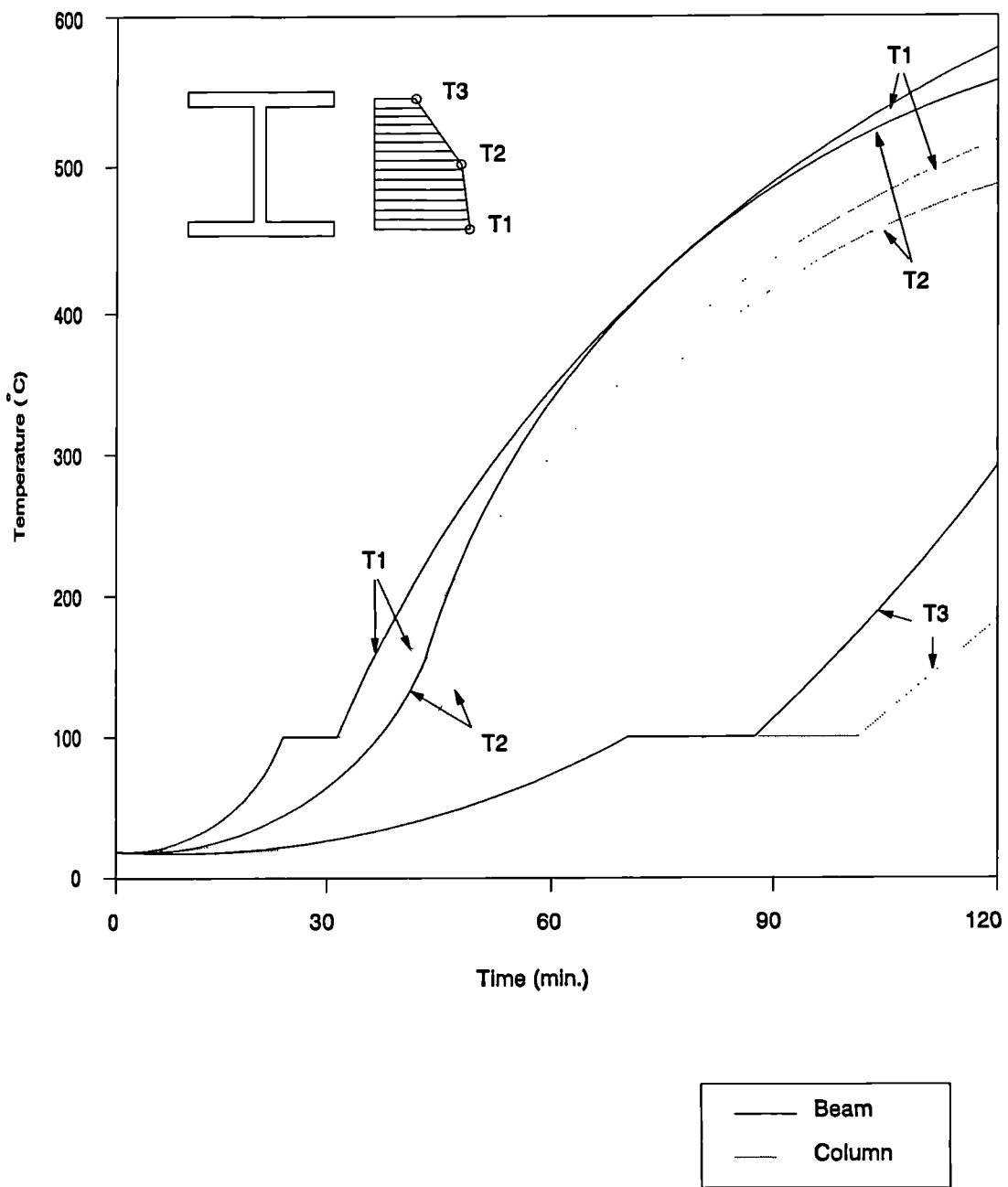
Fig. 4.21 Temperature Profiles for Beam and Column Sections
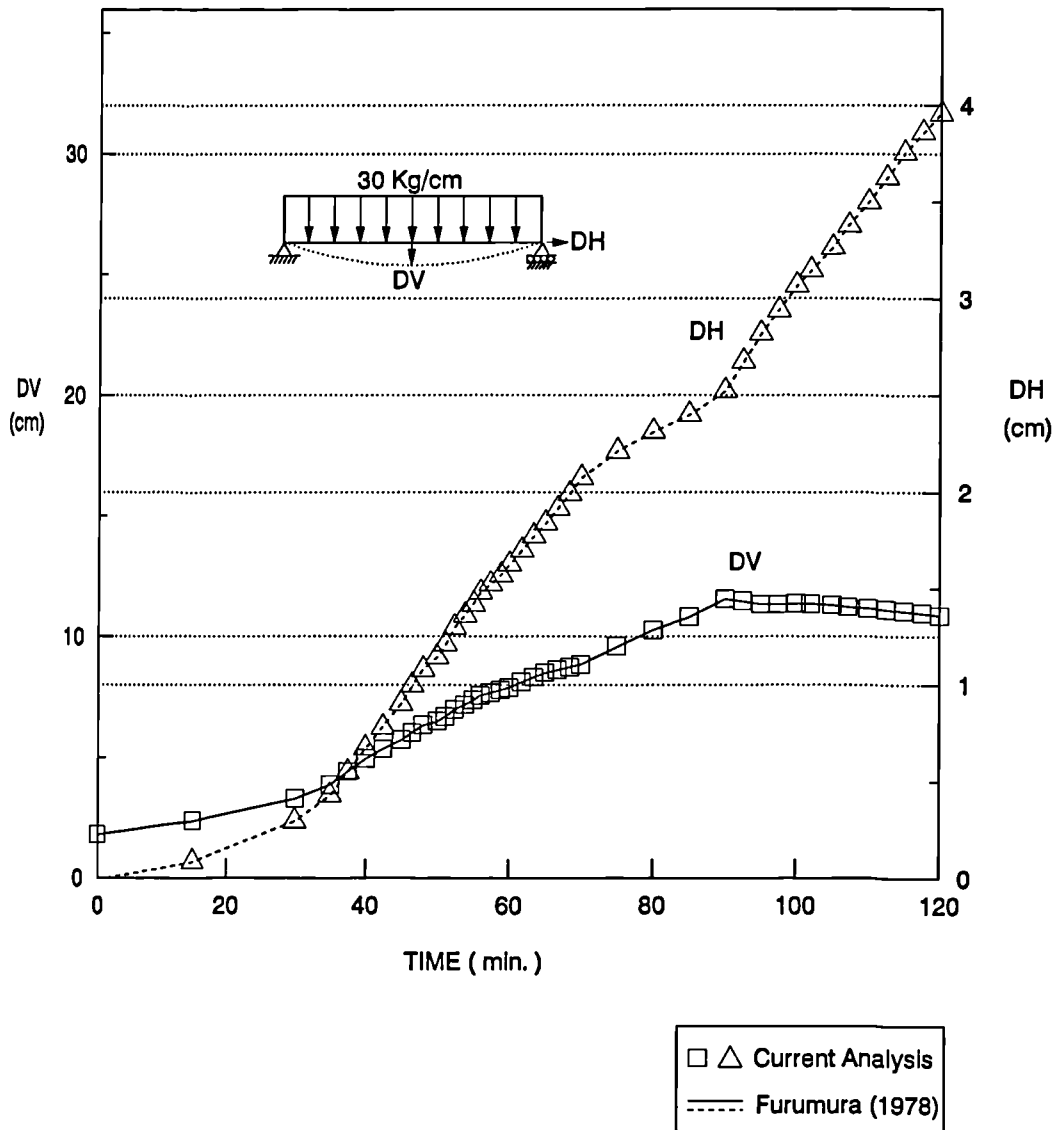
Analysis of Simply Supported Beam Subject to Non-uniform Temperature Profile
Compared to Furumura (1978) Analysis.

Fig. 4.22 Analytical Comparison (Beam Case 1)
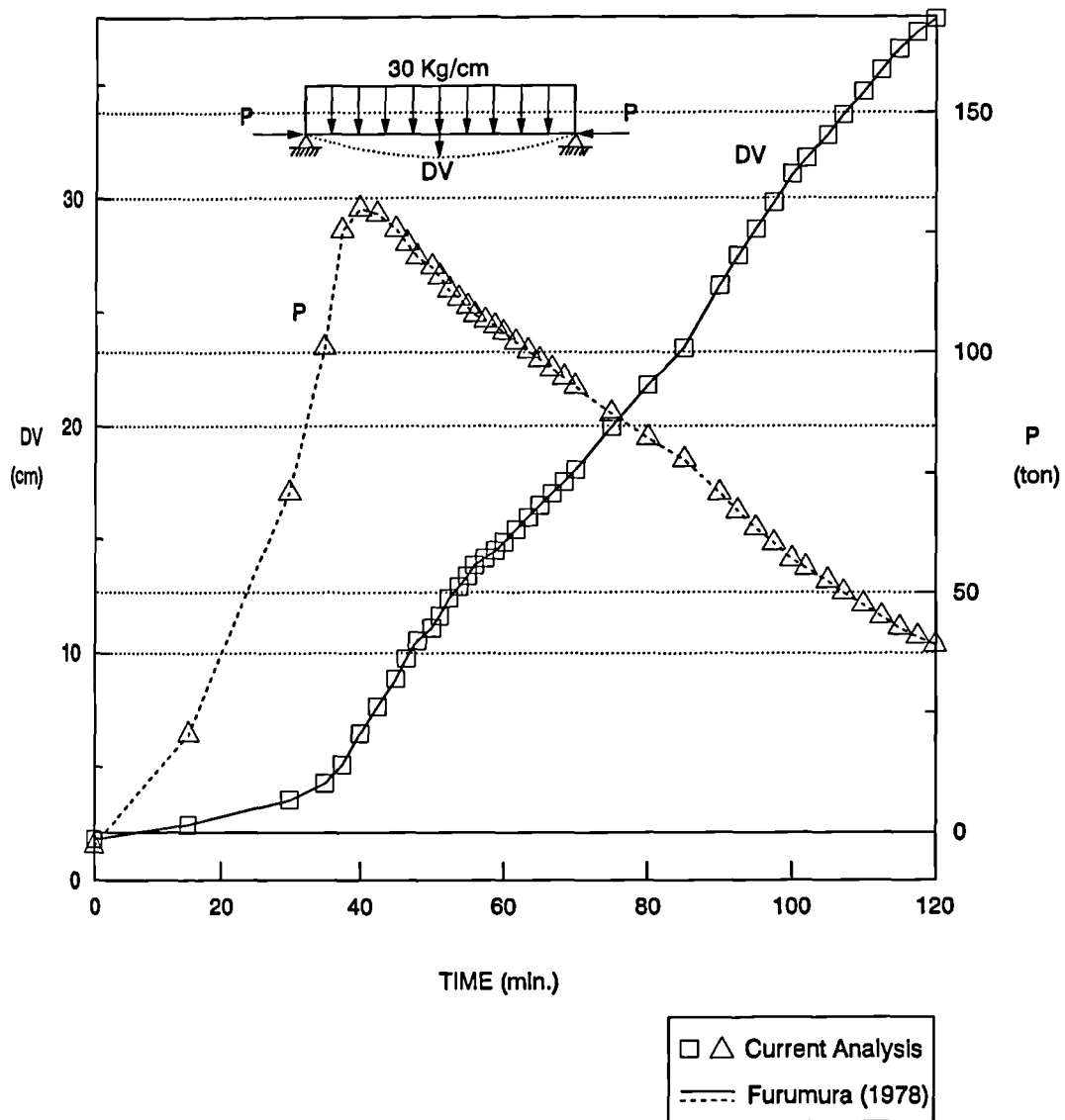
Analysis of Hinge-Ended Beam Subject to Non-uniform Temperature Profile
Compared to Furumura (1978) Analysis.

Fig. 4.23   Analytical Comparison (Beam Case 2)
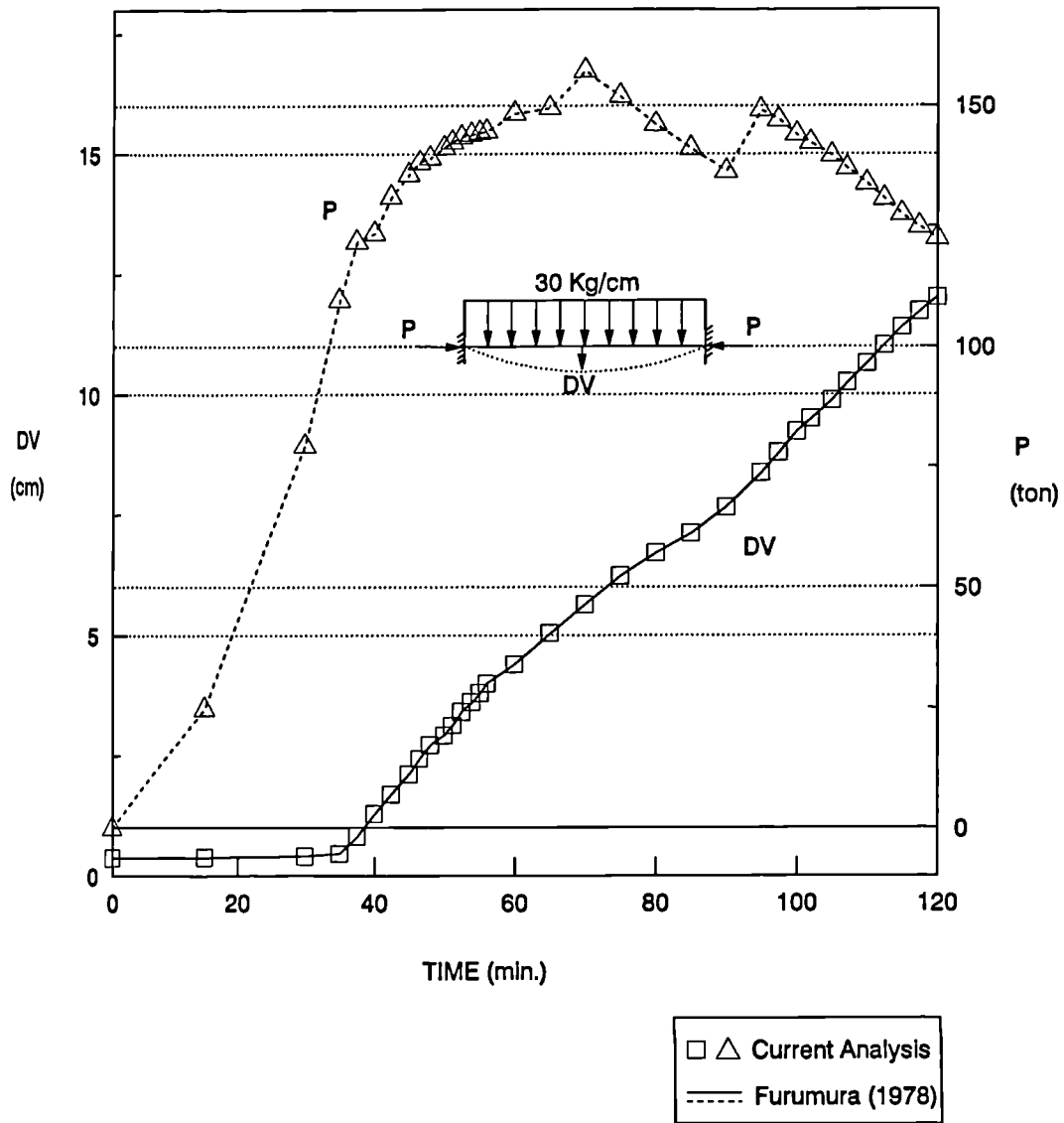
Analysis of Fixed-Ended Beam Subject to Non-uniform Temperature Profile
Compared to Furumura (1978) Analysis.

Fig. 4.24   Analytical Comparison (Beam Case 3)
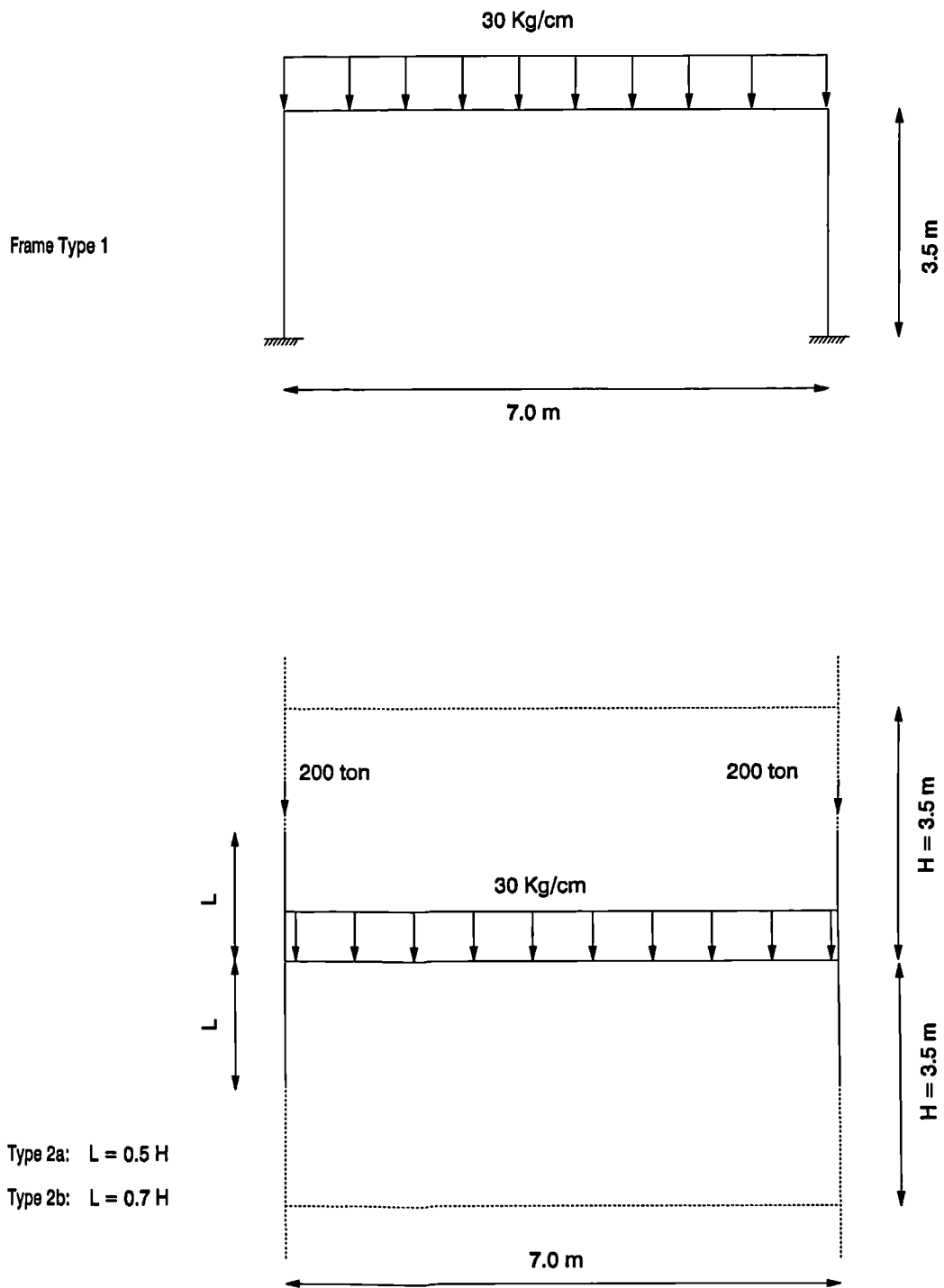
Fig. 4.25 Loading and Dimensions of Furumura (1978) Frames
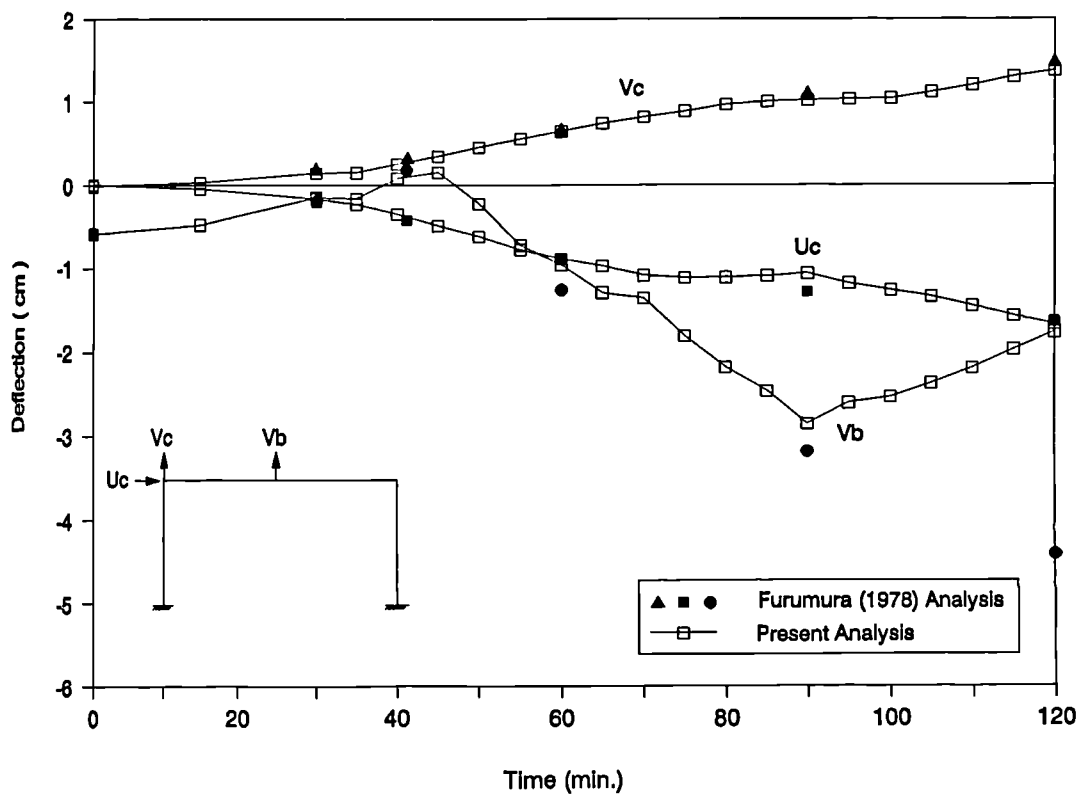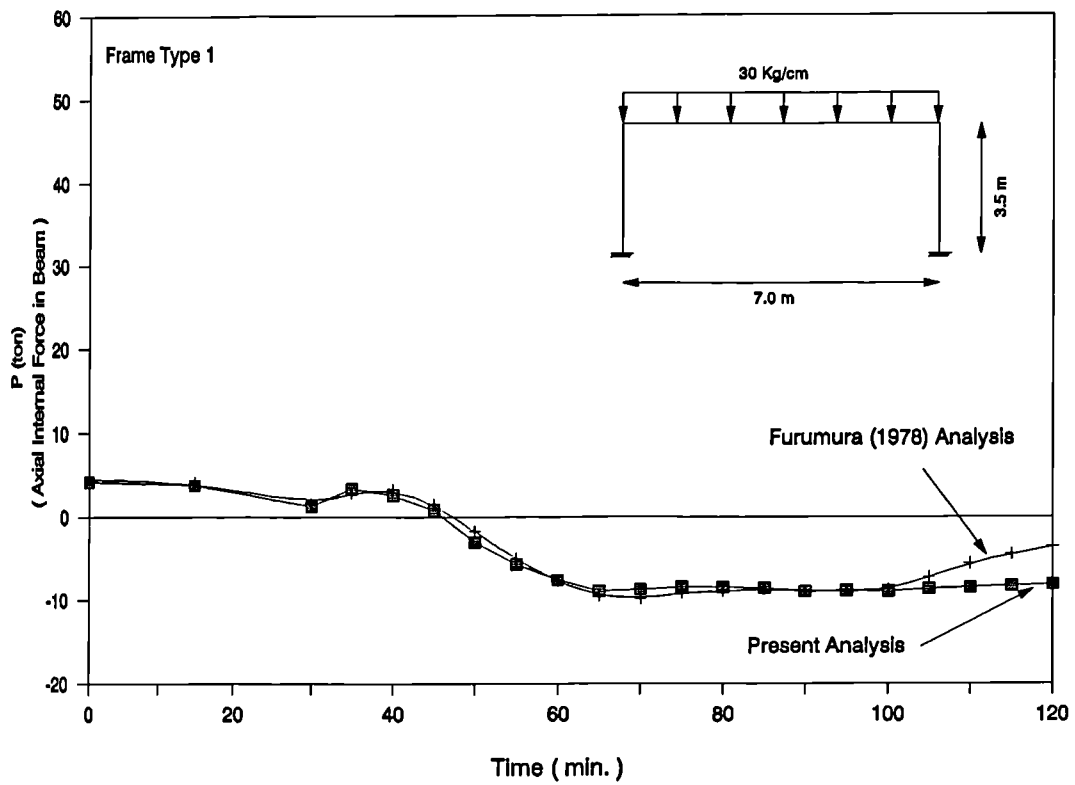
Fig. 4.26 Analytical Comparison (2D Frame Type 1)
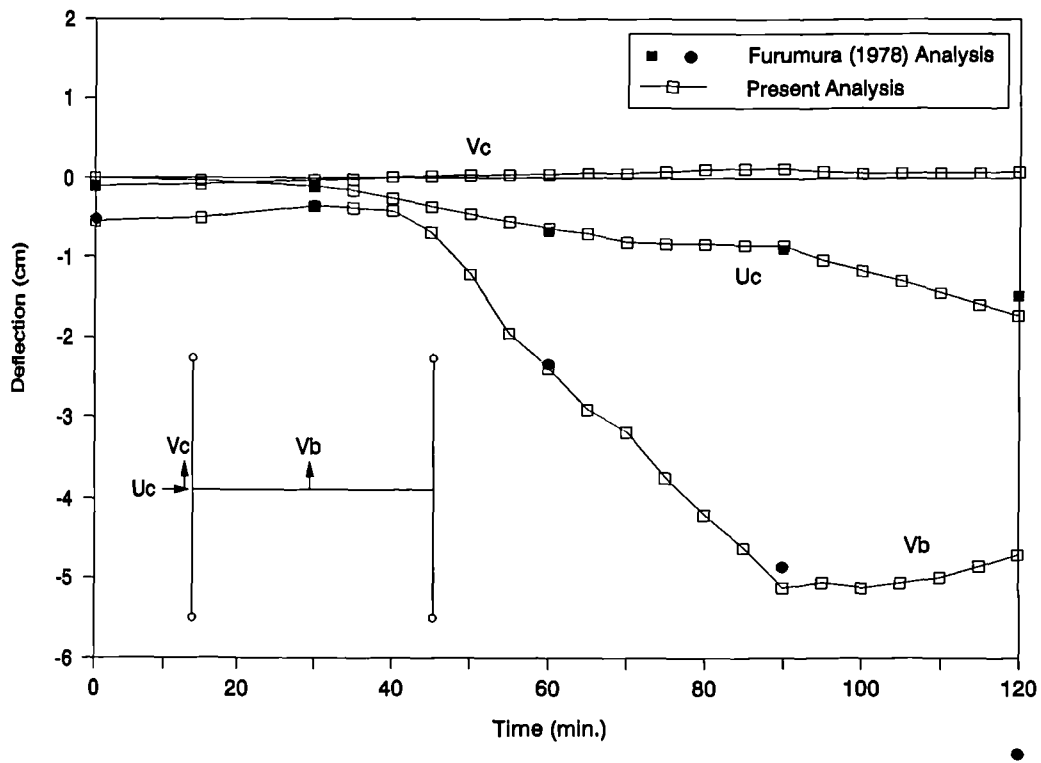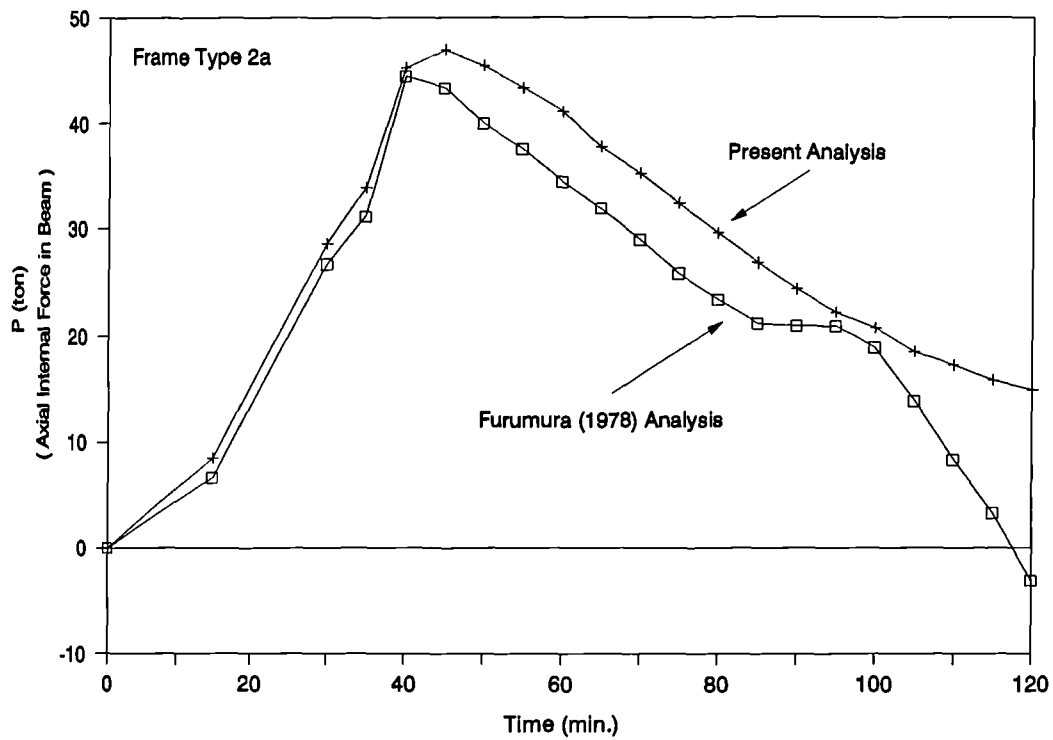
Fig. 4.27   Analytical Comparison (2D Frame Type 2a)
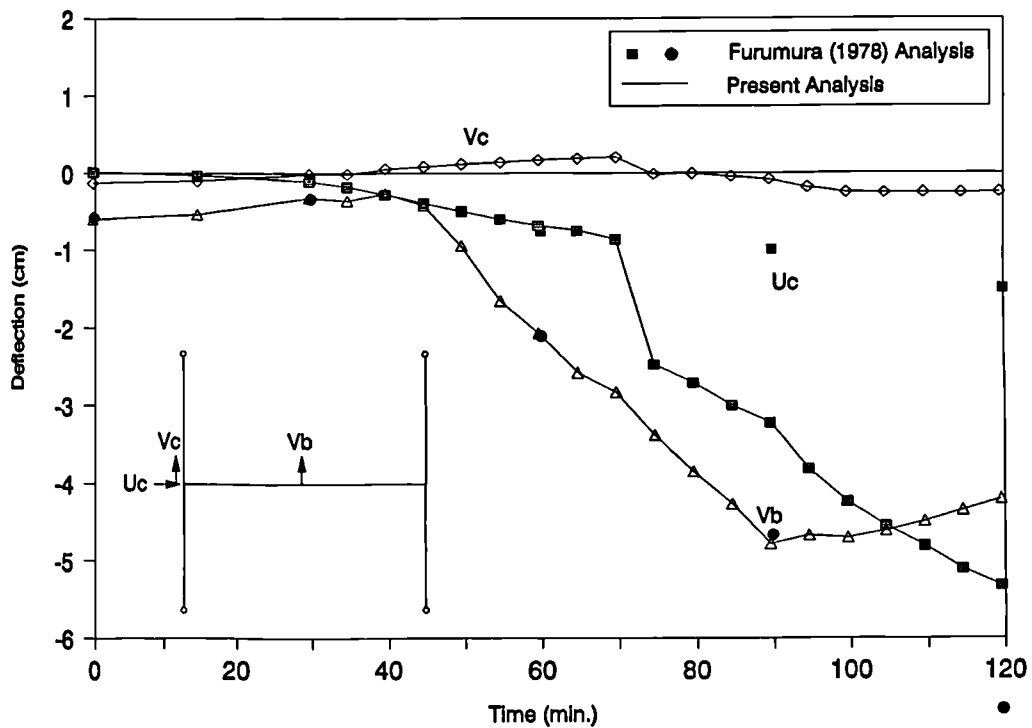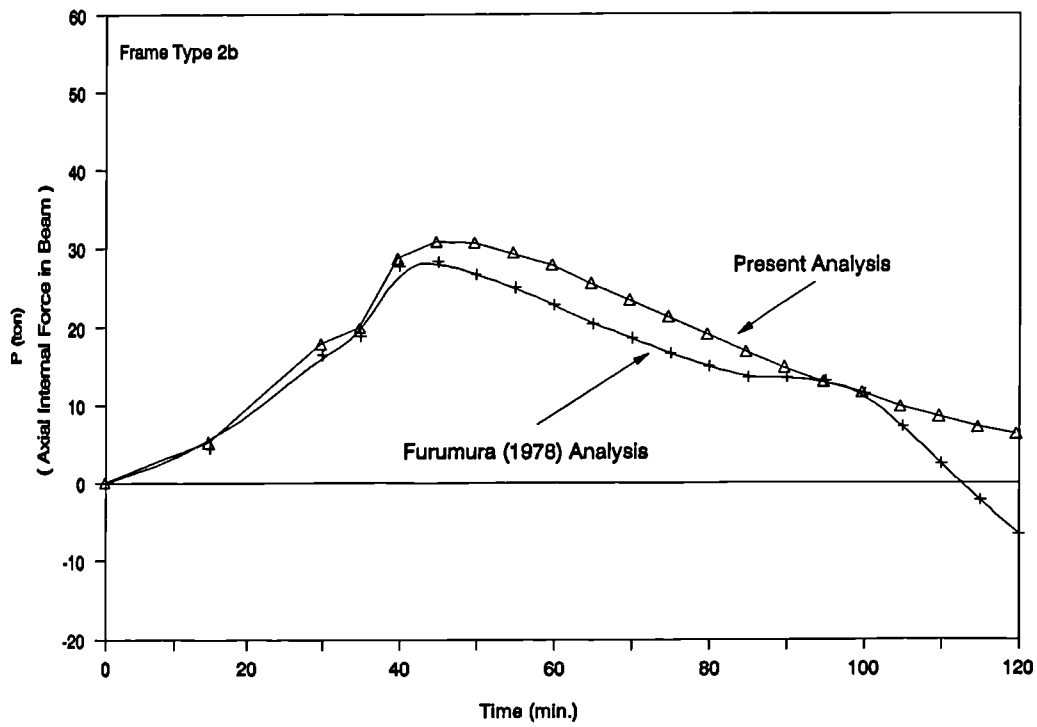
Fig. 4.28   Analytical Comparison   (2D Frame Type 2b)

Furumura including the effect of thermal creep. Since the current analysis does not account for creep, the results are subject to some discrepancy, especially towards the end of the heating scheme. In particular the difference between internal axial forces using both analyses is an apparent result of the creep effect. In the full portal frame case differences between the analyses are insignificant up to a time of 100 minutes, after which the predicted internal force in the beam becomes higher in the present analysis. In both subframes and the full frame it is reasonable that this analysis should overestimate the thermally-induced internal force in the beam, as the absence of creep makes the structure stiffer and capable of sustaining higher levels of internal forces. Consequently, the apparent agreement of both analyses in deflection terms is partly coincidental. The present analysis is expected to yield deformations less than the creep case, but higher internal compressive forces, meaning that the $P - \Delta$ effect contributes to higher deflections. As a result, the opposing effects of both factors have cancelled one another and produced almost the same deflections using non-creep analysis as those produced by creep analysis. The degree of agreement between the analyses is still remarkable and indicates the limited effect of thermal creep on the structural response.

4.5.3.2   Experimental Validation

Many experiments on heated columns have been carried out in continental Europe. A collection of 58 experiments was summarised by Janss and Minne (1982). In Belgium two series of experiments were reported by Vandamme and Janss (1981). The first series consisted of eleven short columns with a slenderness ratio of 25, with different cross-sections and applied loads. The second series of eighteen columns had slenderness ratios between 25 and 102. The actual yield stress was measured

for each column only in the second series. All columns were tested under constant load, and temperature was increased up to failure. In Denmark twelve columns were tested by Olesen (1980) horizontally in a furnace where temperatures were maintained at a constant level and loads increased up to failure. In Germany seventeen columns were tested vertically by Hoffend (1980) with an eccentrically applied load. Temperatures were kept constant while loads were increased up to failure. In France Aribert and Aribert and Randriantsara (1980) carried out two series of tests on fifteen columns. All these columns had a slenderness ratio of 72 with different load ratios. The first series consisted of eight columns maintained at a constant temperature while loads were increased up to failure. In the second series constant loads were applied while temperatures increased up to failure. Analyses were carried out using program 3DFIRE for all these tests. All columns were assumed to have an initial out-of-straightness about both principal axes according to BS449. Loads or temperatures were increased as appropriate in the analysis up to failure. Data and results of the tests, along with analytical results, are shown in tables 4.2, 4.3 and 4.4.

Nominal Size	Slenderness Ratio	Yield Stress N/mm^2	Applied Stress N/mm^2	Ult. Stress N/mm^2	Load Factor BS449	Failure Temp Exp.	Failure Temp Ana.
HEA 300	25.23	235 *	137.3	230.3	0.6	610	504
HEA 300	25.23	235 *	137.3	230.3	0.6	553	504
HEA 300	25.23	235 *	137.3	230.3	0.6	541	504
HEA 300	25.23	235 *	137.3	230.3	0.6	559	504
HEB 300	24.93	235 *	157.0	230.4	0.68	492	466
HEB 300	24.93	235 *	167.6	230.4	0.76	444	410
HEB 300	24.93	235 *	157.0	230.4	0.68	510	466
HEB 400	25.54	235 *	157.0	230.1	0.68	578	466
HEB 300	24.93	235 *	157.0	230.4	0.68	498	466
HEB 300	24.93	235 *	157.0	230.4	0.68	582	466
HEB 300	24.93	235 *	150.5	230.4	0.65	560	480
HEB 300	24.93	274	134.1	268.5	0.50	588	548
IPE 160	102.72	272.5	56.5	133.5	0.42	564	527
IPE 160	102.72	272.5	75.3	133.5	0.56	486	444
IPE 200	84.83	272	69.9	173.8	0.40	559	532
IPE 200	84.83	272	93.3	173.8	0.54	394	445
HEB 120	61.76	266.5	104.7	222.6	0.47	519	516
HEB 120	61.76	266.5	78.5	222.6	0.35	561	566
HEB 180	41.36	279	92.3	261.8	0.35	616	590
HEB 180	41.36	279	136.8	261.8	0.52	560	524
HEA 200	37.95	261	125.8	248.0	0.51	565	518
HEA 300	25.23	267.5	133.9	262.0	0.51	561	539
HEA 220	34.75	252	162.2	241.8	0.67	502	467
HEB 200	37.77	218	89.9	207.6	0.43	549	548
IPE 200	85.49	272	117.0	172.2	0.68	250	324
HEB 140	53.49	247	132.6	219.7	0.60	516	422
HEB 140	53.49	247	90.9	219.7	0.41	576	548
IPE 220	72.22	273	91.9	205.0	0.45	522	499
IPE 220	72.22	273	118.5	205.0	0.58	508	418

* Nominal Value

Table 4.2: Belgian experiments.

Nominal Size	Slenderness Ratio	Yield Stress N/mm^2	Applied Stress N/mm^2	Ult. Stress N/mm^2	Load Factor BS449	Failure Temp Exp.	Failure Temp Ana.
HEA100	144	275 *	86	74.87	1.15	200	20
HEA100	143	275 *	67	75.83	0.88	400	239
HEA100	143	275 *	36	75.83	0.48	550	508
HEA100	143	275 *	62	75.83	0.82	440	272
HEA100	167	275 *	29	56.76	0.51	550	493
HEA100	166	275 *	58	57.41	1.01	400	20
HEA100	167	275 *	50	57.76	0.88	460	236
HEA100	167	275 *	60	57.76	1.06	200	20
* Nominal Value							

Table 4.3: Danish experiments.

Nominal Size	Slenderness Ratio	Yield Stress N/mm^2	Applied Stress N/mm^2	Ult. Stress N/mm^2	Load Factor BS449	Failure Temp Exp.	Failure Temp Ana.
HEA100	72	300	188.0	223.7	0.84	200	228
HEA100	72	300	158.4	223.7	0.71	365	283
HEA100	72	300	149.4	223.7	0.67	400	328
HEA100	72	300	117.5	223.7	0.53	510	449
HEA100	72	300	67.2	223.7	0.30	550	592
HEA100	72	300	51.69	223.7	0.23	600	635
HEA100	72	300	28.67	223.7	0.13	680	722
HEA100	72	300	26.79	223.7	0.12	750	729
HEA100	72	300	169.2	223.7	0.76	235	266
HEA100	72	300	150.4	223.7	0.67	440	328
HEA100	72	300	117.5	223.7	0.53	450	450
HEA100	72	300	94.0	223.7	0.42	480	519
HEA100	72	300	70.5	223.7	0.32	552	582
HEA100	72	300	47.0	223.7	0.21	618	648
HEA100	72	300	22.6	223.7	0.10	701	748

Table 4.4: French experiments.

Although all these experiments involved single columns, both experiments and analyses were conducted in a three-dimensional sense, as no restraints were imposed about either principal axis in any of the experiments. Consequently, the analysis assumes a full 3-D behaviour and initial out-of-straightness was imposed in both principal axis directions according to BS449. Predicted analytical failure temperatures are plotted against the experimental ones on Fig. 4.29. This figure shows that for a considerable number of columns experimental and analytical results lie around the 45° line which represents exact agreement between experiment and analysis. It can also be noticed that where a nominal value of the yield stress is the only one quoted experimental critical temperatures are much higher than analytical predictions.

It is not surprising that there should be a large variation in test results. Even at ambient temperature considerable scatter is observed in series of column tests. The encouraging aspect of the present comparison is that the test results straddle the analytical line very well over most of the range. If imperfection values had been quantified in the tests, and if effective lengths could be properly estimated, then the comparison might be considerably better.

The noticeable outcome from this comparison is the conservative predictions of the present analysis for many columns compared with the experimental results. Although the finite element method is supposed to provide upper bound solutions to physical problems, in this particular case two main factors contributed to the opposite. Actual imperfections were not reported for all columns considered, which has resulted in the assumption of the Code value of imperfection which represents a lower bound value. The other factor is the stress-strain characteristics used which are also based on lower bound rationalisation of experimental data.
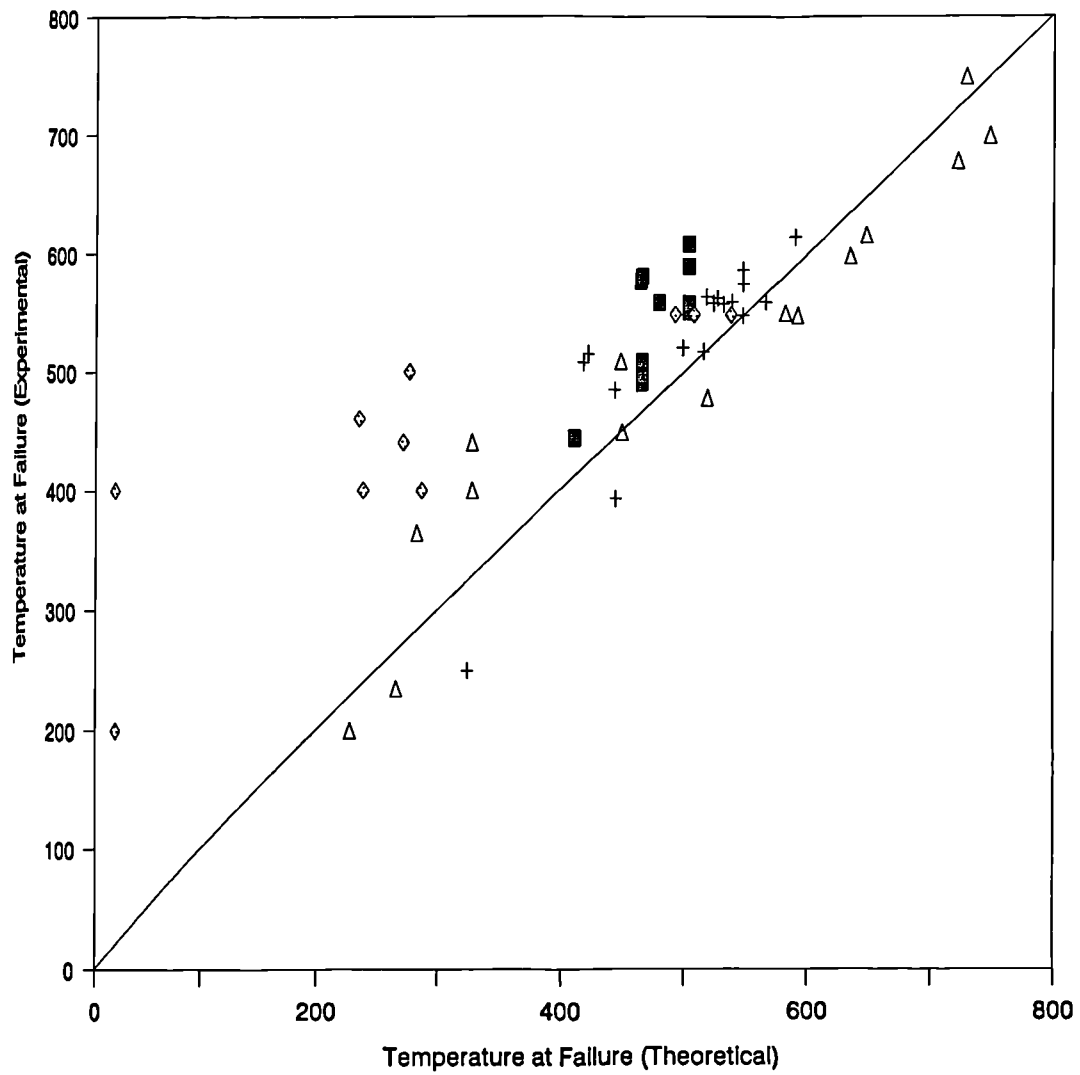
Fig. 4.29 Analytical and Experimental Results for European Tests

The program was also validated against two experiments carried out by British Steel. Both columns were constructed within block/brick walls, with one flange only exposed to fire. To overcome the problem of the end conditions which were reported to have some degree of fixity, the program was used twice for each experiment. The column under consideration was assumed first to be simply supported, and then it was assumed to have one of its ends fixed. It can be seen clearly from the comparison with analysis that the experimental results lie somewhere between these two extremes. No imperfections were considered in the analysis, as no such measurements were reported from these experiments. Figs. 4.30 and 4.31 show the analytical and experimental results for both columns. Although the survival time is clearly rather at variance with the experimental observation, the general form of the behaviour is certainly shown correctly, and the test behaviour is not seen to be really consistent in some respects towards the end of the test.

Cooke and Latham (1987) reported on a full size three-member frame that was tested by the Fire Research Station at the Cardington laboratory. The portal frame consisted of 203 × 203 × 52 columns and a 406 × 178 × 54 beam. The frame was mainly unprotected apart from columns' webs, which were protected by blocking-in. The top flange of the beam was also partially protected by precast concrete slabs. Provision was made to prevent any composite action between the beam and slabs. This frame was analysed using the measured temperature profiles at various parts of the frame. The initial yield stress was assumed to be $275 N/mm^2$ as a nominal value for the steel used in test (grade 43A), since no measured value was reported. Experimental results as reported by Cooke and Latham (1987) are compared with analytical results on Fig. 4.32. The results agree remarkably up to the start of failure where the analysis overestimates deflections. This could be a result of an underestimated yield stress of the steel.
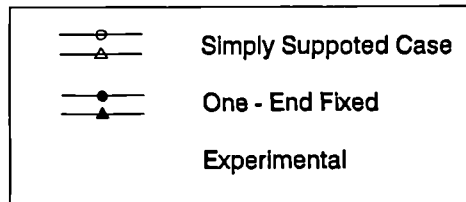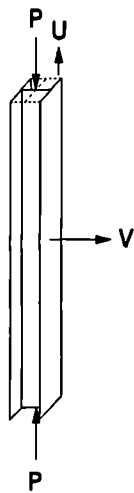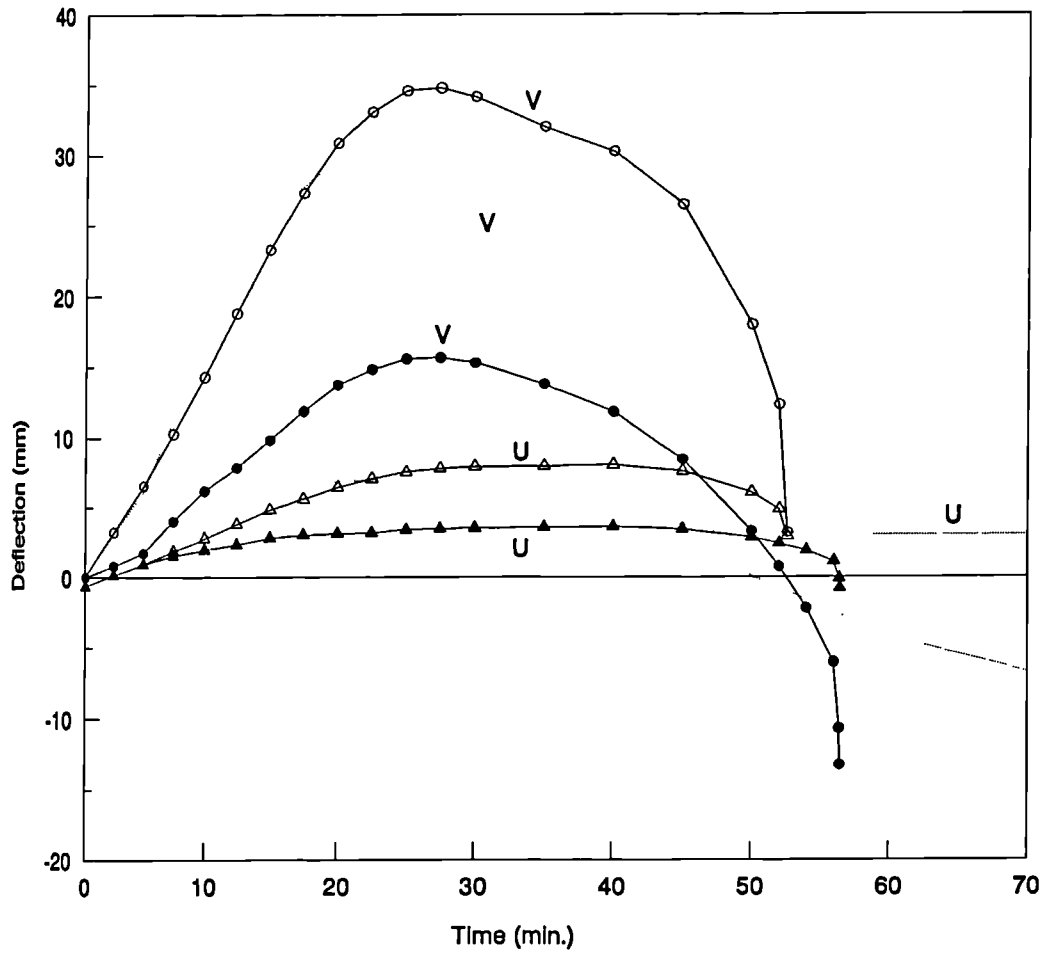
Fig. 4.30   British Steel Experiment - 52
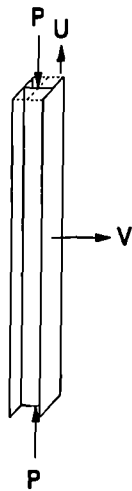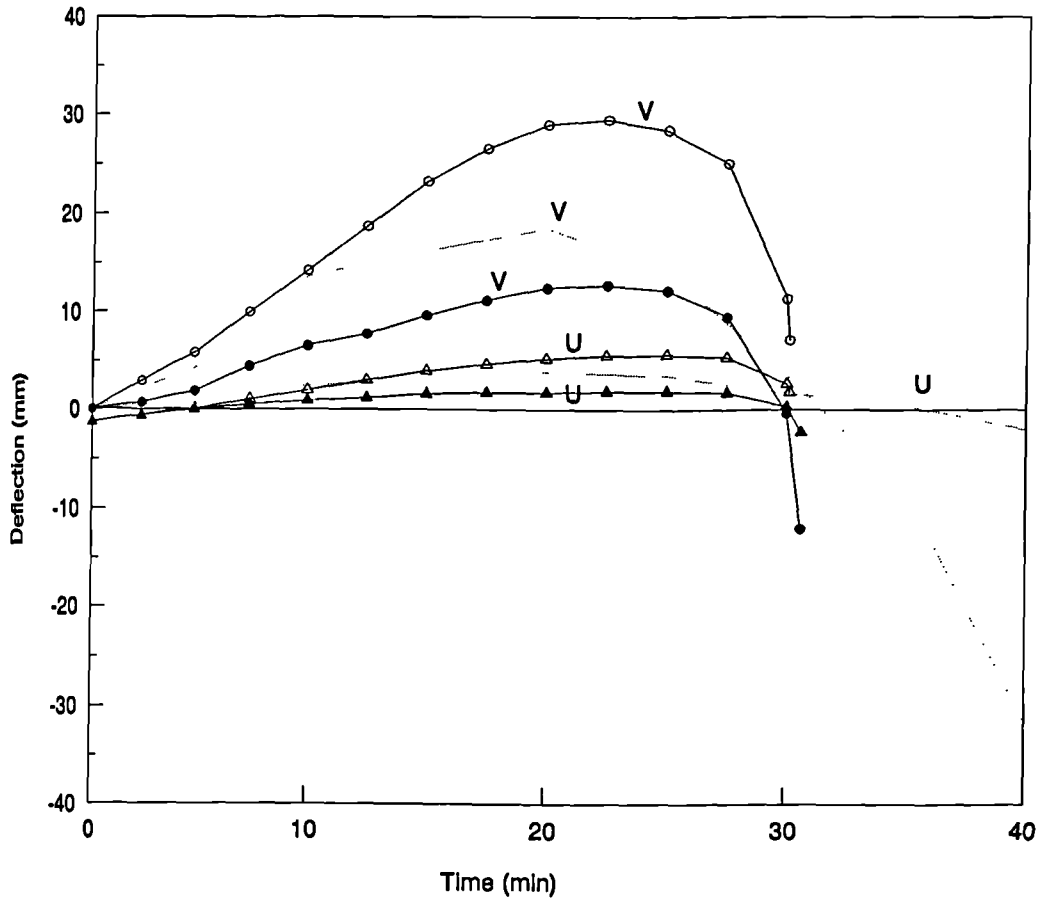
Fig. 4.31   British Steel Experiment - 53
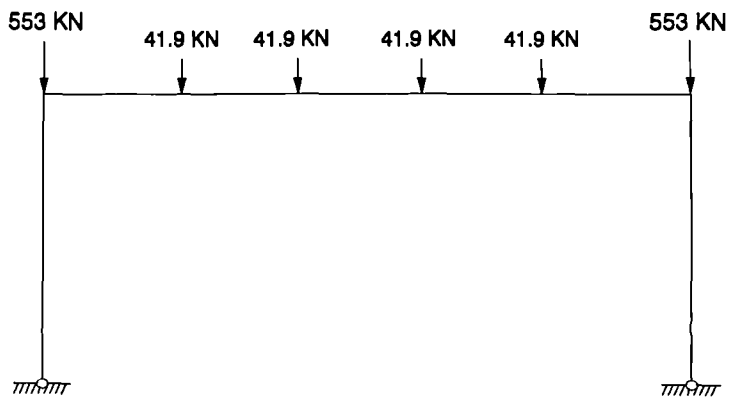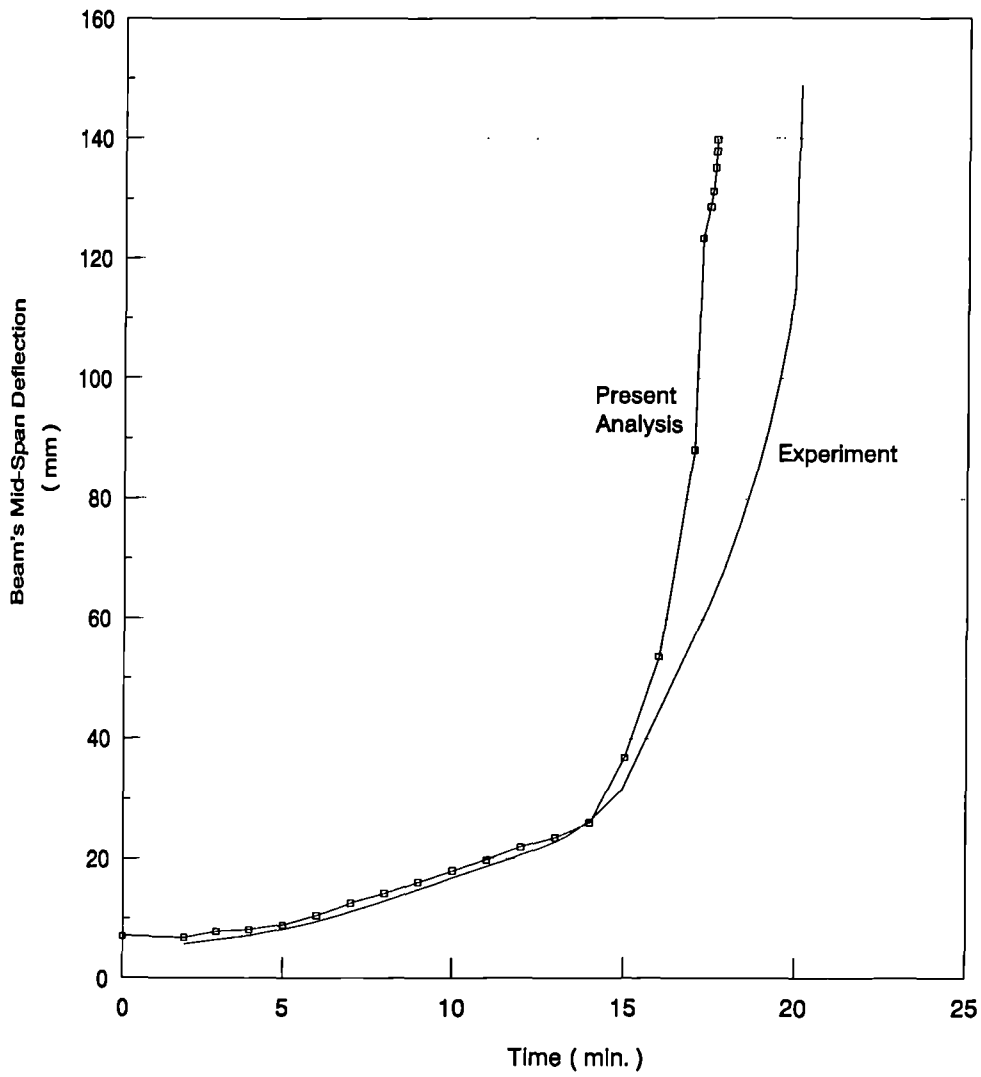
Fig. 4.32 Cardington Frame - 1986

In a retrospective analysis Franssen et al (1993) attempted to analyse this frame using different values for the yield stress. The value of $408 N/mm^2$ gave the nearest correlation with experimentally observed deflections (Fig. 4.33).

4.6 Conclusions

All the aforementioned validations give a high degree of confidence about both the formulation used herein for a three-dimensional element and the correct implementation of this formulation in program 3DFIRE. The proven capability of the analysis to account for moderately large deformations is another desirable advantage in analysing structures in fire conditions. Having established confidence in the software, it will be used in the following chapter to carry out an extensive study on columns as isolated structural members and within framed structures under fire conditions.
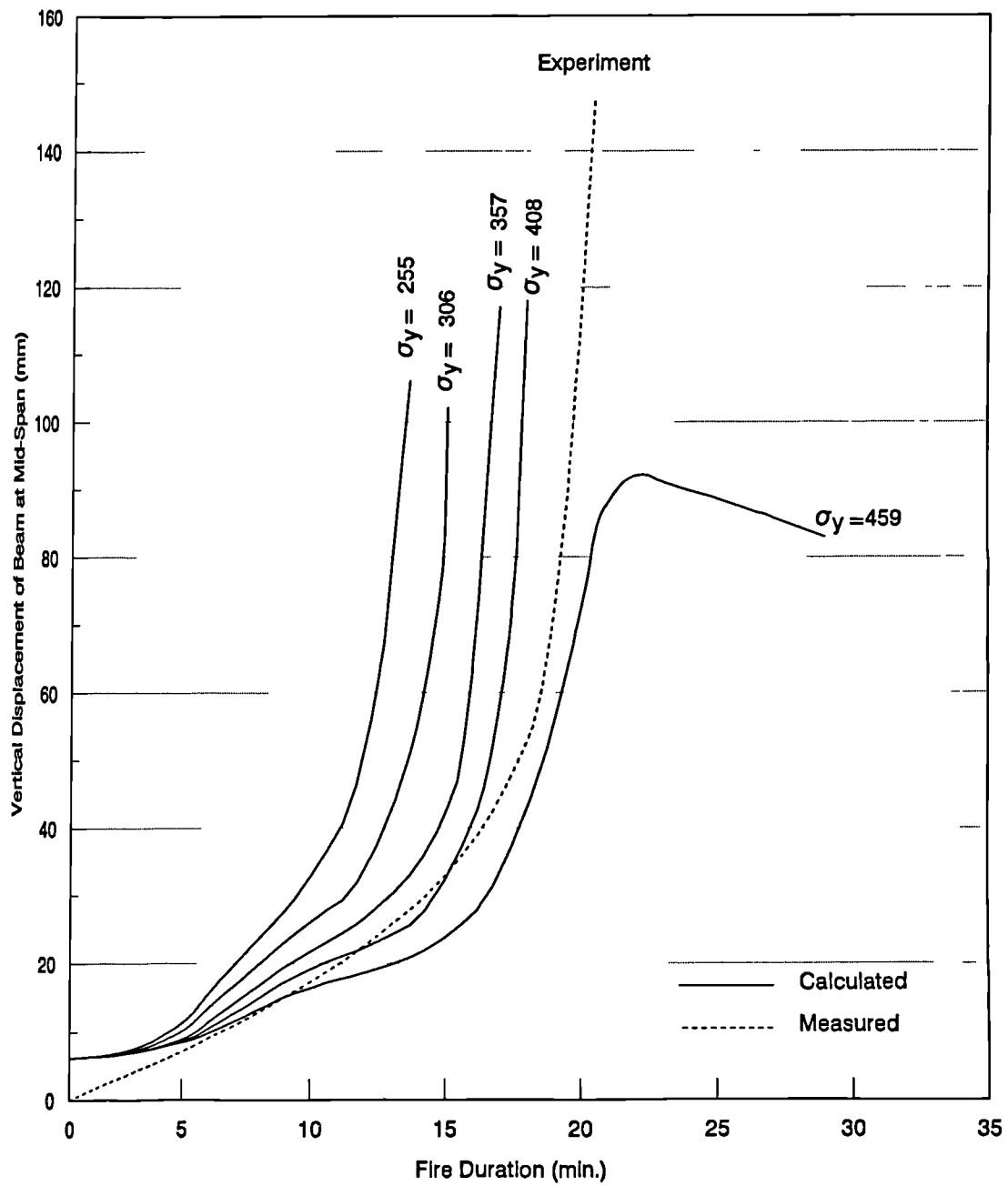
Fig. 4.33 Experimental Results Compared with Analysis by Franssen et al (1993)

CHAPTER 5

Parametric Studies

5.1   Introduction

The strategy that was adopted for this parametric study was to try to find gener-
alised conclusions concerning columns in fire. The particular position of a column
in the structure has a profound effect on its behaviour whether at ambient tem-
perature or at elevated temperatures. Consequently, in this study an attempt will
be made to consider all possible factors that effect columns' capacity in fire as iso-
lated structural elements. Once this task is accomplished, columns can be looked
at again as a part of the framed structure. Another aspect that needs consideration
is the state of temperature within the structural element and its effect on struc-
tural performance. Columns that undergo a uniform thermal distribution across
their sections are expected to respond differently from columns with non-uniform
distribution.

5.2   Assumptions

In order to keep the following studies as consistent as possible certain assumptions
had to be made. The intention of this study was to address practical columns in
fire conditions. Hence there is a need to use specified design guidelines in deciding
the loading and imperfections under which the analysis can be performed. In an
attempt to achieve this, the following assumptions were made in the following
studies:

- The value and the form of imperfection are imposed on all columns in accor-
  dance with BS449. This means that all imperfections that exist in a column
  can be replaced by an initial out-of straightness. The value of this imperfec-

tion can be obtained from any code of practice. The reason for adopting the value from BS449 was that BS449, although outdated, offered a universal value of imperfection for any column, unlike BS5950 or EC3 where different values are quoted for different sections and axes of buckling. Furthermore, the European standard EC3, which is very likely to replace the current British standard BS5950, states that Curve c should be used for fire design purposes for all columns. Curve c provides a value of imperfection almost exactly the same as BS449. In any case, comparisons between various curves of BS5950 and BS449 are made later in this chapter.

- Initial out-of-straightness is imposed about both principal axes of the column.

- Applied load on any column is expressed as a percentage of the ultimate load according to BS449. Although the concept of ultimate load is not used in BS449, it is defined in this study as the load at which the first yield is reached when the BS449 value of imperfection is imposed on the column. This point was made to avoid using permissible stresses, a procedure that is not suitable for analytical studies.

- The value of the yield stress of steel was assumed to be 250 N/mm^2.

- The analyses were performed assuming full three-dimensional behaviour. In other words columns are allowed to translate, rotate, twist and warp at any intermediate point over the column length. At supports translational displacements, twist and warping were restrained.

- Continuous stress-strain characteristics for steel at elevated temperatures, as expressed using a Ramberg-Osgood equation, are used. The reason for adopting this model will be discussed in the next section.

• 'Failure' is reached once the determinant of the stiffness matrix assumes a non-positive value. In this case the value of the increment in temperature is reduced and the analysis is resumed until the increment value is 'sufficiently' small. 'Failure temperature' is quoted as the last temperature before singularity in the stiffness matrix is achieved, provided that the temperature increment assumes the value of $0.2^{\circ}C$. If the temperature increment is larger than this value, the increment is refined until the condition is achieved.

These assumptions are used in all the following studies unless otherwise stated.

5.3 Effect of Stress-Strain Models on Columns' Failure in Fire

A wide range of simplified models of stress-strain characteristics for steel at elevated temperatures are available (Chapter 1). The first issue to be settled before performing this parametric study was as to which of the available stress-strain models could be used to produce reliable results. To test the validity of the stress-strain models with respect to column failure in fire, almost all of them were implemented in combination with a range of columns with different slenderness ratios. For each stress-strain model, 21 columns were analysed starting with slenderness ratios of 5, 10 and then increasing in increments of 10 up to 200. Although very low and very high slenderness ratios are hardly practical, it was considered proper to include them in order to keep the study as comprehensive as possible.

A *UC* 203 × 203 × 52 was chosen for all slenderness ratios, and the length was varied to produce the required slenderness in each case. Each column was loaded

to 60% of its ultimate load according to BS449. All columns were assumed to have imperfection (initial out-of-straightness) about both axes according to BS449.

Failure temperatures were plotted against slenderness ratio in every case (Figs. 5.1 and 5.2). The failure temperature curves for the bilinear stress-strain models (Fig. 5.1) look almost the same in shape. The failure temperatures have the characteristic of ascending from low slenderness ratios up to the point of intersection between Euler and Squash curves, after which the curves generally go flat. This reflects the fact that most bilinear models tend to decrease the value of yield stress at a higher rate than elastic modulus with increase of temperature. By fixing the yield strain for all temperatures, as is the case in the Ramberg-Osgood bilinear model, the failure temperature curve becomes almost flat. Fixing the yield strain means that both strength and stiffness are decreased at the same rate with temperature. The failure curve produced using Furumura's model differs from the rest due to its "plastic" portion having non-zero slope. This explains the higher failure temperatures at very low slenderness ratios in these cases, where the material was allowed to have some stiffness after yielding. The same can be said about the results of using a trilinear approximation of the EC3 model (Fig. 5.2), for which failure temperatures were considerably lower because the assumption of a lower level of first yield resulted in reduction of both strength and stiffness for the whole range of slenderness ratios.

Regarding the shape of the failure temperature curves, none of the bilinear models used were capable of predicting the failure shape produced by the experimentally-based model (Ramberg-Osgood). Using another experimentally-based stress-strain model such as that of EC3, has produced more acceptable comparisons. Fig. 5.2 shows these results.

Failure Temperature for Columns Loaded to 60% of BS449
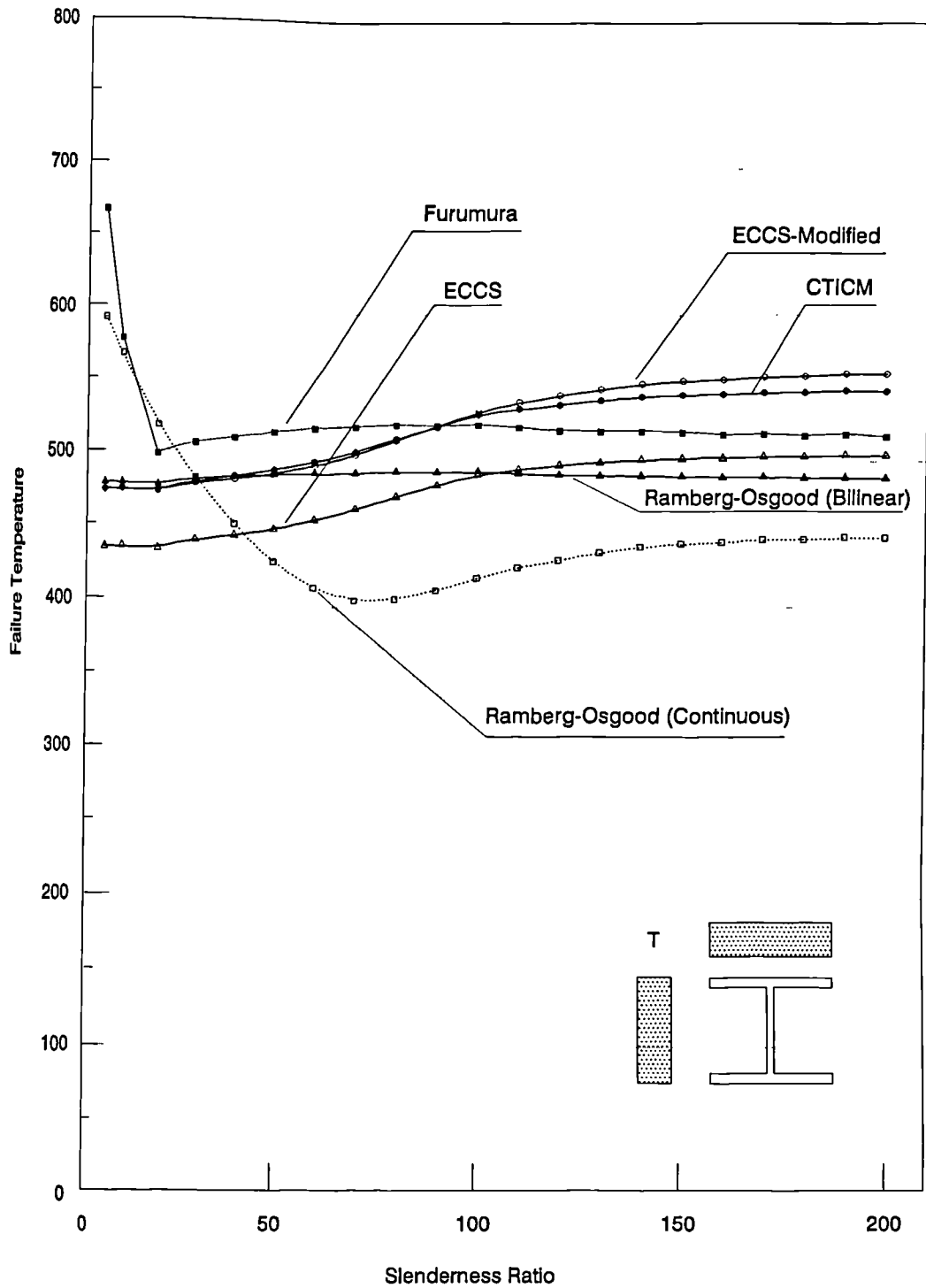
Fig. 5.1 Comparison of Various Bilinear Stress-Strain Models
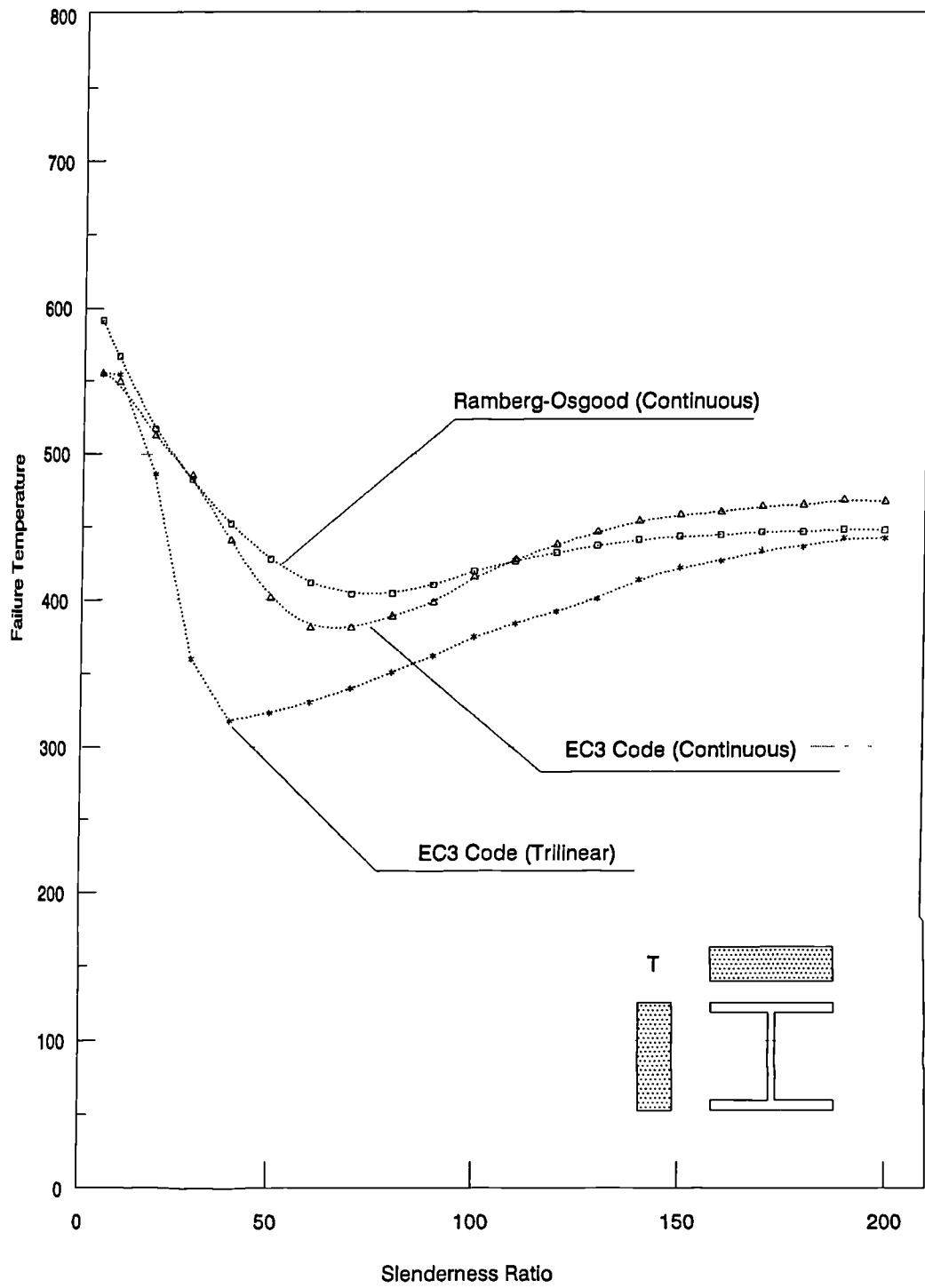
Fig. 5.2 Comparison of Various Continuous Stress-Strain Models

A selected number of temperature-deflection curves are plotted on Figs. 5.3, 5.4, 5.5, 5.6, 5.7 and 5.8 as an example of the actual behaviour in each case. Columns of slenderness ratios 40, 90, and 150 were chosen for this purpose. It is clear from the temperature-deflection curves for all the cases that the columns have failed by buckling about their minor axes, as would be expected for the case of uniform heating. It can also be observed that deflections for all cases are similar at low temperatures, or in the region of what can be thought of as "elastic" behaviour, regardless of the stress-strain model. At higher temperatures bilinear or trilinear models exhibit small deflections compared with the continuous models. This is a reasonable consequence of the material losing its stiffness instantaneously in the multi-linear models, compared with the gradual loss of stiffness in continuous models.

The most obvious conclusion from Figs. 5.1 and 5.2 is the fact that bilinear models failed to produce a similar variation of failure temperatures compared with the experimentally-based models. Consequently a decision was made to use the continuous Ramberg-Osgood model for the rest of this study.

5.4 Isolated Columns

In this section various aspects of isolated column behaviour will be studied. The effect of imperfection always has a dominant role in column studies at ambient temperatures. This effect is second only to that of slenderness ratio. As a result it was decided to look at important imperfections along with other aspects such as end conditions. In all cases every factor is studied over a wide range of slenderness ratios. In the following sections a uniform temperature distribution over the length
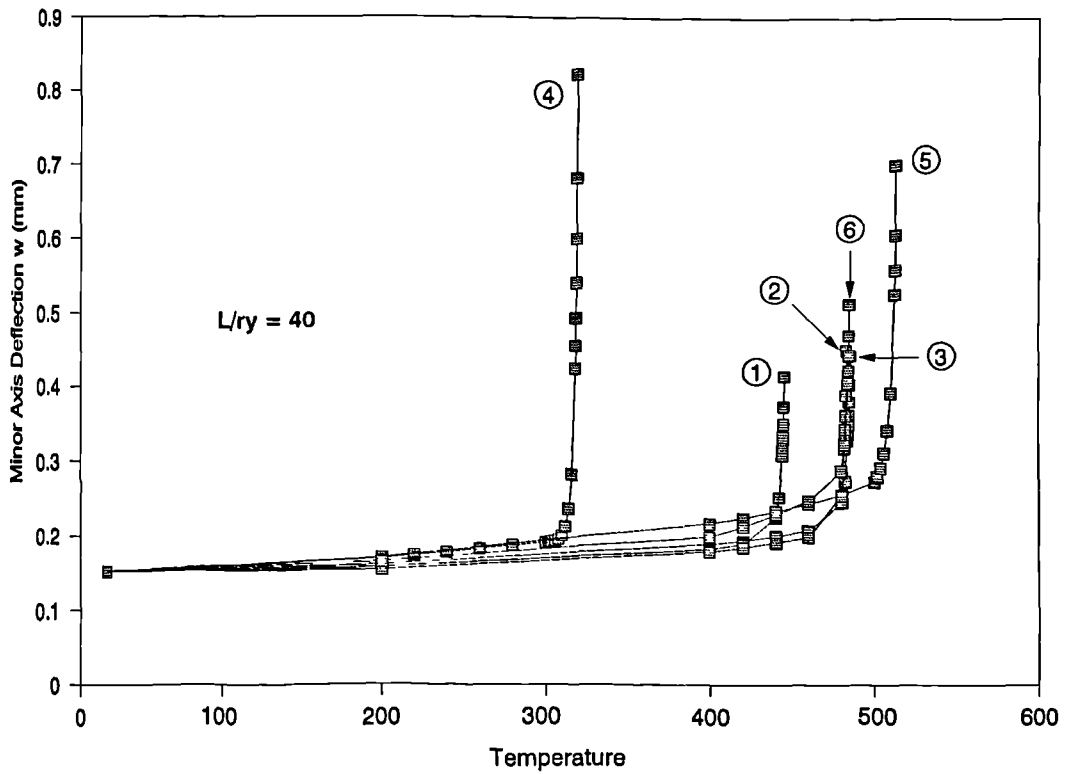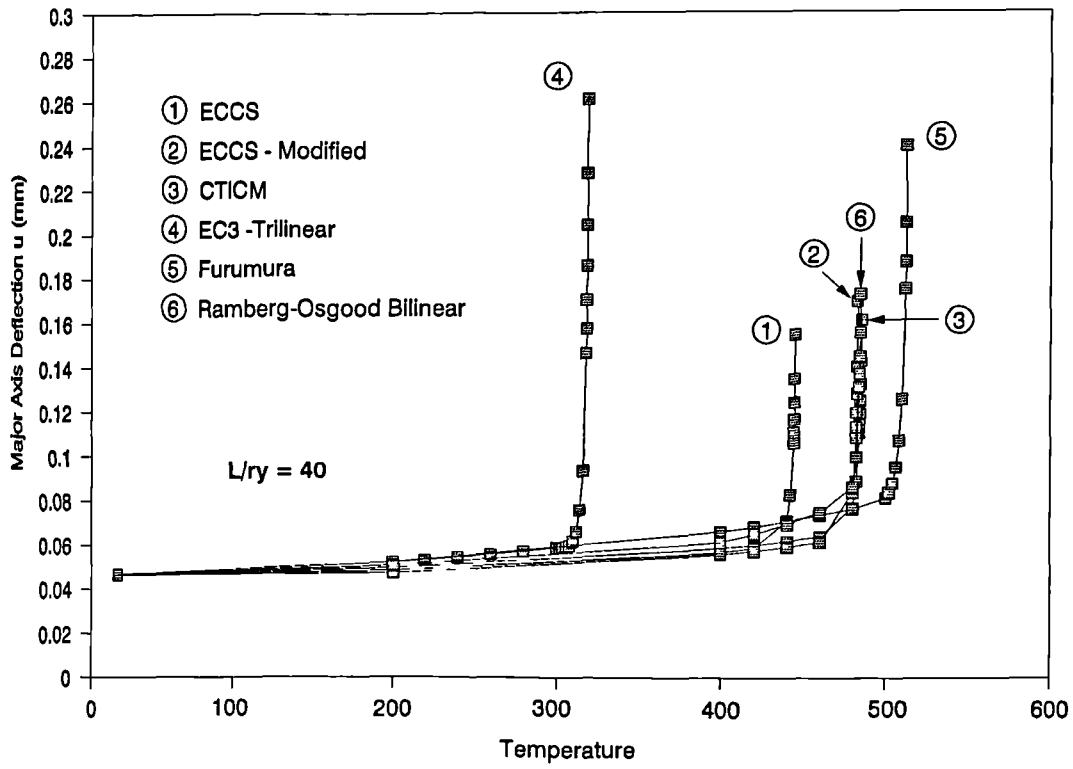
Fig. 5.3 Comparison of Different Bilinear Stress-Strain Models

(Midspan Deflections)
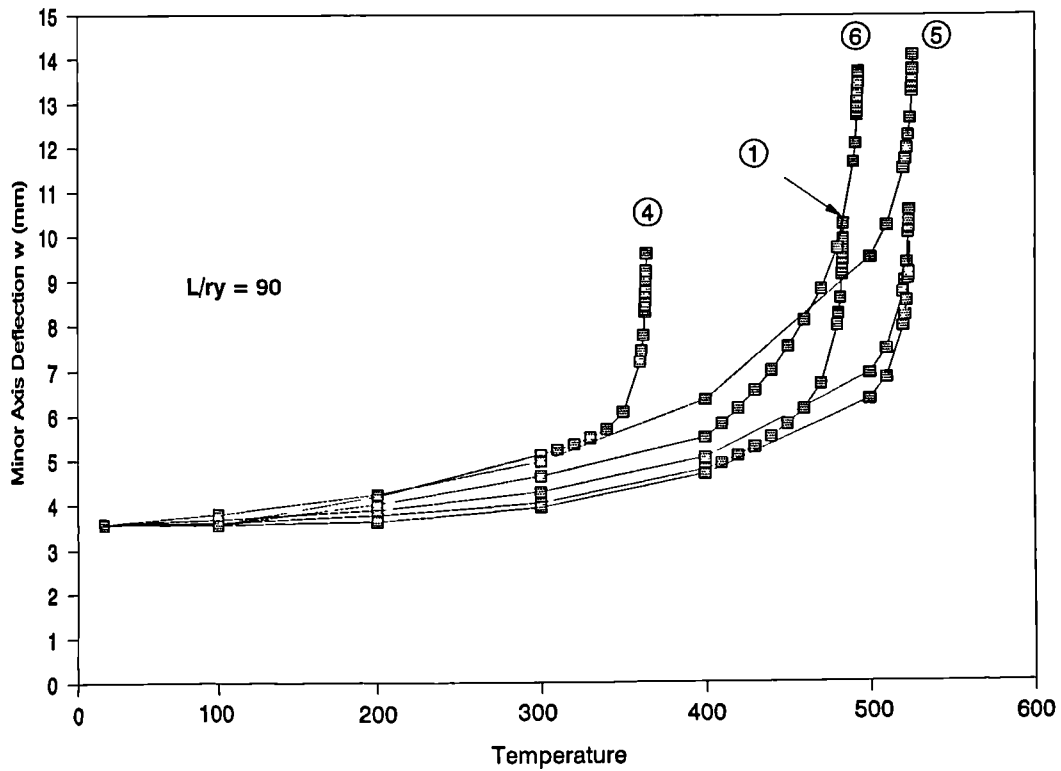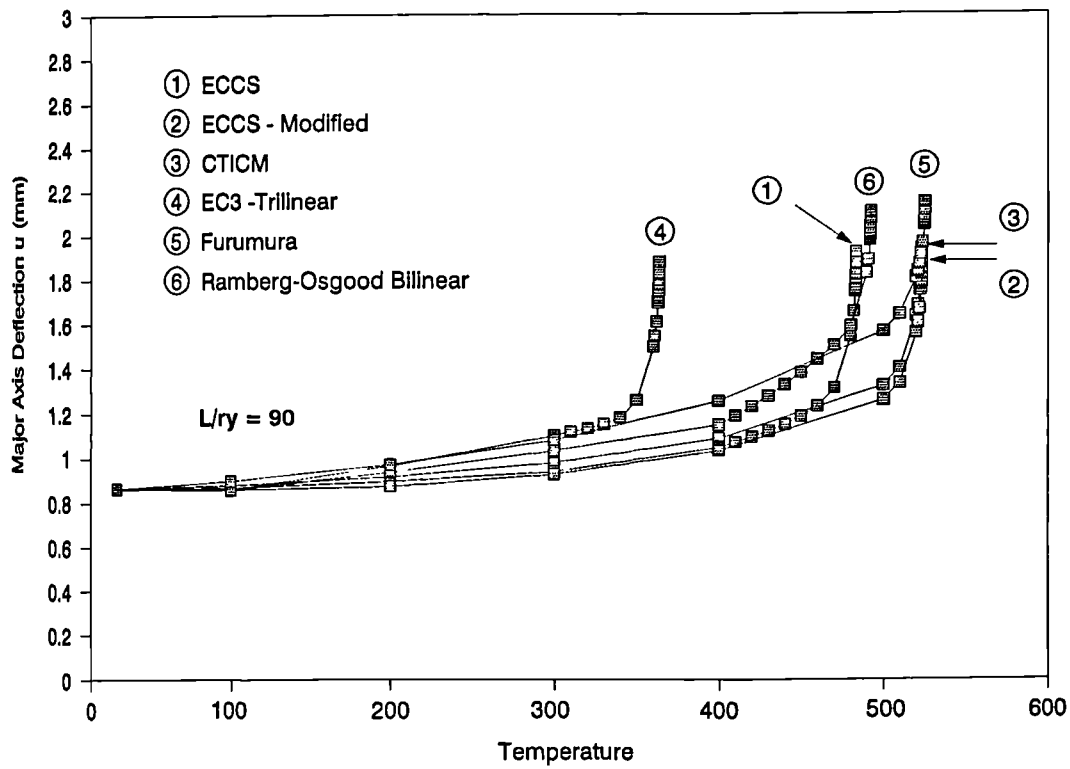
Fig. 5.4 Comparison of Different Bilinear Stress-Strain Models
(Midspan Deflections)
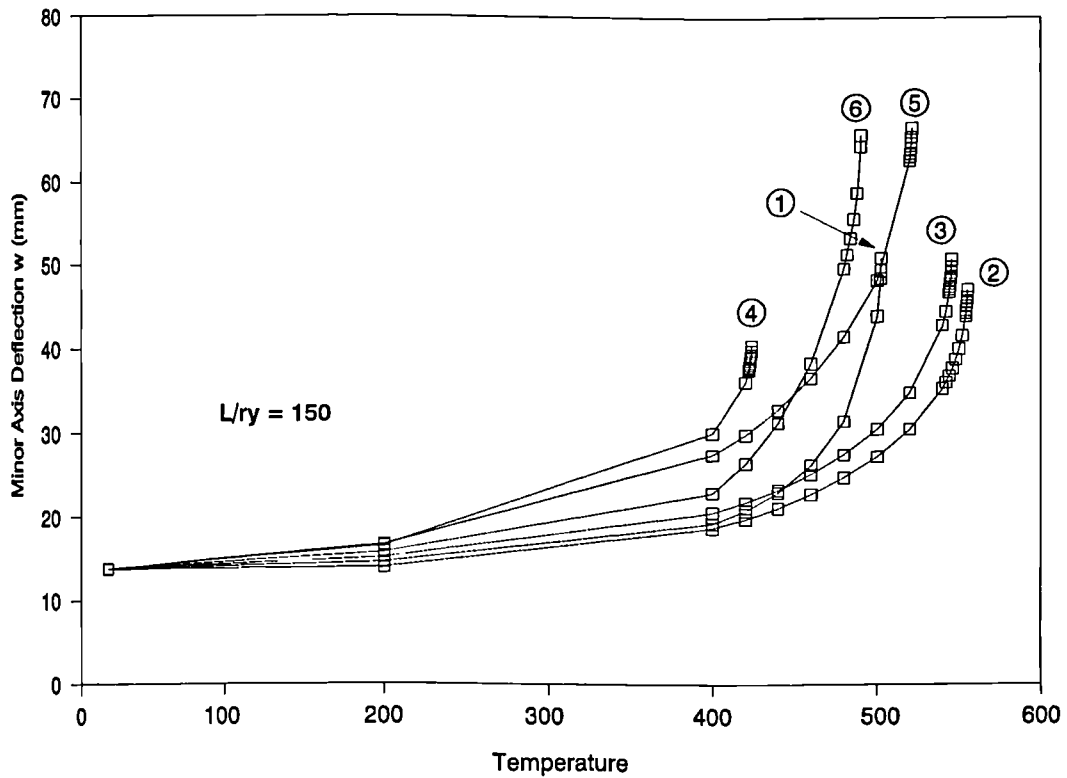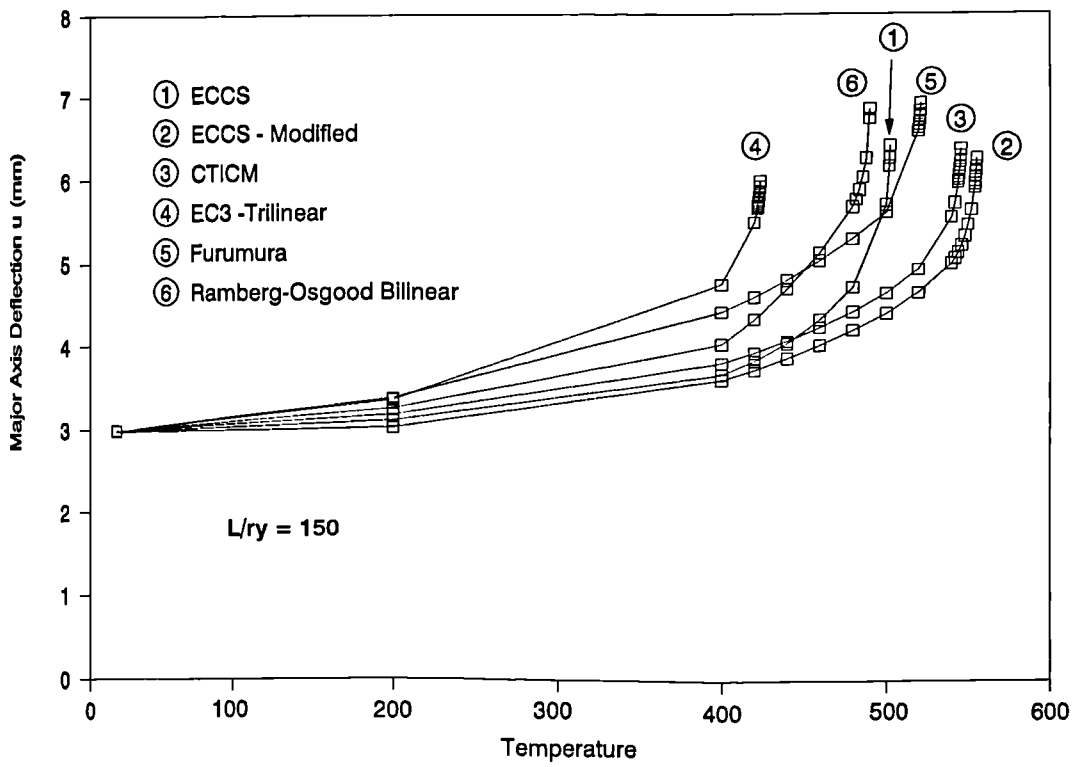
Fig. 5.5 Comparison of Different Bilinear Stress-Strain Models

(Midspan Deflections)
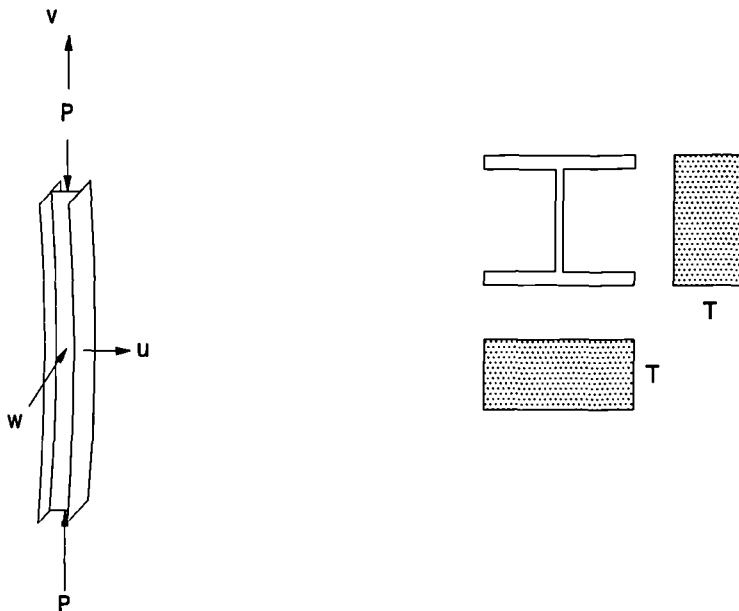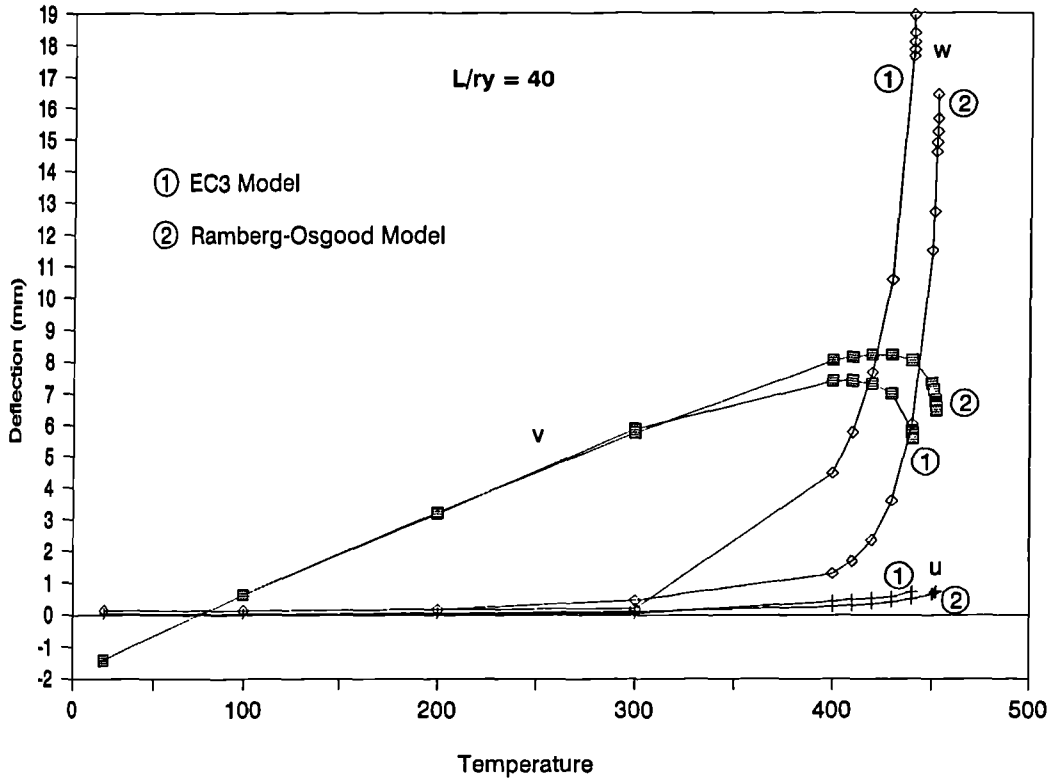
Fig. 5.6 Temperature-Deflection Curves for a Uniformly Heated Column
(Comparison Between EC3 and Ramberg-Osgood Stress-Strain Models)
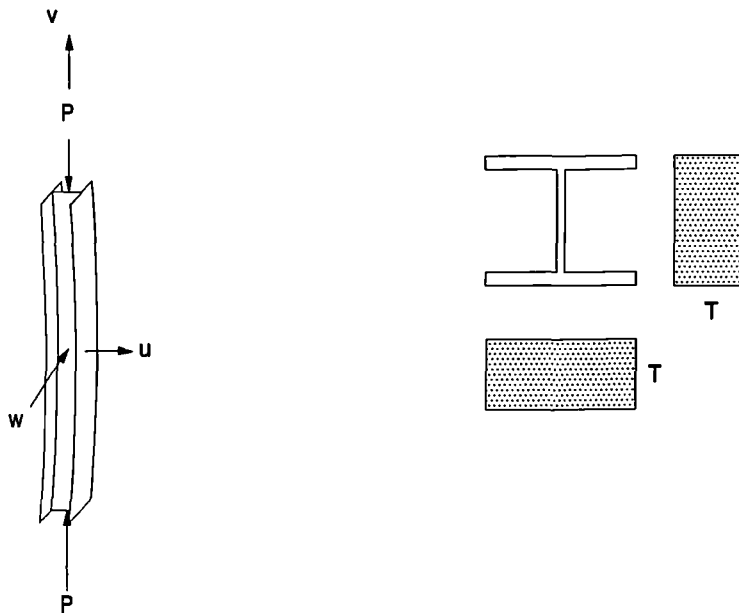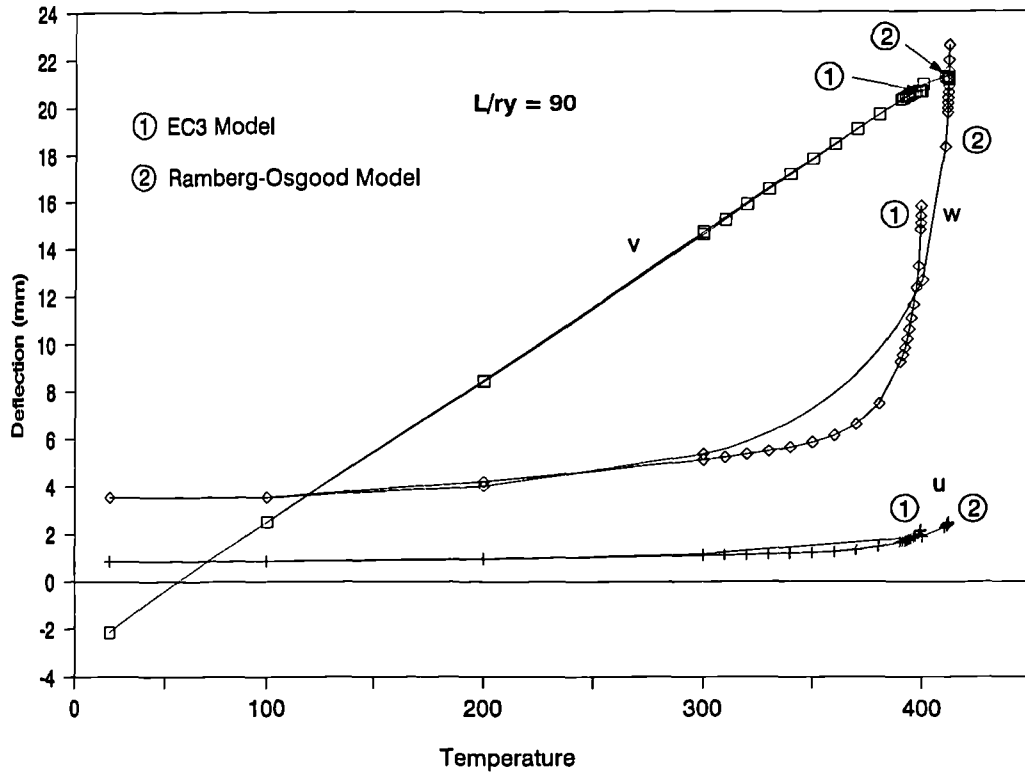
Fig 5.7 Temperature-Deflection Curves for a Uniformly Heated Column

(Comparison Between EC3 and Ramberg-Osgood Stress-Strain Models)
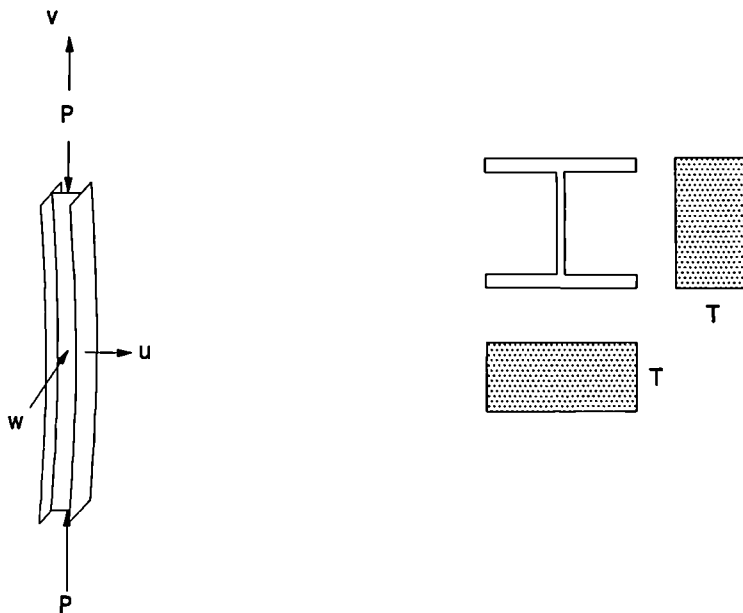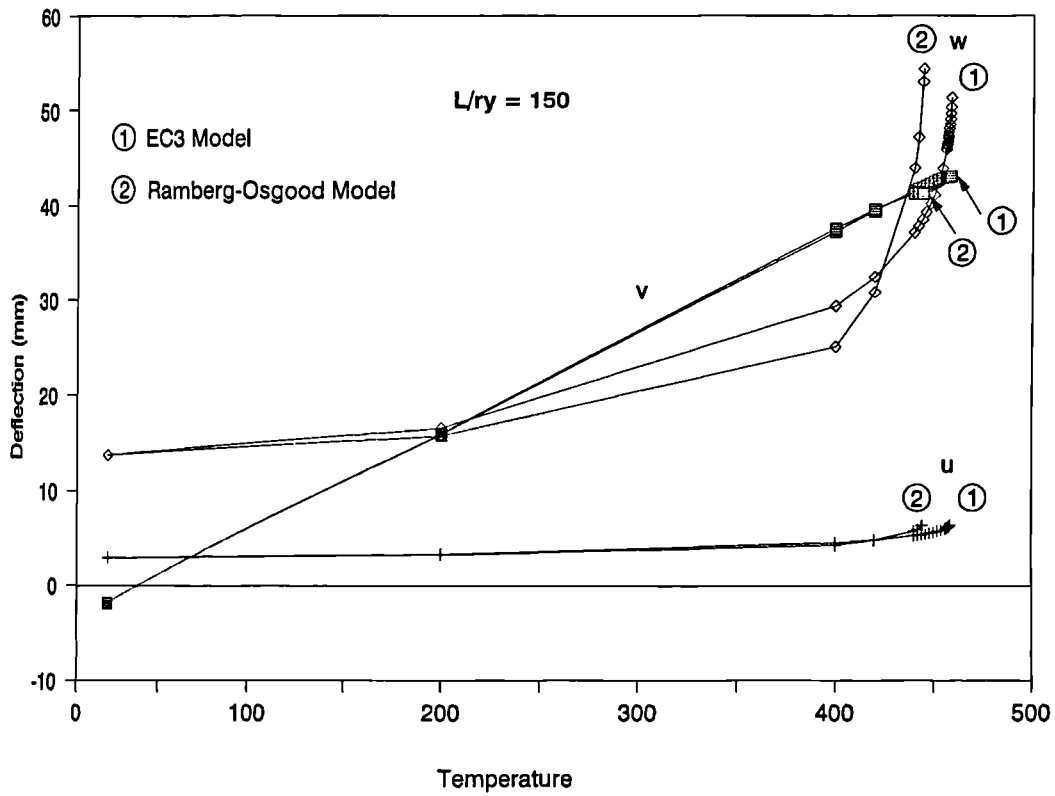
Fig 5.8 Temperature-Deflection Curves for a Uniformly Heated Column

(Comparison Between EC3 and Ramberg-Osgood Stress-Strain Models)

and across the section of the column will be assumed. Once various aspects of uniformly heated columns' behaviour have been studied, columns subject to thermal gradients will be considered.

5.4.1 Effect of Initial Out-of-Straightness

Another set of analyses has been carried out for the same columns without introducing any imperfection to them. Loads were assumed to be the same for both perfect and imperfect columns (60% of ultimate load to BS449), and the Ramberg-Osgood model was used to represent the change of stress-strain characteristics. Failure temperatures were the same for perfect columns as for imperfect columns at low slenderness ratios, while higher failure temperatures were evident for perfect columns at intermediate and high slenderness ratios. It is clear that, both at ambient and elevated temperatures, the intermediate and high ranges of slenderness ratios are more affected by imperfections than the low range. Whether for perfect columns or imperfect ones, the relative reduction of failure temperatures is evident in the intermediate range of slenderness ratios. This phenomenon resembles that for imperfect columns at ambient temperature where the reduction of the axial load-capacity is larger in the same range. Failure took place by buckling about the minor axis for all columns considered in this case.

To assess the effect of reducing the value of the initial imperfection on failure temperatures half the BS449 value was assumed and analyses were conducted for the same range of slenderness ratios. Applied loads in all columns were assumed to be the same for each slenderness ratio regardless of the amount of imperfection. This implies that perfect columns, for example, effectively carry a lower load ratio than imperfect columns though they carry the same load. In any case, design

loads are calculated based on the imperfection value specified by the Code rather than the actual value. Results of these analyses are shown on Fig. 5.9. along with the perfect case and the fully imperfect case to BS449. These results illustrate clearly the effect of imperfection on failure temperatures. Halving the imperfection produced critical temperatures almost half-way between the perfect and fully imperfect cases.

5.4.2 Effect of Axis of Imperfection

If initial out-of-straightness is imposed about one axis only while the other axis is left perfectly straight, keeping in mind that all columns buckled about their minor axis, it is to be expected that columns with minor axis imperfection will fail as those with imperfections about both axes, while columns with major axis imperfection will fail as perfect ones. To test this assumption two sets of columns were analysed and compared with columns from the pervious section.

Results of these analyses, which are shown on Fig. 5.10, support this assumption and illustrate the sensitivity of column failure to initial imperfection. Again all columns failed in this case by buckling about the minor axis.

5.4.3 Effect of Load Ratio

By varying the load ratio as a percentage of the ultimate load to BS449, the effect of load ratio on failure can be observed. The same 21 columns were analysed for load ratios of 20, 40, 50, 60, 70 and 80% of the ultimate load to BS449. Failure temperatures for columns loaded with different ratios are shown on Fig. 5.11. It is fair to conclude that the relationship between failure temperature and load ratio

Failure Temperature For Columns Loaded to 60% of BS449
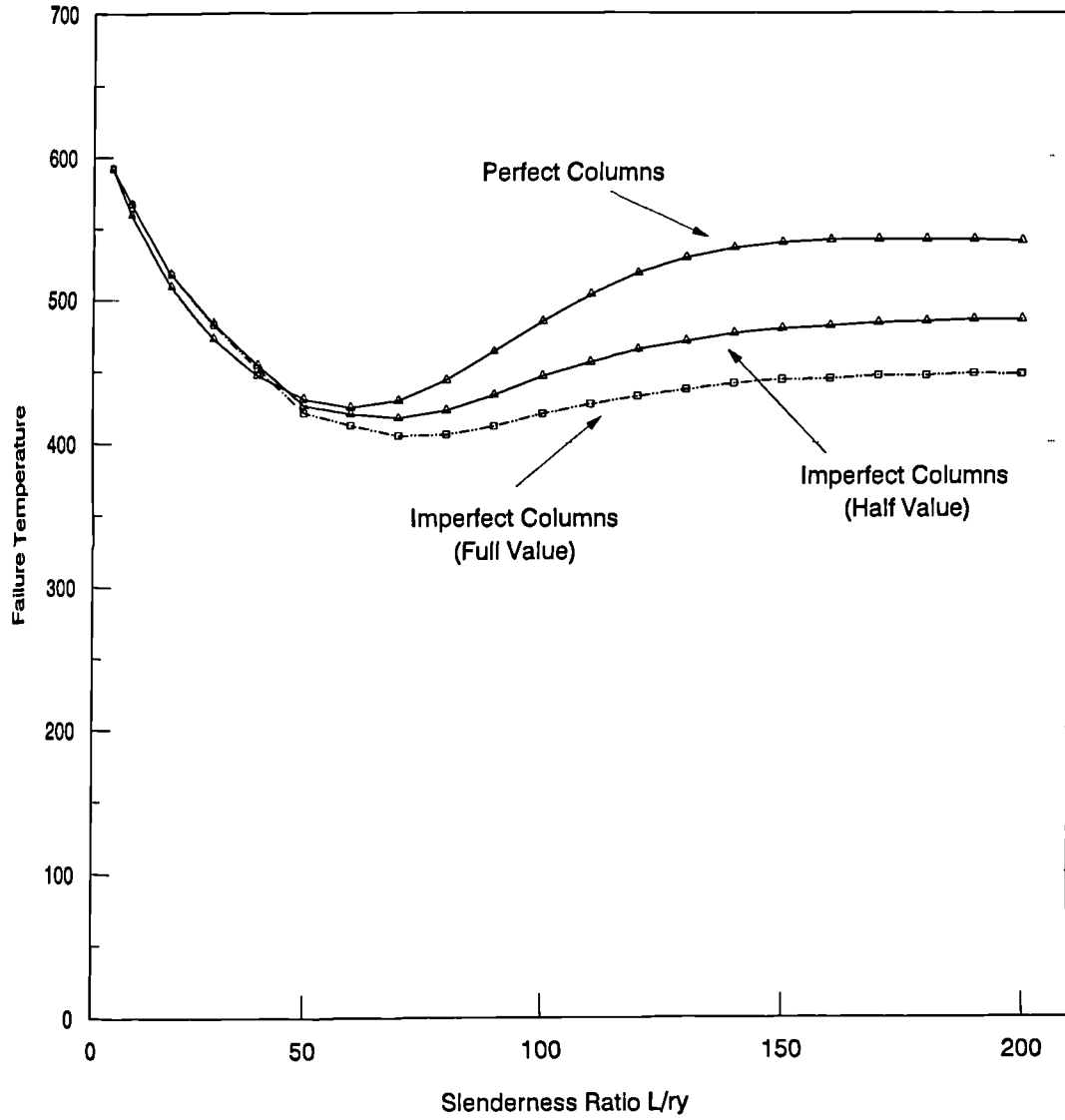
All columns uniformly heated

Fig. 5.9   Effect of Initial Out-of-Straightness

Failure Temperature For Columns Loaded to 60% of BS449

Major Axis Imperfection

Perfect Columns

Imperfect Columns
Both Axes

Minor Axis Imperfection

Failure Temperature

Slenderness Ratio L/ry
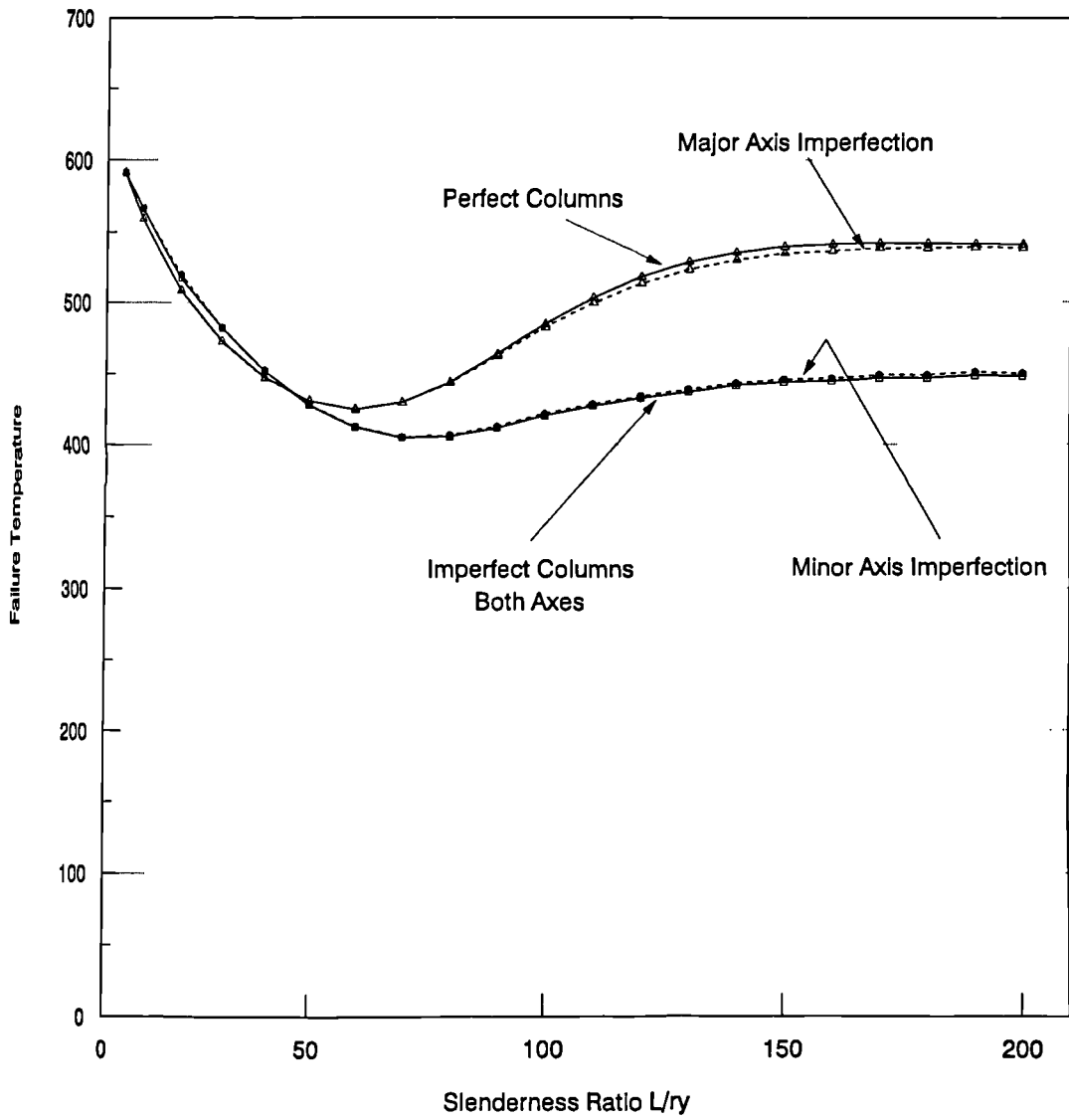
All columns uniformly heated

Fig. 5.10   Effect of Axis of Imperfection
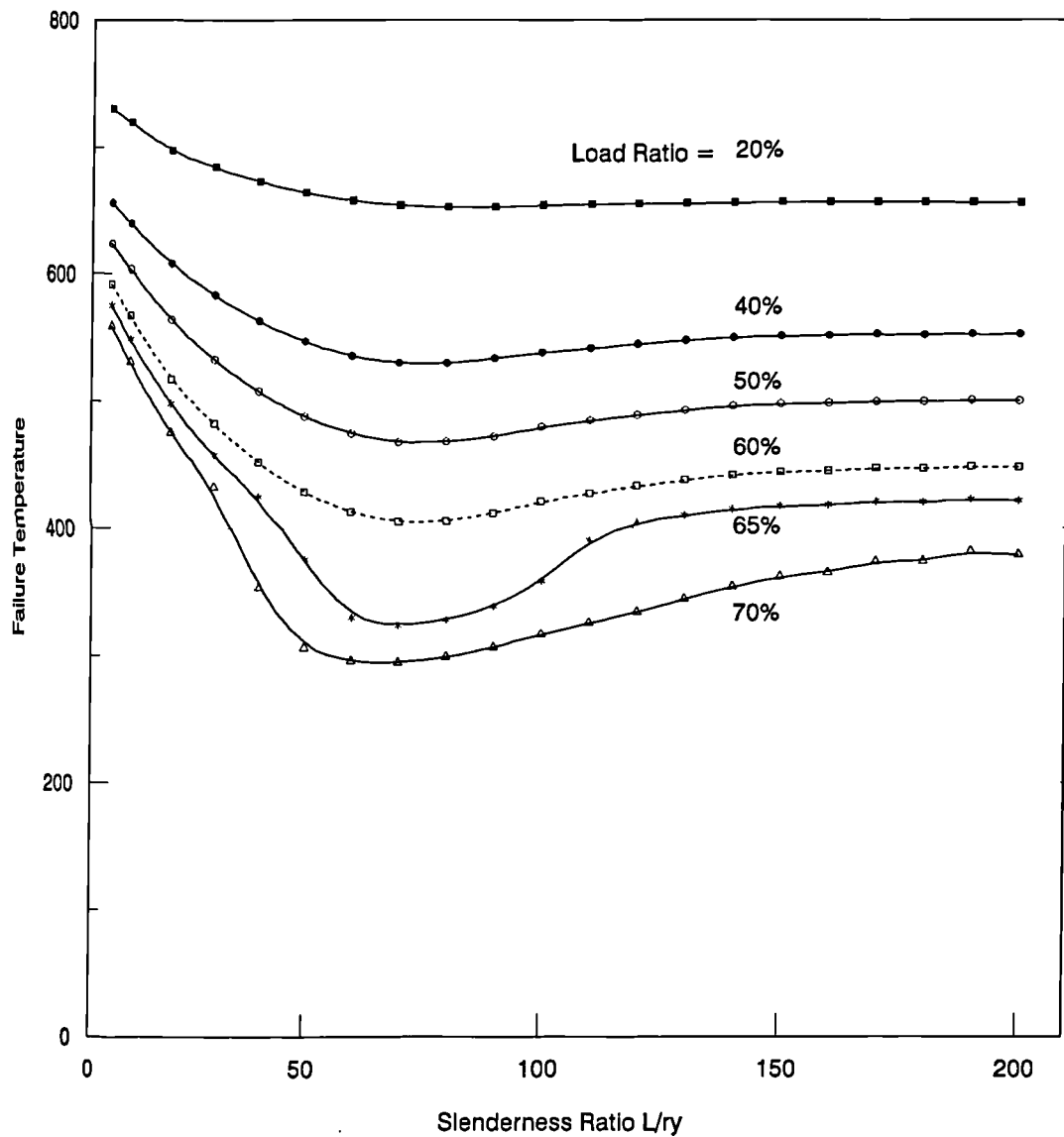
All columns with Imperfections In Both Principal Axis Directions

All columns uniformly heated

Fig. 5.11   Effect of Load Ratio

for a given slenderness ratio is linear up to a load ratio of 60%. Beyond this load ratio the linearity is generally lost.

The case of a load ratio of 65% was considered, to establish where the non-linear relationship between load ratio and failure temperatures starts. The failure temperature curve corresponding to the load ratio of 65% shows that this linearity is still maintained for most of the range except for slenderness ratios between 40 and 110.

It seems clear that 60% load ratio is the upper bound beyond which the effect of load ratio starts to magnify the reduction in failure temperatures for columns within the intermediate range of slenderness, as can be seen from the 65% load ratio case. This magnification of the effect of load ratio spreads to a wider range at both ends of the intermediate range of slenderness at higher load ratios as can be seen from the 70% load ratio case. In any case, loads beyond the ratio of 60% are not expected to be found in real constructions and going beyond this level can be regarded as a purely academic exercise. As a result the failure temperature for any practically-loaded column can be linearly interpolated between any known failure temperatures at given load ratios for a known slenderness.

All columns analysed for this load ratio effect have failed by buckling about their minor axes. All columns were assumed to have both their principal axes initially imperfect to the BS449 value.

5.4.4   Effect of End Conditions

To establish the effect of end conditions, a well established case of clamped-ended columns was considered. The applied loads were the same as for the pinned-ended

columns (60% of the ultimate load to BS449). The length of the fixed-ended columns was considered to be twice the length of the simple ones, assuming an effective length of half the actual length. Initial out-of-straightness was imposed on the pinned-ended columns in the form of a half sine wave. To arrive at an equivalent imperfection for the fixed-ended columns the same half sine wave was imposed on the middle half of the column length while a quarter of that wave was imposed on both end quarters of the column length. This arrangement gives the fixed-ended column an initial shape as shown on Fig. 5.12.

Results shown on Fig. 5.12 illustrate clearly that the difference in failure temperatures between the cases is trivial. This comparison shows clearly that, once the effective length is defined from the end conditions, the slenderness ratio becomes the prominent factor in deciding the failure temperature regardless of the end conditions. This observation is similar to that for columns at ambient temperature, where the end conditions are used just to define the effective length. Unfortunately the effective length is more difficult to establish for practical cases such as those in multi-storey frames, contrary to the analytically-clear case of clamped-ended columns.

5.4.5 Effect of Residual Stresses

The existence of initial residual stresses in hot-rolled and welded structural members is a well-known phenomenon. These stresses result from the cooling process during manufacture or fabrication, where different parts of the cross-section lose heat at different rates. Although in self-equilibrium, residual stresses are added to the internal stresses due to loads, and contribute to failure at lower loads as a result of the material at certain parts of the cross-section reaching yield earlier. The

Failure Temperature For Columns Loaded to 60% of BS449
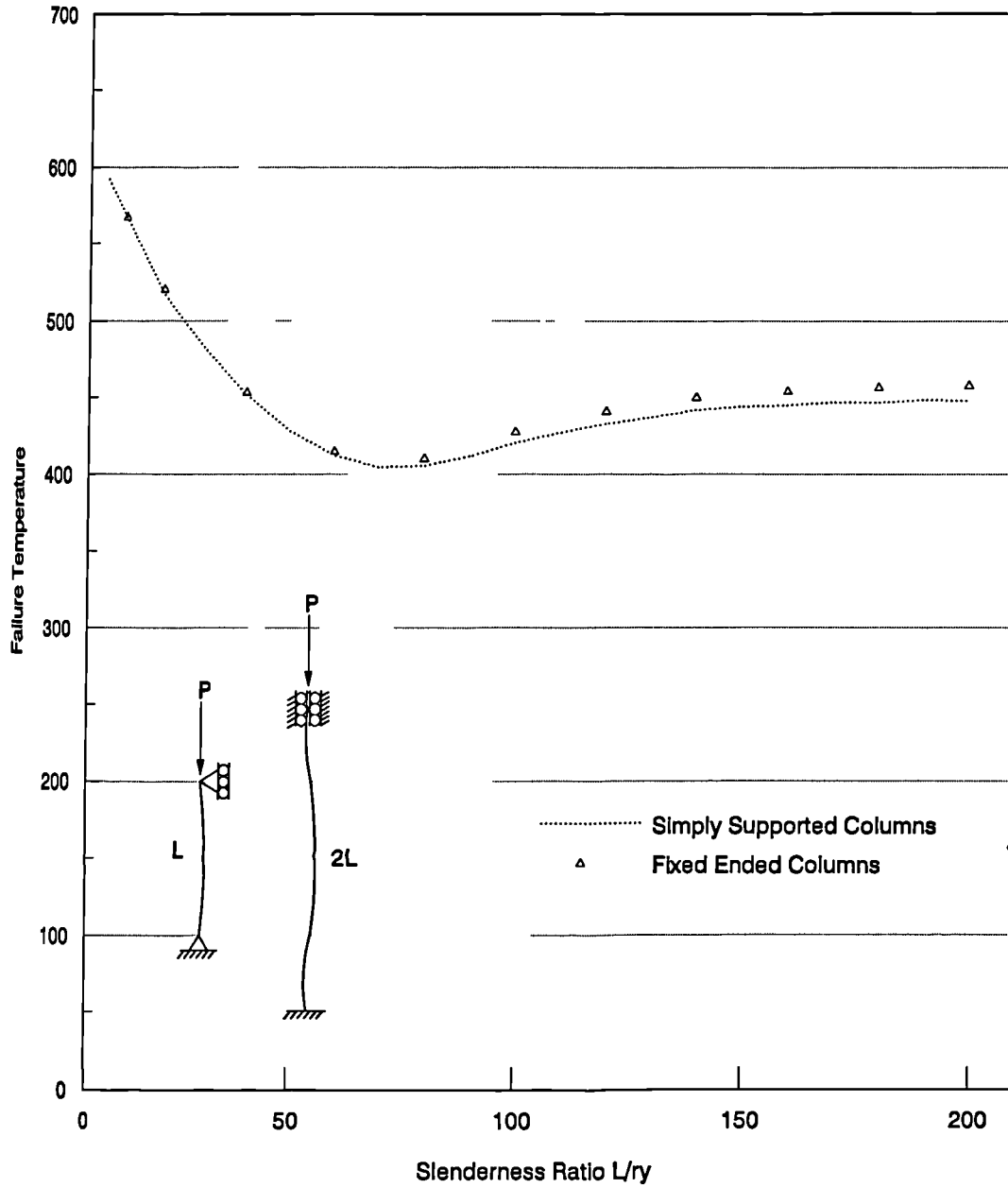
All columns with Imperfections in Both Principal Axis Directions

All columns uniformly heated

Fig. 5.12 Effect of End Conditions

current practice in Europe is to include their effect implicitly in the design codes as a part of the initial out-of-straightness. This is not necessarily the case in other countries; in the United States for example some design codes place a great emphasis on the residual stresses rather than initial out-of-straightness. This means that there is a need to investigate their influence on columns under fire conditions.

Initial residual stress patterns were added to the perfect columns of the previous section. A linear distribution of residual stresses was assumed and three values of peak residual stresses (1/6, 1/3 and 1/2 of the yield stress at ambient temperature) were considered. The effect of the initial residual stress patterns on failure temperatures is shown on Fig. 5.13. All columns considered in Fig. 5.13 have no initial out-of-straightness and residual stresses are the only imperfections imposed on them. These results show the effect of residual stresses as an isolated factor on columns failure at elevated temperatures. They contribute to the reduction of failure temperature, especially in the intermediate and high ranges of slenderness. Their effect on the low range of slenderness can hardly be visualised on the graph. This effect has produced failure curves of comparable shape as that produced by initial out-of-straightness, for all levels of residual stress. The only exception is the extremely high level of residual stress (0.5 σ_y), at which disproportionate reduction in the failure temperature is evident between slenderness ratios 60 and 120.

So far the effects of two different types of imperfection have been studied separately. Hence, it is necessary to investigate the effect of combining both types of imperfection on column failure in fire. If the initial out-of-straightness according to BS449 is added to the residual stresses the effect of this combination is as shown on Fig. 5.14. Adding more imperfection to the columns reduced the failure temperature further, with the greatest effect of this combination of imperfections
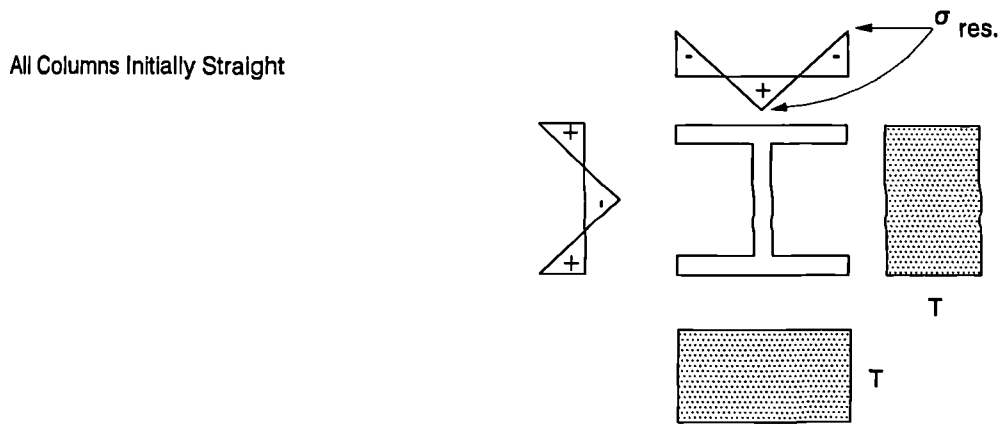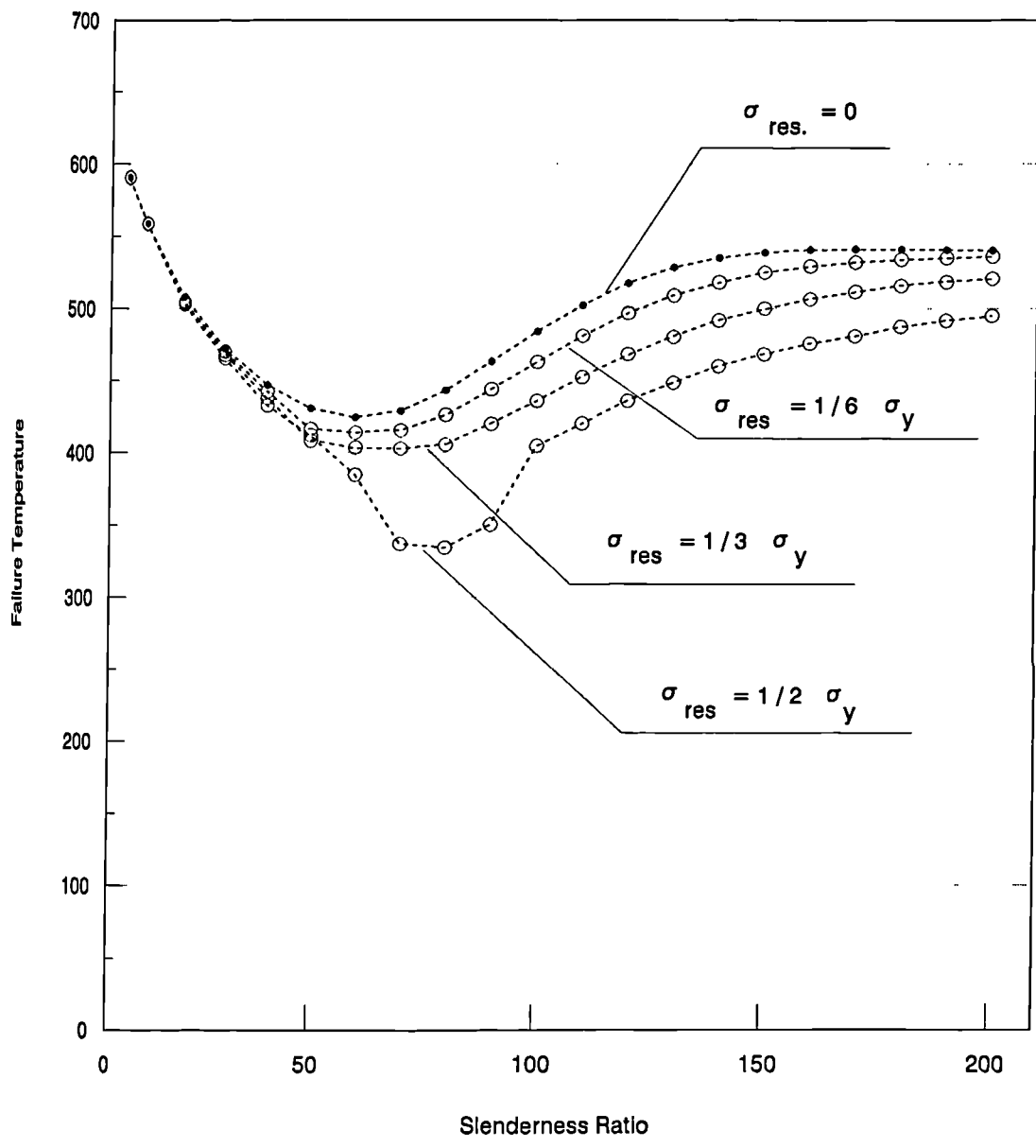
Fig. 5.13 Effect of Residual Stresses on Perfect Columns
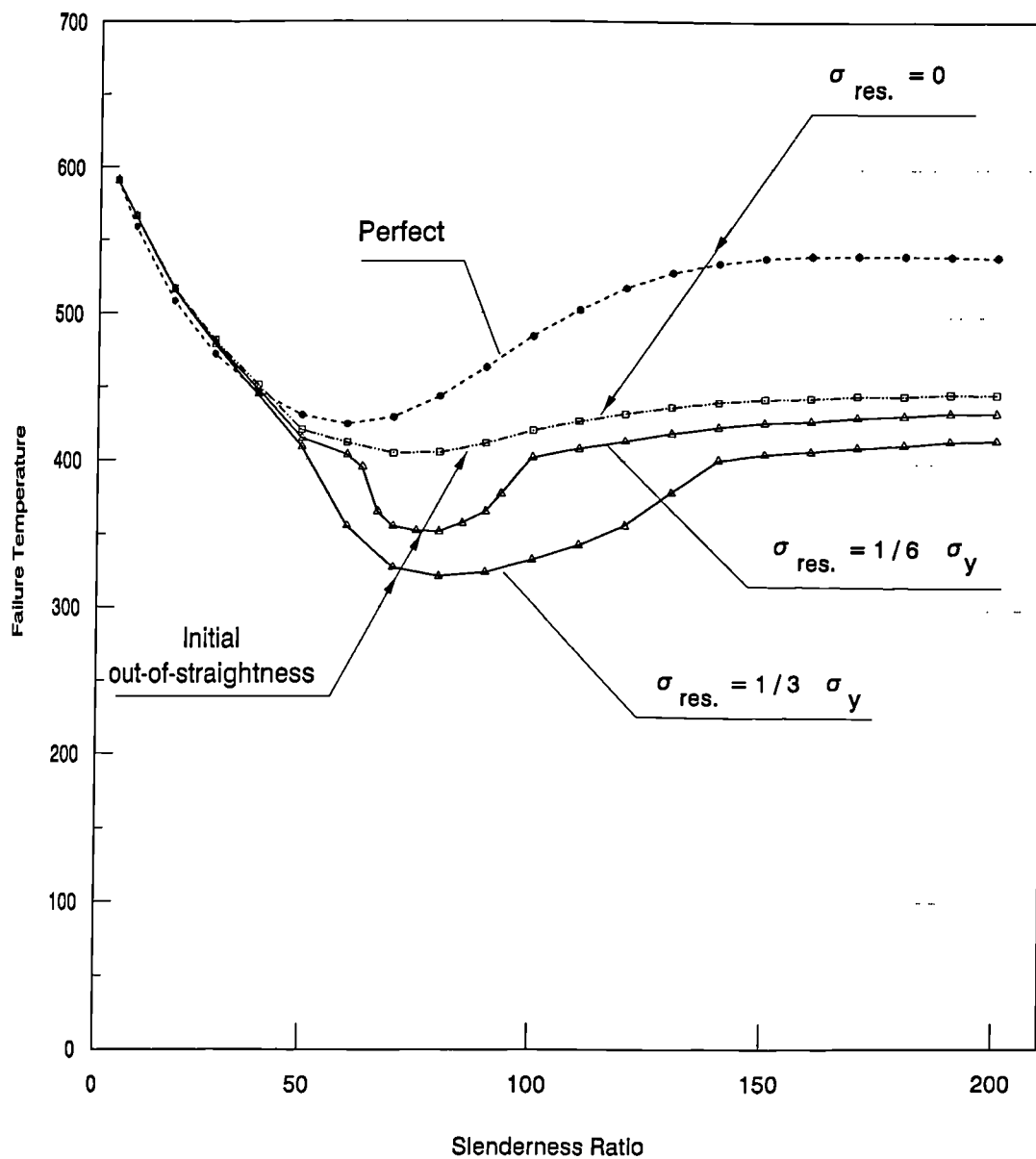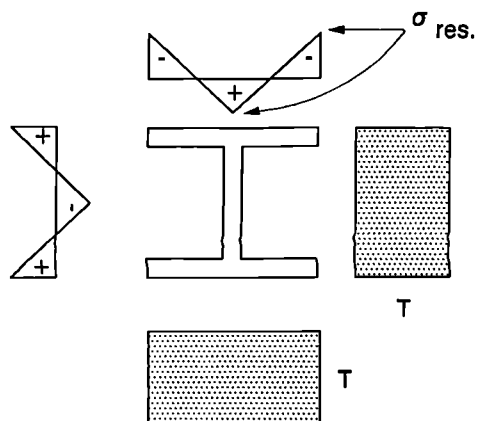
Fig. 5.14 Effect of Residual Stresses Compared with Initial out-of-straightness

exhibited in the intermediate slenderness range. It can also be noticed that this disproportionate reduction in failure temperatures spreads at both ends of the intermediate range if the amount of imperfection is increased.

It was thought that some combination of these two prominent imperfections which is equivalent to the initial out-of-straightness might exist, confirming the old Perry-Robertson assumption of regarding all imperfections as a single initial out-of-straightness. An attempted combination consisting of half the initial out-of-straightness and a residual stress pattern of the value $1/6^{th}$ of the yield stress was analysed. Results of this case along with all other residual stress cases are plotted on Fig. 5.15 for comparison purposes. This attempted combination shows reasonably good correlation with the full BS449 initial out-of-straightness for all slenderness ratios and gives almost exactly the same results up to a slenderness ratio of 80, after which differences are still small. This shows that the Perry assumption of regarding all imperfections as an initial out-of- straightness can be justified for columns under elevated temperatures.

Sample temperature-deflection curves for a column of slenderness ratio 90 are shown in Fig. 5.16. Deflections for various residual stress levels exhibit the same behaviour as in ambient temperature cases where the applied load is increased instead of the temperature. Deflections in what can be thought of as the 'elastic' range assume almost the same value regardless of the residual stress level. The only effect of residual stresses on the temperature-deflection history is to reduce the level at which excessive deformations take place, leading to earlier failure.
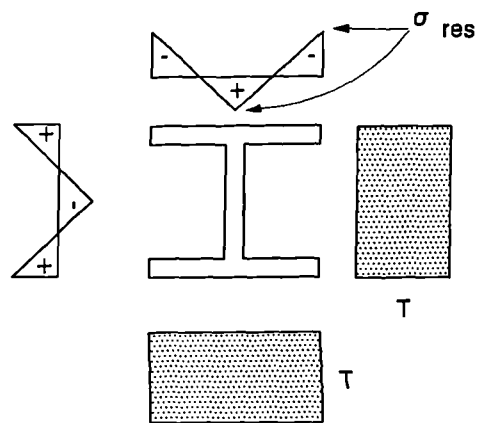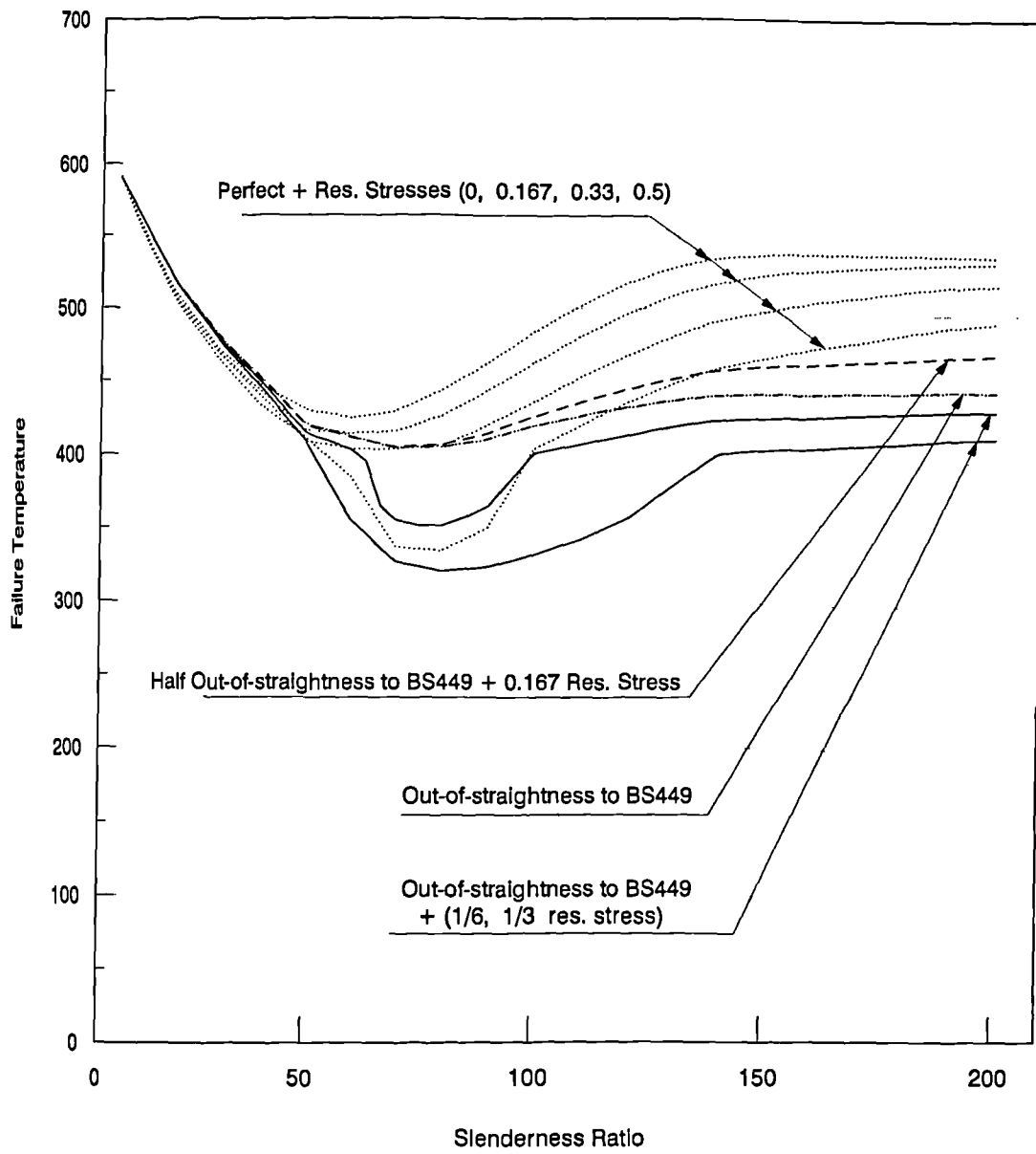
Fig. 5.15 Effect of Different Residual Stresses/Imperfection Schemes
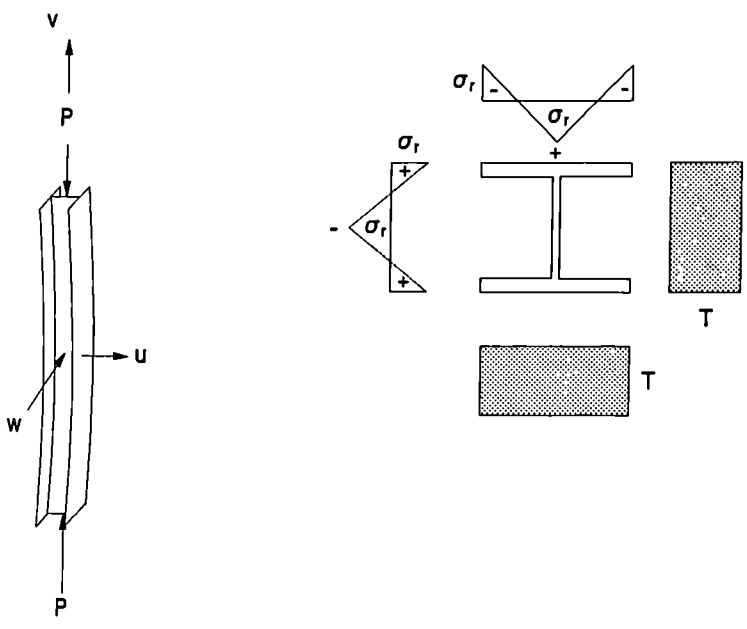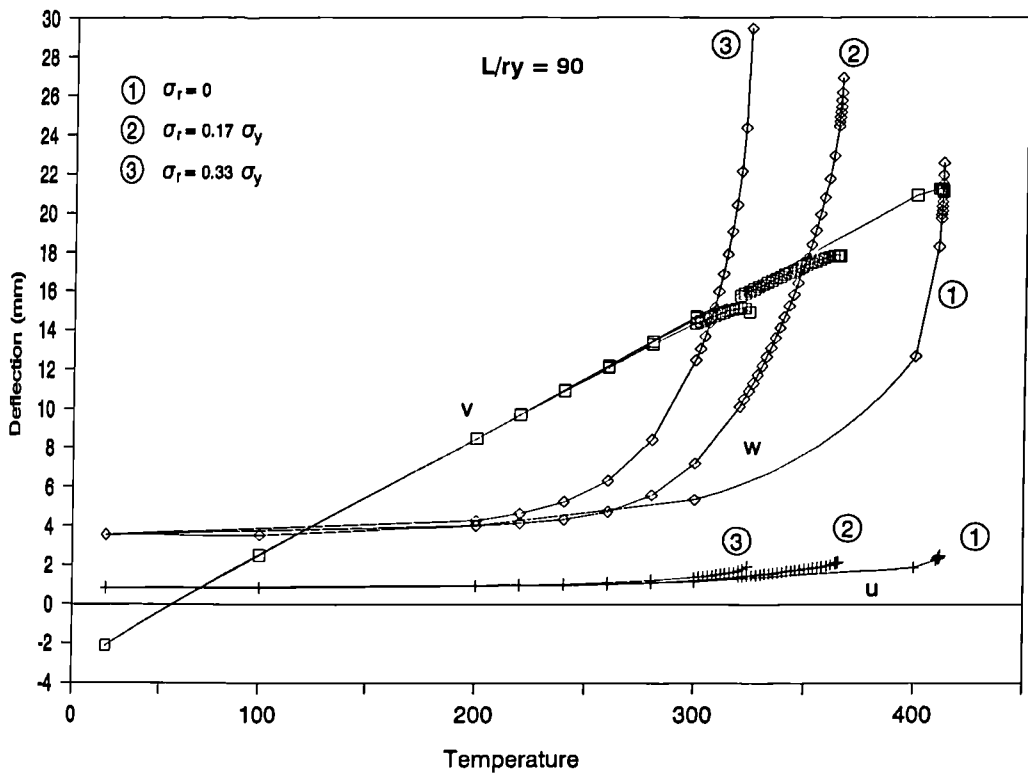
Fig. 5.16 Temperature-Deflection Curves for Column with Residual Stresses

5.4.6 Columns Under Thermal Gradients

All the previous studies were concentrated on uniformly-heated columns. This is not necessarily the case for all columns that undergo a rise in temperature in a real fire. Even in an experimental environment it is almost impossible to produce an exactly uniform pattern of temperature for columns or any other structural members.

The temperature distribution across the cross-section of a steel column may assume a variable profile due to the presence of fire-resistant partitions. In construction practice, such partitions are frequently placed between the flanges of columns causing a thermal gradient in fire situations. Hence, it is necessary to investigate whether the effect of thermal gradients has the same impact on the fire resistance of such columns or a different one. Although columns under thermal gradients are expected to exhibit different structural behaviour from uniformly-heated columns, the main interest in the following study is to assess whether this effect is beneficial or adverse.

5.4.6.1 Major Axis Thermal Gradients

Experiments on columns with walls built between their flanges have shown that the ratio between temperatures of the protected and the exposed flanges is in the range of 1:10. Fire tests were carried out by British Steel Corporation (1987) in which columns were constructed within block/brick walls with one side of the column exposed to fire. Temperature distributions across the tested sections show that this ratio is acceptable. Thermal analysis results illustrated in Chapter 2 (Fig. 2.1) show also that this ratio compares well with numerical predictions. To

assume a lower ratio was regarded as improper, due to the consequent assumption of a constant temperature (20°C) for almost the whole process of heating up to failure; an assumption which would be highly impractical.

The same range of columns was analysed assuming a linear thermal gradient across the cross-section with the cool flange having 10% of the hot flange temperature but not less than 20°C. All columns were loaded to 60% of their ultimate load according to BS449 and imperfections were applied about both principal axes according to the same Code. Initial out-of-straightness was applied in the same direction as the thermal bowing in order to ensure that the cases considered are 'worst' cases.

Results of these analyses compared with the uniform-temperature case are shown on Fig. 5.17. If the thermal gradient is reduced towards the uniform case the gradient curves should converge to the uniform one. Another four sets of analyses were performed for that purpose, results of which are illustrated on the same figure. It is clear from this figure that at a cool:hot flange ratio of 8:10 the gradient curves start to converge to the uniform-temperature curve.

To establish the reason for the unusual shape of the temperature gradient curves, especially those with high gradients, compared with the uniform-temperature curve, three columns of different slenderness ratios were selected to illustrate their temperature-deflection history (Figs. 5.18, 5.19 and 5.20). It seems that columns of different slenderness ratios have different characteristics in terms of a tendency to reverse their direction of deflection before failure. One can conclude that columns within the descending part of the curve (slenderness ratio between 5-30) exhibit full deflection reversal with respect to axial expansion and thermal bowing deformation. Fig. 5.18 shows clearly that thermal bowing reversed direction completely on the threshold of failure. Columns within the ascending part of the failure curve (slen-

Failure Temperature For Columns Loaded to 60% of BS449
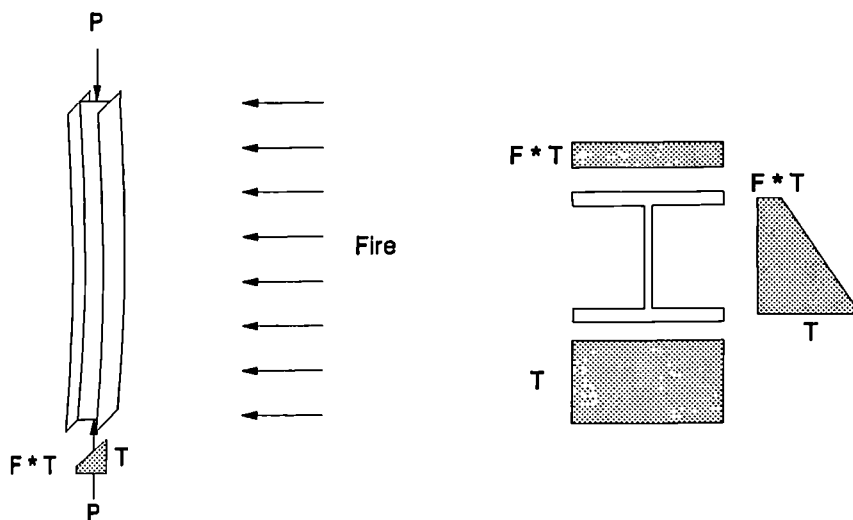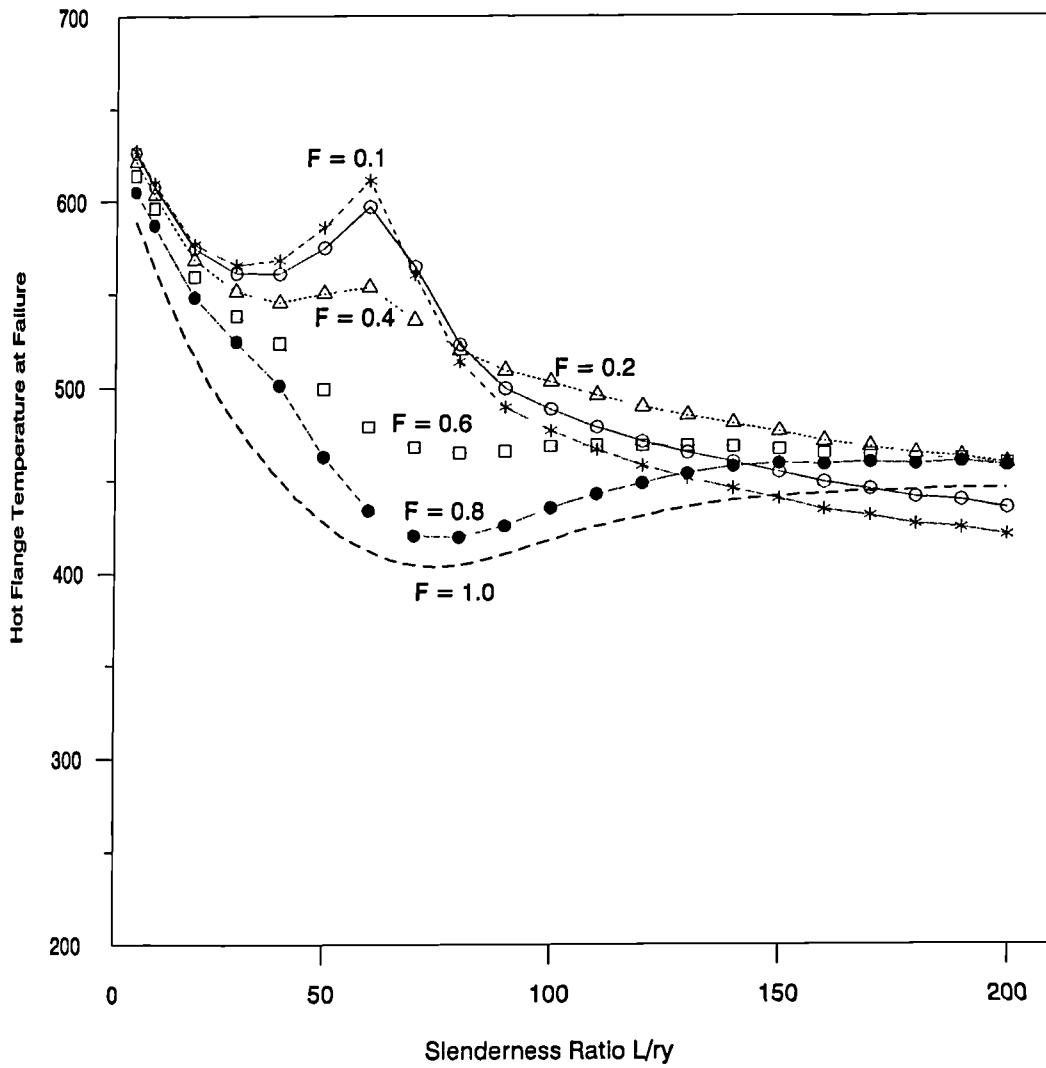
Fig. 5.17 Effect of Thermal Gradient about the Major Axis
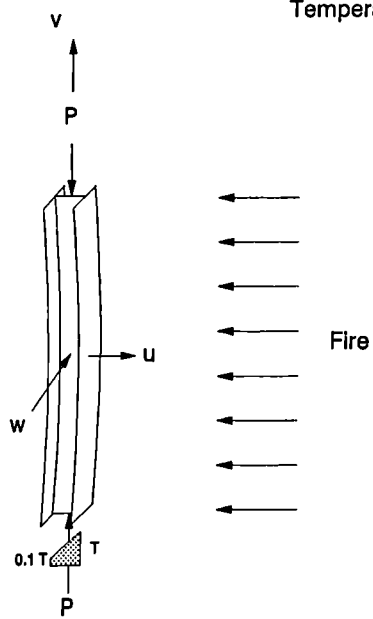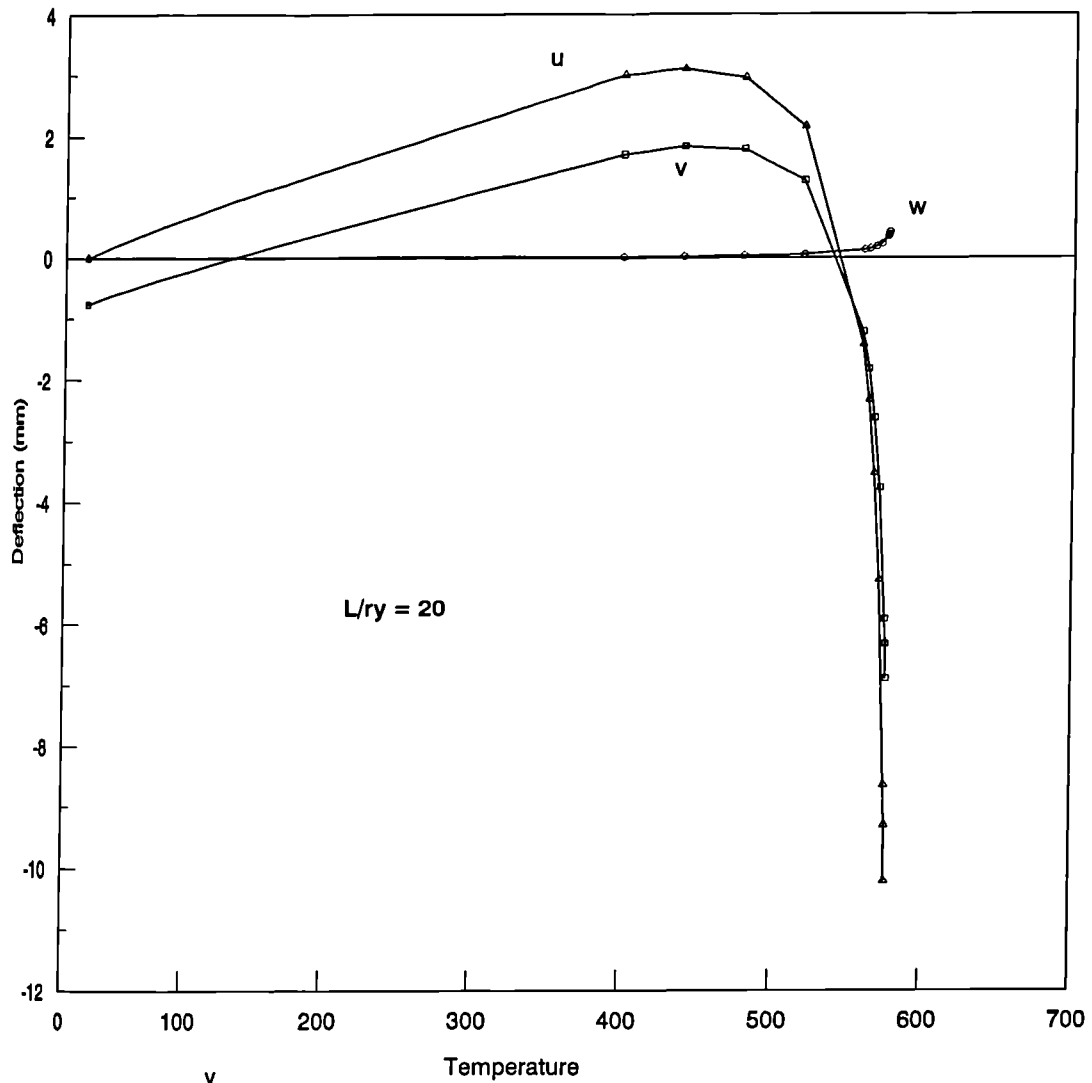
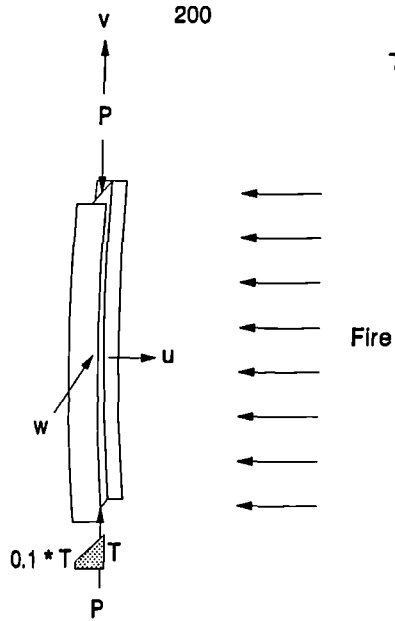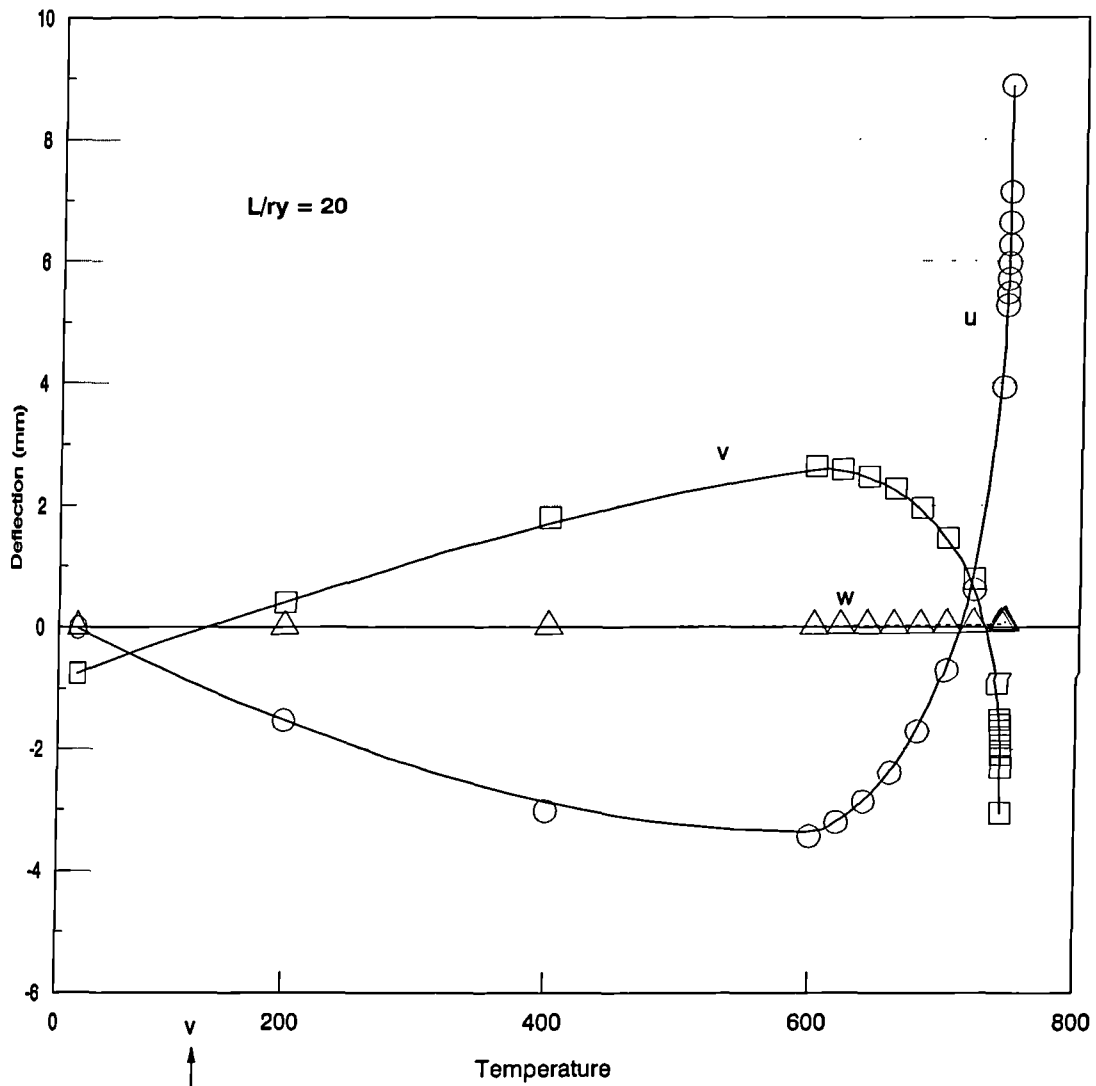Fig. 5.18 Temperature-Deflection for a Column with Thermal Gradient
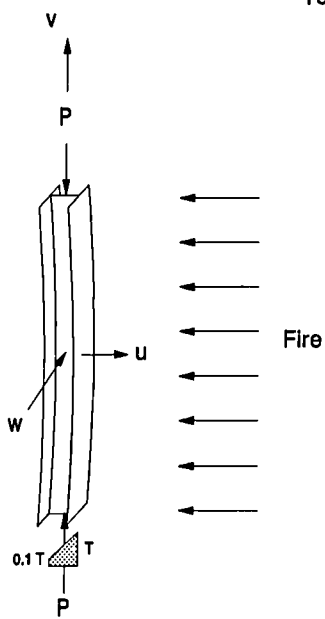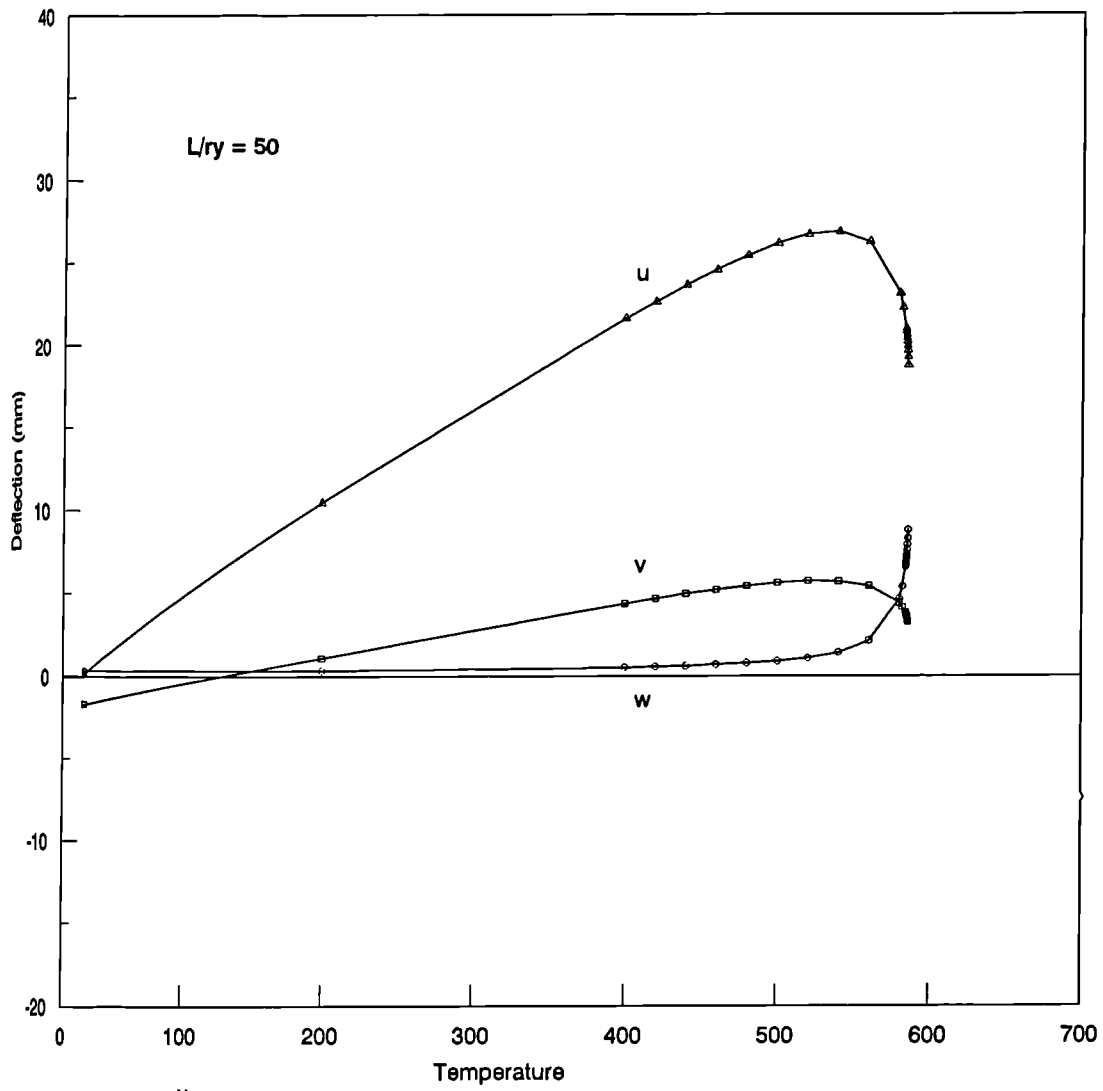
Fig. 5.19 Temperature-Deflection for a Column with Thermal Gradient
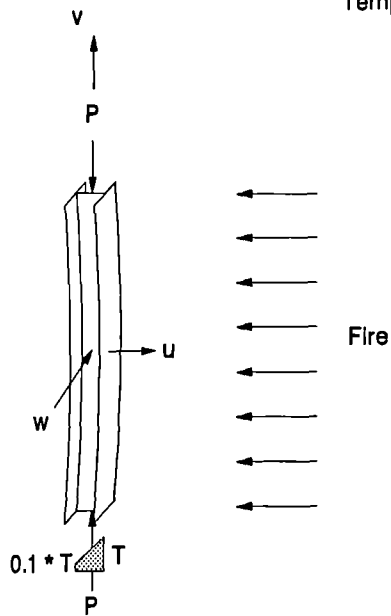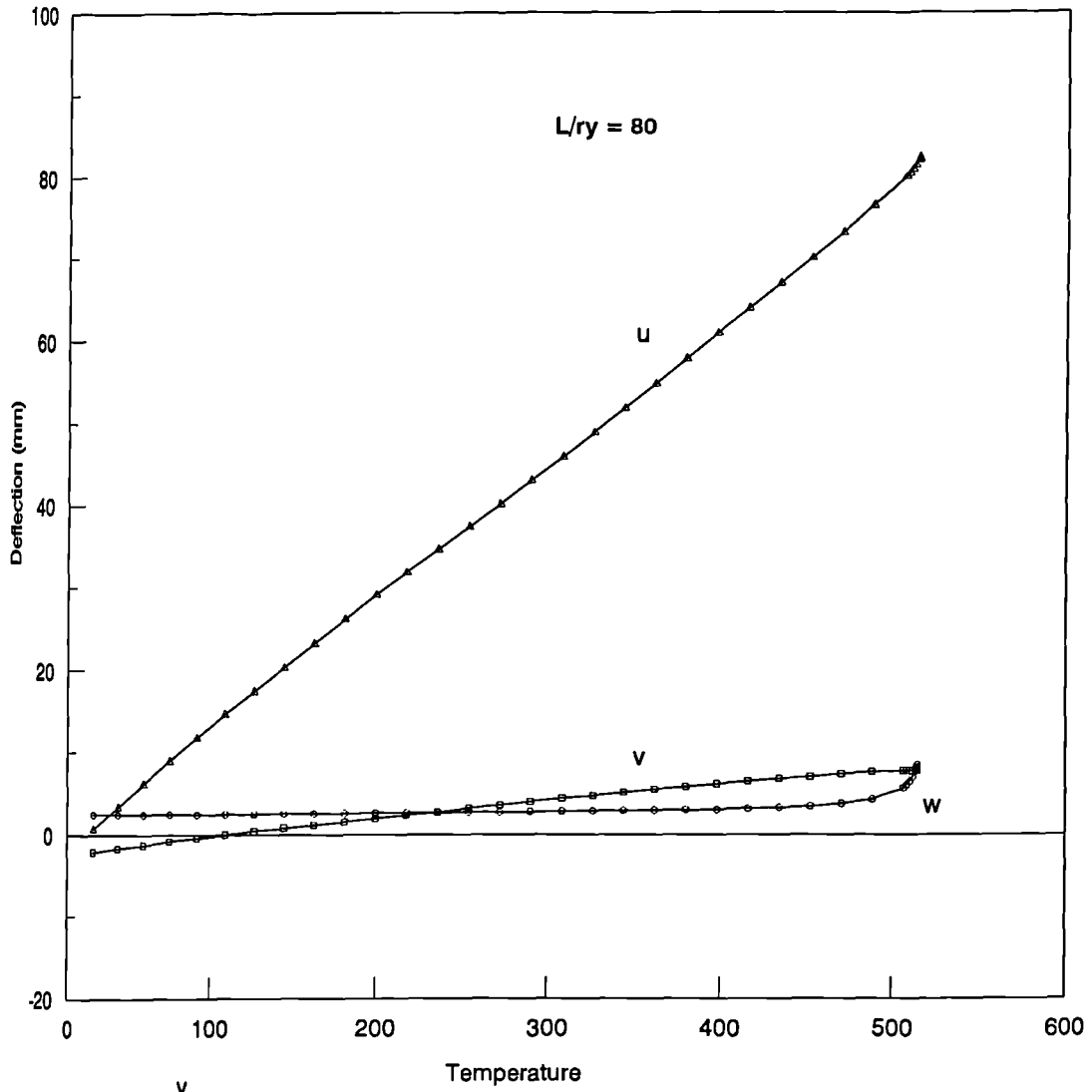
Fig. 5.20 Temperature-Deflection for a Column with Thermal Gradient

derness ratio between 40-60) reverse these deflections to some extent but without going beyond the initial configuration at ambient temperature. All columns within the second descending part of the curve (slenderness ratio above 60) do not exhibit any deflection reversal. This phenomenon of thermal bowing reversal has been observed in column tests under thermal gradient. Although it is being predicted in this study by a finite element analysis, it is still possible to understand it using the Perry approach developed in Chapter 2. The thermal gradient causes thermal bowing which contributes to the rise of deflections in the direction towards the fire source. At the same time the centroid of the section shifts in the opposite direction due to the non-uniform loss of stiffness across the section. Keeping in mind that the axial load is still applied at the original centroid (mid-web), this shift introduces a load eccentricity that causes deflections in the opposite direction to the thermal bowing. It seems that deflections due to this load eccentricity, although contributing to the reduction of the rate of thermal bowing in all cases, become the dominant part of the deflections before failure, especially for stocky columns.

It is notable that all columns with major axis gradients failed in a mixed mode, with all the three prominent mid-length deformations increasing excessively on the threshold of failure. Apart from columns with slenderness ratio higher than 150 and with 1:10 flange temperature ratio, all other columns failed at higher temperatures compared with uniformly heated columns. The failure temperature of the small number of columns with slenderness ratio above 150 is clearly not very far from the failure temperature of the uniform case.

5.4.6.2 Minor Axis Thermal Gradients

Though it is practically difficult to envisage situations where columns undergo thermal gradients across the minor axis, it was decided to undertake a similar study considering minor-axis gradients for the sake of completeness.

The same set of columns was used for this purpose with thermal gradient across the minor axis of the column. Initial out-of-straightness is applied about both principal axes and in the same direction as the thermal bowing. Six different temperature ratios (1:10, 2:10, 5:10, 7:10, 9:10 and 9.5:10) have been considered. The temperature ratio in this case represents the ratio between the extreme fibres of the flanges and the temperature of the web assumes the average value of temperatures at the extreme fibres.

Results of this study are shown on Fig. 5.21 along with the uniformly heated case. It is still clear that stocky columns with minor-axis thermal gradient have much higher fire resistance than the uniformly heated columns. This is true for columns of slenderness ratio less than 50. The significantly low failure temperatures for columns with high thermal gradients and high slenderness ratios is not surprising. The fact that the cool flange in the major-axis case retains a considerable fraction of the column's stiffness is in sharp contrast to the minor-axis case, where a negligible part of each flange remains stiff.

Figs. 5.22, 5.23 and 5.24 show the temperature-deflection history for three columns selected across the slenderness range for 1:10 temperature ratio. The behaviour of the column of slenderness ratio 20 shows reversal of thermal bowing and axial expansion unlike the other two columns of slenderness 50 and 80. It is clear that the reversal of thermal bowing allowed the stockiest columns with minor-axis thermal
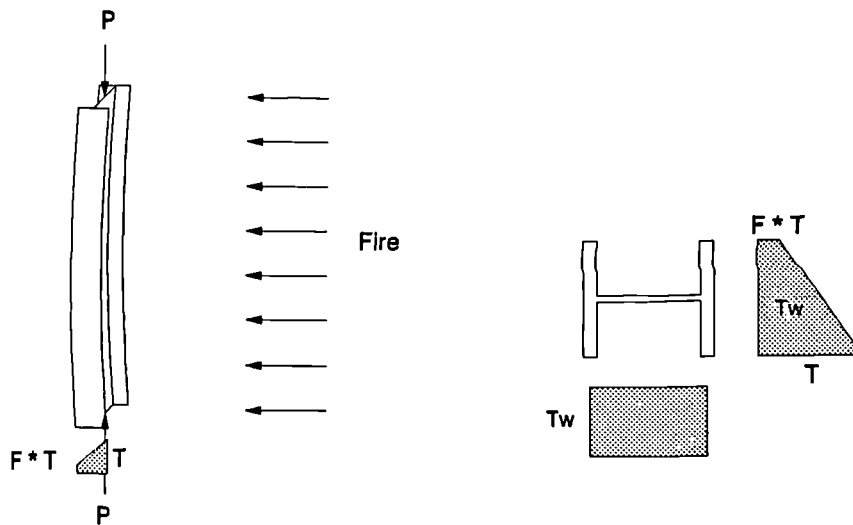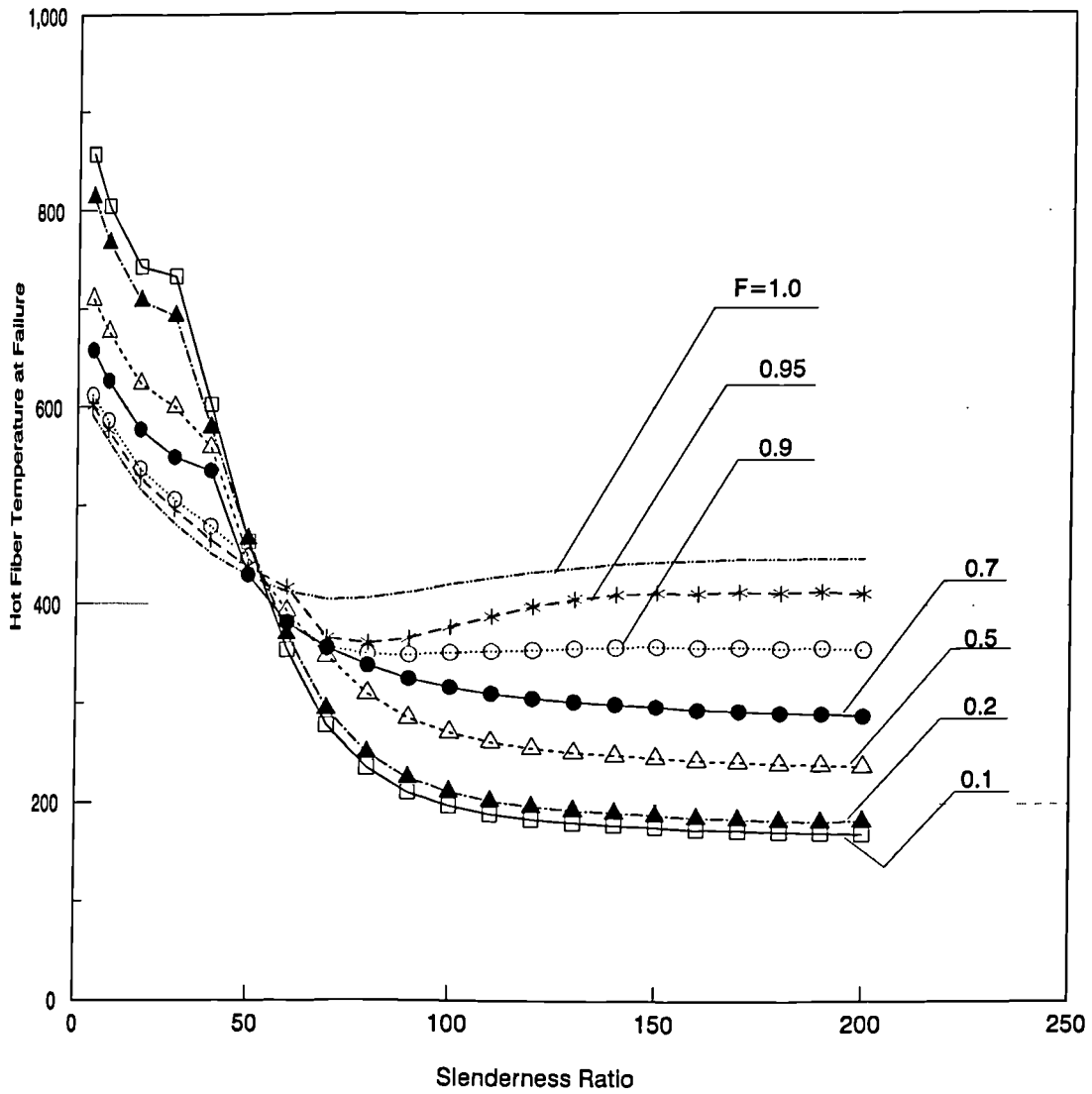
Fig. 5.21 Effect of Thermal Gradient about the Minor Axis

Fig. 5.22 Column Heated with Gradient about Minor Axis - Temperature-Deflection
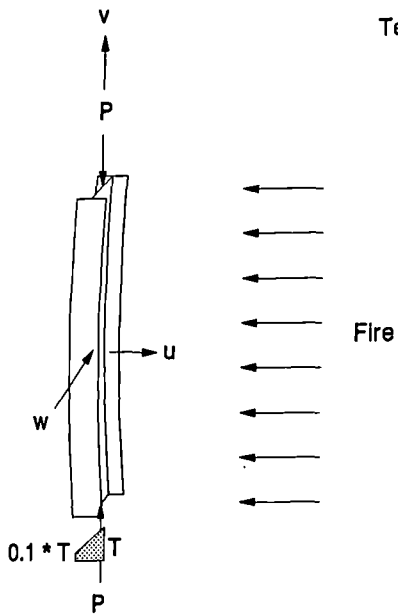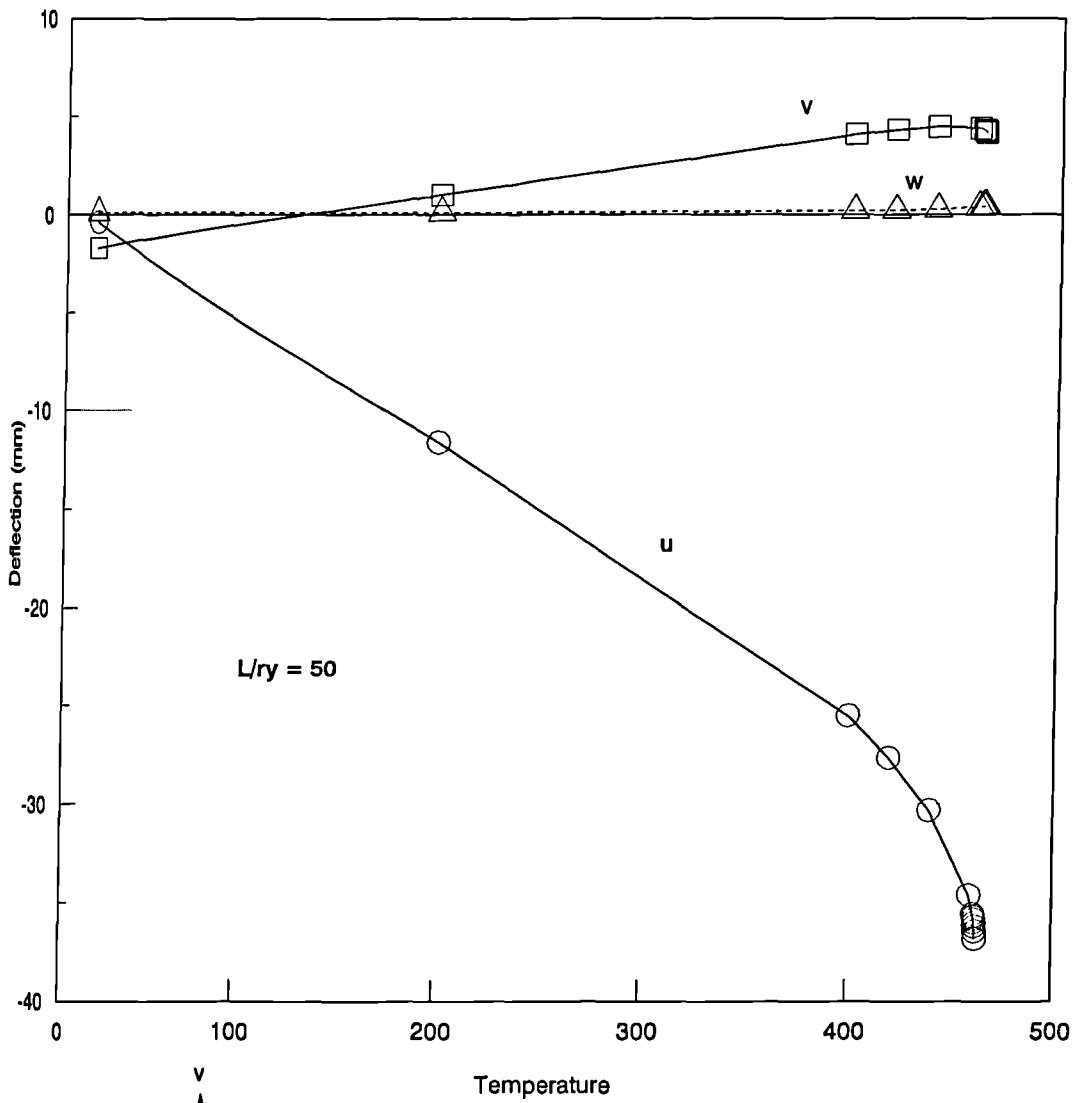
Fig. 5.23 Column Heated with Gradient about Minor Axis - Temperature-Deflection
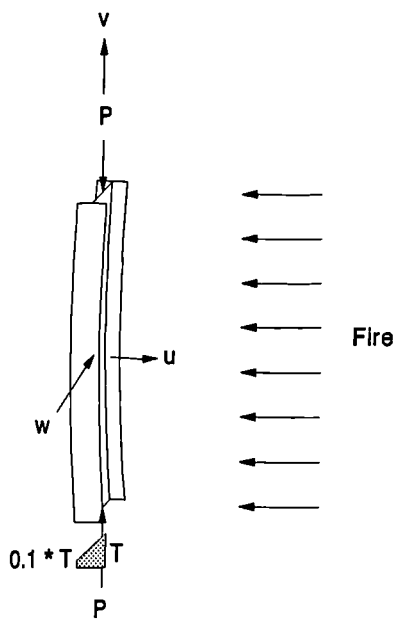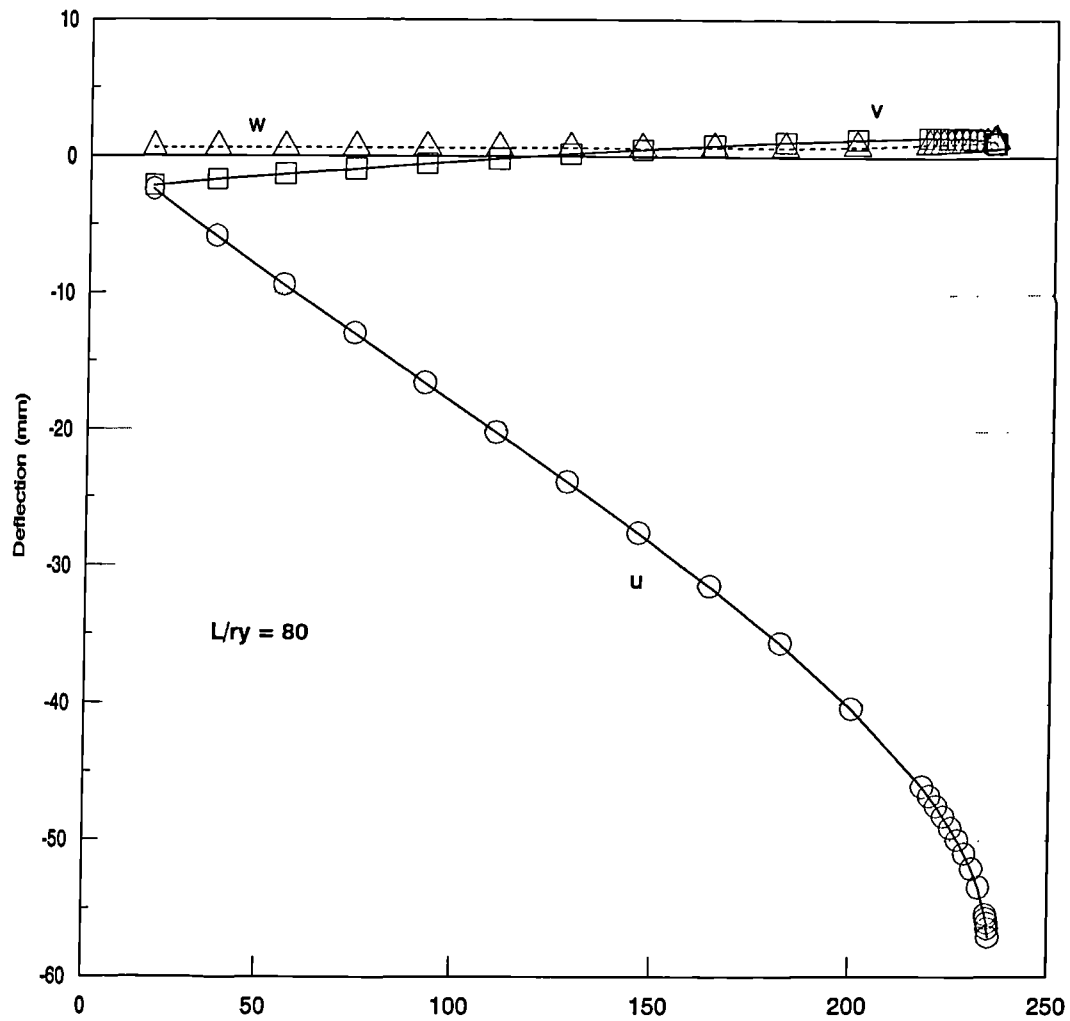
Fig. 5.24 Column Heated with Gradient about Minor Axis - Temperature-Deflection

gradients to sustain much higher temperatures.

5.4.6.3 Columns with Biaxial Thermal Gradients

Two sets of analyses for the same range of slenderness ratios were carried out to consider more general situations for columns experiencing thermal gradients. Assumed temperature profiles for each set are shown on Fig. 5.25. These profiles assume that a column with a flange exposed to fire will have a thermal gradient across its major axis. The temperature ratio of the protected flange is expected to be of the order of 10% of that of the exposed flange. While it is reasonable to assume that no significant gradient will take place across the minor axis, it was decided to investigate the effect of having a small gradient across the minor axis; a situation that might be more general than assuming no gradient at all. The ratio of the temperatures of the extreme fibres of the flanges was taken to be 95% and 90% in two separate sets of analyses. The reason for performing these analyses was to attempt a more realistic simulation of practical columns embedded within walls in fire conditions. A high thermal gradient across the major axis is expected in this case while a small variation in temperature across the minor axis is also expected.

The results of these analyses are shown on Fig. 5.25 along with the previous results for uniform temperature and major-axis gradient for the purpose of comparison. It is clear from the illustrated results that columns with biaxial gradient will fail at temperatures somewhere between the failure temperatures for single-axis gradient when each temperature gradient axis is considered separately. Fig. 5.25 shows clearly that adding a small minor-axis thermal gradient contributed to higher failure temperatures compared to uniformly heated columns and even to columns with

Failure Temperature For Columns Loaded to 60% of BS449
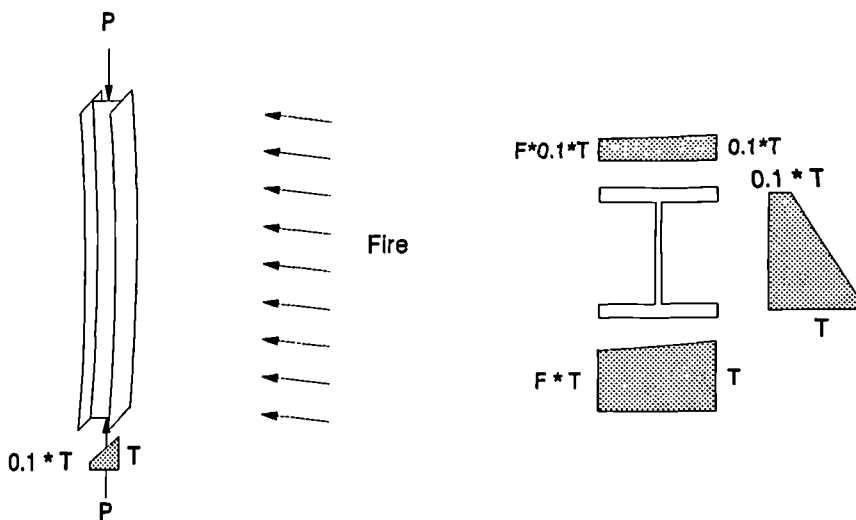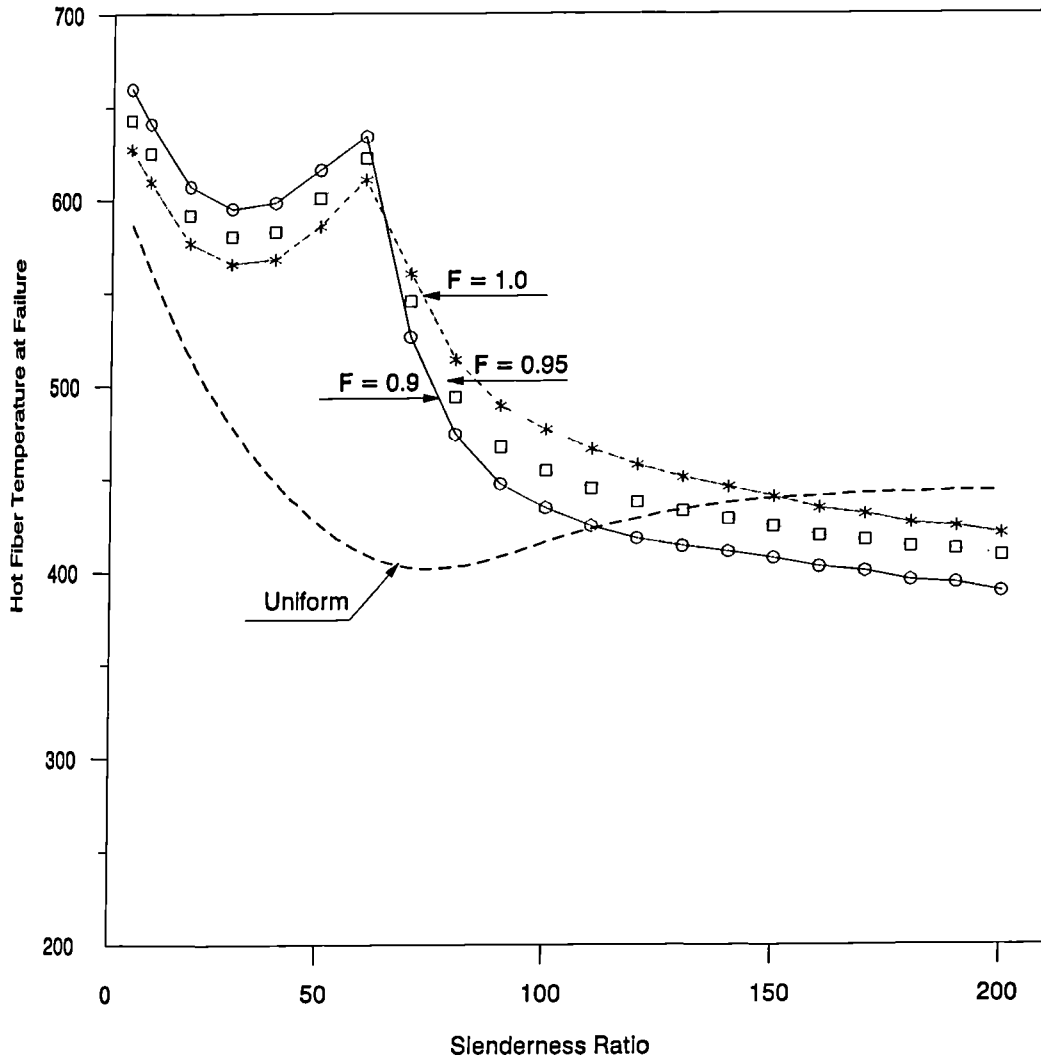
Fig. 5.25 Effect of Thermal Gradient about Both Principal Axes

major-axis thermal gradient. This is evident for columns with slenderness ratio between 5 and 60. For the rest of the range of slenderness adding the same minor-axis thermal gradient contributed to lower failure temperatures compared to the major-axis case.

Figs. 5.26, 5.27 and 5.28 show the temperature-deflection history for three columns of different slenderness ratios. Temperature-deflection characteristics are very similar to those of the major-axis case (Figs. 5.18, 5.19 and 5.20). Columns with slenderness ratio between 5-30 show full deflection reversal with respect to thermal bowing while columns between 40-60 slenderness show deflection reversal that did not going beyond the initial position of the column. The rest of the columns with slenderness higher than 60 show no deflection reversal.

It should be pointed out that all columns considered in all thermal gradient studies have unrestrained out-of-plane behaviour. In practice, columns subject to thermal gradient are very likely to be embedded within walls. These walls constitute an effective restraint against out of plane buckling which implies an even better fire resistance for such columns.

5.4.7 Effect of Cross-Section

All the studies in the previous sections were carried out using a single Universal Column cross-section from the British Steel tables. Different slenderness ratios were obtained by changing the columns' lengths. It is necessary, for the sake of completeness in this study, to consider whether the use of different cross-sections from the tables causes different behaviour. To avoid extensive repetition of work, three slenderness ratios were selected for re-analysis, using various cross-sections
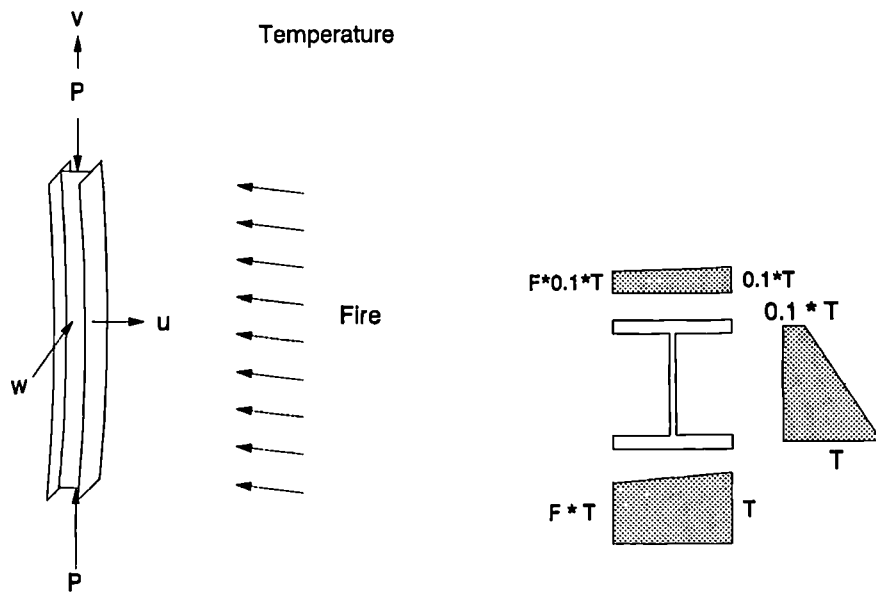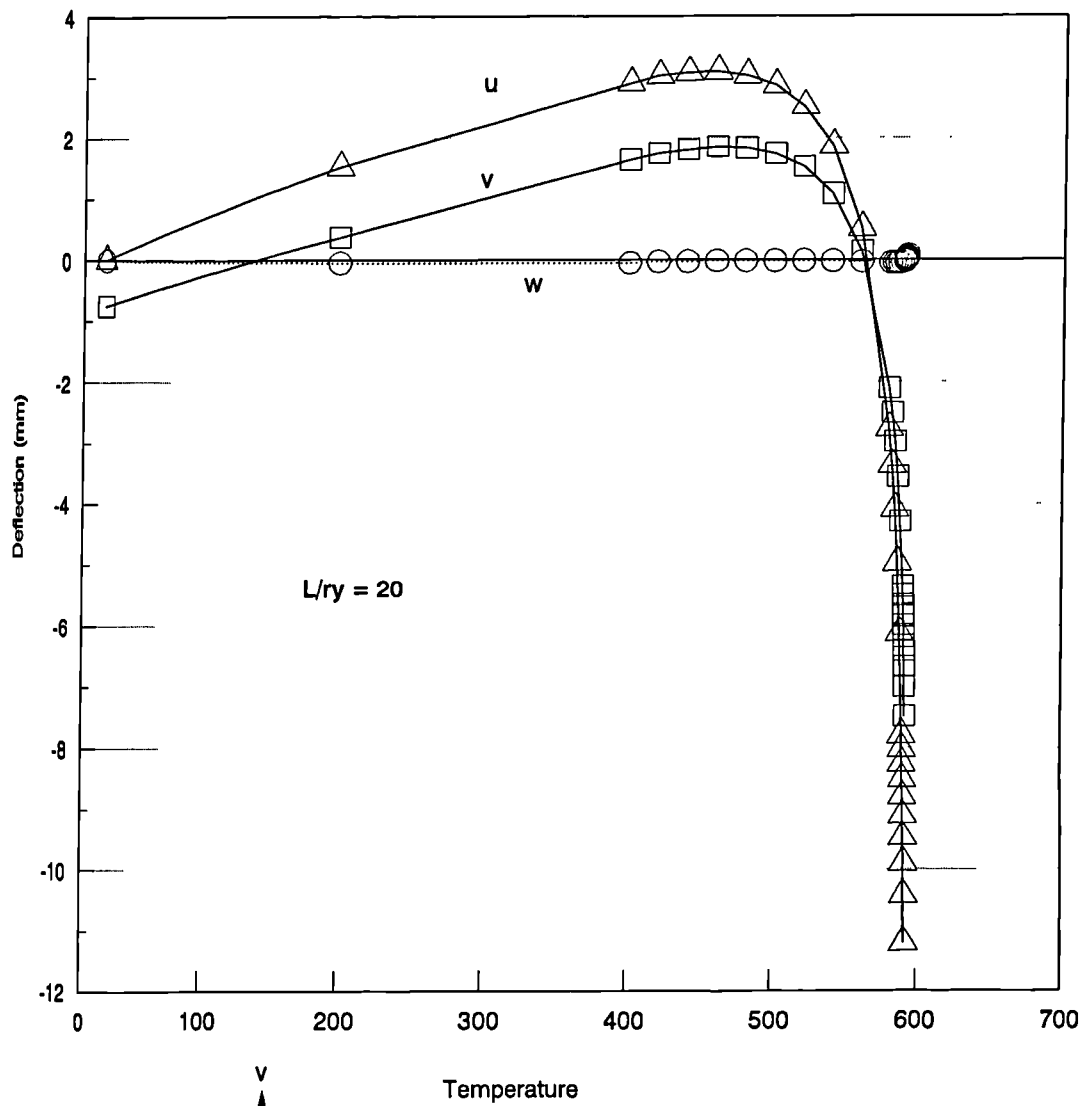
Fig. 5.26 Temperature-Deflection for a Column with Biaxial Thermal Gradient
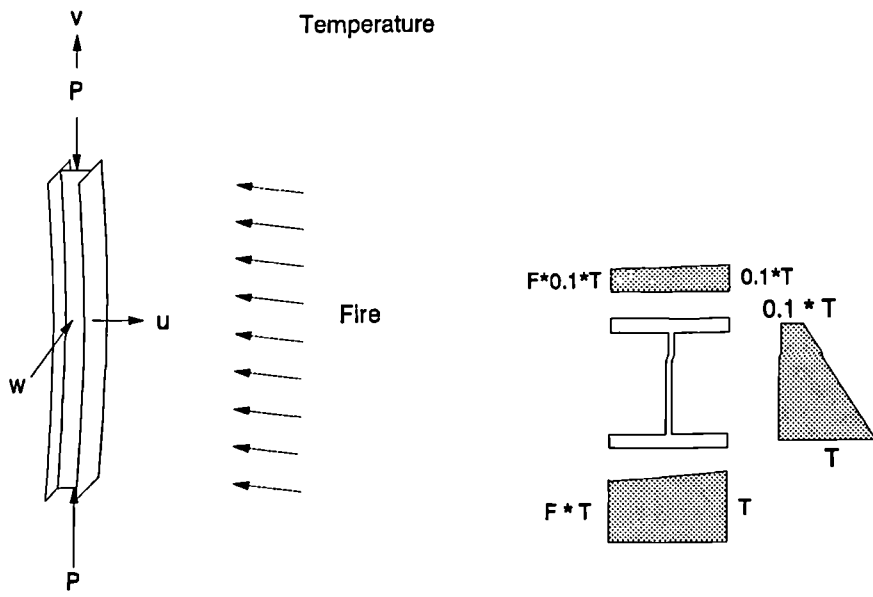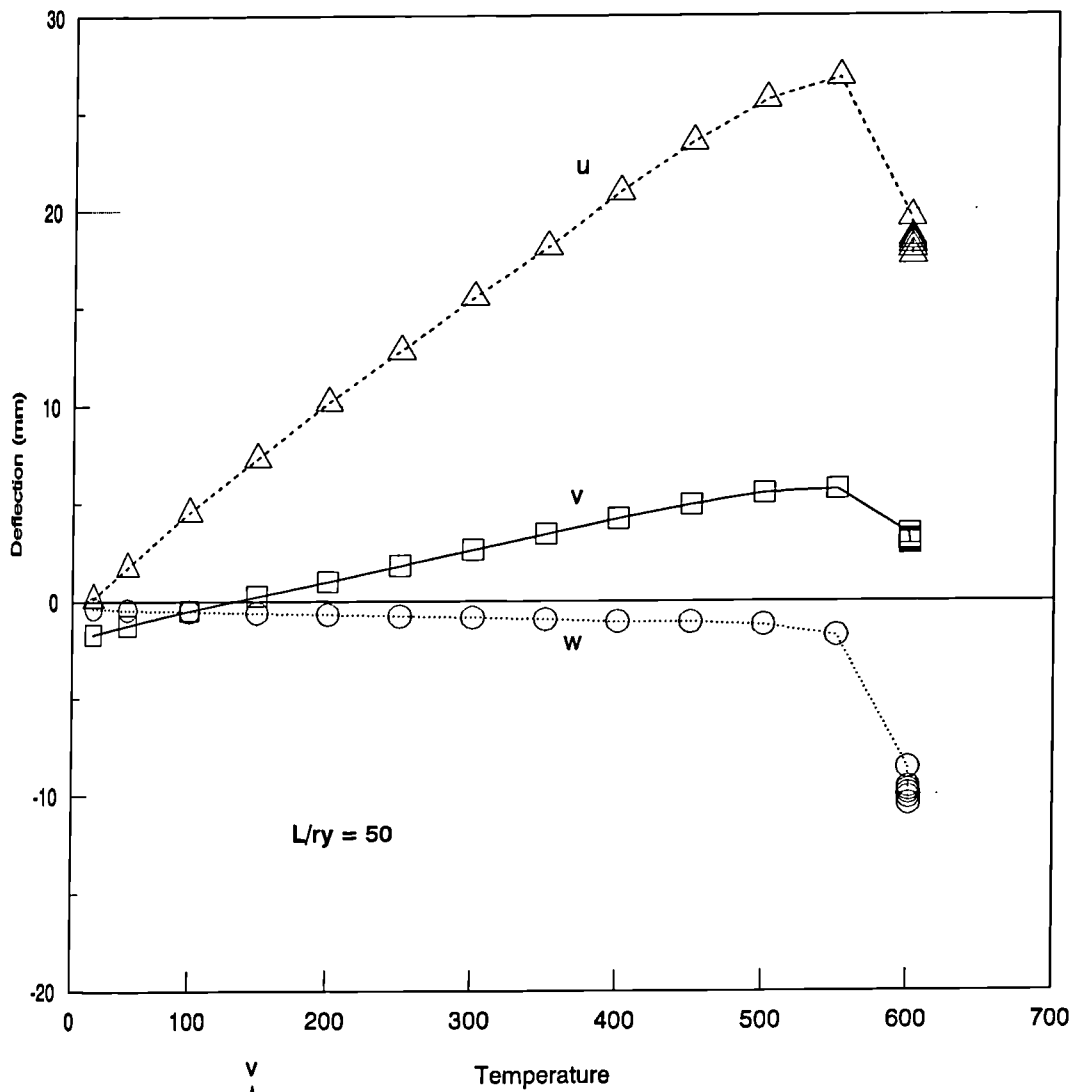
Fig. 5.27 Temperature-Deflection for a Column with Biaxial Thermal Gradient
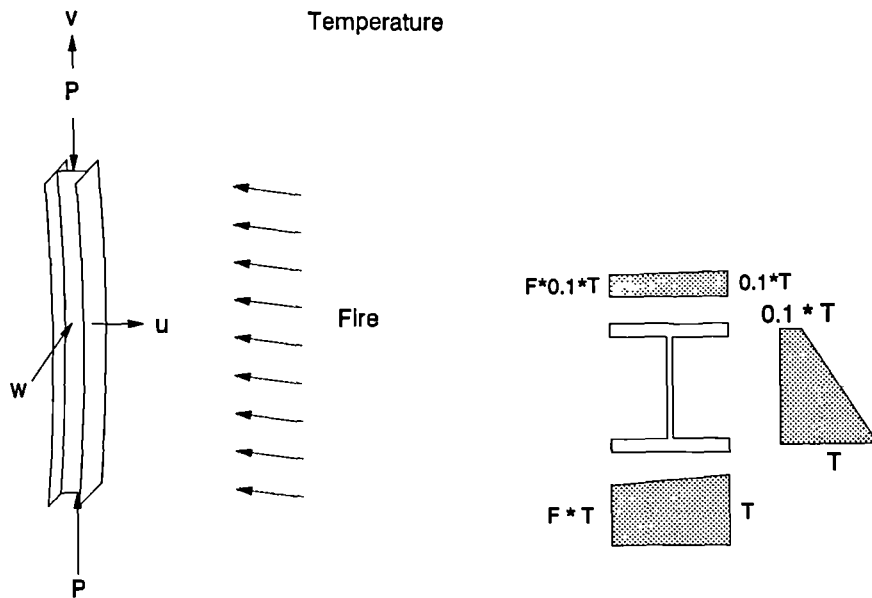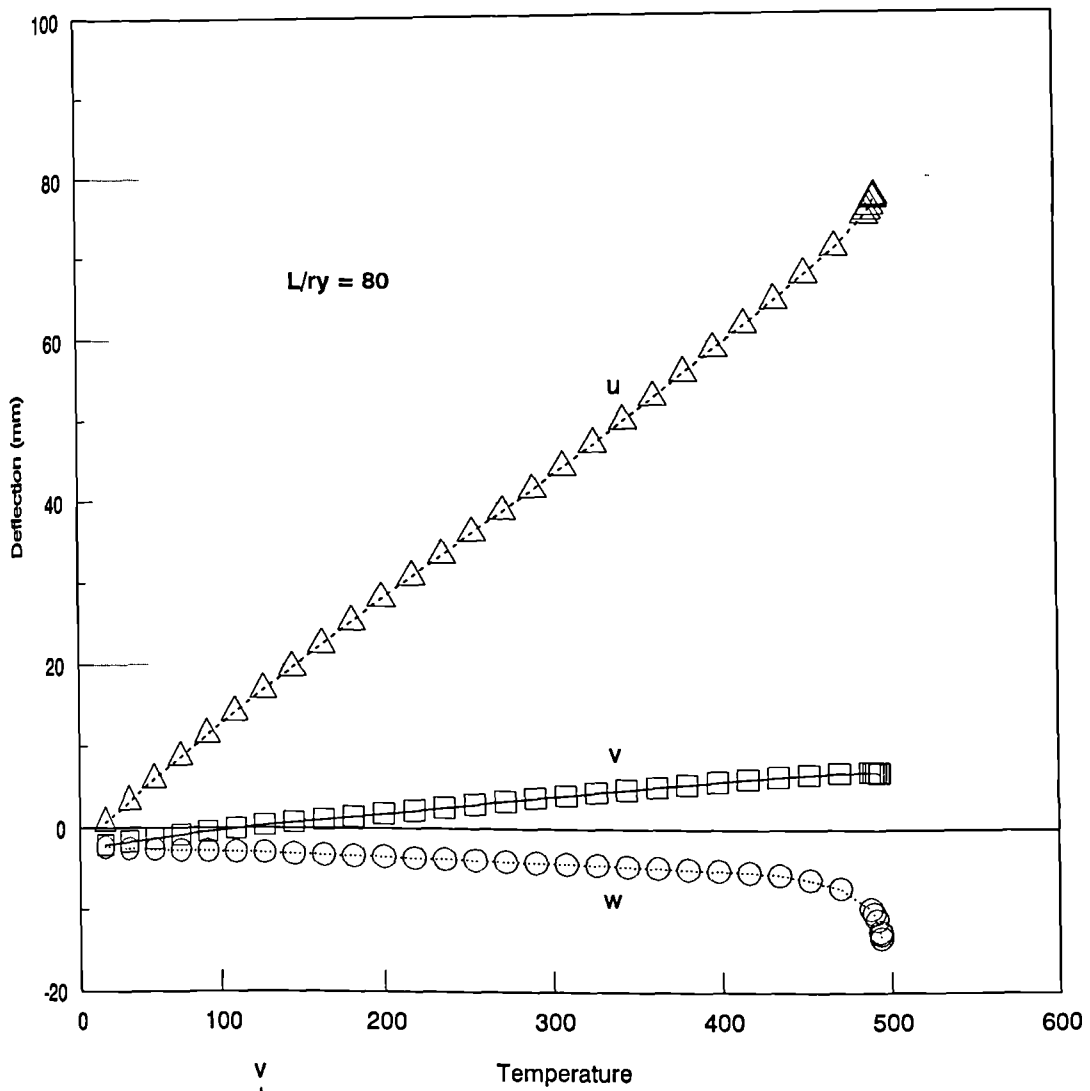
Fig. 5.28 Temperature-Deflection for a Column with Biaxial Thermal Gradient

selected across the table. All the sections selected were analysed for cases of both uniform and non-uniform temperature profile.

Fig. 5.29 shows the failure temperatures for 10 columns heated uniformly and loaded to 60% of their capacity to BS449. Slenderness ratios of 30, 80 and 130 have been considered as a good sample of the practical range of slenderness ratios. The failure temperatures of the $UC203 \times 203 \times 52$, which has been used for all the previous studies, are represented as a reference temperature by the broken line on Fig. 5.29. The scatter of failure temperatures when other sections are used can be seen to be extremely small.

The same exercise has been carried out using the same assumptions with the exception that a thermal gradient has been applied across the major axis of all the columns (Fig. 5.30). Failure temperature variations in this case, although higher than the uniform case especially for intermediate and high slenderness ratios, are still clearly acceptable. The variations in failure temperature for the stocky column (slenderness ratio 30) are clearly very small and compare better with results obtained by using the reference column.

5.5 Columns Within 3-D Subframes

In steel construction it is a common practice to use one column section over several storeys despite the fact that successive smaller columns could carry the applied loads at different levels. This practice is quite sensible in order to facilitate the construction procedures, to reduce the piece-count and to offset excessive connection cost if different sections were used. This fact makes it worthwhile studying the effect of continuity into cool storeys on the fire resistance of such frames, an-
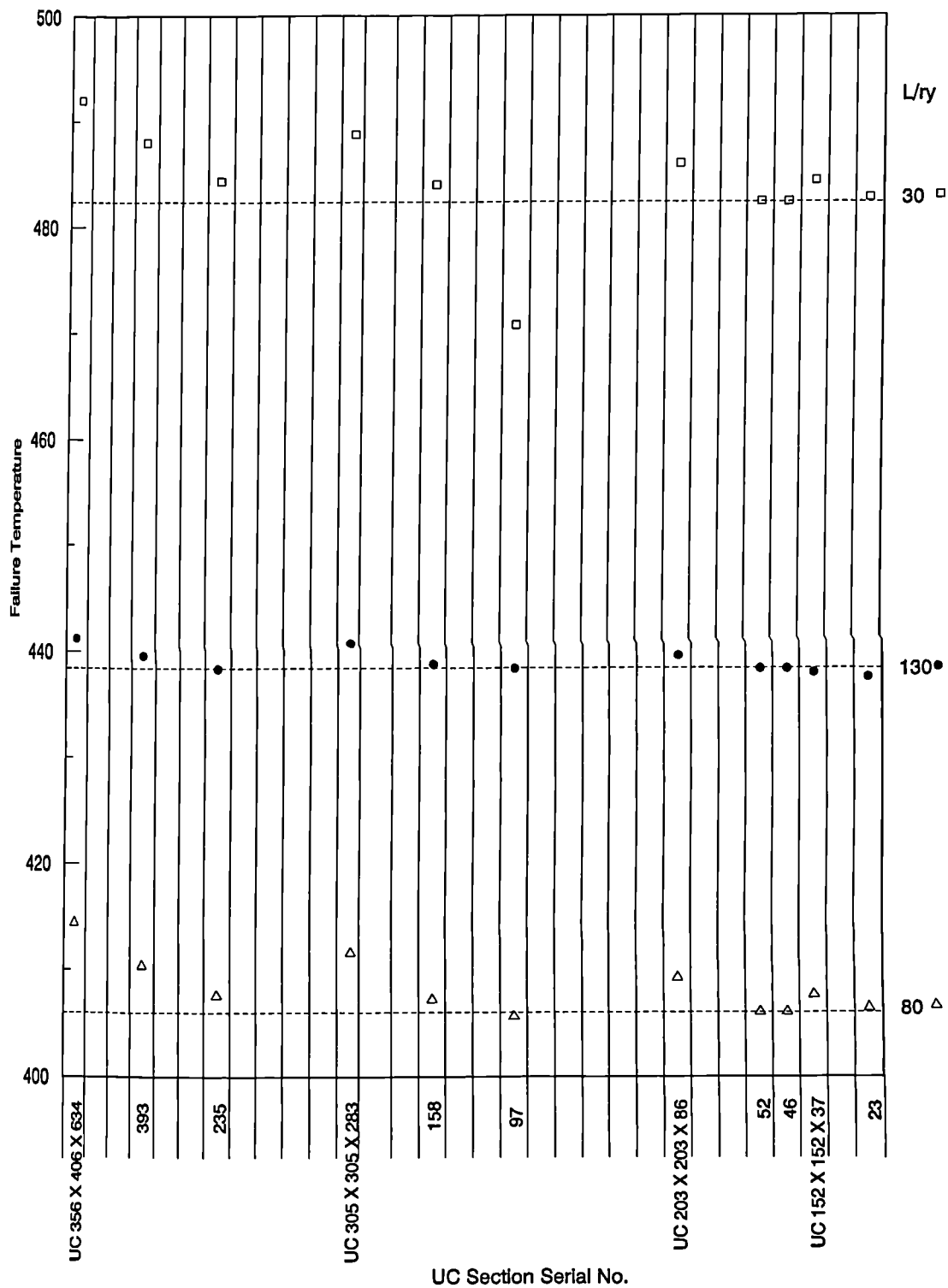
Fig. 5.29 Effect of Cross-Section on Failure Temperature for Uniformly Heated Columns
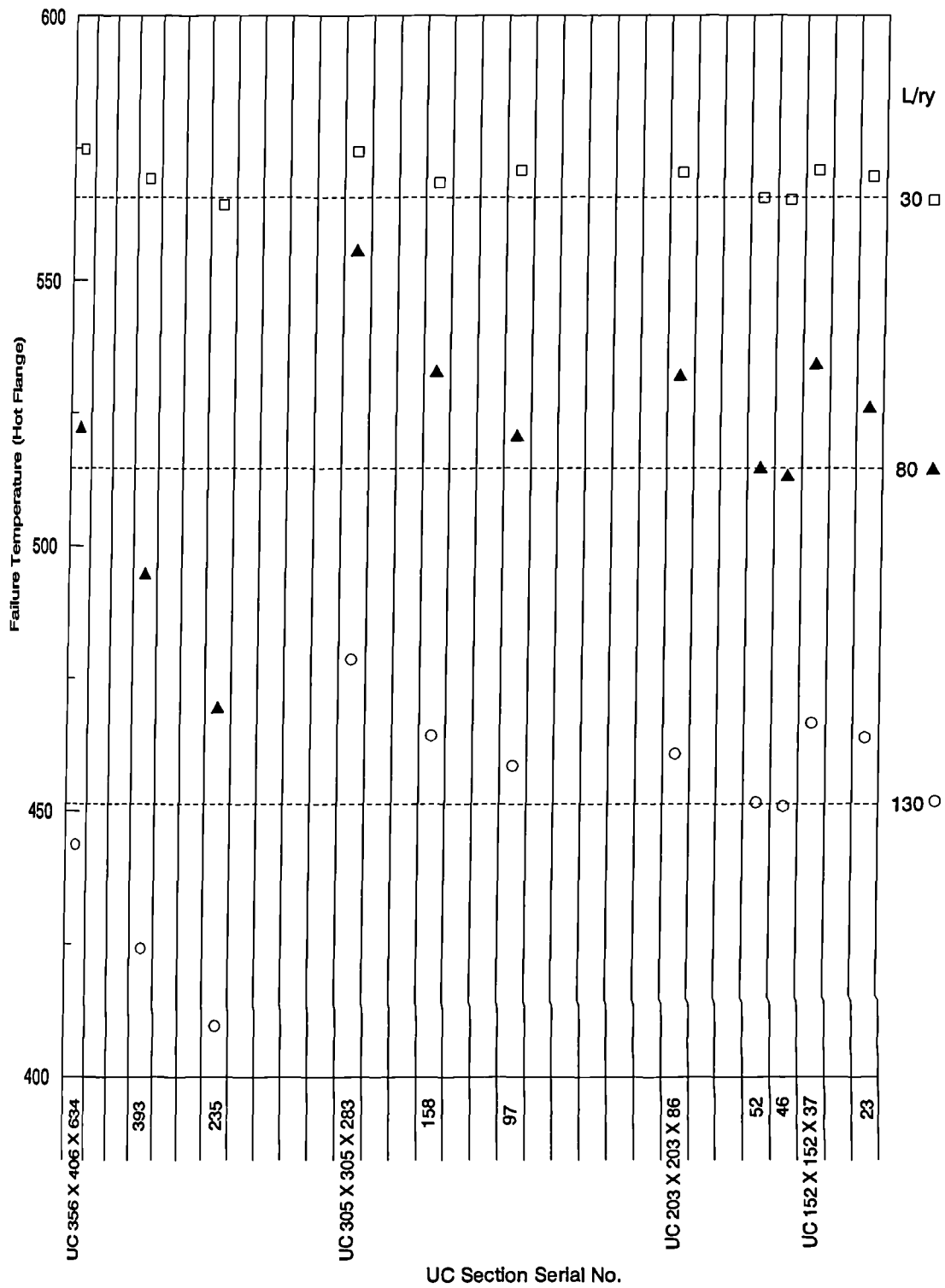
Fig. 5.30 Effect of Cross-Section on Failure Temperature for Columns with Gradient

ticipating better fire resistance especially for columns in higher storeys which are bound to carry reduced load ratios.

5.5.1 Uniformly Heated Columns Within Subframes

In the following study, three-storey subframes are used with the same column section and height for all storeys. The storey height was varied between subframes in order to obtain different slenderness ratios, while the section $UC203 \times 203 \times 52$ was again used in all the subframes. The same section ($UB406 \times 178 \times 74$) and length ($6m$) were used for beams meeting the column at each floor level in all subframes. This arrangement resulted in a lower storey column loaded to 60%, the middle column loaded to 40% and the upper-storey column loaded to 20%, of capacity. The reason for keeping the beams the same for all cases is to ensure that the column parameters are the only variables in this study. For the same reason all beams were kept at ambient temperature in all the following analyses. Equal loads have been applied at the mid-span of the beams at all floor levels so that the lowest column carries 60% of its ultimate load to BS449. Assuming full symmetry with adjacent bays, the analysis has been carried out using half the spans of the beams with restrained rotations and unrestrained vertical displacements. To study rigidly-connected frames beams were introduced as described above. In the simply-connected frames the beams were removed, and columns were restrained in position and unrestrained in direction at each floor level. This arrangement was used as a result of the present analysis being capable of handling only rigid frames.

First the lower column, which carries a constant load of 60% of its ultimate load

was heated uniformly. Failure temperatures for both cases of simple and rigid connections are shown on Fig. 5.31 along with results of the isolated case considered previously. The difference between failure temperatures of simple and rigid subframes is very small; about 30 degrees for the most slender column and almost zero for the stockiest one. Nevertheless, there is a remarkable improvement of the fire resistance of the columns in the subframe compared with the isolated ones, which ranges between $30^\circ C$ and $70^\circ C$.

The same subframes were also analysed heating the middle-storey column which carries 40% of its ultimate load. Failure temperatures for this case are shown on Fig. 5.32, which shows an even better improvement; an increase in the failure temperature of $40^\circ C$ − $120^\circ C$ compared with isolated columns that carry the same loads.

The third set of analyses has the upper column heated and carrying 20% of its ultimate load. The difference in failure temperatures can hardly be seen when comparing the simply and rigidly connected cases shown in Fig. 5.33. Nevertheless, the same improvement can be seen when comparing isolated columns and subframes carrying the same loads.

Results from all the three cases are plotted together on Fig. 5.34, from which a rise in failure temperature of the order of $120^\circ C$ is evident between the higher and lower-storey fires.

Temperature-deflection curves for three columns with slenderness ratios of 20, 70 and 150 are shown on Figs. 5.35, 5.36 and 5.37 for the simply connected subframe case. Similar curves for the rigidly connected case are shown on Figs. 5.38, 5.39 and 5.40. All columns on Figs 5.35-5.40 are loaded at the 60% level. It is diffi-
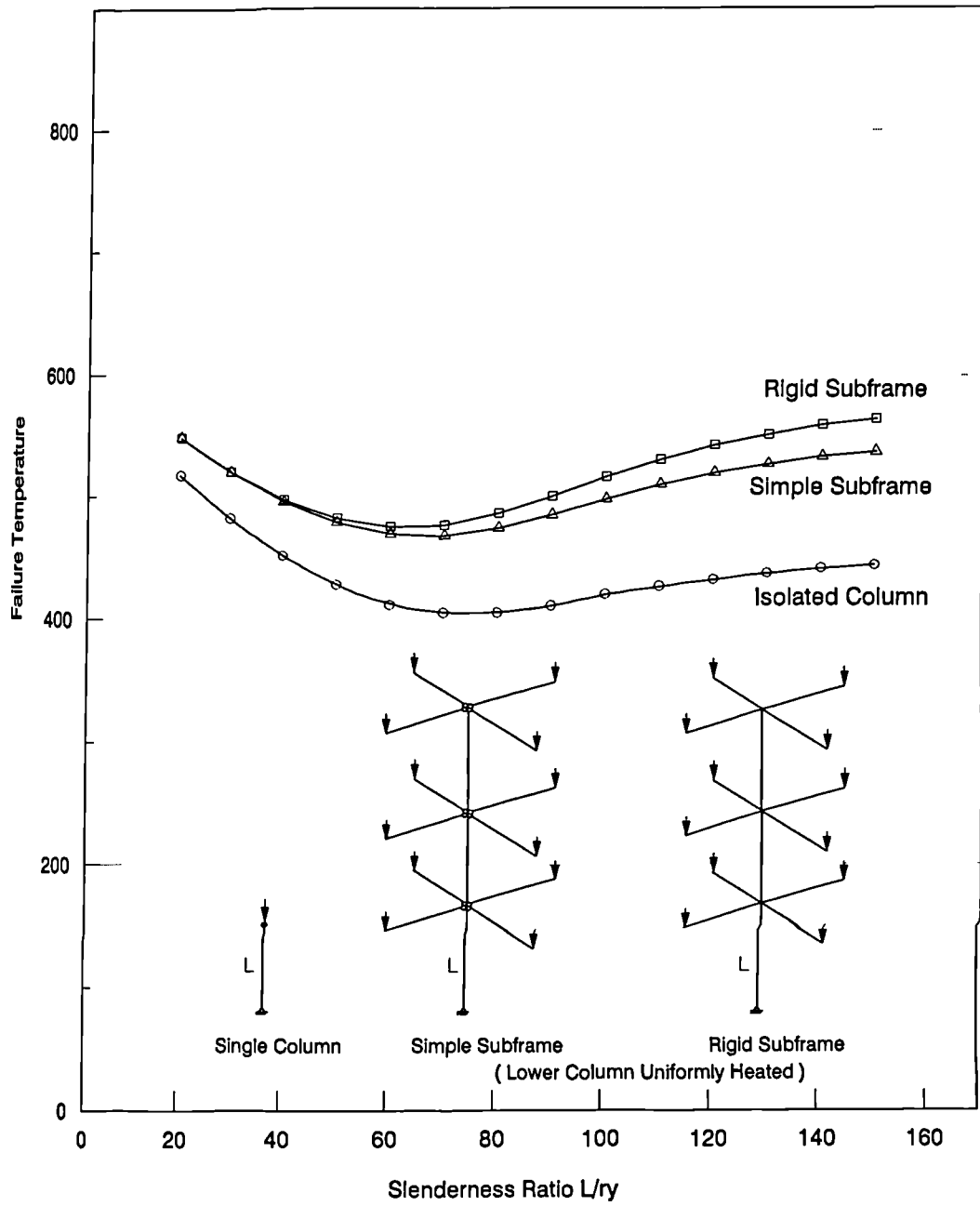
Heated Column Loaded with 60% of Ultimate Load to BS449

Fig 5.31 Failure Temperature for Subframes
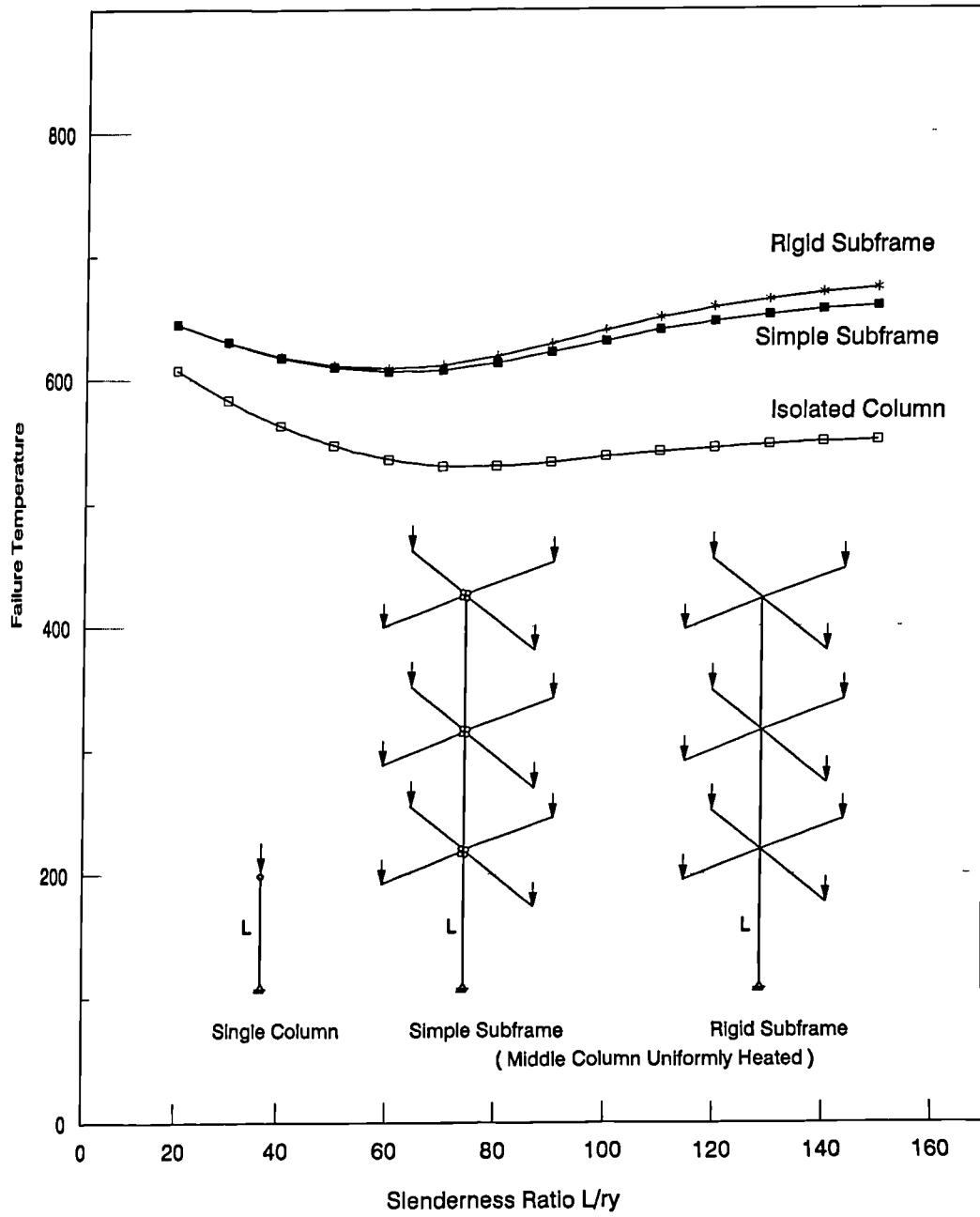
Fig 5.32 Failure Temperature for Subframes
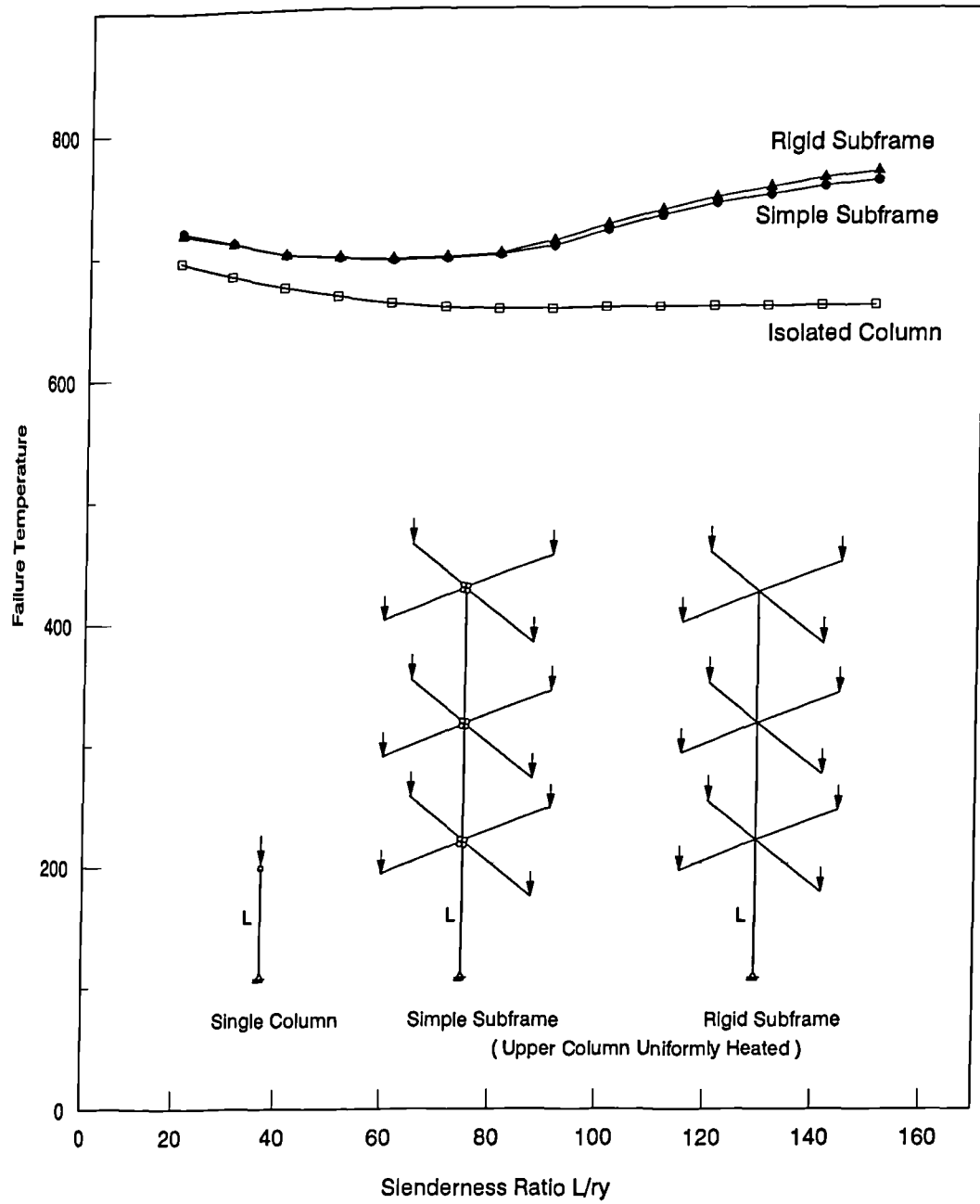
Heated Column Loaded with 20% of Ultimate Load to BS449

Fig 5.33 Failure Temperature for Subframes
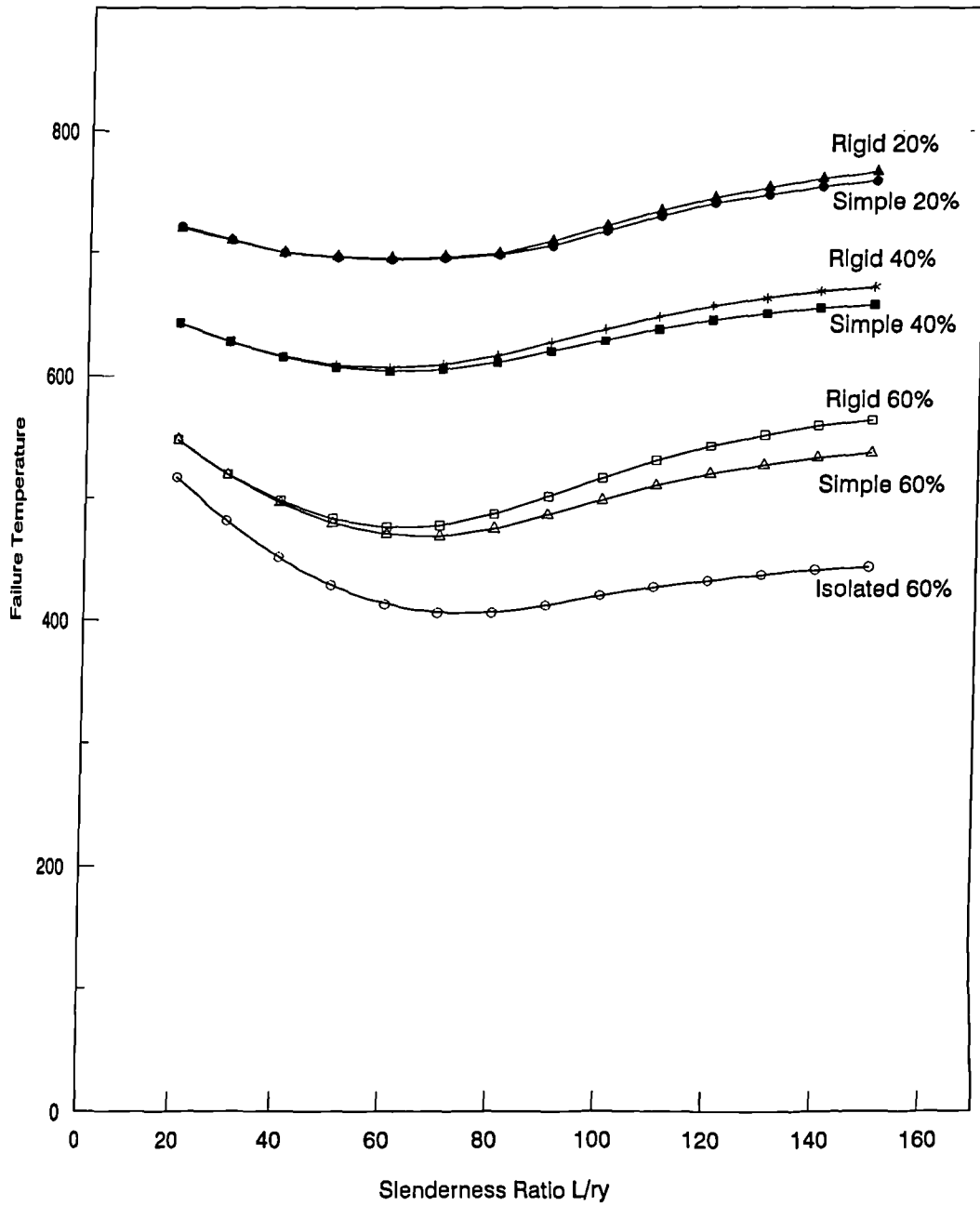
Heated Column Loaded with 20%, 40% and 60% of Ultimate Load to BS449 -Comparison

Fig 5.34 Failure Temperature for Subframes
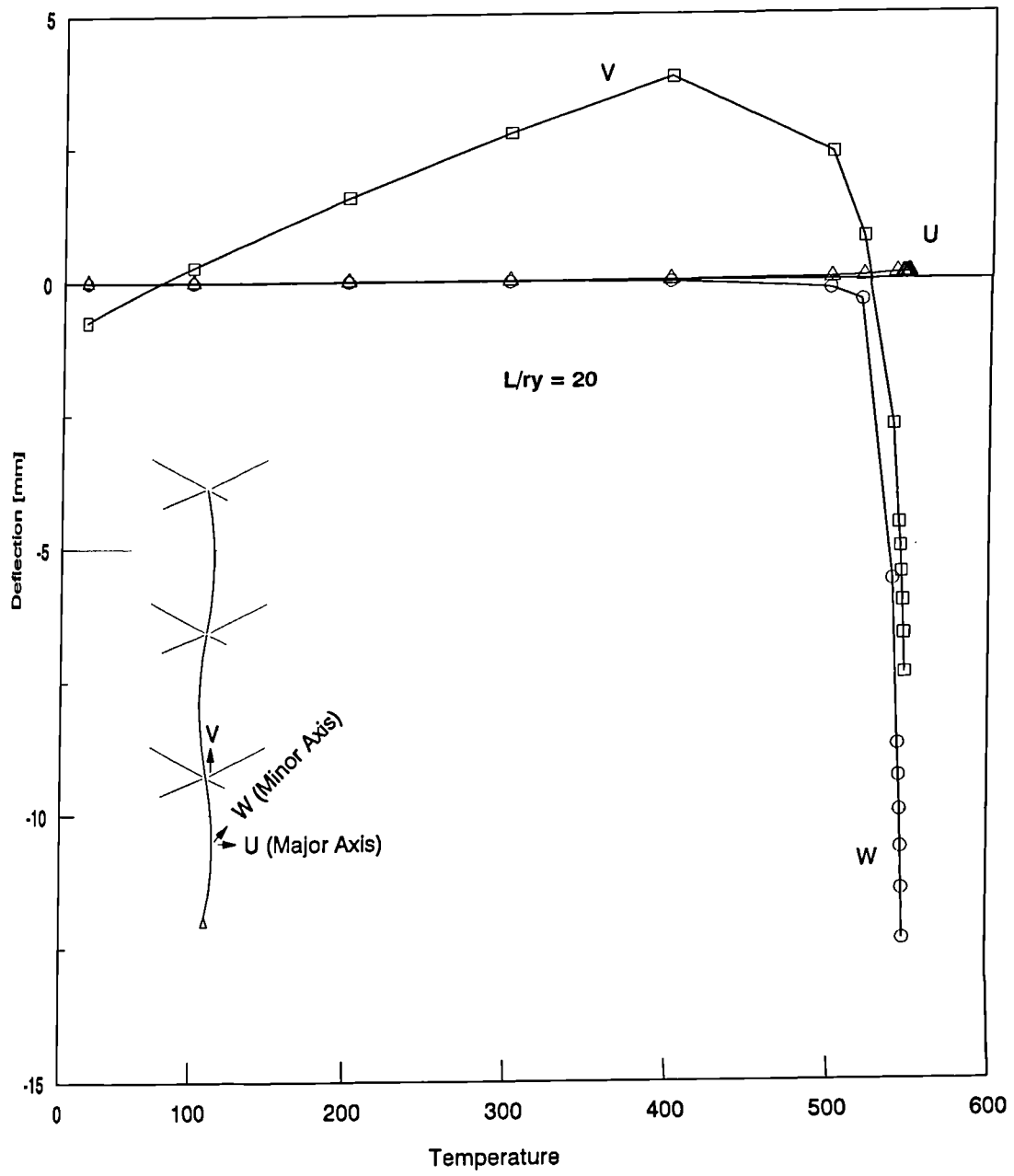
Fig 5.35 Temperature-Deflection In Simple Subframe
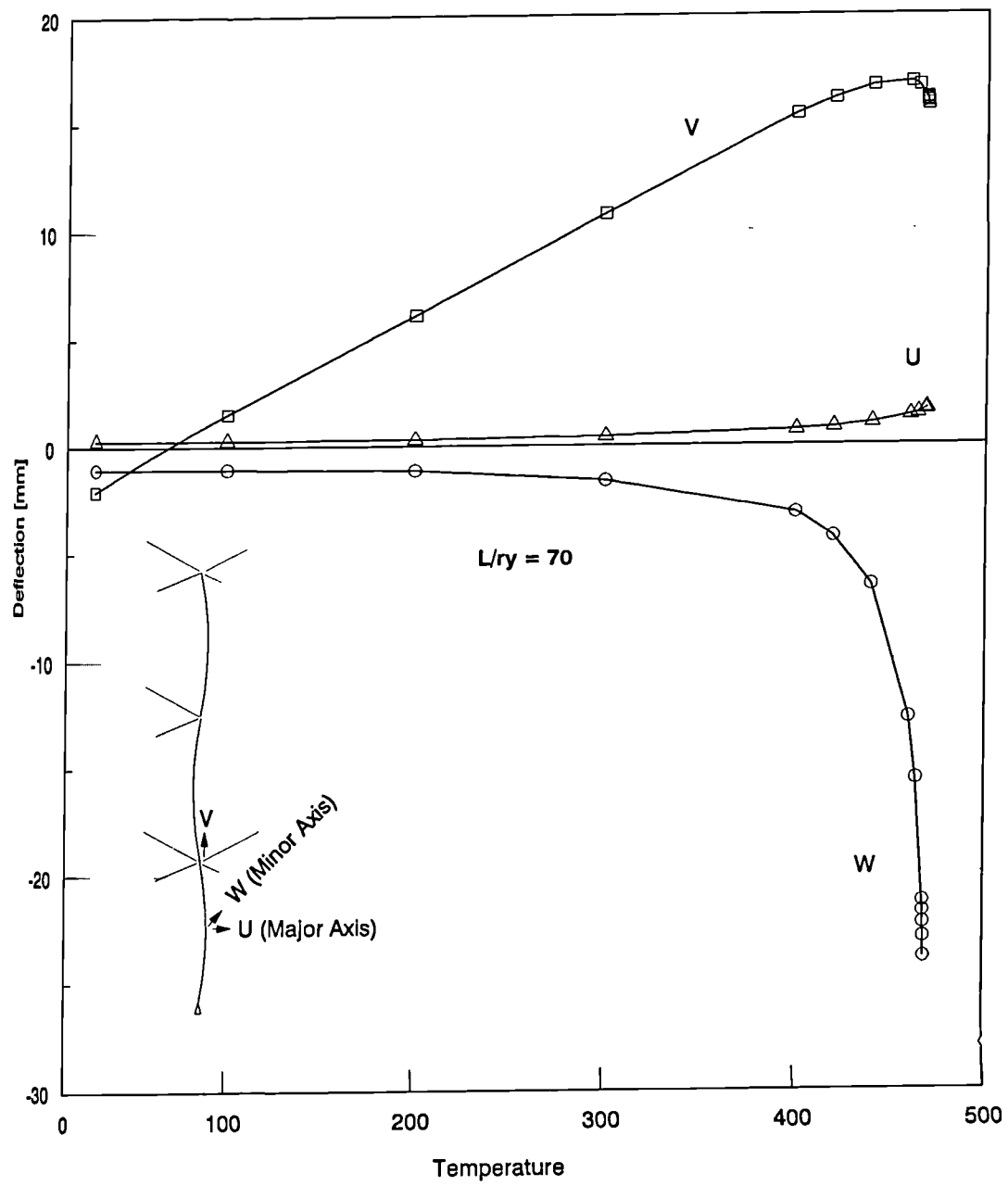
Fig 5.36 Temperature-Deflection in Simple Subframe
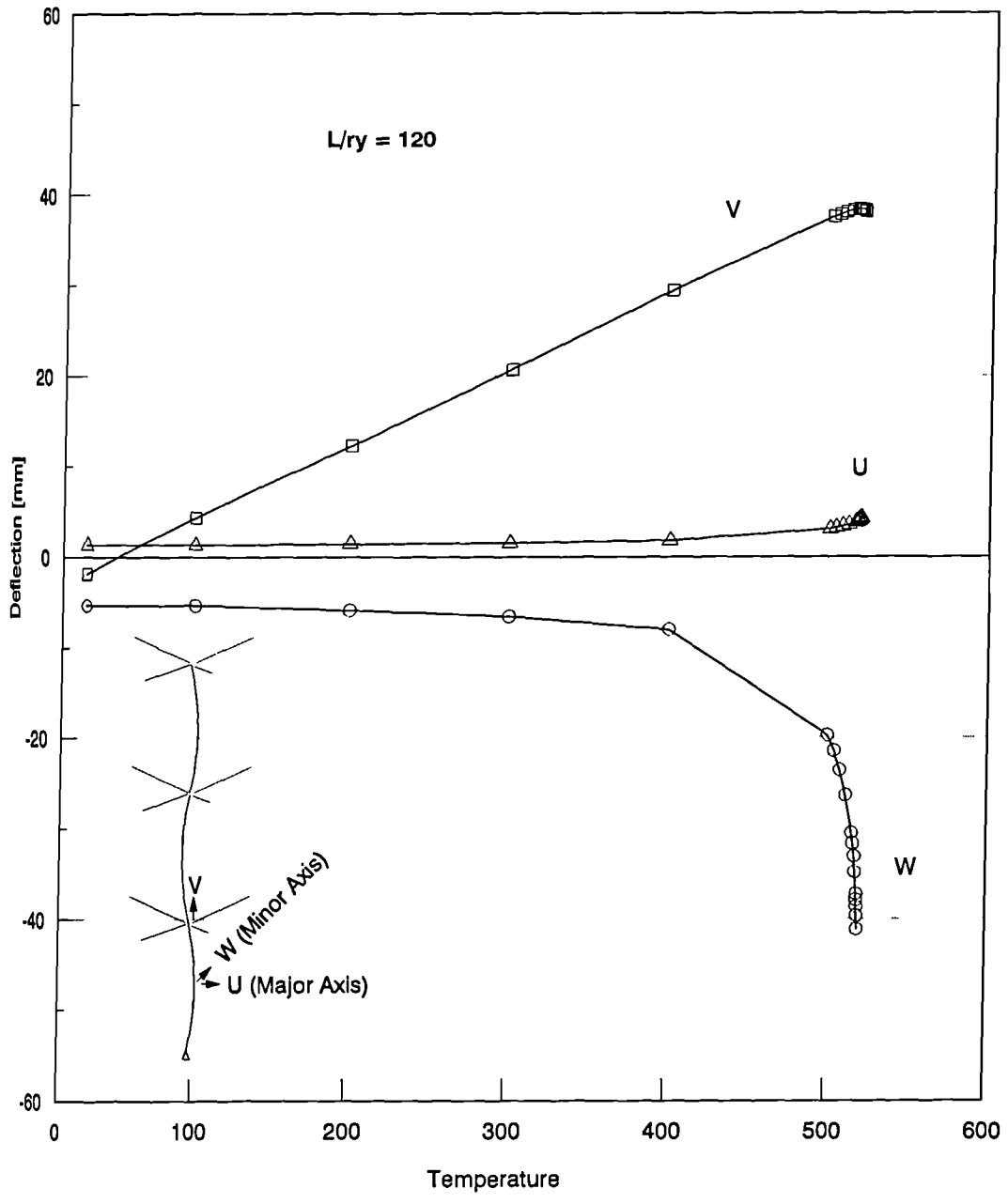
Fig 5.37   Temperature-Deflection In Simple Subframe
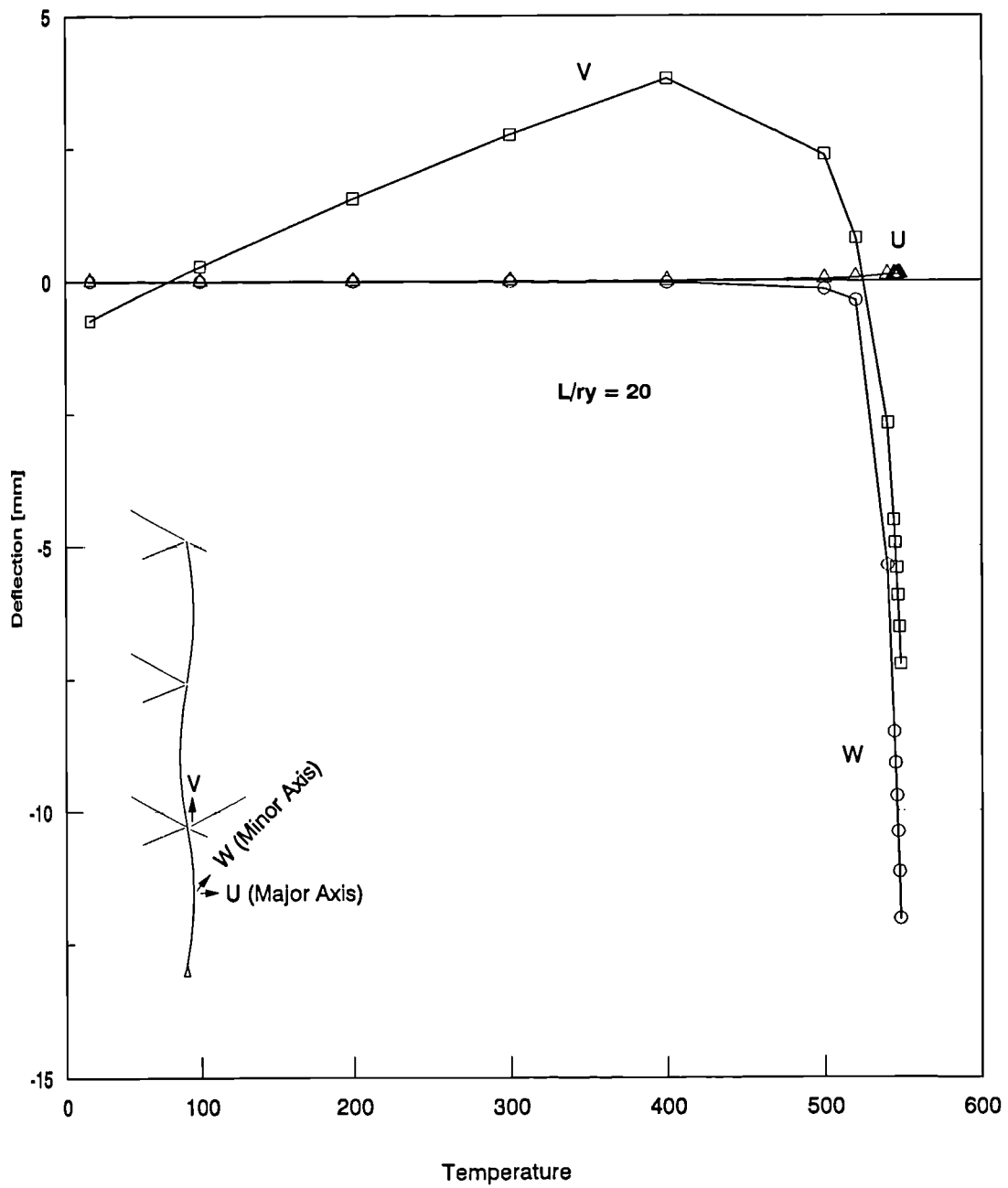
Fig 5.38   Temperature-Deflection In Rigid Subframe
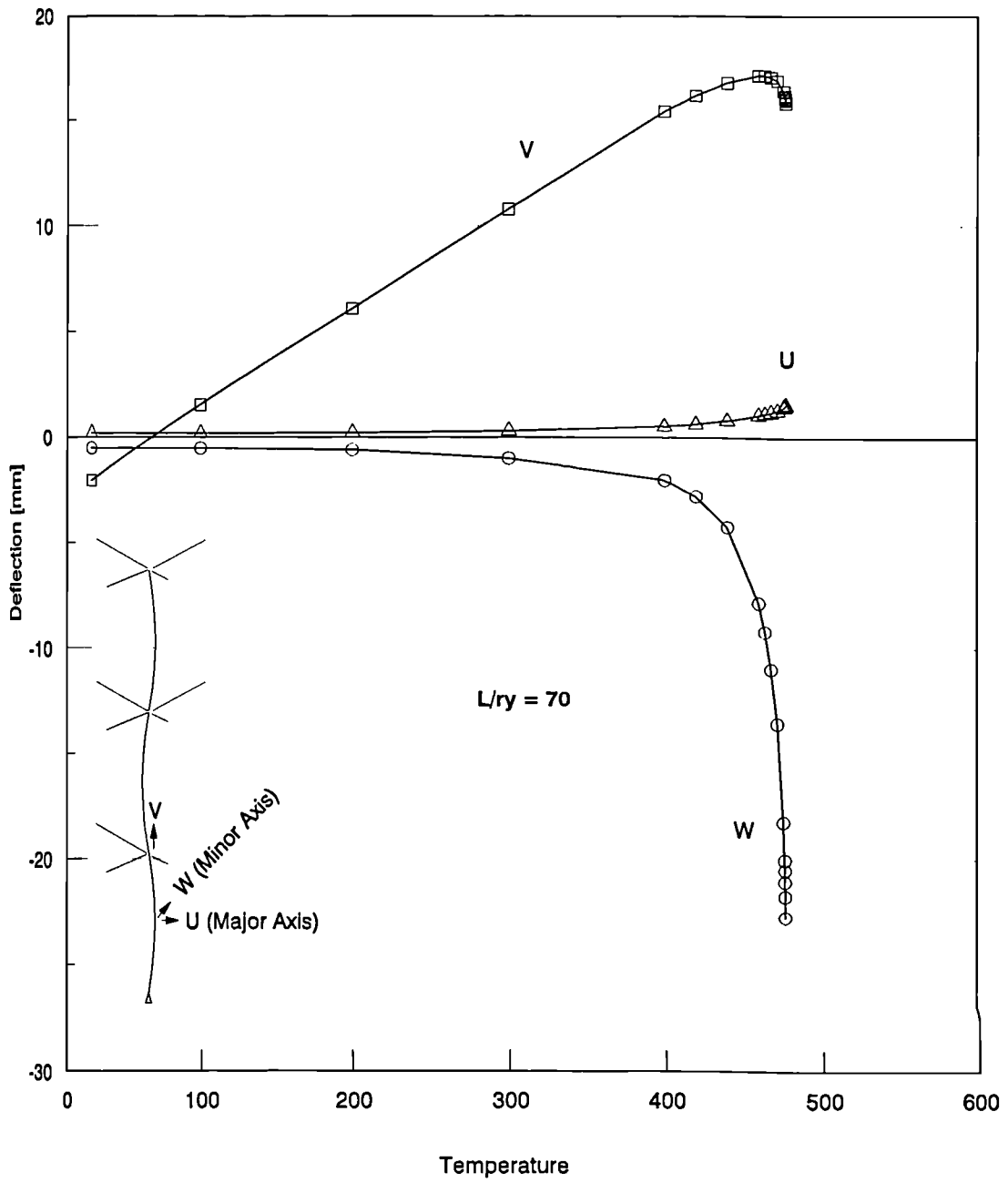
Fig 5.39 Temperature-Deflection in Rigid Subframe
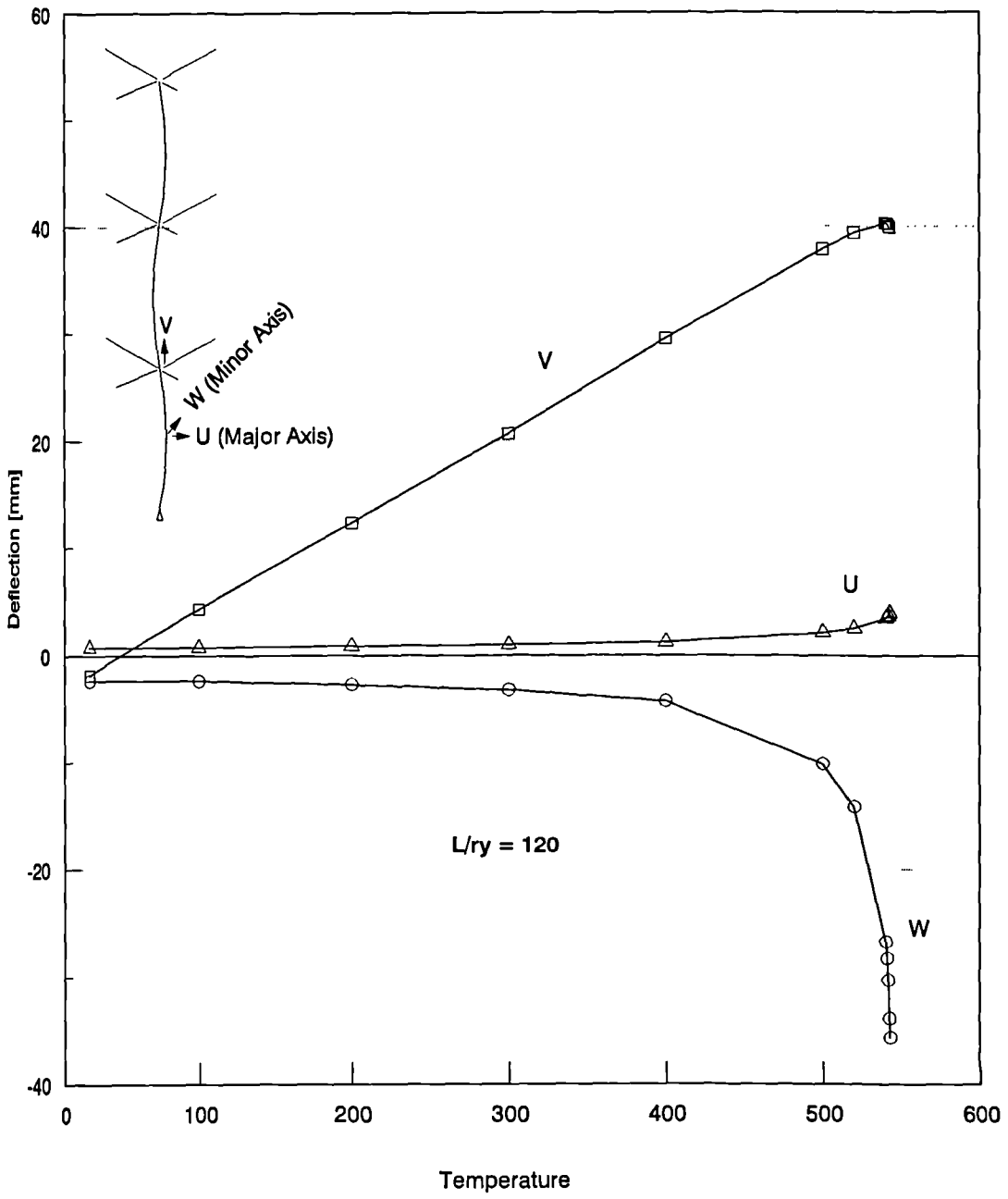
Fig 5.40 Temperature-Deflection in Rigid Subframe

cult to see any real difference in the deflection histories of columns with the same slenderness but different connections, a fact that was reflected in the similarity of failure temperatures. It is clear from the deflection curves that all columns failed by buckling about their minor axes, though the reversal of the axial expansion is prominent at low slenderness ratios and less visible at higher ratios.

The obvious observation is that columns with reduced load ratios, an inherent feature in multi-storey buildings, exhibit better fire resistance.

The most important observation is the enhanced fire resistance of framed columns compared with identical isolated columns. This phenomenon can be explained in the context of the additional end restraints provided by the cool column or columns at unheated levels. This additional end-stiffness acts almost as a rigid boundary to the heated column. This effect can be seen if the deflected shape of the column is plotted. Fig. 5.41 shows the deflected shapes of three columns of 20, 90 and 150 slenderness ratio at various stages in the heating scheme. While the deflection of an isolated column assumes a sinusoidal shape, the framed columns show a completely different shape towards the threshold of failure. The clear points of contraflexure within the heated column indicate the amount of stiffness provided by the cool columns, to the extent that the heated column can be thought of as fixed-ended. This clearly means that the slenderness ratio of the heated column is considerably reduced, providing it with extra stiffness. The extent of this reduction will be considered later in this study.

The apparent conclusion is that this improvement in the fire resistance of framed columns is mainly the result of the cool columns rather than the beams. When the beams are removed altogether, as in the simple-connection case, the resulted reduction in the column fire resistance can be seen to be minimal and confined to the
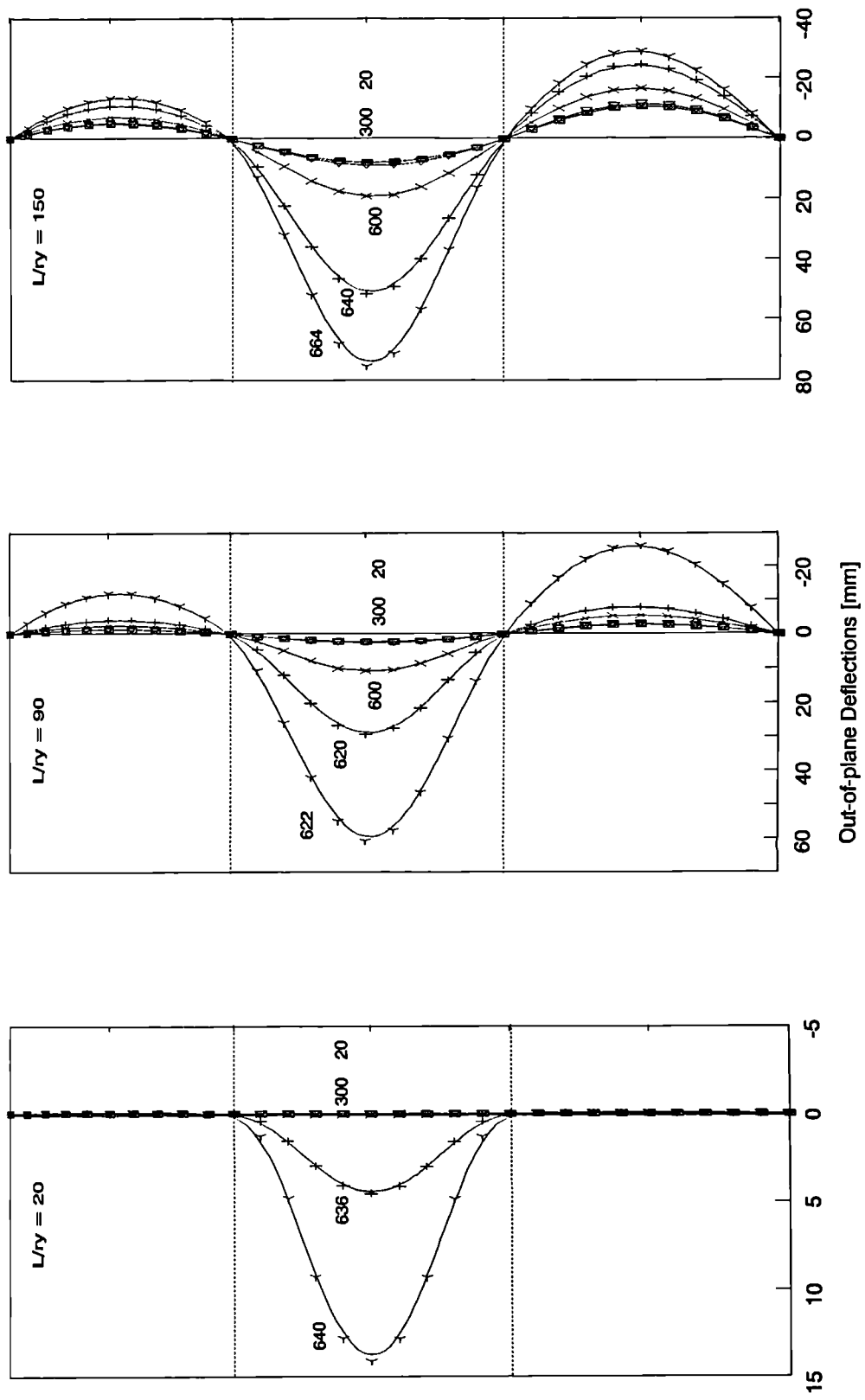
Fig. 5.41 Deflected Shapes of Subframes with Simple Connections

high slenderness range. This very small contribution of the beams to the overall stiffness of the assembly can be misleading. The reason for this is the existence of a theoretical upper limit in terms of the reduction of the heated column slenderness ratio. Once the cool columns have provided the heated column with an extra end-stiffness to give it a slenderness ratio of nearly half that of an isolated column with the same length, the connecting beams can add very little to the heated column stiffness. The beams' contribution can increase the column's fire resistance only within the high range of slenderness ratio. Nevertheless, to assess the influence of the connecting beams on the column capacity, a larger beam-section and two smaller beam-sections were used with some columns of high slenderness ratio and the same cases were re-analysed. Different beam sections ($UB533 \times 210 \times 92$), ($UB356 \times 171 \times 51$) and ($UB305 \times 165 \times 46$) have been used to replace the original beam section ($UB406 \times 178 \times 74$) . These beams have moment capacities of approximately twice, half and one quarter of the original beam respectively. In all cases the increase or reduction in failure temperature due to using stronger or weaker beam sections can hardly be seen, as illustrated in Fig. 5.42. Results obtained by using various beam sections confirm clearly that the beams are not capable of providing significant extra stiffness to the heated column.

To assess the effect of the connecting beams separately the same columns were considered to be connected to beams only, as shown in Fig. 5.43. Failure temperatures of this new assembly compare well with results obtained from the full assembly. This shows clearly that rotational restraint can be provided to the heated columns either by the continuity of the column or by rigidly connected beams. However it is obvious that whatever the stiffness of the assembly might be, it can only restrain the heated column up to the point of decreasing its effective length to nearly half its actual length. The exact amount of the reduction in slenderness of continuous
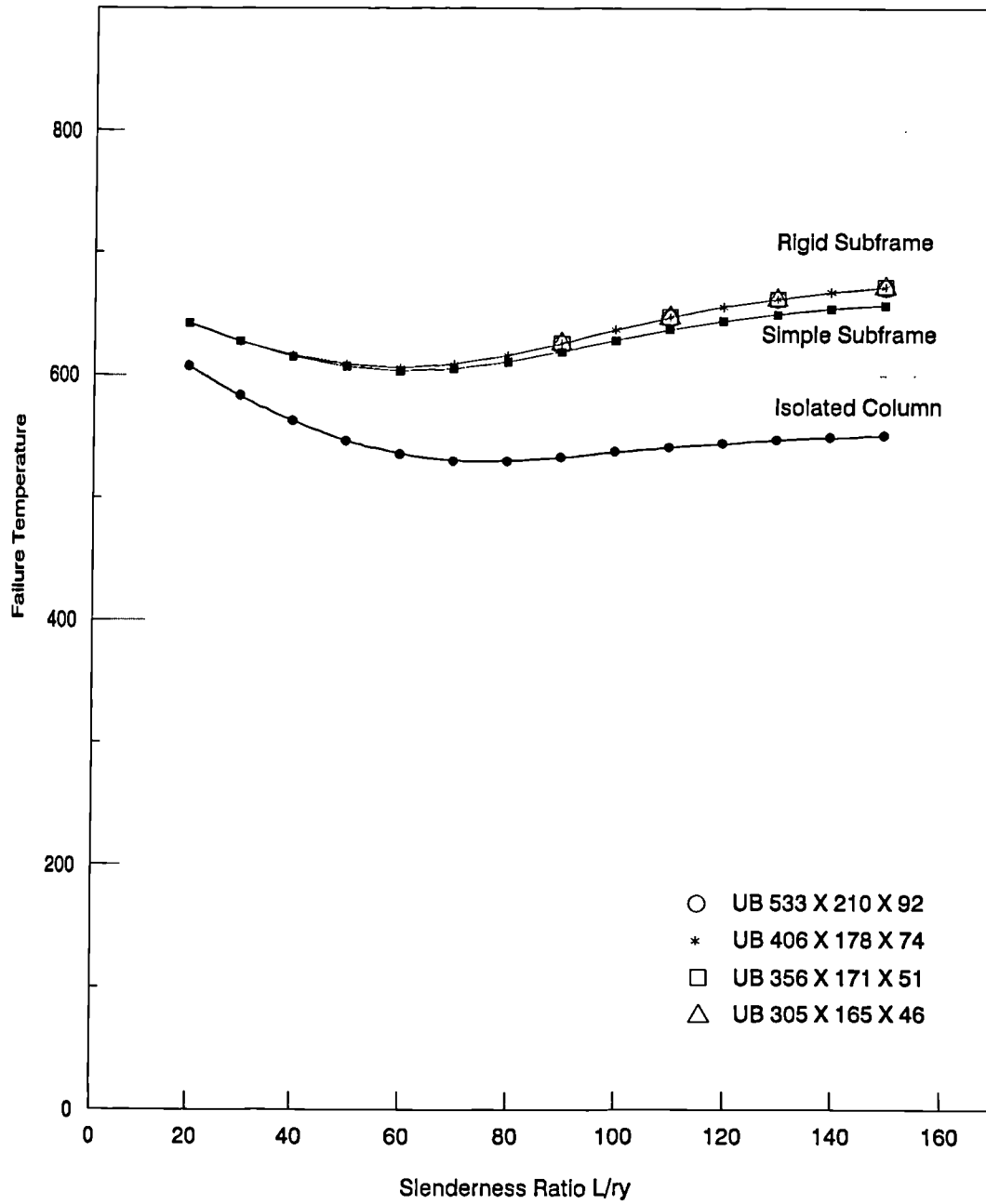
Fig 5.42 Failure Temperatures for Subframes

Effect of the Connecting Beam Cross-Section
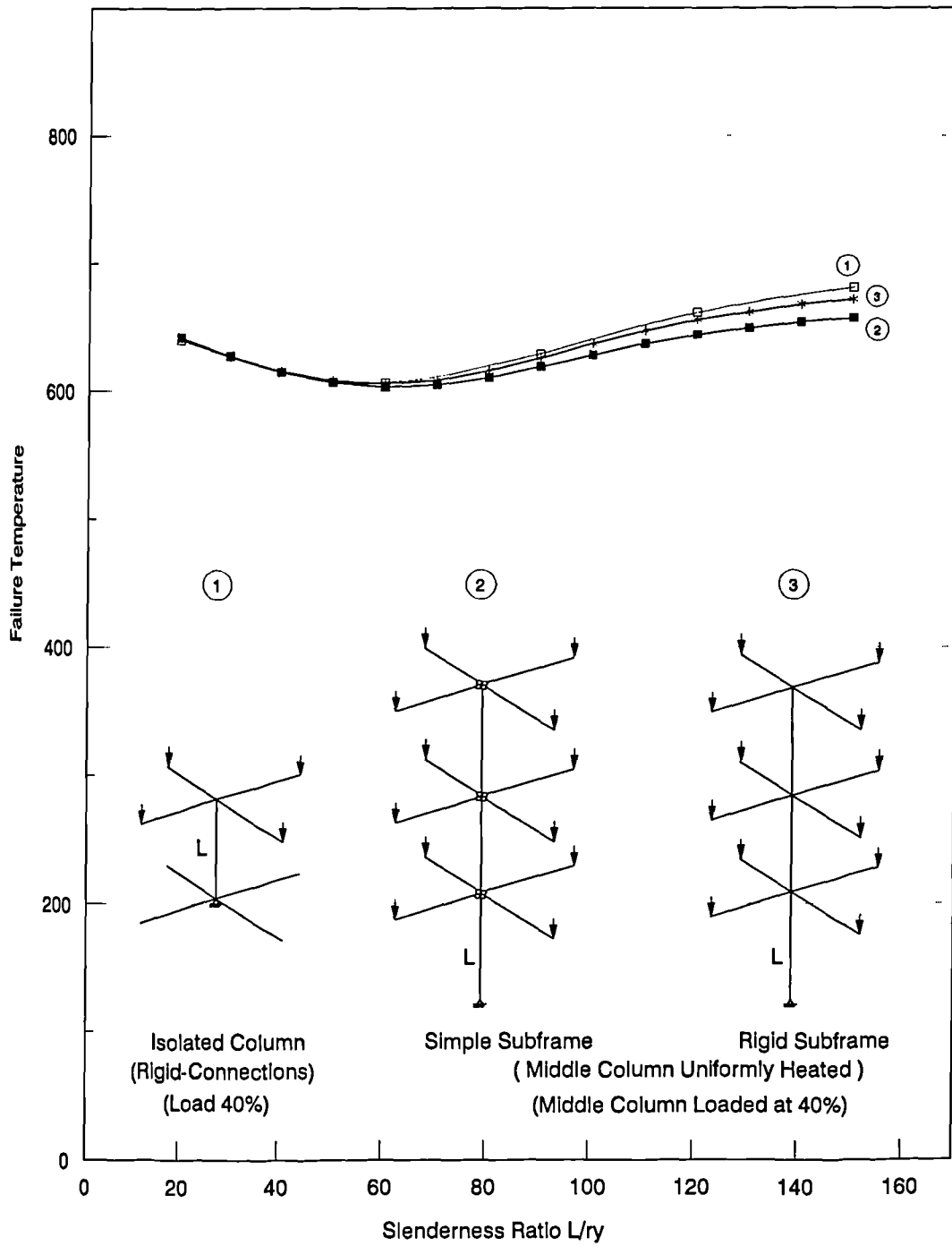
Fig. 5.43 Effect of Connecting Beams on the Column's Stiffness

columns will be considered later in this chapter.

It is noticeable in the case of beams connected to an isolated column that the failure temperature at high slenderness ratios (120 and 150) is slightly higher than that of an identical assembly with the upper and lower columns included. The immediate conclusion about the result of adding extra columns to the assembly is that it is bound to increase the overall stiffness of the heated column. This could be true if the additional columns function as an additional stiffness provider to the heated column. Actually the additional columns also influence the heated column in another way. In the case of an isolated column, the connecting beams can induce no rotations to the heated column end due to the symmetry in the beams and the applied loads. The upper and lower columns behave differently, by introducing some rotation to the heated column as a result of their initial out-of-straightness. The extent of the adjacent column rotation can be seen on Fig. 5.41 which shows the deflected shape of the three spans of the column. In the slender range this behavioural pattern contributed to a slight increase in the failure temperature when connecting columns were excluded. This not the case with stocky columns. Again referring to Fig. 5.41 the deflected shape of the stocky column ($\lambda = 20$) shows the very limited rotations produced by unheated columns.

All the assemblies previously considered herein have one level heated while other levels remain at ambient temperature. It is also worthwhile considering the effect of having fire at all levels of the assembly, a situation that can take place in actual spreading fires. The same set of columns with simple connections has been analysed with columns heated at all levels. The failure temperatures corresponding to this case compared with the temperatures of the case of heated lower-column and isolated columns are shown on Fig. 5.44. It is apparent that, when columns
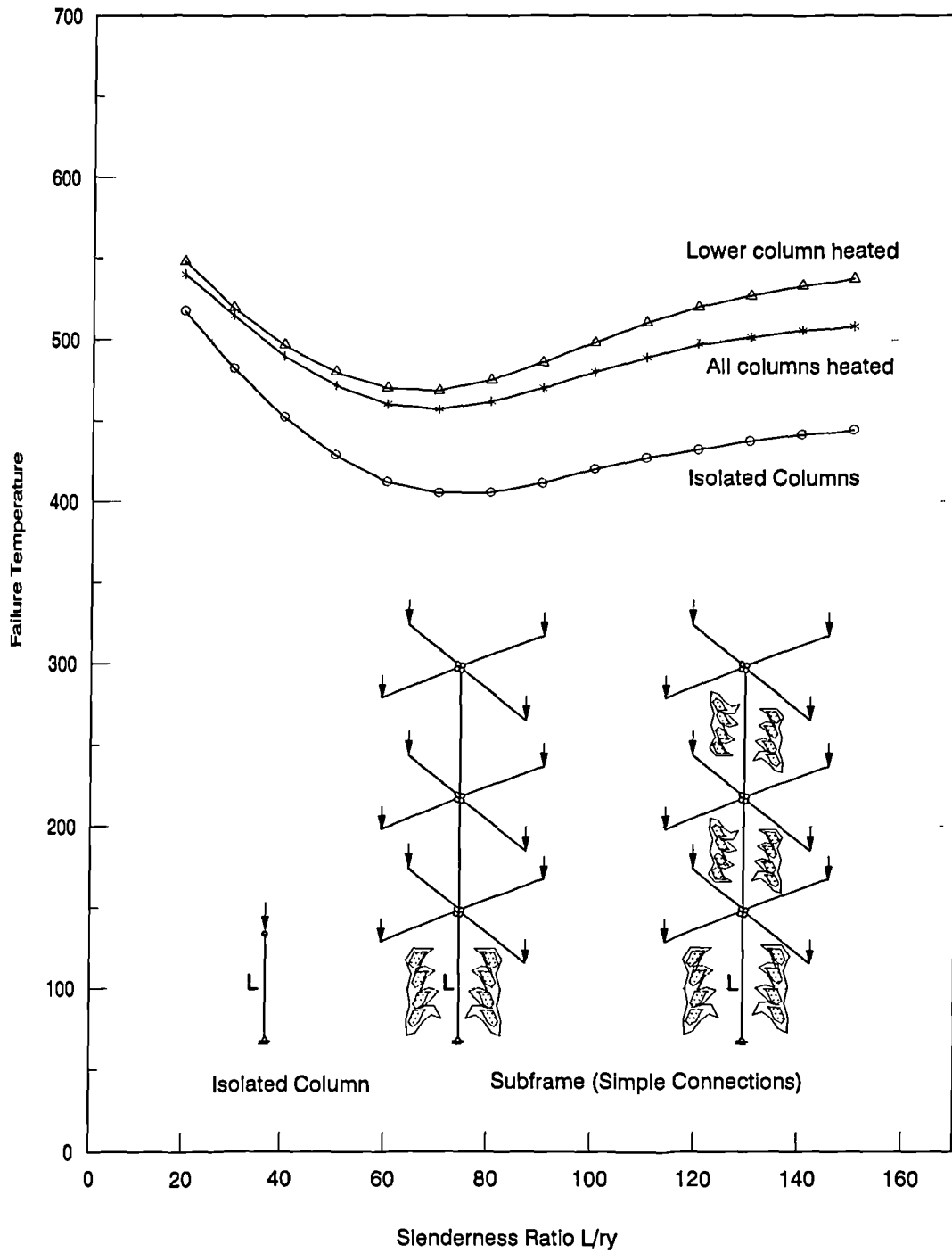
Fig. 5.44   Subframes with Simple Connections -Different heating schemes

are heated at all levels, they exhibit lower fire resistance compared with that of a heated lower column in isolation. Nevertheless, heating columns at all levels showed much higher fire resistance compared with isolated columns. It is clear in this case that the lower column which carries the highest load level is the critical one, yet the middle-storey column is still capable of providing rotational restraint to the lower column. Although the middle column is heated at the same temperature as the lower column, its rotational stiffness is considerably higher than the lower column due to its lower level of load. This effect produced a significant increase in the fire resistance of the assembly compared with the case of isolated columns.

5.5.2 Columns Within Subframes -Thermal Gradient

Isolated columns subject to major-axis thermal gradient have generally exhibited better fire resistance compared with uniformly heated columns. Although it is expected that thermal gradients are bound to produce the same effect in multi-storey assemblies, it is still desirable to investigate their influence on subframes. Columns within subframes with the same specifications used in the previous section have been analysed with thermal gradient about the major axis. Temperature distribution across the section is assumed to be linear with the cool flange temperature at 10% of the hot flange and with no temperature below $20^{\circ}C$. Only columns which carry 60% of their ultimate loads have been re-analysed for this purpose.

Fig. 5.45 shows the failure temperatures for cases of both simple and rigid connections compared with those for the uniformly heated subframes and for isolated columns. This figure again shows a considerably higher fire resistance for most columns within subframes compared with isolated columns under thermal gradi-
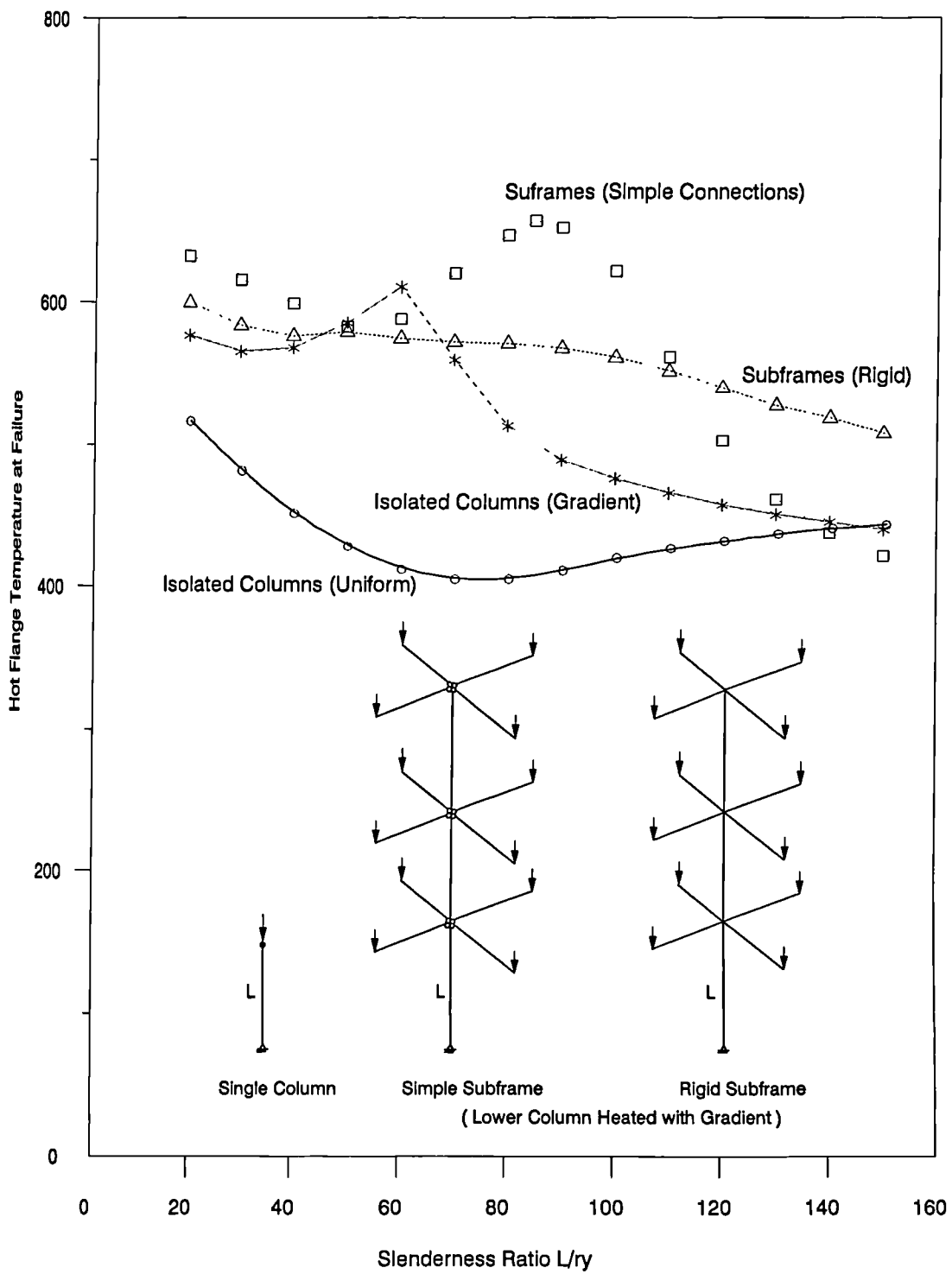
Fig 5.45 Failure Temperatures for Subframes

ent.

Figs. 5.46, 5.47 and 5.48 show temperature-deflection histories for columns of three slenderness ratios (20, 70 and 120) for the simply-connected case. The pattern of behaviour is similar to that of the isolated columns. The stocky column of $\lambda = 20$ sustains a rise in temperature up to the point where the axial and major axis displacements reverse considerably. On the other hand the column of $\lambda = 70$ showed some reversal while the slender column of $\lambda = 120$ showed no reversal at all.

A similar pattern of behaviour is evident for the same columns with rigid connections. Figs. 5.49, 5.50 and 5.51 illustrate the temperature-deflection history for these columns.

5.5.3 Effective Length of Columns Within Subframes

So far loads have been calculated for all subframes assuming that the effective length is equal to the actual length of the column within the subframe. This assumption is hardly realistic, due to the fact that designers invariably allow for some degree of restraint in multi-storey buildings by reducing the design effective length.

To assess the effect of such assumptions in fire, the loads applied to columns need to be adjusted to take into account the assumed effective length in design. For this purpose, the same set of subframes has been re-analysed with the middle column uniformly heated, and the applied loads have been adjusted for different assumed effective lengths. For the simply-connected case, effective length ratios of 0.85,
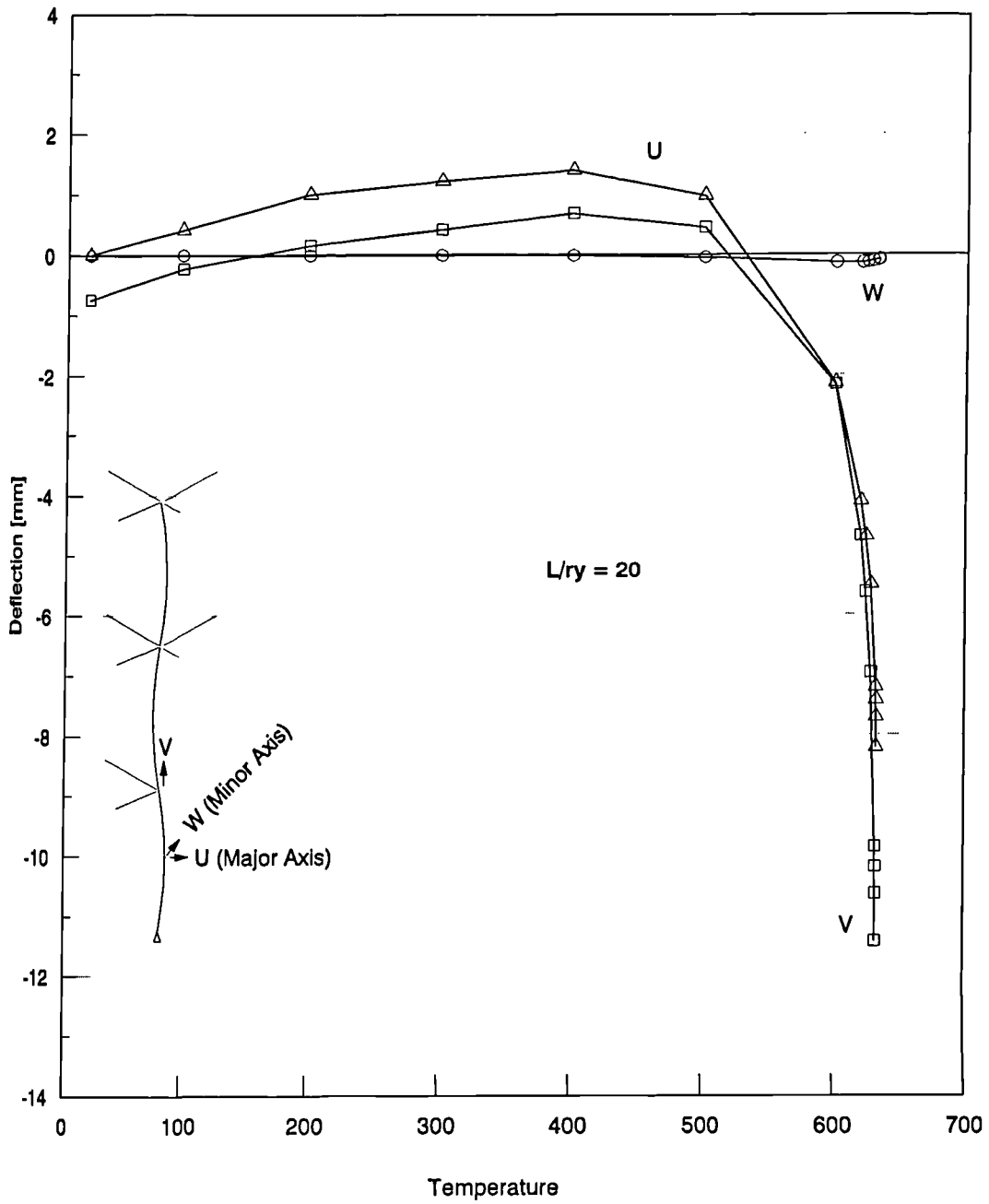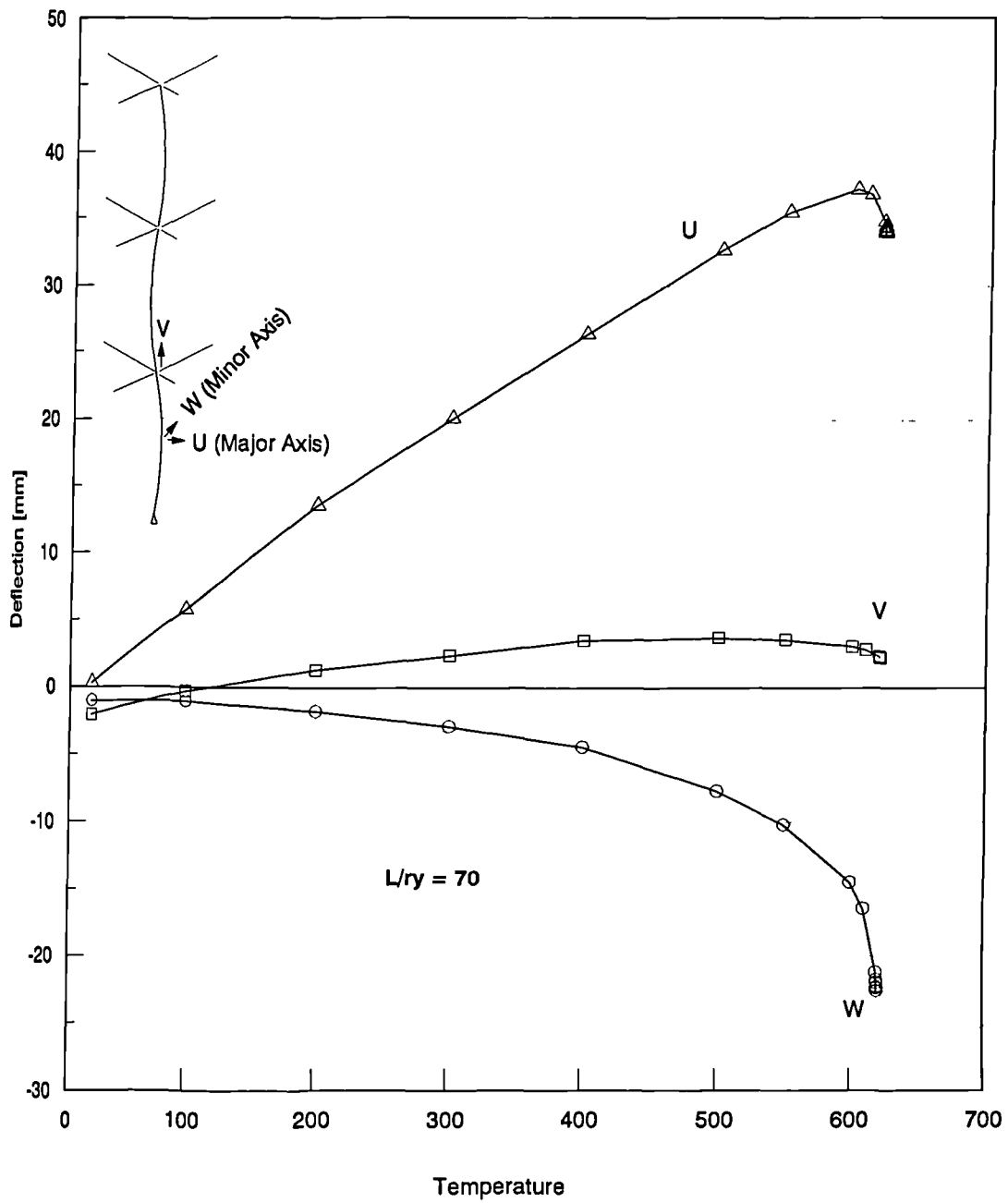
Fig 5.46   Temperature-Deflection in Simple Subframe

Fig 5.47 Temperature-Deflection in Simple Subframe
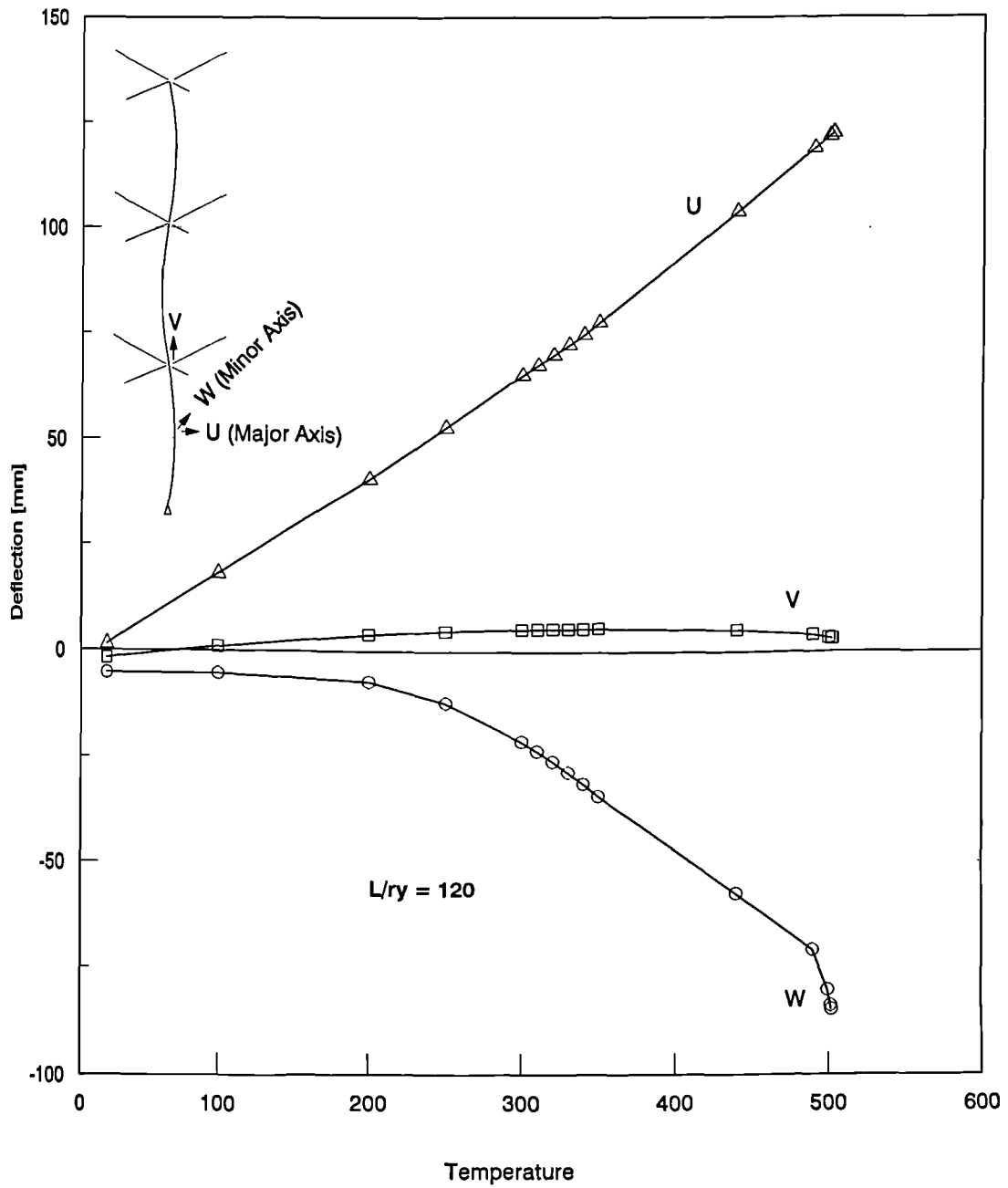
Lower Column Heated with Temperature Gradient about Major Axis (T2=0.1T1)

Fig 5.48   Temperature-Deflection In Simple Subframe
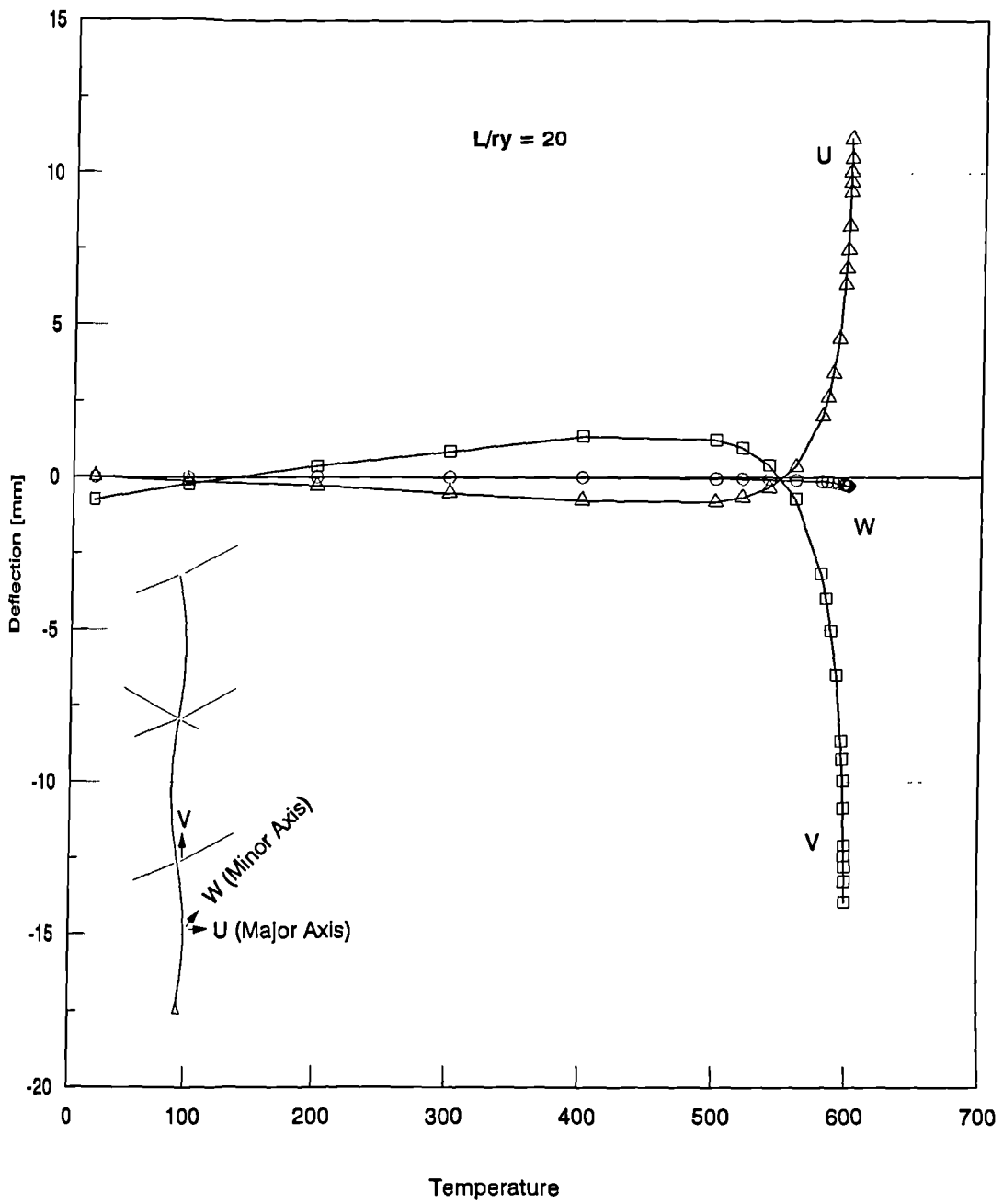
Lower Column Heated with Temperature Gradient about Major Axis (T2=0.1T1)
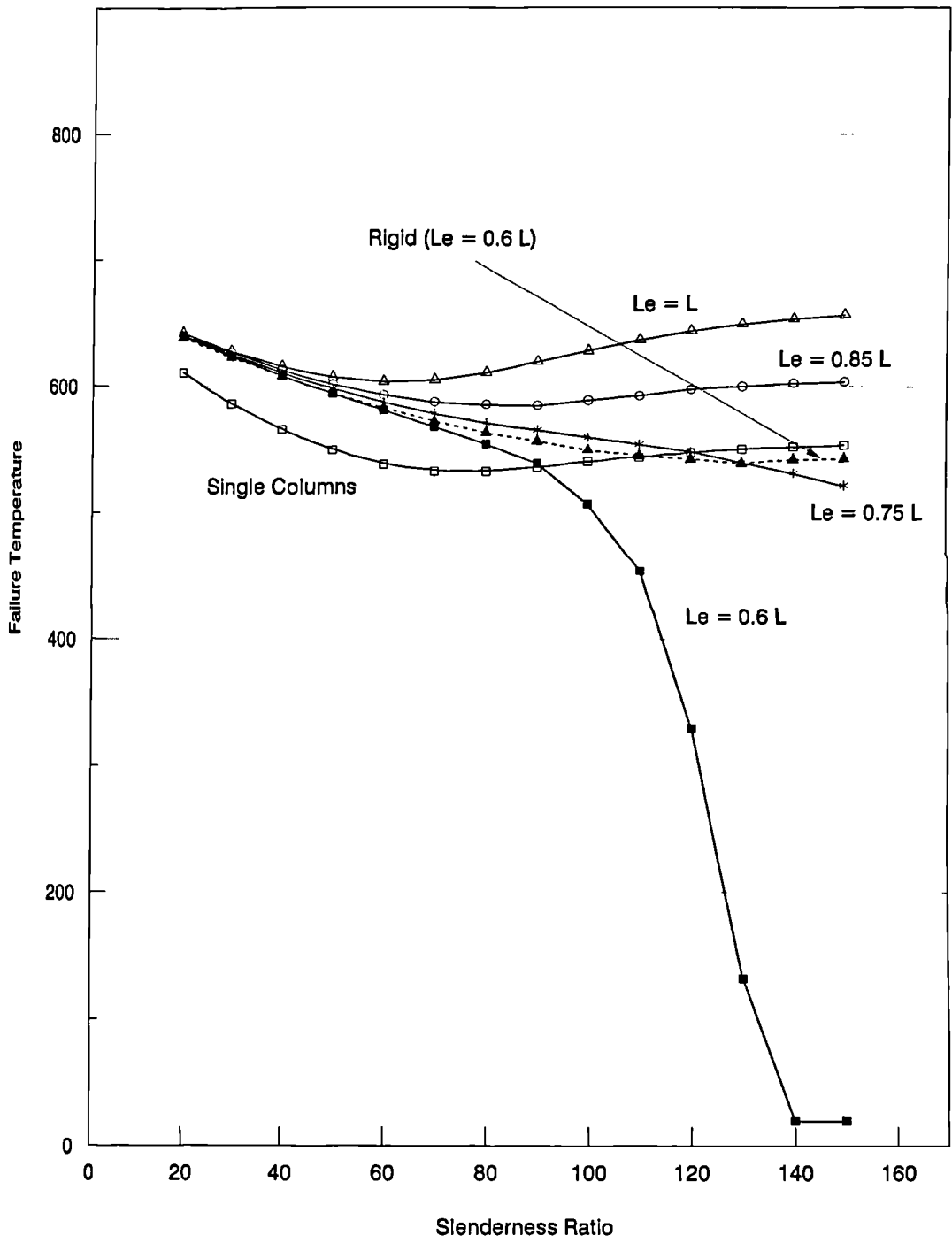
Fig 5.49   Temperature-Deflection in Rigid Subframe
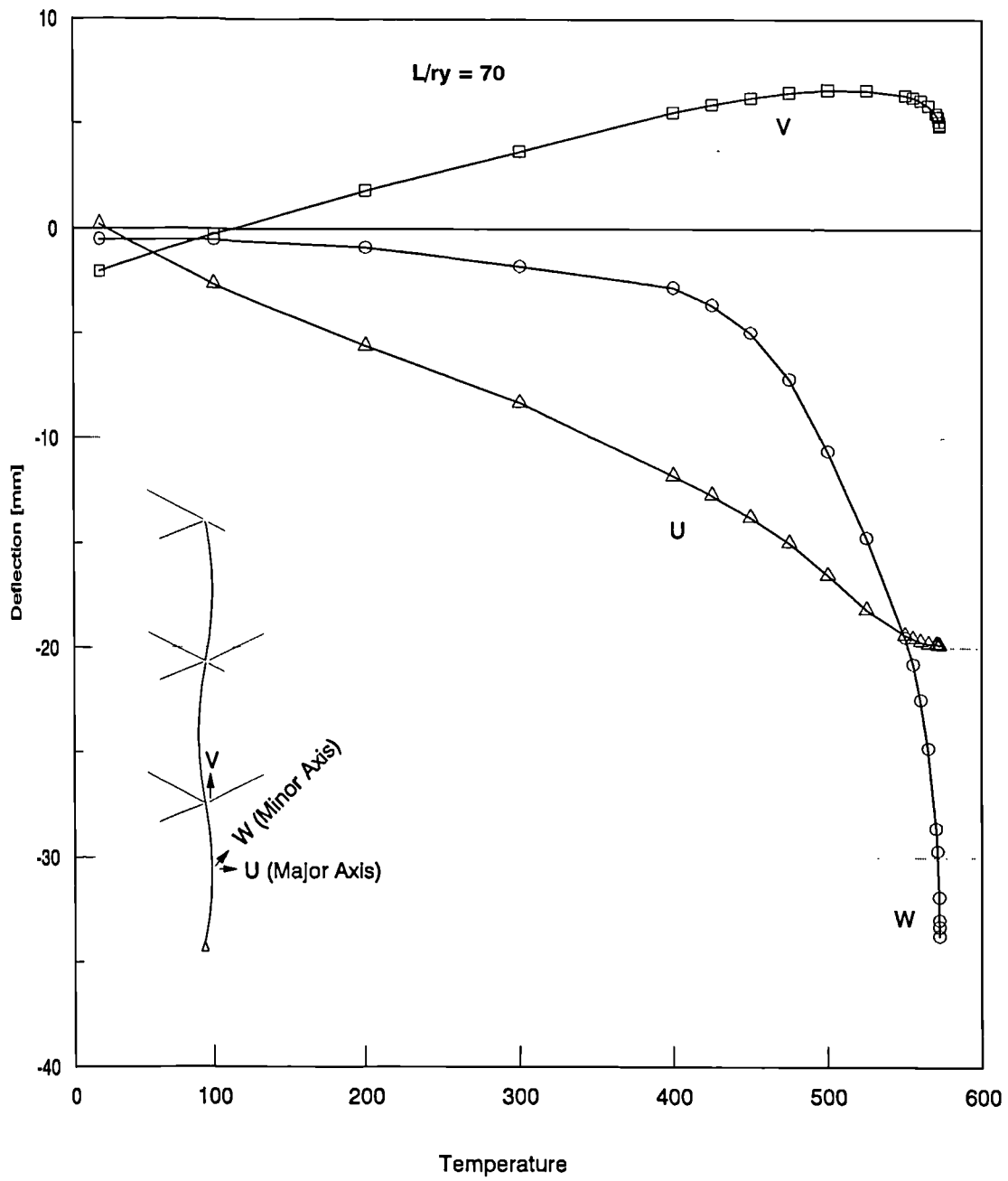
Lower Column Heated with Temperature Gradient about Major Axis (T2=0.1T1)

Fig 5.50   Temperature-Deflection In Rigid Subframe

Fig 5.51   Temperature-Deflection in Rigid Subframe

Fig. 5.52 Effect of different assumptions of the effective length

0.75 and 0.6 of the actual column length were considered. The failure temperatures corresponding to these cases are shown on Fig. 5.52. The results from these analyses show that any reasonable effective length such as 0.85 L produced higher failure temperatures than isolated columns for all slenderness ratios. Even the unlikely ratios of 0.75 L and 0.6 L produced higher failure temperatures for most of the practical range of slenderness ratios. This is due to the increase in the axial load-capacity of columns within the stocky range with reduction in slenderness ratio being small compared with the same increase in slender columns.

The procedure has been repeated for the rigidly connected subframes for an effective length factor of 0.7 of the actual column length. Results from this are plotted on the same figure, producing failure temperatures comparable to the simply-connected case where an effective length ratio of 0.85 was used. Results from all the above cases show that for low and intermediate slenderness ratios failure temperatures are well above those of the isolated column case, even if an extremely high degree of restraint was assumed in the load calculations.

The European code, EC3 Part 10 (1990), accounts for the assembly effect on the fire resistance of columns by reducing the effective length of the column under consideration. This reduction is conditional on considering each storey as a fire compartment. As a result EC3 states that the effective length of column situated in an intermediate storey can be taken as 0.5 of the 'system length' and for a column on the top floor as 0.7 of the 'system length'. It should be pointed out that this reduction in the effective length can only be used for the fire resistance calculations. On the other hand BS5950 Part 8 (1990) does not account for the assembly effect explicitly.

In order to compare this EC3 recommendation with results obtained from the

present analysis, the following study has been undertaken. Isolated columns considered previously have been re-analysed with their actual length reduced to different ratios of their original length. At the same time the applied loads corresponding to the original effective length were retained. This reduction can simulate the reduction of the effective length of a column due to the assembly effect. Failure temperatures obtained from these analyses are plotted in Fig. 5.53 for adjusted lengths of 0.5, 0.6, 0.7 and 0.85 of the original length. Results obtained from the subframe analysis for columns carrying the same loads are compared with above results on the same figure. Loads applied at isolated columns correspond to 40% of their ultimate load based on the full length of the isolated column. The subframe loads correspond also to 40% of ultimate load as the middle storey column is heated in this comparison. It can be seen that the subframe failure temperatures coincide with those of columns with effective length factor of 0.5 in the slenderness range below 40. Beyond this slenderness the subframe failure temperature curve diverges progressively from the effective length factor of 0.5 to reach somewhere between the 0.6 and 0.7 effective length factor curves. It is clear that it is very difficult for slender columns to acquire enough end-stiffness to reach the upper limit of an effective length factor of 0.5. The interactive nature of the relationship between the heated and unheated columns within an assembly, as pointed out in the previous section, simply does not allow this. While the heated column induces extra rotations to the adjacent cool columns, the heated column undermines its own beneficial stiffness from such columns towards the threshold of failure. Just before failure it can be seen (Fig 5.41) that the slender cool columns are subjected to considerable deformations.

The same exercise has been carried out for the lower storey column which, unlike the middle storey column, has column continuity at one end only and carries 60%
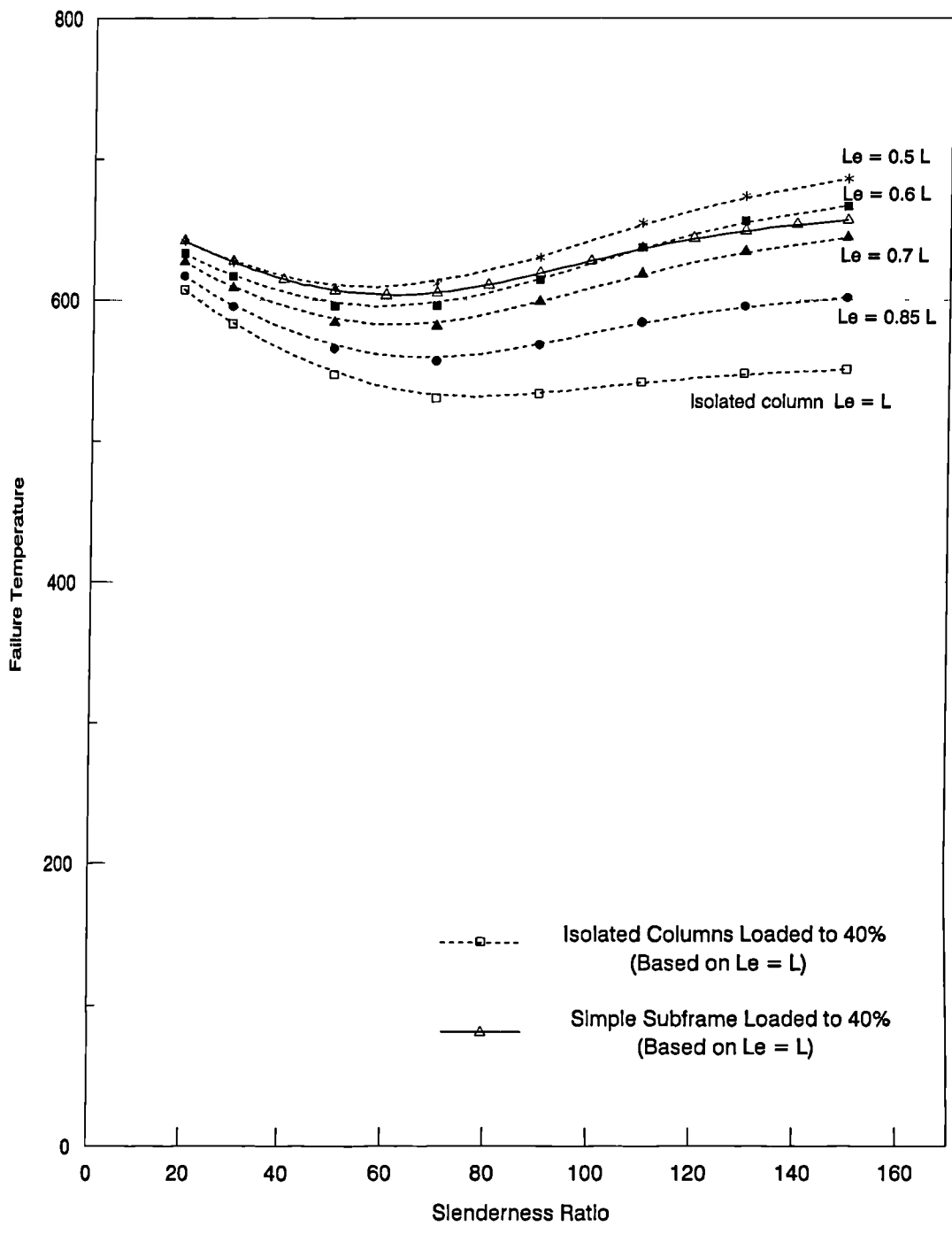
Fig. 5.53 Effective Length of Intermediate Columns

of its ultimate load. The isolated columns have reduced length as in the previous case but carry 60% of their ultimate load. Results obtained from these analyses are shown on Fig. 5.54. In this case the effective length of the lower storey column should assume the value of 0.7 of the actual length if it is assumed to be fixed at one end and pinned at the other. Again it is clear that the ability of the unheated upper column to provide full restraint at the upper end of the heated column is limited to the stocky range. At the slender end of the curve the cool column provided enough stiffness to the heated column for it to reach an effective length factor of about 0.8 rather than 0.7.

5.6 Generalised Results

In this section an attempt has been made to produce easily understood results concerning the fire resistance of columns. Engineers are used to thinking of column failure in the context of Perry reduction to Squash-Euler curves. To produce similar curves for isolated columns in fire, a constant temperature has to be imposed on columns while their applied loads are increased up to failure. Temperature profile increments were set at intervals of 100° C, covering the range between 100^oC and 700^oC, resulting in seven curves that define the critical stress for any temperature of the above range. The results of these analyses are shown on Figs. 5.55, 5.56, 5.57 and 5.58 using two styles of presentation and two values of yield stress.

The reason for using two values of the yield stress (250 and 350 N/mm^2) is to assess the effect of changing this parameter, which was kept constant at 250 N/mm^2 in all the previous studies. For this purpose the aforementioned results were reproduced on a single graph by normalising the slenderness ratio. Fig. 5.59 shows
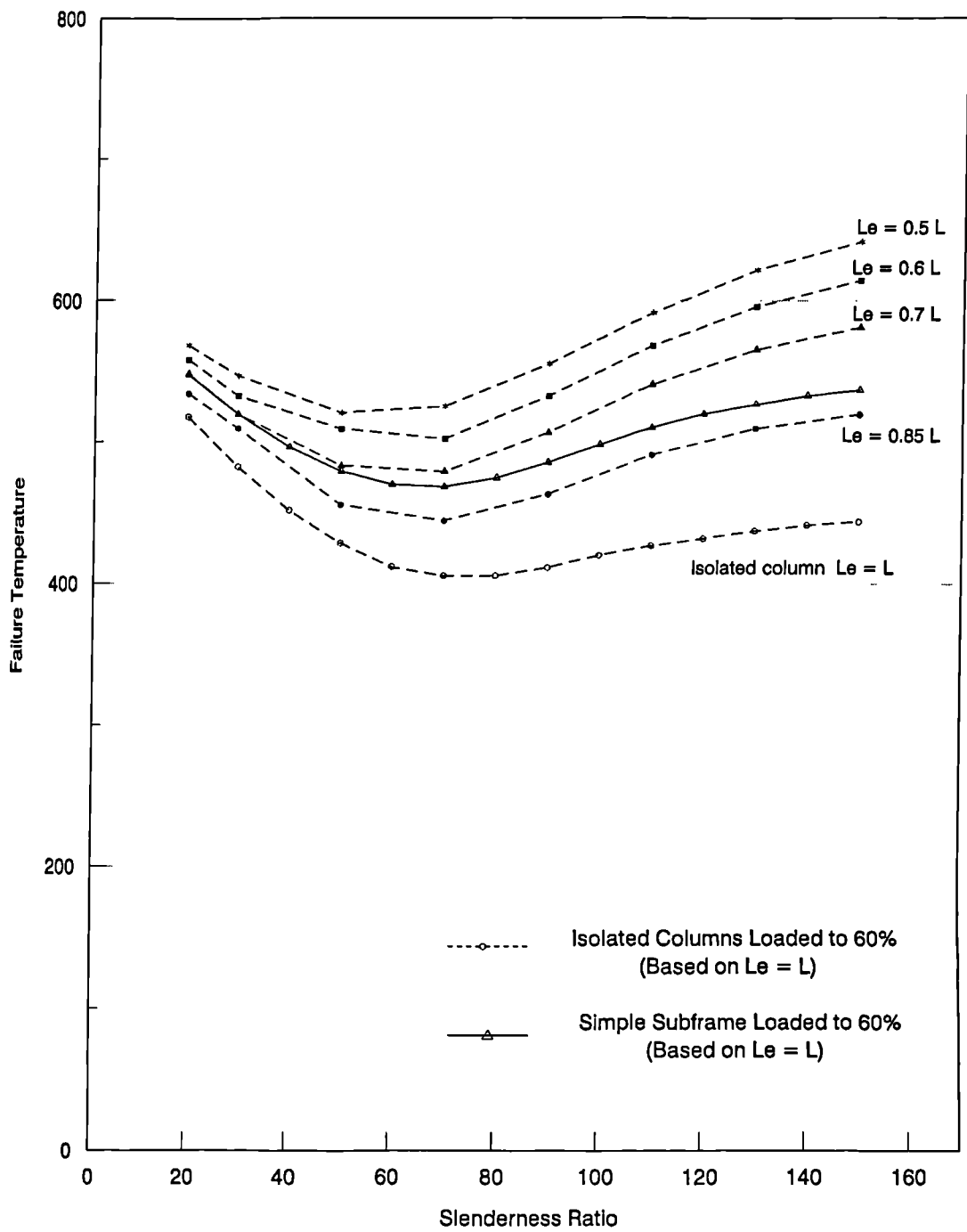
Fig. 5.54 Effective Length of Lower-Storey Columns
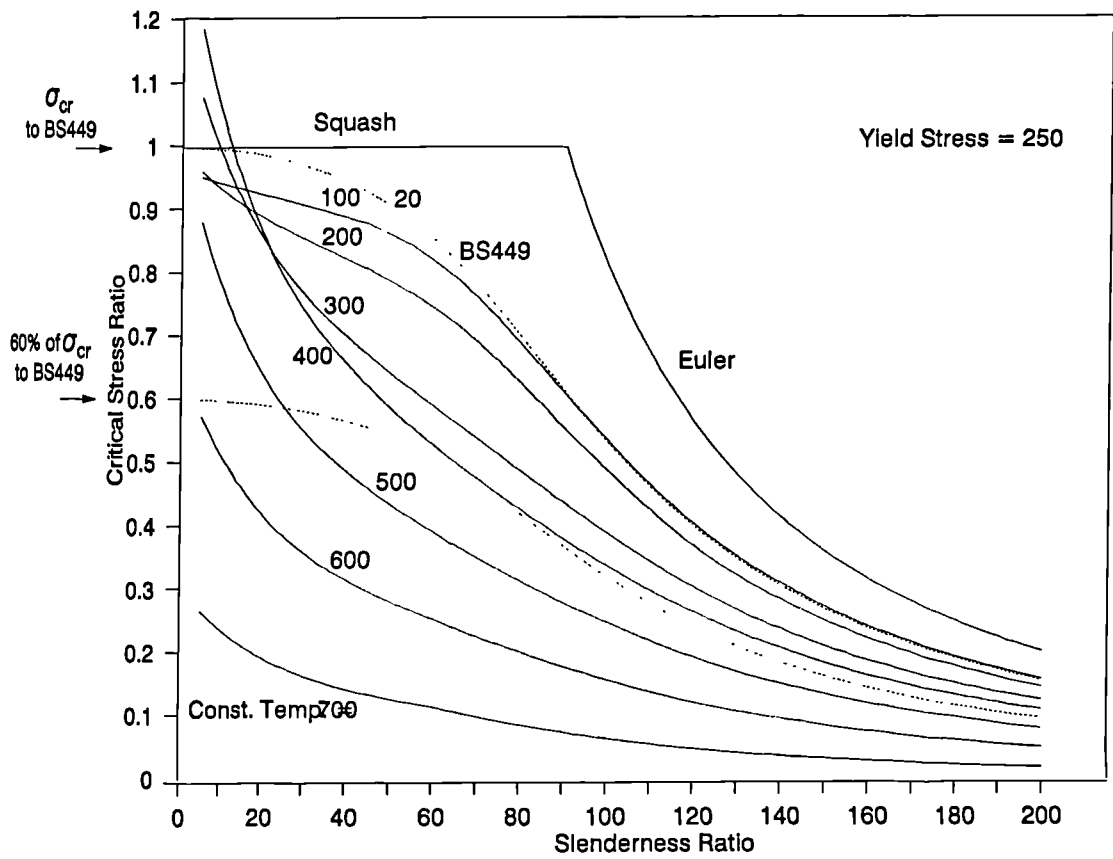
Fig. 5.55 Failure Stresses for Columns Heated to a Constant Temperature
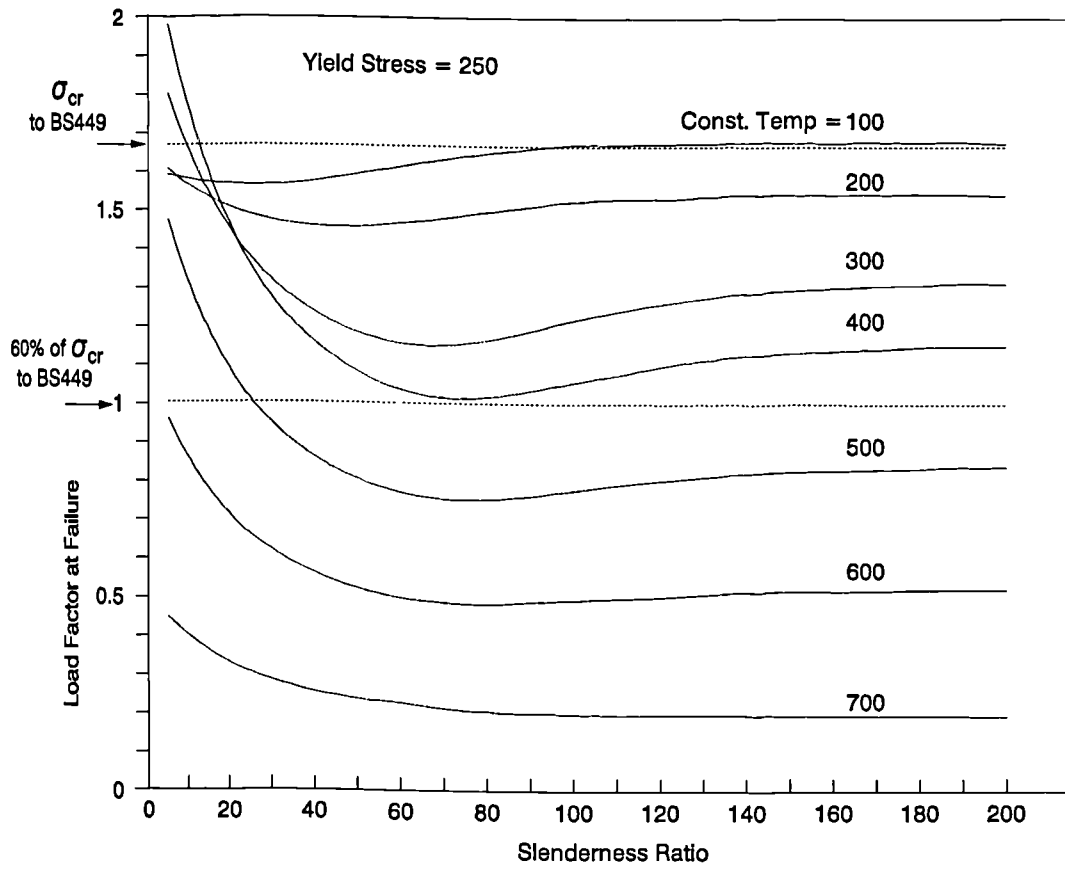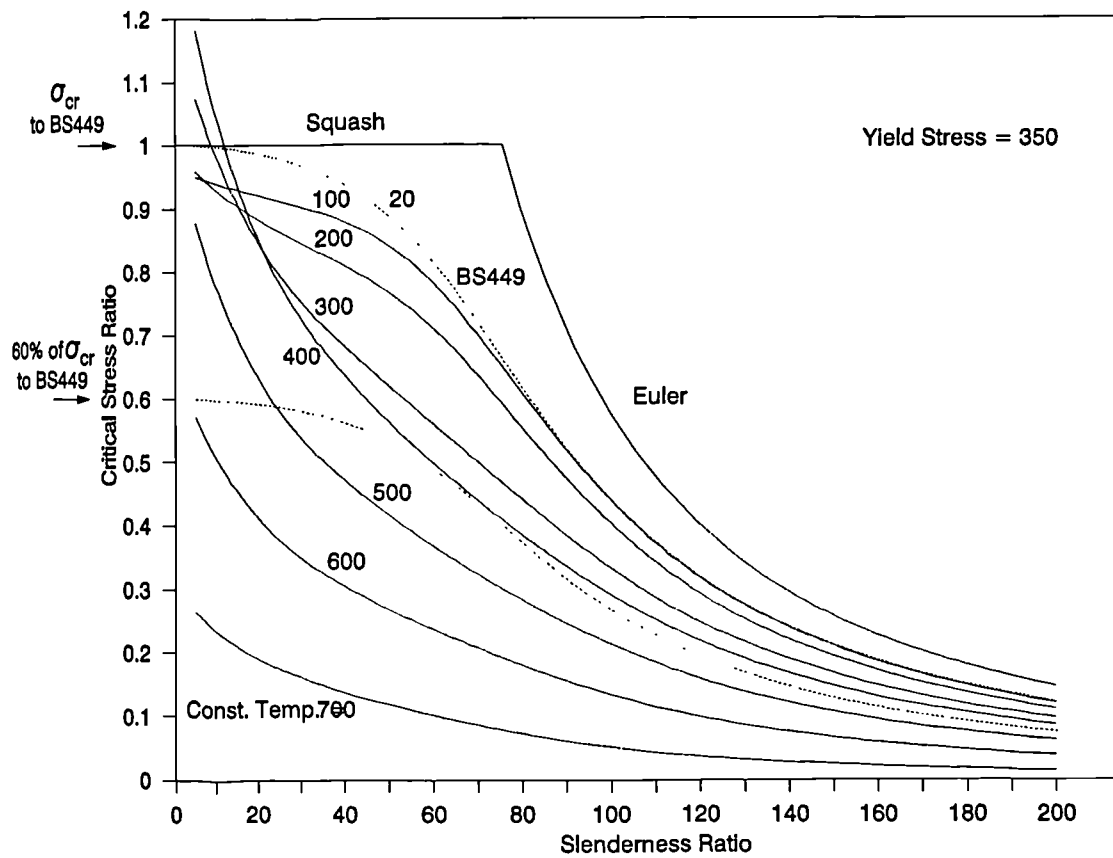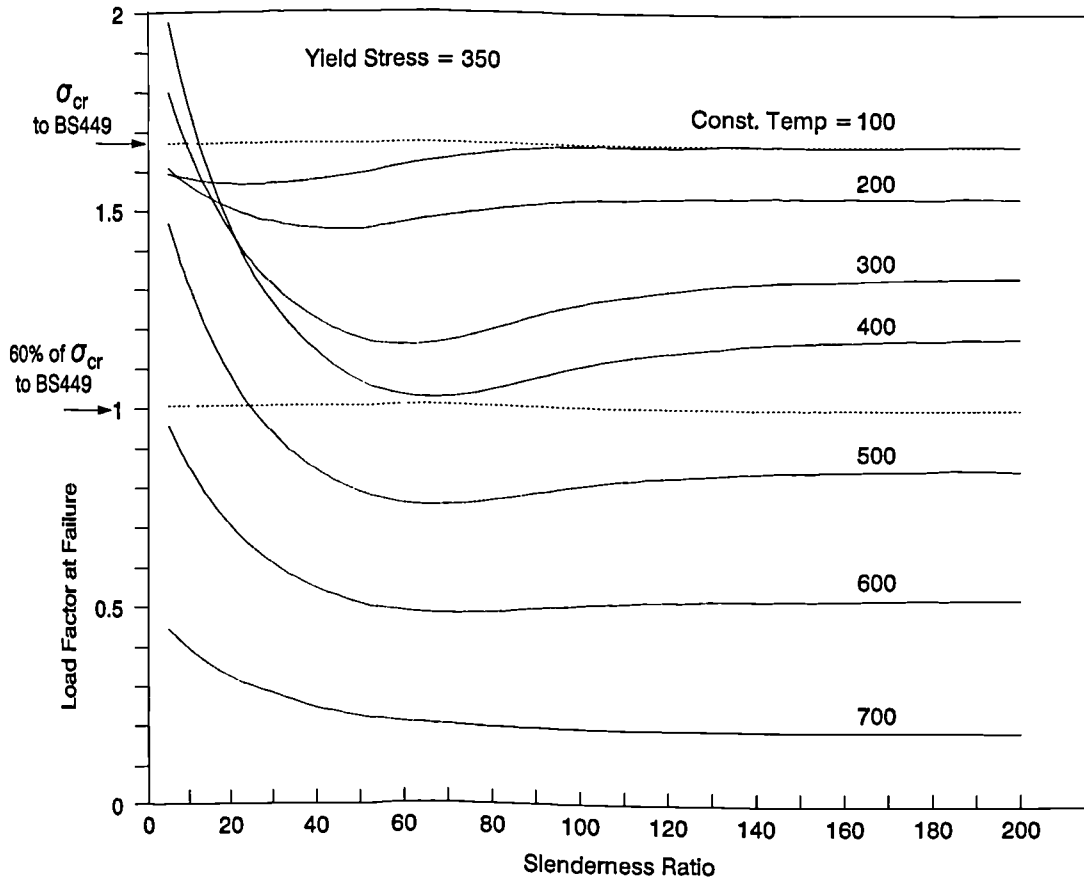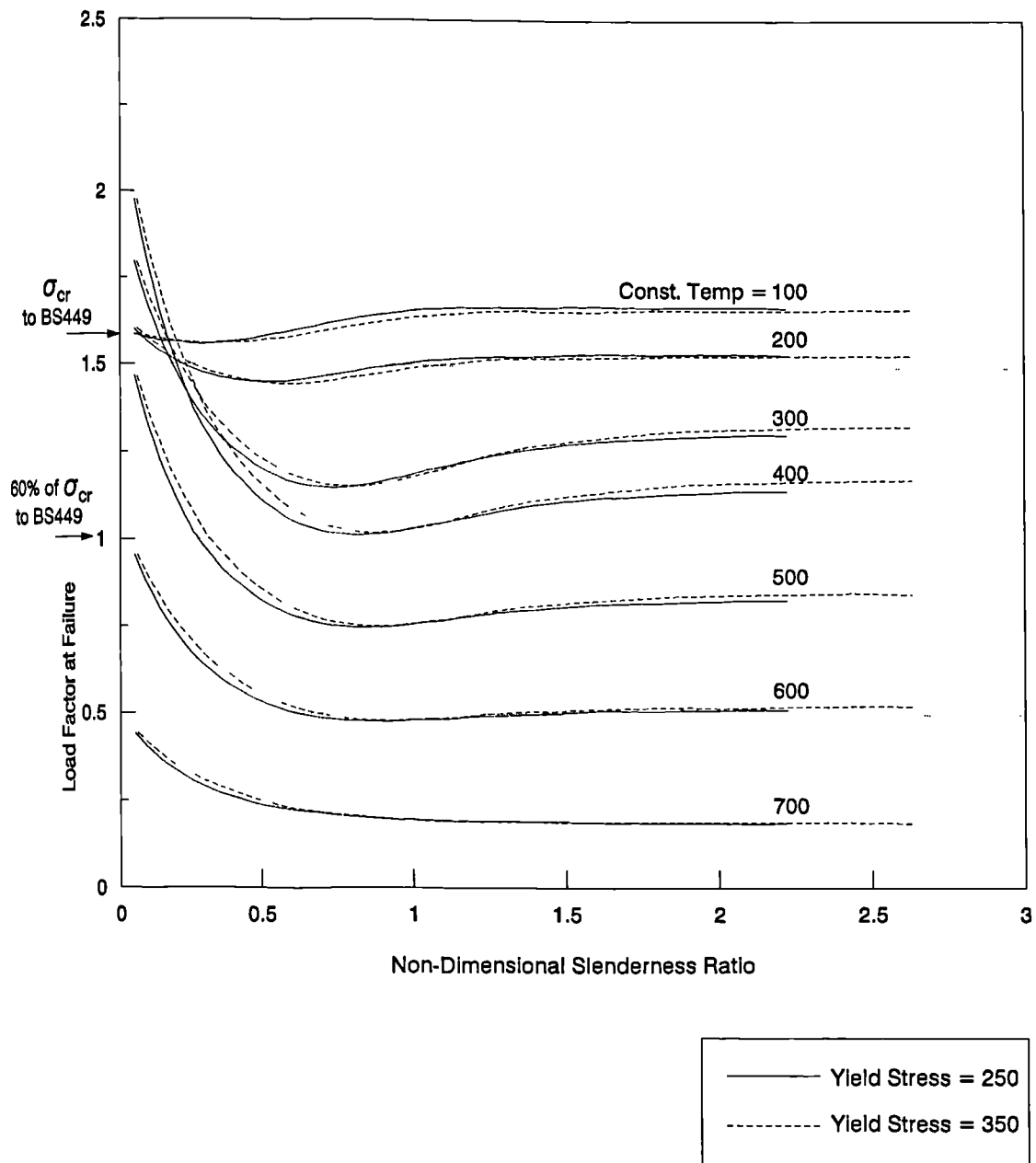(normalised w. r. t. the yield stress)

Fig. 5.56 Failure Load Factors for Columns Heated at a Constant Temperature (Normalised w. r. t. 60% of the ultimate load to BS449)

Fig. 5.57 Failure Stresses for Columns Heated to a Constant Temperature
(normalised w. r. t. the yield stress)

Fig. 5.58 Failure Load Factors for Columns Heated at a Constant Temperature (Normalised w. r. t. 60% of the ultimate load to BS449)

Fig. 5.59 Failure Load Factors for Columns Heated at a Constant Temperature
(Normalised w. r. t. 60% of the ultimate load to BS449)

no significant difference in the normalised critical stresses using either value of the yield stress.

5.7 BS449, BS5950, EC3 and the Present Analysis

BS5950 Part 8 is the first UK Code or Standard to deal specifically with the fire resistance of steel structures. As a result it is worth while comparing predictions of the present analysis with the Standard recommendations applied to steel columns in fire. On the other hand, the BS449 criteria for column imperfections and first yield loads at ambient temperatures have been used for simplicity in the previous studies. This fact makes it appropriate to compare assumptions from both Standards with the present analysis. On the other hand it is widely accepted that the current British Standard is very likely to be the last of its type due to plans to replace it by the European Standards in the future. It is thus reasonable to compare the present analysis with the recommendations of EC3 in the fire context.

At ambient temperature, failure loads as specified by BS449 and BS5950 curves **a**, **b, c** and **d** are shown on Fig. 5.60. These curves are produced using a Perry formula with different imperfection parameters. Applied loads of 60% of the ultimate load and initial out-of-straightness as recommended by both Standards were applied to the same set of isolated columns used in the previous studies. All columns were then heated uniformly up to failure and the failure temperatures compared with the limiting temperatures as specified by BS5950 Part 8 in Fig. 5.61. The resulting curves suggest two main conclusions. Firstly the Standard specifies unsafe failure (limiting) temperatures for most of the range of slenderness ratios. Secondly, any
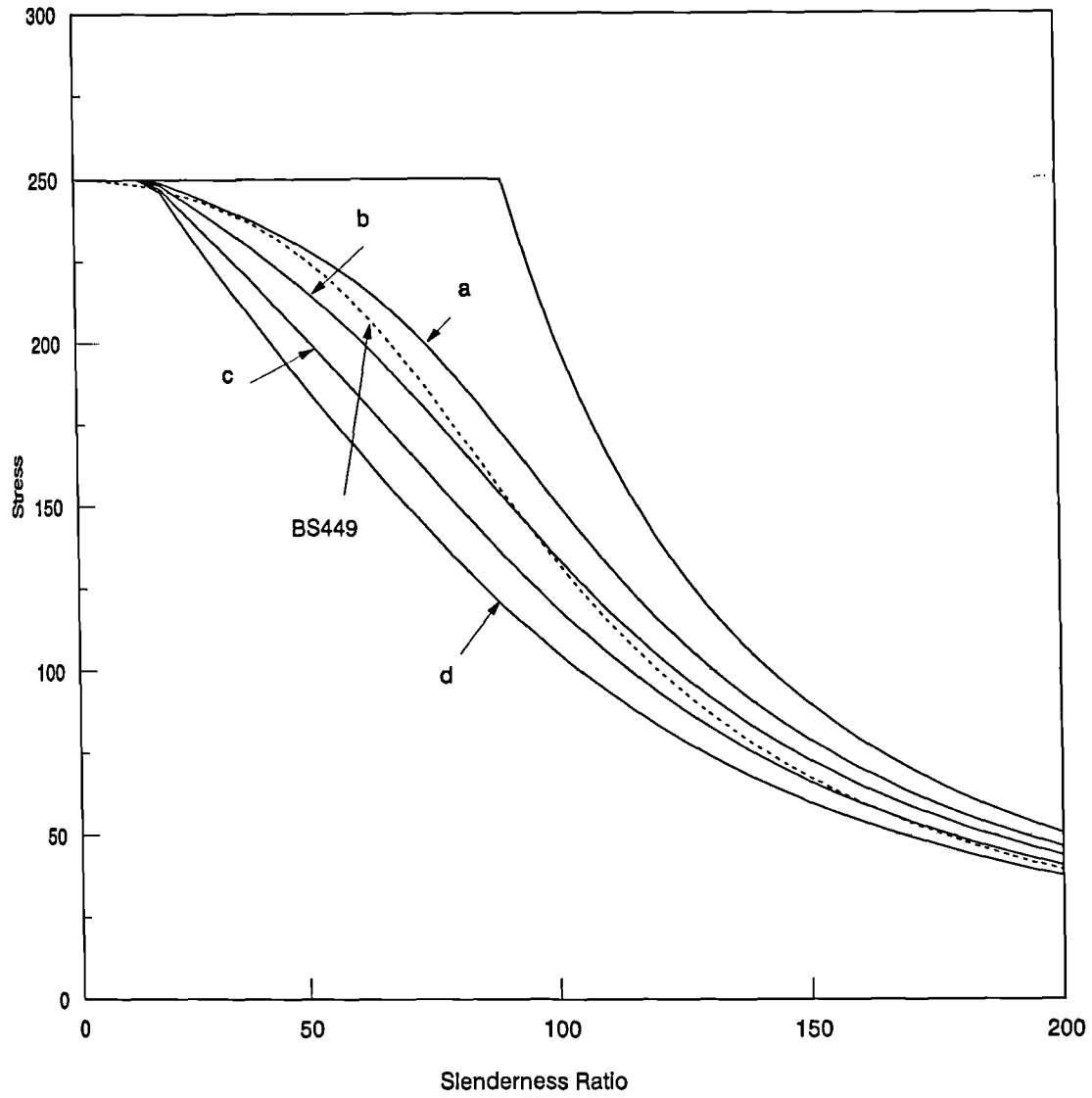
Fig. 5.60 Ultimate Stress For Columns In Compression

Comparison Between BS449 and BS5950
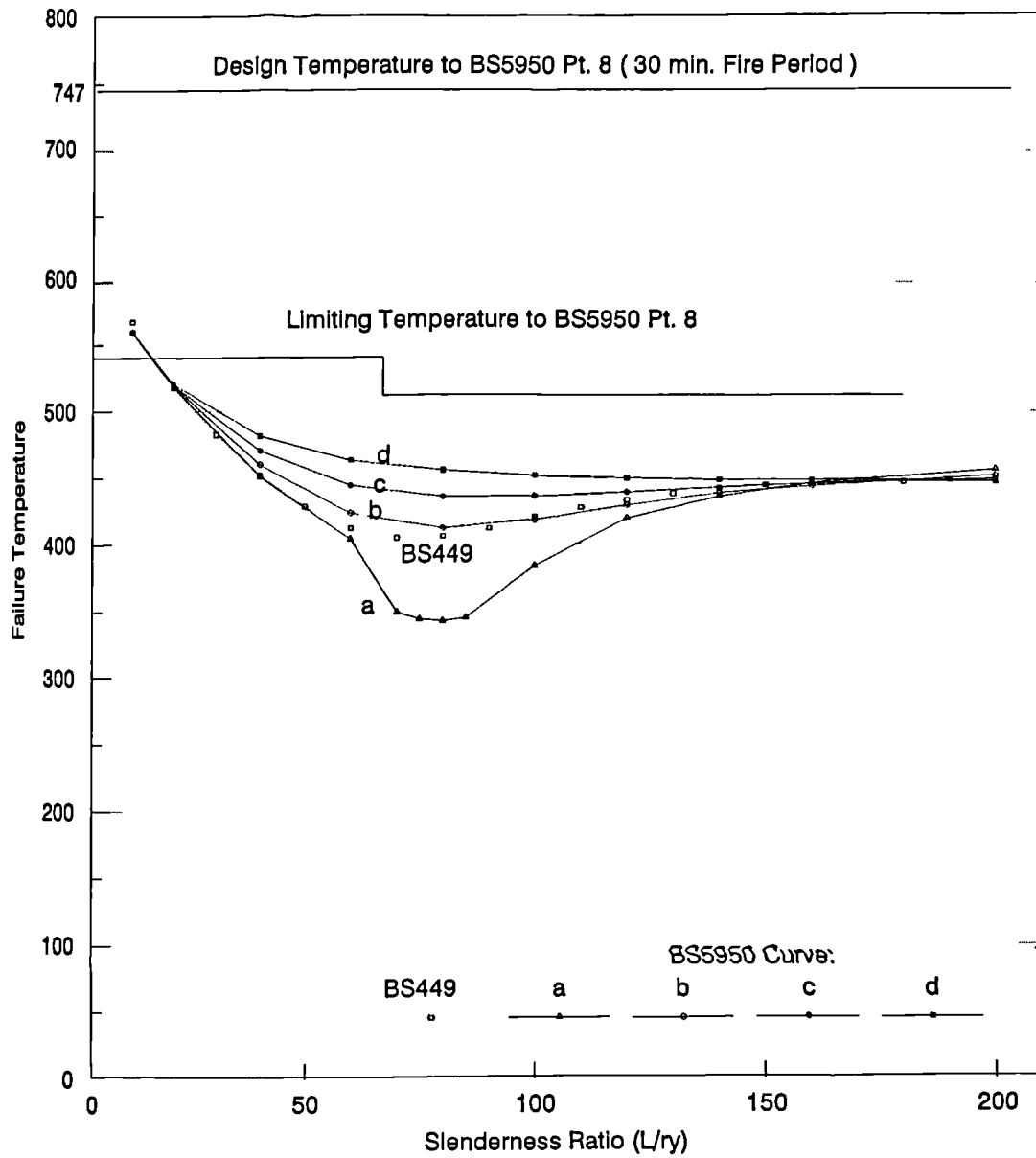
Fig. 5.61 Columns Loaded to 60% of the Ultimate Laod w.r.t Relevant Code

increase in load-bearing capacity of columns at ambient temperature, and hence in the applied loads suggested by BS5950 using different curves, resulted in lower failure temperature for the columns concerned. This implies that any beneficial increase in the load-bearing capacity of a column due to using a higher curve, for example curve **a**, is offset in fire conditions by a lower failure temperature.

The apparently unsafe limiting temperatures can easily be explained. While columns analysed in this study are isolated, the Standard is concerned with columns within multi-storey buildings, which have shown higher fire resistance in previous studies once they were placed within subframes. As a matter of fact the BS5950 limiting temperature curve is derived solely from experiments. In these experiments only isolated columns were considered, the boundary conditions of which were set deliberately to simulate columns within multi-storey buildings.

With respect to the second observation, although the analytical curves use the accurate assumptions of BS5950, they were produced by using standard universal columns. This is contrary to the assumption of BS5950 that other curves as well as curve **c** apply to different sections and different failure axes.

Accordingly it may be appropriate to compare BS5950 limiting temperatures with cases which correlate more accurately with the experimental conditions. In these experiments as reported in the Compendium of UK standard fire test data by British Steel Corporation (1987) the applied loads were calculated based on an assumed effective length less than the actual length and end conditions were designed to provide a considerable rotational stiffness to column ends. Fig 5.62 shows the failure temperatures of the subframes considered previously, compared with BS5950 limiting temperatures. In this case the subframe columns are loaded to 40% of their capacity based on an effective length factor of 0.85. As a result
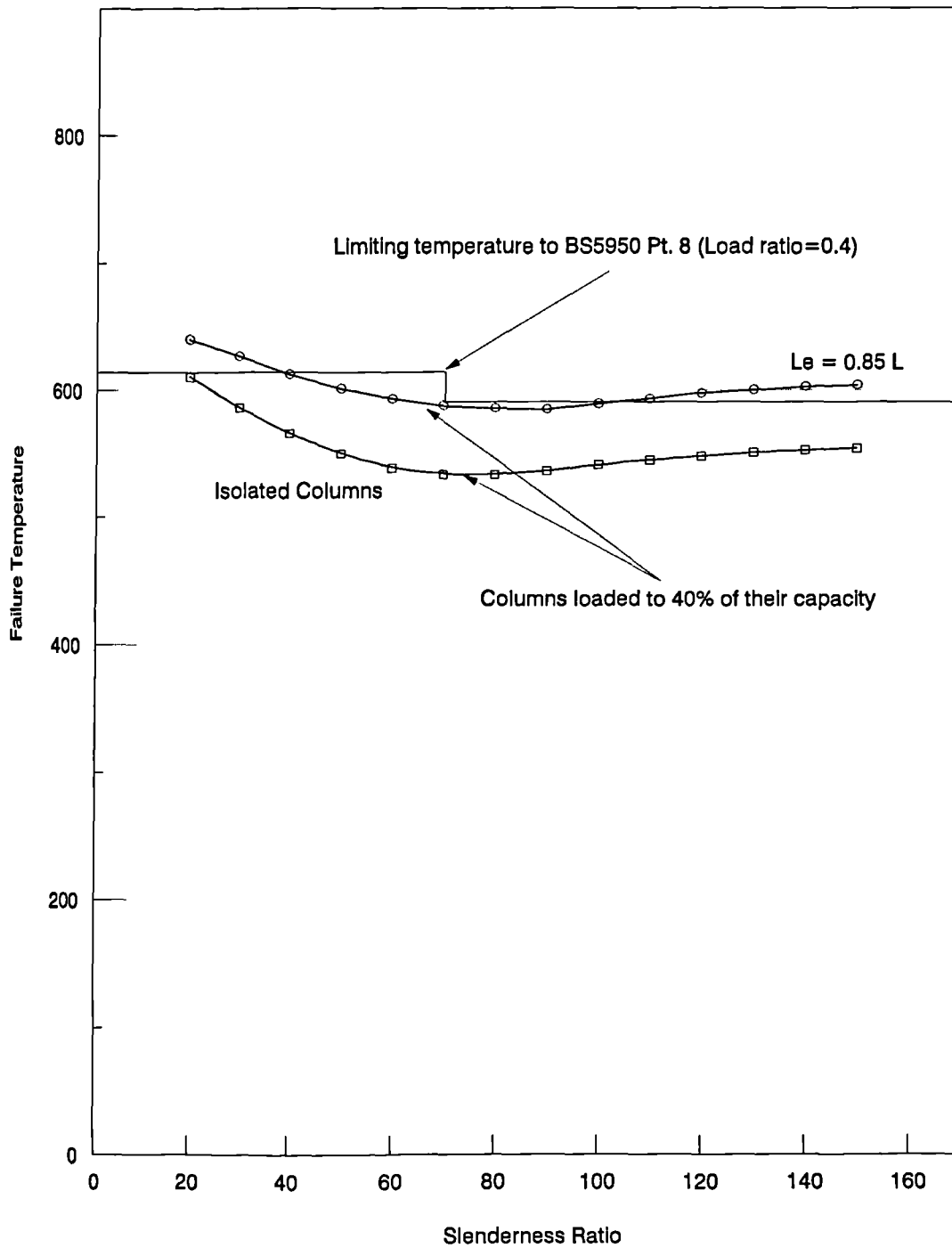
Fig. 5.62 BS5950 Limiting Temperature and the Present Analysis

it can be seen that the limiting temperatures of BS5950 become more comparable with the analytical results. The failure temperatures of the isolated columns which carry the same level of load (40%) can still be seen on the same figure to be much lower than the Standard limiting temperatures.

To compare the current analysis with EC3, the same set of columns considered previously is compared with 'critical' temperatures obtained from EC3 on Fig. 5.63. Results obtained previously from subframe analysis are also compared on the same figure, with EC3 critical temperatures modified to account for the assembly effect. Again in both cases it is clear that EC3 results are on the unconservative side compared with the analytical results.

5.8 Conclusions

The parametric studies undertaken in this chapter have shown the capability of the developed software to produce meaningful results. Studies regarding isolated columns are thought to be comprehensive in identifying the most important factors which influence their fire resistance. As far as multi-storey columns are concerned, the present studies provide a reasonable insight into their behaviour in fire though not a conclusive one. The brief comparison with the recommendations of the present UK standard can constitute a starting point for further consideration of the methods of the considered Standards in concluding and presenting such recommendations.

Generalised conclusions and recommendations as suggested by this study will be laid out in the next chapter.
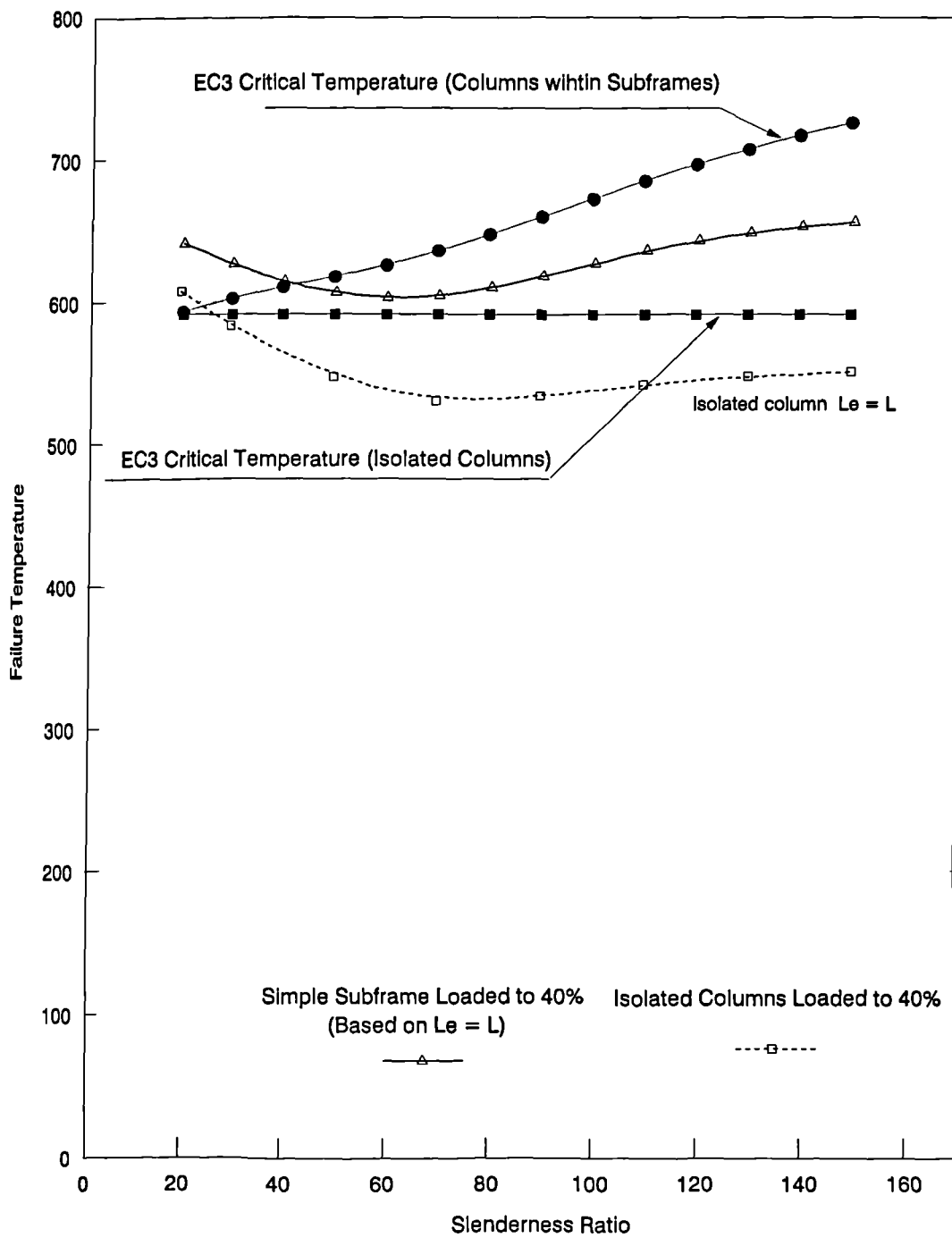
Fig. 5.63 EC3 Pt. 10 Compared with the Present Analysis

CHAPTER 6

Conclusions

6.1 Introduction

The work presented in this thesis has been concerned with the development of a numerical tool for the three-dimensional analysis of steel frames in fire conditions. The analytical approach is based on the finite element method in which structural members are modelled as beam elements. A computer program, 3DFIRE, based on the developed model has been extensively validated against available analytical and experimental results. The program has then been used to carry out various studies on columns. The results of these have indicated the existence of consistent patterns in the structural behaviour of columns in fire conditions. Such patterns are valid both for isolated columns and for columns within frames.

6.2 Isolated Columns

Based on the large number of analytical results concerning the behaviour of isolated columns in fire, valuable conclusions can be made. These conclusions can be summarised as follows:

- Simplified bilinear stress-strain models for steel at elevated temperatures may provide an adequate tool for design purposes, but they have proven not to provide good accuracy in analysis. Hence, recourse to continuous models such as Ramberg-Osgood or EC3 is necessary to perform more accurate analysis.

- The well-known column sensitivity to imperfections at ambient temperature is still applicable to columns at elevated temperatures. Imperfect columns lose part of their bearing capacity compared with perfect columns that conform to the 'Euler-and-Squash' curve. This loss is not constant; while columns

with very low and very high slenderness ratio tend to lose the least, columns in the intermediate range tend to lose most. This well-established fact at ambient temperature still holds good at elevated temperatures. Failure-temperature curves for columns, perfect or otherwise, have shown that columns within the intermediate range of slenderness have exhibited less fire resistance compared with stocky or slender columns. To different extents, this phenomenon is evident whether initial imperfections are imposed prior to the heating regime or not. This observation may allow the 'fire' to be thought of as another imperfection.

- Initial out-of-straightness and residual stresses have a similar effect on the failure temperatures of columns in fire. This effect can be arrived at by applying both imperfections simultaneously or by applying them individually. This shows clearly that Perry's assumption that all imperfections can be replaced by an equivalent initial out-of-straightness, which has produced a successful design analysis model for isolated columns at ambient temperature, is still valid at elevated temperatures.

- Slenderness ratio and imperfection have been shown to be the most prominent factors that influence the fire resistance of columns. End conditions, although influencing the slenderness ratio, cannot be regarded as an independent factor in the fire context, as is the case at ambient temperature. The same conclusion can be drawn with respect to the nature of the cross-section. It has been shown clearly that once the slenderness ratio of a column is defined, it exhibits the same fire resistance under a given load almost regardless of its cross-section.

- The relationship between load ratio and failure temperature assumes a linear pattern for columns loaded within the practical limits of design guidelines. Fig. 6.1, which is a reproduction of Fig. 5.11, shows the linearity of this relationship up to load ratio 60% for columns of different slenderness ratios. Applied load ratios beyond 60% have no practical interest as it is inconceivable that any column designed according to Standard will bear loads exceeding this ratio, especially at the fire limit state.

- The fire resistance of uniformly-heated columns can usually be regarded as a lower bound to that of columns heated otherwise. The fire resistance of columns with major-axis gradients have been seen to be higher than that of uniformly-heated columns. The only exception to this statement is the case of columns with minor-axis gradients and high slenderness ratios. Even columns with minor-axis gradients and low slenderness ratio have exhibited better fire resistance than uniformly-heated columns with the same slenderness ratio.

In any case, it difficult to think of practical cases where columns might undergo large minor-axis gradients. On the other hand, the kind of major-axis gradients which have proved to influence columns' fire resistance beneficially compared with the uniformly-heated case are very likely to occur in fire situations where the column is embedded within fire-resistant walls.

Generally, the failure temperature curves produced in the previous studies for uniformly-heated isolated columns subject to different load levels (Fig. 5.11) can be regarded as an absolute lower bound. Almost all other column cases considered, such as those with thermal gradients, invariably exhibit better fire resistance compared to the uniformly-heated case. Fig 5.17 illustrates this conclusion very
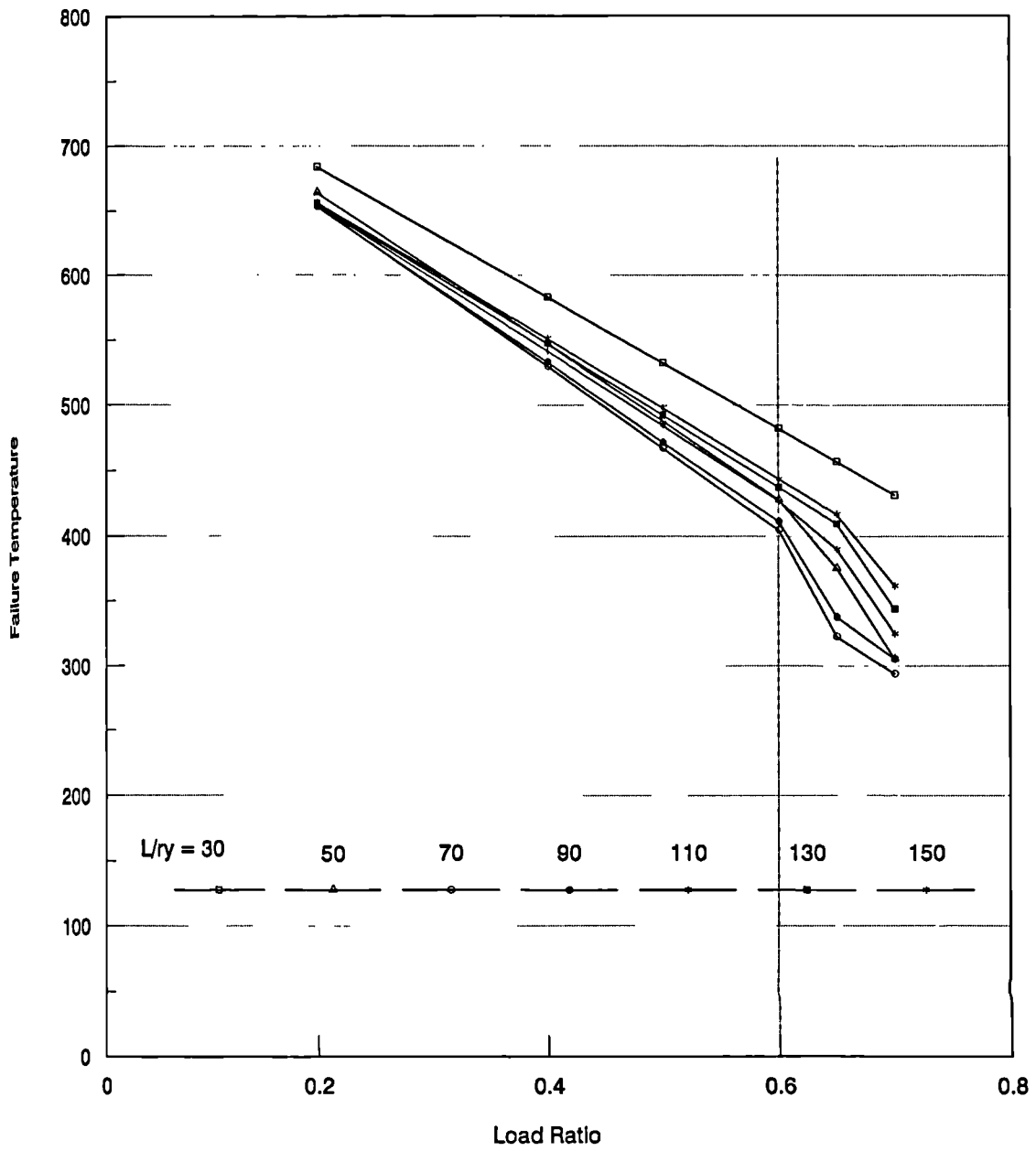
Fig. 6.1 Relationslp between Load Ratlo and Failure Temperature

clearly.

6.3   Columns within Frames

In modern steel structures, columns are as widely used within multi-storey con-
structions as in single-storey buildings. The existence of columns in multi-storey
structures presents certain difficulties in defining some essential parameters such
as the effective length and therefore the slenderness ratio. On the other hand, the
same fact presents certain opportunities, especially in terms of the fire-resistance
of such columns.

Although the number of analyses performed for columns within subframes was less
in extent than that of isolated columns, important and meaningful conclusions can
still be drawn from the analytical results. A column which is situated within a
braced framed structure is well-known to have higher axial load-bearing capacity
compared to an identical isolated column at ambient temperature. This *assembly
effect*, a term used in this work to describe the effect of the assembly on the fire
resistance of framed columns, has proven to have more influence in fire conditions.
Conclusions concerning this effect may be summarised in the following points:

- the assembly effect on the fire resistance of columns in fire has been shown to
  enhance this resistance in all cases. This benefit can be provided to columns
  either by the continuity of the column over several storeys or by connected
  beams. The basic reason for this increase in the column's fire resistance
  is the end-stiffness provided by other connected structural members of the
  assembly, which reduces the column's effective length.

- The extent of this effect depends on the column's slenderness ratio and on the arrangement of structural elements within the assembly. It has been shown that columns within the high slenderness range benefit less from this effect. A column situated in an intermediate storey that can be regarded as a fire compartment performs in a nearly similar way to a fixed-ended column. However a column situated in the top floor or the ground floor with its lower end pinned to the foundation performs similarly to an isolated column with one of its ends fixed and the other pinned.

- Even if the storey in which the column is situated cannot prevent the fire spreading to other storeys, and cannot consequently be regarded as a fire compartment, the assembly effect can still enhance the fire resistance of columns in such situations. The reason for this is the inherently different load levels of columns in multi-storey buildings. It has been shown that the upper column can provide significant end-stiffness to the critical lower column due to its lower load level, even despite being subject to the same temperature.

- The assembly effect has been shown to enhance the fire resistance of framed columns subject to thermal gradients. Such columns exhibit a better fire resistance compared to uniformly-heated columns. Thermal gradients have the same influence on framed columns as on isolated columns. Consequently failure temperatures obtained from the uniform-temperature case can be regarded as lower bounds to all failure temperatures.

- Whether framed columns are designed to carry loads based on an effective length factor of 1.0 or otherwise, they exhibit significantly enhanced fire resistance compared to isolated columns. In fact it is unlikely that designers

would normally assume an effective length factor of 1.0 in multi-storey buildings. It is more likely that effective length factors of 0.85 or 0.7 would be used. It has been shown that framed columns designed to carry loads based on any reasonable effective length factor still have significantly higher fire resistance than do isolated columns.

6.4 Codes of Practice

A limited number of studies has been undertaken to compare the present analytical results with the recommendations of both BS5950 Pt. 8 and EC3 Pt. 10. As a result, interesting preliminary conclusions can be drawn concerning the expected conservatism of both Standards. The following conclusions can be regarded as indicative rather than conclusive.

- BS5950 Pt. 8 'limiting' temperatures seem to considerably overestimate the fire resistance of isolated columns in the normal slenderness range. This is still the case, but to a lesser extent, with framed columns, for which the Standard still overestimates their fire resistance over an important part of the practical range of slenderness.

- The same conclusion seems to apply to the 'critical' temperatures of the European Standard EC3 Pt. 10. Comparisons between the present analysis and the Code have shown unconservative fire resistance estimates for both framed and isolated columns.
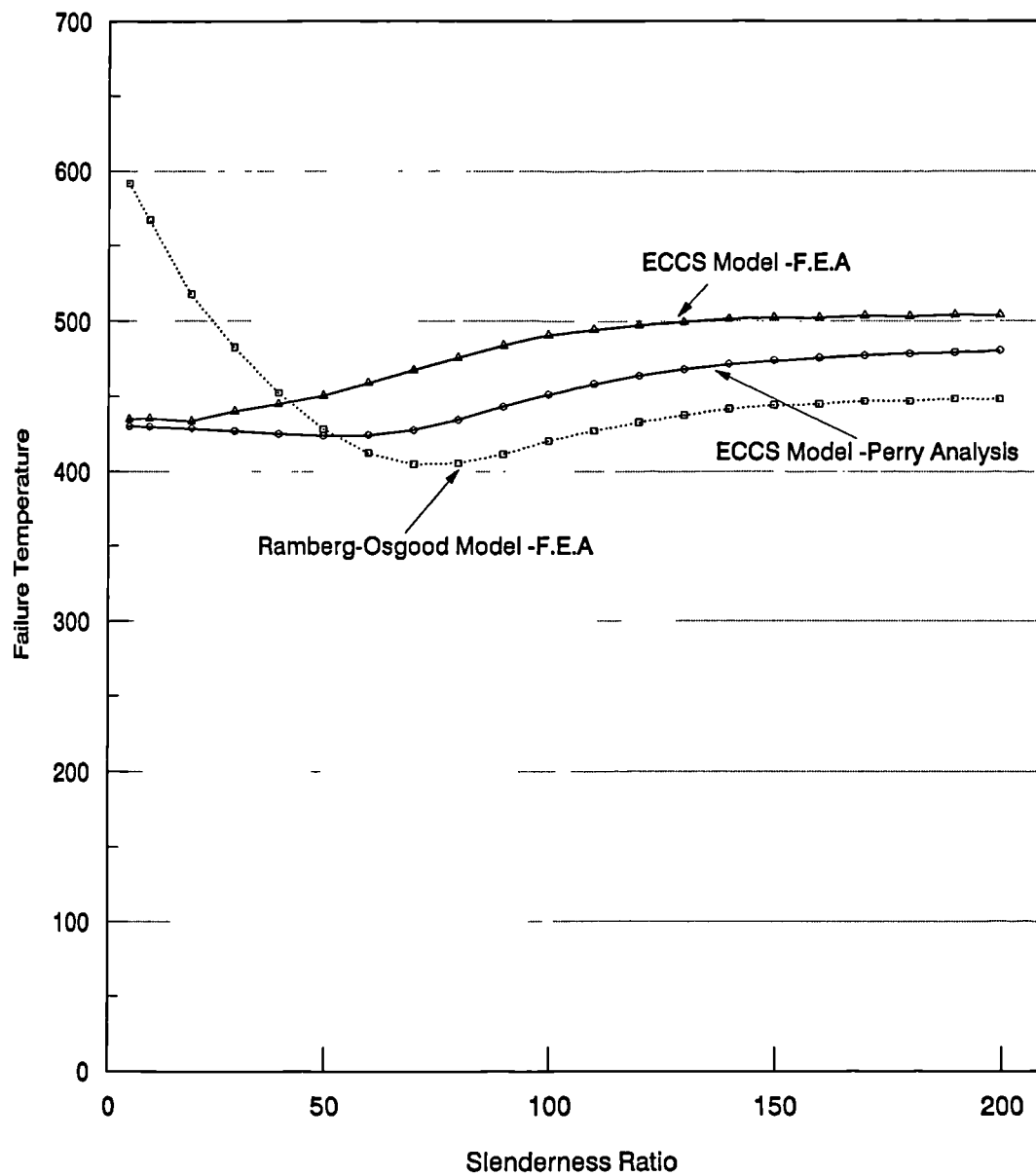
Fig. 6.2 Comparison between Perry Analysis and Finite Element Analysis

6.5 Perry Analysis and the F.E.M

The simplified approach developed in Chapter 2 can be regarded as a complement rather than a substitute for the finite element analysis. Fig. 6.2 shows a comparison between failure temperatures produced by a first-yield analysis (Perry) and the finite element analysis using stress-strain characteristics of the ECCS bilinear model and the Ramberg-Osgood continuous model. Perry results were also based on using the ECCS model. It is natural for failure temperatures produced by the first yield analysis to fall below those produced by inelastic analysis. On the other hand first yield analysis produces results more comparable with those produced using experimentally based stress-strain characteristics. Another study carried out by Burgess and Najjar (1993) using Perry analysis has shown good correlation with the large number of experimental results reported in Chapter 4 pp. 115-118. In this study an attempt has been made to find a bilinear rationalisation of the EC3 continuous stress-strain characteristics. As can be seen on Fig. 6.3 the best correlation with experimental data has been obtained by using the average of the upper and lower yield stresses of EC3 in the first yield analysis.

The importance of Perry analysis is that it can be used as a means of understanding the structural behaviour in fire based on elementary mechanics principles. This is important for non-academics who need not have blind faith in results produced by complicated numerical methods. On the other hand it may well be used, after sufficient development, as a practical tool for design purposes.
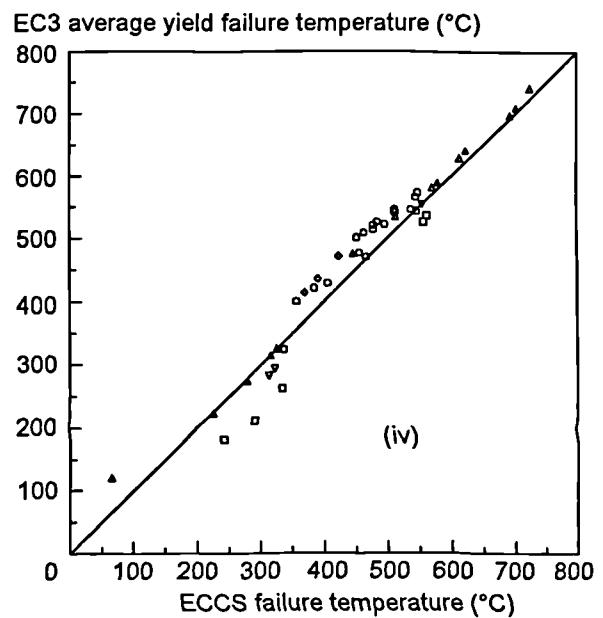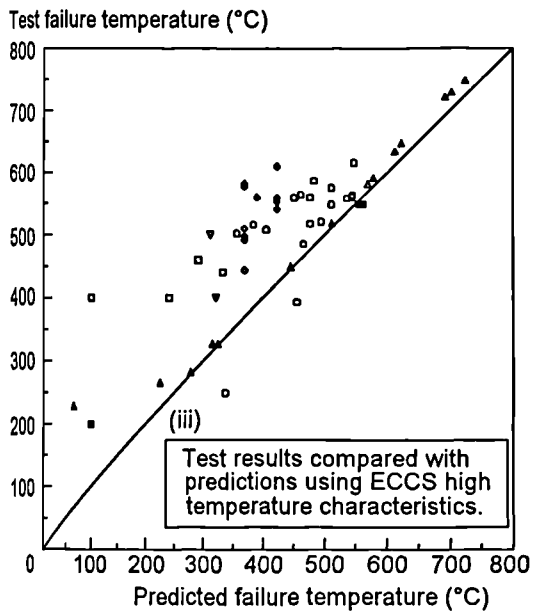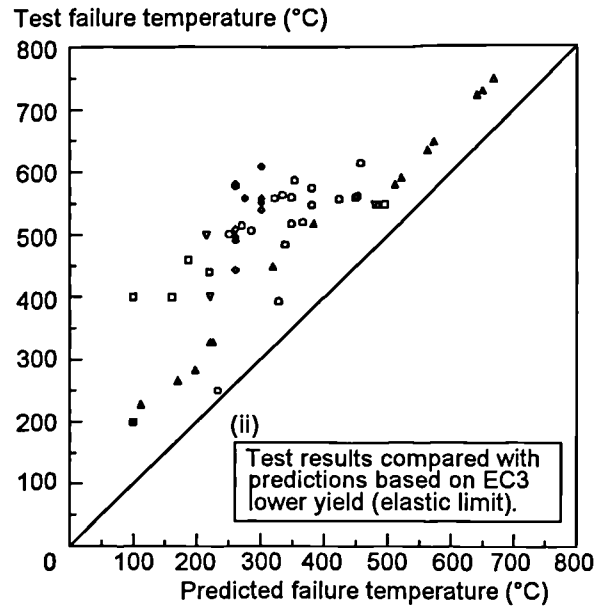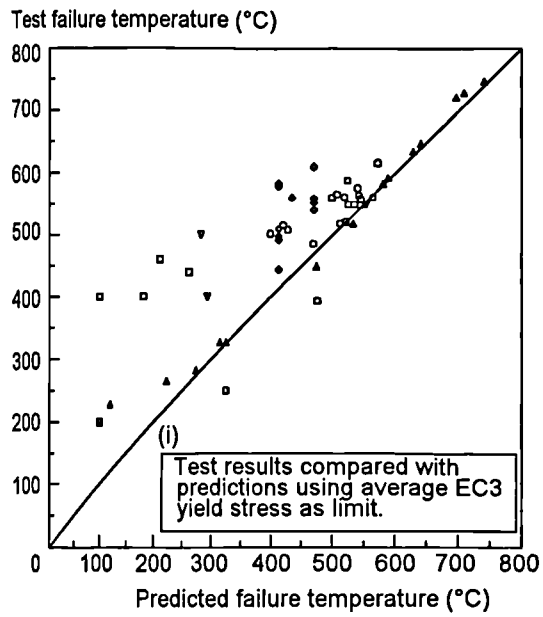
Fig. 6.3 Perry Anlysis Using Various Stress-Strain Models

6.6 Recommendations

The developed analysis has been shown to provide robust and reliable finite element solutions for columns in fire. Further developments based on the present analysis can be summarised in the following:

- The capability of the developed software can be extended to study semi-rigid connections as well as rigid ones. This can be done by one of three methods. Spring elements which have a moment-rotation capacity based on experimental data can be introduced to represent the connection semi-rigidity. Another possible route is to develop the present beam element to account for semi-rigidity at its end. This implies that a modification is required to the present cubic shape functions to account for semi-rigidity. A third route which could be explored is to introduce a physical element to represent the actual connection. The connection after all is a physical entity which consists mainly of bolts, plates and welds. Hence there is no reason why such connections should not be modelled as they exist in reality. Although the first method looks the easiest to implement, the third presents a great opportunity to abandon the need for experimental input into the analysis and restricts such input to validation and modelling purposes.

- The developed space transformation of coordinates (Chapter 3) allows the extension of the present software to a full three-dimensional flooring system. This can be achieved by the introduction of two-dimensional elements to represent slabs in addition to the present one-dimensional elements. This line of development requires considerable reformulation due to the current formulation being based on open thin-walled section assumptions. These

assumptions imply that normal strains are the prominent strain component in defining the stress state of the structural element and hence the structural behaviour of such sections. That may not be true in slab elements. In structural elements where shearing strains contribute significantly to overall deformations the inherent thin-walled assumptions, which neglect the effect of shearing deformations, cease to provide a good representation of the actual behaviour. Consequently shearing deformation may need to be included in such developments.

• The present formulation, as can seen in Chapter 3, is highly non-linear. Although this feature is beneficial in terms of the accuracy acquired by the analysis, it may be a handicap in terms of the time required to analyse extremely large problems. Hence is may be desirable to reduce the present non-linearity, for example in developing the present software to accommodate flooring systems.

One other possible development is to extend the present analysis to account for composite beams. This development has already been accomplished in the context of some analyses performed for a related research study (Najjar et al 1993; Najjar et al 1994). Due to the fact that this development was not planned as a part of this project, it will be illustrated briefly in Appendix A.

References

[1] Aribert, J. -M. and Abdel Aziz, M., **1987**
Simulation du comportement à l'incendie de poteaux comprimés et fléchis en présence de gradients quelconques de température.
Construction Métallique, Vol. 24, No. 2, pp 3-40.

[2] Ayrton, W. E. and Perry, J., **1886**
On struts.
The Engineer, 62, pp. 464.

[3] Baba, S. and Nagura, H., **1985**
Effect of material properties on the deformation of steel frames in fire.
Proc. of JSCE Structural Eng./Earthquake Eng., Vol. 2, No. 1, pp. 47-57.

[4] BRE, **1993**
Cardington Newsletter.
Building Research Establishment, Issues 1, 2 and 3.

[5] Bresler, B., **1977**
FIRES-T2, a computer program for the fires response of structures -Thermal.
Report No. UCB FRG 77-15, University of California, Berkeley.

[6] Birnstiel, C., **1968**
Experiments on H-columns under biaxial bending.
J. of the Structural Division, ASCE, Vol. 94, No. ST10, pp. 2429-2449.

[7] British Steel Corporation, **1987**
Compendium of UK standard fire test data on unprotected structural steel.
Report RS/RSC/S10328/1/87/B.

[8] Brockenbrough, R., **1970**
Theoretical stresses and strains from heat curving.
J. of the Structural Division, ASCE, Vol. 96, No. ST7, pp. 1421-1444.

[9] BS5950, **1985**

Structural use of steelwork in building: Part 1. Code of practice for design in simple and continuous construction: hot rolled sections.

British Standards Institution, London.

[10] BS5950, **1990**

Structural use of steelwork in building: Part 8. Code of practice for fire resistant design.

British Standards Institution, London.

[11] Burgess, I. W., Olawale, A. O. and Plank, R. J., **1992**
Failure of steel columns in fire.
Fire Safety Journal, Vol. 13, No. 2, pp. 183-201.

[12] Burgess, I. W. and Najjar, S. R., **1993**
A simple approach to the behaviour of steel columns in fire.
J. of Constructional Steel Research, (accepted for publication).

[13] Chen, W. F. and Atsuta, T., **1977**
Theory of beam-columns; Vol. 2 - Space behaviour and design.
McGraw-Hill Book Company, Inc., New York.

[14] Cheng, W. and Mak, K., **1975**
Computer analysis of steel frames in fire.
J. of the Structural Division, ASCE, Vol. 101, No. ST4, pp. 855-867.

[15] Cheng, W., **1983**

Theory and application on the behaviour of steel structures at elevated temperatures.

Computers and Structures, Vol. 16, No. 1-4, pp. 27-35.

[16] Cooke, G. M. E., **1987**

The structural response of steel I-section members subjected to elevated temperature gradients across the section.

PhD thesis, City University, London.

[17] Cooke, G. M. E. and Latham, D. J., **1987**
The inherent fire resistance of a loaded steel framework.
Steel Construction Today, No. 1, pp. 49-58.

[18] Corradi, L., Poggi, C. and Setti, P., **1990**
Interaction domains in steel beam-columns in fire conditions.
J. of Constructional Steel Research, Vol. 17, No. 3, pp. 217-235.

[19] CTICM (Centre Technique Industriel de la Construction Métallique), **1982**
Méthode de prévision par le calcul du comportement au feu des structures en acier.
Construction Métallique, 3, pp. 39-79.

[20] Culver, C. G., **1972**
Steel column buckling under thermal gradients.
J. of the Structural Division, ASCE, Vol. 98, No. ST8, pp. 1853-1865.

[21] Department of the Environment and The Welsh Office., **1985a**
Approved document B, B/2/3/4 Fire spread.
Department of the Environment and The Welsh Office, HMSO.

[22] Department of the Environment and The Welsh Office., **1985b**
Manual to the building regulations.
Department of the Environment and The Welsh Office, HMSO.

[23] Dotreppe, J. -C., **1986**
Structural models for fire analysis.
IABSE Periodica, No. 3, pp. 101-112.

[24] ECCS (European Convention for Constructional Steelwork), **1983**
European recommendations for the fire safety of steel structures.
Elsevier, Amsterdam.

[25] El-Rimawi, J. A., **1989**
The behaviour of flexural members under fire conditions.
PhD thesis, University of Sheffield.

[26] El-Rimawi, J. A., Burgess, I. W. and Plank, R. J., **1993**
Modelling the behaviour of steel frames and subframes with semi-rigid connections in fire.
Proc., Third CIB/W14 Workshop on Fire Modelling, Rijswijk, Ed. Twilt, L. (In press).

[27] El-Zanaty, M. H. and Murray, D. W., **1983**
Non-linear finite element analysis of steel frames.
J. of Structural Engineering, ASCE, Vol. 109, No. 2, pp. 353-368.

[28] Eurocode EC3, **1988**
Design of steel structures. Pt. 1: General rules and rules for buildings (final draft).
Commission of the European Communities.

[29] Eurocode EC3, **1990**

Design of steel structures. Pt. 10: Structural fire design (draft).

Commission of the European Communities.

[30] Eurocode EC4, **1992**

Design of composite steel and concrete structures. Pt. 1.2: Structural fire design (draft).

Commission of the European Communities.

[31] Franssen, J. -M., **1987**

Etude du comportement au feu des structures mixtes acier-béton.

PhD thesis, Université de Liège.

[32] Franssen, J. -M, **1989**

Modélisation et influence des contraintes résiduelles dans les profils métalliques soumis à l'incendie.

Construction Métallique, Vol. 24, No. 2, pp 3-40.

[33] Franssen, J. -M, Cooke G.M.E. and Latham, D. J., **1993**

Numerical simulation of a full fire test on a loaded steel framework.

J. of Constructional Steel Research, (submitted for publication).

[34] Furumura, F. and Shinohara, Y., **1978**

Inelastic behaviour of protected steel beams and frames in fire.

Report of the Research Laboratory of Engineering Materials, No. 3, pp. 1-14.

[35] Giżejowski, M., **1986**

In-plane stability of imperfect frames at elevated temperature.

Second Regional Colloquium on Stability of Steel Structures, Hungary, Proc., pp. 287-294.

[36] Harstead, G. A., Birnstiel, C. and Leu, K. C., **1968**

Inelastic H-columns under biaxial bending.

J. of the Structural Division, ASCE, Vol. 94, No. ST10, pp. 2371-2398.

[37] Hoffend, F., **1980**

Brandverhalten von stahlstutzen bei ausmittiger lasteinleitung, dehnbehinderung oder teilweiser bekleidung.

Technische Universitat, Braunschweig, Germany.

[38] Jain, P. and Rao, R., **1983**

Analysis of steel frames under fire environment.

Int. Journal for Numerical Methods in Engineering, Vol. 19, pp. 1467-1478.

[39] Janss, J. and Minne, R., **1982**
Buckling of steel columns in fire conditions.
Fire Safety Journal, Vol. 4, No. 4, pp. 227-235.

[40] Jeyarupalingam, N. and Virdi, K. S., **1991**
Steel beams and columns exposed to fire hazard.
Int. Seminar on Structural Design for Hazard Loads, Brighton UK, 17-19 April.

[41] Kirby, B. R. and Preston, R.R., **1988**
High temperature properties of hot-rolled structural steels for use in fire engineering design studies.
Fire Safety Journal, Vol. 13, No. 1, pp. 27-37.

[42] Knight, D. C., **1975**
Predicting the performance of steel members during fire conditions.
IABSE Symposium 'Steel and composite structures for user needs', Dresden.

[43] Kruppa, J., **1979**
Collapse temperature of steel structures.
J. of the Structural Division, ASCE, Vol. 105, No. ST9, pp. 1769-1787.

[44] Lawson, R. M. and Newman, G. M., **1990**
Fire resistance design of steel structures; a handbook to BS5950: Pt. 8.
The Steel Construction Institute, Ascot, UK.

[45] Malhotra, H. L., **1986**
Fire safety in buildings.
Building Research Establishment Report, Fire Research Station, Borehamwood, UK.

[46] Morino, S. and Lu, L. W., **1971**
Analysis of space frames.
Fritz Engineering Laboratory, Report No. 331.13, March.

[47] Najjar, S. R. and Burgess, I. W., **1992**
Perry analysis and the failure of steel columns in fire.
Stress Analysis and the Personal Computer (SAPC'92) Meeting, The Institute of Physics.

[48] Najjar, S. R. and Burgess, I. W., **1993**
Non-linear analysis of three-dimensional steel frames in fire conditions.

Civil Engineering Department Report No. DCSE/93/S/06, University of Sheffield.

[49] Najjar, S. R., Burgess, I. W. and Plank, R. J., **1993**
Non-linear studies of the Cardington composite frame in fire conditions using 3DFIRE.
Civil Engineering Department Report No. DCSE/93/S/05, University of Sheffield.

[50] Olawale, A. O., **1988**
Collapse behaviour of steel columns in fire.
PhD thesis, University of Sheffield.

[51] Olesen, F. B., **1980**
Fire tests on steel columns.
Inst. Technol. Struct. Eng. Aalborg, Denmark.

[52] Ossenbruggen, P. J., Aggarwal, V. and Culver, C. G., **1973**
Steel column failure under thermal gradients.
J. of the Structural Division, ASCE, Vol. 99, No. ST4, pp. 727-739.

[53] Ramberg, W. and Osgood, W. R., **1942**
Description of stress-strain curves by three parameters.
NACA Technical Note No. 902.

[54] Robertson, A., **1925**
The strength of struts.
I.C.E Selected Engineering Papers, No. 28.

[55] Rojahn, C., **1968**
Large deflections of elastic beams.
Thesis for the degree of engineer, Stanford University.

[56] Saab, H. A., **1990**
Non-linear finite element analysis of steel frames in fire conditions.
PhD thesis, University of Sheffield.

[57] Saab, H. A. and Nethercot, D. A., **1991**
Modelling steel frame behaviour under fire conditions.
Engineering Structures, Vol. 13, No. 4, pp. 371-382

[58] Saada, A. S., **1974**
Elasticity theory and applications.
Pergamon Press Inc., New York.

[59] Schleich, J. B., **1986**
Fire engineering design of steel structures.
Steel Construction Today, No. 2, pp. 39-52.

[60] Schleich, J. B., Dotreppe, J. -C. and Franssen, J., -M., **1986**
Numerical simulations of fire resistance tests on steel and composite structural
elements or frames.
IABSE Periodica, No. 3, pp. 101-112.

[61] Soltis, L. A. and Christiano, P., **1972**
Finite deformations of biaxially loaded columns.
J. of the Structural Division, ASCE, Vol. 98, No. ST12, pp. 2647-2661.

[62] Timoshenko, S. P. and Gere, J. M., **1978**
Mechanics of materials.
Van Nostrand Reinhold Company Ltd., New York.

[63] Uddin, T. and Culver, C. G., **1975**
Effect of elevated temperature on structural members.
J. of the Structural Division, ASCE, Vol. 101, No. ST7, pp. 1531-1549.

[64] Vandamme, M. and Janss, J., **1981**
Buckling of axially loaded steel columns in fire conditions.
IABSE Periodica, Vol. 3, pp. 43-81.

[65] Vinnakota, S., **1976**
Inelastic H-columns under biaxial bending.
Canadian Journal of Civil Engineering, Vol. 3, No. 2, pp. 186-197.

[66] Virdi, K. S. and Dowling, P. J., **1973**
The ultimate strength of composite columns in biaxial bending.
Proc., The Institute of Civil Engineers, No. 55, pp. 251-272.

[67] Virdi, K. S. and Dowling, P. J., **1976**
The ultimate strength of biaxially restrained columns.
Proc., The Institute of Civil Engineers, Pt. 2, No. 61 pp. 41-58.

[68] Virdi, K. S., **1981**
Design of circular and rectangular hollow section columns.
J. of Constructional Steel Research, Vol. 1, No. 4, pp. 35-45.

[69] Vlasov, V. Z., **1961**
Thin-walled elastic beams.
English Translation., National Science Foundation, Washington D.C., Oldbourne Press.

[70] Wang, J. C. and Moore, D. B., **1991**
Fire resistance of steel beams.
Int. Seminar on Structural Design for Hazard Loads, Brighton UK, 17-19 April.

[71] Witteveen, J. and Twilt, L., **1975**
Behaviour of steel columns under fire action.
Int. Colloquium on Column Strength, Paris 1972, Proceedings IABSE, Vol. 23, Zurich.

[72] Witteveen, J., Twilt, L. and Bijlaard, F. S. K., **1976**
Theoretical and experimental analysis of steel structures at elevated temperatures.
IABSE, 10th Congress, Tokyo, Final report, Zurich.

[73] Witteveen, J., Twilt, L. and Bijlaard, F. S. K., **1977**
The stability of braced and unbraced frames at elevated temperatures.
Second Int. Colloquium on Stability of Steel Structures, Liège, Preliminary report, Zurich.

[74] Zbirohowski-Kòscia, K., **1967**
Thin walled beams.
Crosby Lockwood & Son, London.

[75] Zienkiewicz, O. C., **1971**
The finite element method in engineering science.
McGraw-Hill Book Company, Inc., New York.

[76] Zienkiewicz, O. C. and Taylor, R. L., **1991**
The finite element method; 4th Ed., Vol. 2., Solid and fluid mechanics and nonlinearity
McGraw-Hill Book Company (UK) Limited.

APPENDIX A

Analysis of Composite Frames

A.1 Introduction

A full-scale testing facility has been made available for building research by the construction of an eight-storey steel-framed structure at Cardington. This facility will provide the opportunity to perform static, dynamic, explosive and fire tests on a real structure (BRE 1993). Testing full-scale structures under fire conditions is an expensive undertaking financially and a complicated one technically. Consequently, in the run-up period before fire testing is undertaken in 1994-95 on the full-scale eight-storey composite test frame at Cardington, it was thought prudent to carry out a series of pre-test analyses in order to help in making the final decisions concerning test arrangements. Provisional decisions had already been made about the areas within the structure in which the compartments for the natural fires should be located, but it is important that the structural behaviour in the fires should cover a sufficient range of distortion to provide a fair test for numerical modellers while not causing severe collapse to occur. One key parameter to which a value needs to be set at this stage is the loading level at the floor above the fire compartment, but it is also necessary to have predictions of behaviour in order to design and position instrumentation. Research workers at BRE, City University, Sheffield University and the Université de Liège have been involved in the numerical modelling work.

A.2 Problem Modelling and Program Validation

Prior to this work the program 3DFIRE had been developed for three-dimensional analysis of rigidly-connected steel skeletons under temperature profiles caused by fire conditions, and had been validated against a wide range of analytical and

experimental work. The Cardington frame is a steel structure with composite steel-concrete flooring. For this reason the analysis has been extended to include composite beams, particularly to include concrete as a material. The development of the composite beam element is described, followed by simple validation examples.

A.2.1 Problem Model

As is illustrated in Fig. A.1 the steel I-section is divided into a minimum of twelve segments to allow for a fairly detailed temperature profile to be introduced. A concrete slab is connected to the top flange of the steel section, and this is divided into a variable number of layer segments. To account for mesh or bar reinforcement a single layer consisting of two segments is included within the concrete slab at any required position. This arrangement allows the full three-dimensional effect of any variation in temperature across the depth and the width of the slab. The elastic centroid of the composite cross-section is calculated based on the transformed section at ambient temperature using the modular ratios for the materials at zero strain. At this centroid the single node at each end of the beam element is fixed.

A.2.2 Simple Validation Examples

To assess the proposed composite beam model a few simple examples have been analysed to compare results from both the finite element analysis and basic structural mechanics principles. Fig. A.2 shows a cantilever composite beam subject to an end moment causing tension on the concrete fibre of the beam. In order to simplify the example no reinforcement has been used. The centroid of the un-

cracked composite section lies just above the flange of the I-section, so that the concrete would actually be almost wholly in tension over the whole length of the beam, if tension could be sustained. The EC4 model for a concrete stress-strain relationship has been used in this analysis, with zero strength and stiffness being assumed in tension, while the steel is kept in the elastic range. In structural terms this last assumption makes the analysis identical to that for a steel beam. If vertical end displacement is calculated using the normal elastic formula $v = \frac{ML^2}{2EI}$ a result of 30.24mm is obtained, compared with 30.27mm produced by the program. It is interesting to note that the program produced also an apparent axial expansion of the beam, even though a tiny horizontal translation is expected in the opposite direction. This phenomenon is consistent with the positioning of the nodes at both ends of the elements at the uncracked composite beam's centroid, just above the upper flange of the I-section. The program therefore calculates the axial displacement of the upper flange rather than the centroid of the steel section. The expansion indicated is therefore the strain at the node position multiplied by the length of the beam. Strains and stresses predicted by the program are similar to what would be expected from the steel beam alone.

In Fig. A.3 an axial tensile force has been applied to the free end of the same composite beam in place of the moment. The same stress-strain relationship for concrete as used previously has been used, resulting in an effective reduction of the problem to that of a steel beam with an axial end force, applied eccentrically from the centroid of its section. The normal representation of this case assumes an applied end moment due to the eccentrically applied load, resulting in a reaction moment at the support consisting of this moment plus that produced by the $P - \Delta$ effect. This solution is correct if all calculations are based on the assumption that the reference axis coincides with the centroid of the steel section. On the other

hand the program produces a reaction moment given by the $P - \Delta$ effect only. This a reasonable outcome, since the program calculations are based on the composite section's centroid as the reference axis, and converts to the usual solution if the reference point is displaced by half the depth of the steel section. Again deflections, strains and internal stresses at the support, as indicated by the program, are similar to those produced by hand calculations.

A.3   Stress-Strain Model for Concrete

The composite construction Eurocode EC4 (1992) suggests a convenient stress-strain model for lightweight concrete, consisting of a hyperbolic curve for concrete in compression. EC4 allows the use of up to 10% of the compressive strength of concrete as a tensile strength. It also allows the use of a linear descending path for the stress-strain curve after maximum stress has been attained. Four versions (Fig. A.4) of the EC4 model have been incorporated in the analysis to assess their effects in combination with the EC3 models for structural steel and reinforcement. The concrete models are identical in their rising compression curves at any temperature level, but vary in their treatment of post-ultimate compression and of tension. The fixed-ended composite beam illustrated in Fig. A.4, with a point load applied at mid-span, has been used to study these combinations. Axial movement of one of the fixed ends is allowed, so that the case under consideration is kept reasonably simple. Fig. A.5 shows the vertical (mid-span) and axial (end) displacements of this beam as it is heated up to failure, using the four models for concrete stress-strain characteristics. Deflections produced by all the models are clearly very close and failure temperatures are impossible to separate. Fig. A.6 shows the bending moment diagrams for models 1, 3 and 4 at selected temperatures. Model 2

produced the same results as model 3 due to the fact that concrete in compression never reached the descending path of the stress-strain curve. It is clear that the hogging moment at supports is lowest for model 1 while a little improvement is evident for model 3 as a result of the additional strength of some of the concrete in tension. The initial value of hogging moment in case 4 was much higher due to the additional strength of all the concrete in tension. These differences at ambient and low temperatures disappear quickly at higher temperatures, producing effectively identical distributions of moment at failure.

Model 3 has been selected as the concrete model to be used in the analyses, as it offers a more realistic representation of concrete in tension than does model 1. Model 4 has been ruled out because of numerical difficulties which are experienced once concrete reaches its descending path in tension, forcing the use of very small temperature increments and long run-times.

A.4 Analyses of the Cardington Frame

In order to obtain results which can be compared directly with those from other workers, it has been agreed that common assumptions should be made about the frame details and material stress-strain characteristics in fire. EC3 stress-strain models for both structural and reinforcing steel in fire are used in the following analyses. The EC4 model for light-weight concrete is also incorporated in the analysis as described in Section A.3. The geometry and loading regime of the 2-D section through the frame are shown in Fig. A.7. Fig. A.8 shows cross-section details and a proposed heating scheme to be implemented in the analyses.

Two tests are planned to take place in compartments directly below Levels 4 and

7, which stretch completely across the depth of the structure. In the following analyses the pre-existing general load level (Fig. A.7) will be used with the exception of the heated levels (4 and 7) on which loads will be multiplied by factors of 1.0, 1.33, 1.78 and 2.22. This exercise has been proposed to order to bracket the range of practical loadings at the heated level, in order to decide the actual load level under which the fire tests will carried out.

Figs. A.9 and A.10 show the absolute vertical displacements of an outer column, an inner column, and the mid-span points of the outer and inner beams for Level 4. The same information is shown on Figs. A.11 and A.12 for Level 7. In order to attempt to separate beam and column behaviour it was decided also to plot beam deflections relative to the average deflection of the columns at the beam ends. These net deflections are shown in Figs. A.13 and A.14 for both Levels 4 and 7 for all the load cases. Figs. A.15 and A.16 show column head rotations for all cases. It is noticeable that the column head rotation at Level 4 initially exhibits a clockwise direction, and reverses direction as heating proceeds due to the expansion of the beams, before resuming its original direction as the beams become softer and deflect rapidly. At Level 7 the same phenomenon takes place, but without the rotations reversing their direction. This is likely to be a result of the different column sections and superstructure loadings at the different levels.

Figs. A.17 and A.18 show the internal axial forces in the outer and inner beams at Levels 4 and 7 for all load cases. It is clear that the inner beam sustains more axial force that the outer beam. This is logical; the inner beam is subject to axial restraint from more columns, as well as reacting to the force generated in the outer beam.

Figs. A.19 and A.20 show the internal axial force in both the outer and inner

columns for all cases. The variation in the axial load of the columns is a result of moment redistribution within the beams. It can be observed that the outer column starts to sustain a higher level of axial force towards the end of the heating scheme, thus relieving the middle column to some extent from its share of the beam reactions. This is true for all cases at both levels, although to a lesser extent as the load factor is increased.

Moments at the outer beam-column junction, within the outer beam, at the inner junction and within the inner beam at Level 4 are shown on Figs. A.21 to A.24. The same information is given in Figs. A.25 to A.28 for Level 7. At the outer connection it can be seen that the heated column develops a large moment due to its non-uniform heating, which is balanced in turn by that on the upper unheated column. Unlike the outer column, the inner column is uniformly heated, and as a result most of the moment developed in it can be regarded as a transfer of the unbalanced moments of the beams.

A.5 Comparison with Other Analyses

More such analyses will take place before the key decisions are made on the test parameters. In the meantime, it is encouraging that the results produced from the 3DFIRE software and reported here are generally in accordance with those produced by the other modelling tools used. Due to the fact that results produced by other researchers are not published yet it is probably inappropriate to quote them in this work. The analyses reported here are all for plane frames, and one interesting study still to be undertaken is an investigation of the amount of support

in the fire test which is likely to be provided by the secondary beams. This will be looked at by means of 3-D subframe models in the next section.

A.6   3-D Subframe Analyses

All the previous analyses have been performed assuming in-plane behaviour only. In order to investigate some of the out-of-plane behavioural aspects of the locations where fire tests are proposed, a series of three-dimensional analyses has been carried out. In the following a description to these analyses is presented.

- All 8 cases have been re-analysed as 2-D subframes with the columns unrestrained against out-of-plane action except at floor levels where columns assumed to be restrained in position but not in direction. No initial imperfections have been introduced to the columns in this set of analyses. The failure temperatures and deflection histories were identical to those produced by in-plane analyses.

- The same cases have been re-analysed again with the same boundary conditions (out-of-plane behaviour permitted except translation at floor levels), but with initial out-of-straightness introduced in the minor-axis direction. The value of this initial imperfection was assumed to be 1 in 1000 of the actual column height. Small reduction in the failure temperatures was observed in this case. The following table shows the failure temperatures of the imperfect cases compared to those of the perfect cases.

Level/Load Ratio	Perfect Case	Imperfect Case
4 / 1.00	717.0	705.0
4 / 1.33	708.0	700.0
4 / 1.78	653.0	649.0
4 / 2.22	614.0	614.0
7 / 1.00	760.0	748.0
7 / 1.33	712.0	705.0
7 / 1.78	664.0	660.0
7 / 2.22	574.6	572.4

Table A.1: Effect of initial imperfections.

This shows clearly that there is no danger of out-of-plane buckling on the frames under consideration. The slight reduction in failure temperatures was a result of the out-of-plane imperfection which introduced twist to the heated columns producing a combined major/minor-axis failure.

- Various three-dimensional subframes have been analysed to establish the effect of the secondary beams on the stiffness of the main-frame beams. Fig. A.29 shows the applied loads on the assembly. These loads do not correspond exactly to the applied loads on the two-dimensional subframe considered in Fig. A.7 but represent a load ratio of about 2.3. This study was carried out independently of the 2-D cases. The extent of these subframes and their boundary conditions are shown in Table A.2 together with the predicted failure temperatures.
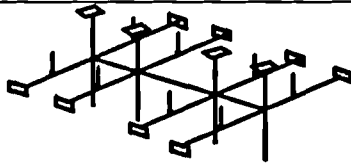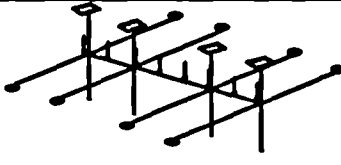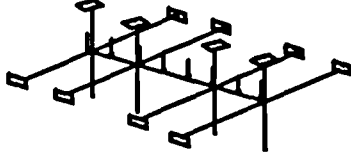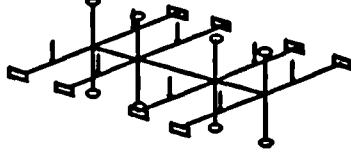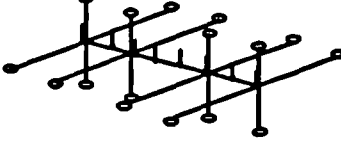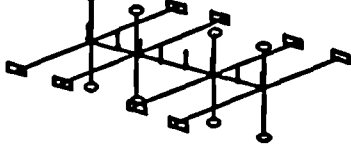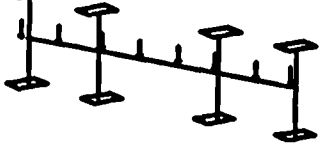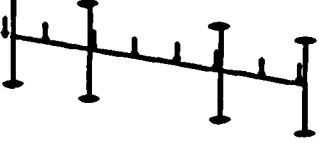
No.	Temp$_{cr}$	Description	Subframe
1	601.0	L_{column} = full length Columns and beams with fixed-ends. Loads applied at secondary beams.	
2	622.5	L_{column} = full length Columns with fixed-ends. Beams with pinned-ends. Loads applied at main beams.	
3	630.0	L_{column} = full length Columns with fixed-ends. Beams with fixed-ends. Loads applied at main beams.	
4	567.4	L_{column} = half length Columns with pinned-ends. Beams with fixed-ends. Loads applied at secondary beams.	
5	563.1	L_{column} = half length Columns with pinned-ends. Beams with pinned-ends. Loads applied at main beams.	
6	562.0	L_{column} = half length Columns with pinned-ends. Beams with fixed-ends. Loads applied at main beams.	
7	667.4	L_{column} = full length Columns with fixed-ends. Loads applied at main beams.	
8	661.3	L_{column} = half length Columns with pinned-ends. Loads applied at main beams.	

Table A.2 Subframe arrangement and failure temperatures.

The reason for applying loads at the main beams instead of the secondary ones apart from case 1 is due to the failure of the secondary beams at ambient temperature if the remote ends of the secondary beams were assumed to be pinned. This assumption produced greater hogging moments at the near ends of the secondary beams which rendered a large area of the concrete flange fully cracked. Hence case 1 could not be repeated for pin-ended secondary beams. Case 2 shows a comparable failure temperature to case 3. On the other hand cases 4, 5 and 6 show almost the same failure temperatures, which are considerably reduced compared to cases 2 and 3. It seems that the extent of the subassembly plays an important role in the determination of the fire resistance of the frame. An important parameter is the heating regime of the columns; the lower part of each heated column was assumed to be subject to lower temperatures than the rest of the column (Fig. A.8). The loss of this stiffer part of the column when half of its length was considered (cases 4, 5 and 6) produced a considerable reduction in the fire resistance of the assembly. This stiffer part is likely to reduce the effective length of the column, as was demonstrated in Chapter 6. In any circumstances this interpretation of the results does require further investigation. Cases 7 and 8 for two-dimensional subframes show higher failure temperatures than those of 3-D subframes. This shows that the out-of-plane behaviour is more critical in subframe models compared to the full-frame model considered in Table A.1. This is another point which deserves further investigation in the context of reducing the structure into subframes.

The effect of the secondary beams on the overall behaviour of the main frame proved to be insignificant. Fig. A.30 shows a comparison of the net deflections of the inner and outer beams for cases 1, 2 and 7. This result is

by no means surprising due to the relatively small stiffness of the secondary beam compared to the main-frame beam in terms of its smaller cross-section and longer span. Yet one should keep in mind that modelling the floor's restraining effect into secondary beams with concrete flanges is rather an underestimate. Consequently the membrane effect of the floor is likely to prove more significant during the actual testing.

Apart from the failure temperatures the deflection history of all the three-dimensional subframes is qualitatively very similar to the results presented for the two-dimensional analyses. In order to avoid extensive repetition typical temperature-deflection characteristics of case 2 are presented in Fig. A.31.

A.6   3-D Conclusions

It is early at this stage to draw generalised occlusions from the analyses presented in this appendix. Nevertheless, these analyses indicate certain points worth further consideration:

- The 2-D frame analyses show that failure is bound to be column-led under the assumed heating and loading schemes.

- The 3-D frame analyses indicate that the secondary beams are the critical elements in the design of the Cardington frame. Main-frame beams are evidently over designed to the extent that they can bear the ultimate design load up to temperatures of the order of $600^\circ C$. This an important point to consider in the final loading arrangement of the proposed test. Although it is desirable to apply reasonably high loads on the main beams this may not

be achieved through loading slabs supported by the secondary beams.

- At ambient temperature it is invariably acceptable to take a subframe to represent the entire frame using certain rules. This notion may still be acceptable at elevated temperatures if theoretical cases, such as uniformly heated members, are considered. On the other hand if more realistic heating schemes are to be considered, such as that of this study, the use of subframes needs more fundamental re-thinking. While it is difficult to conclude any generalised rules from the limited number of subframes performed in this study, it at least indicates the need for more rigorous studies in this area.
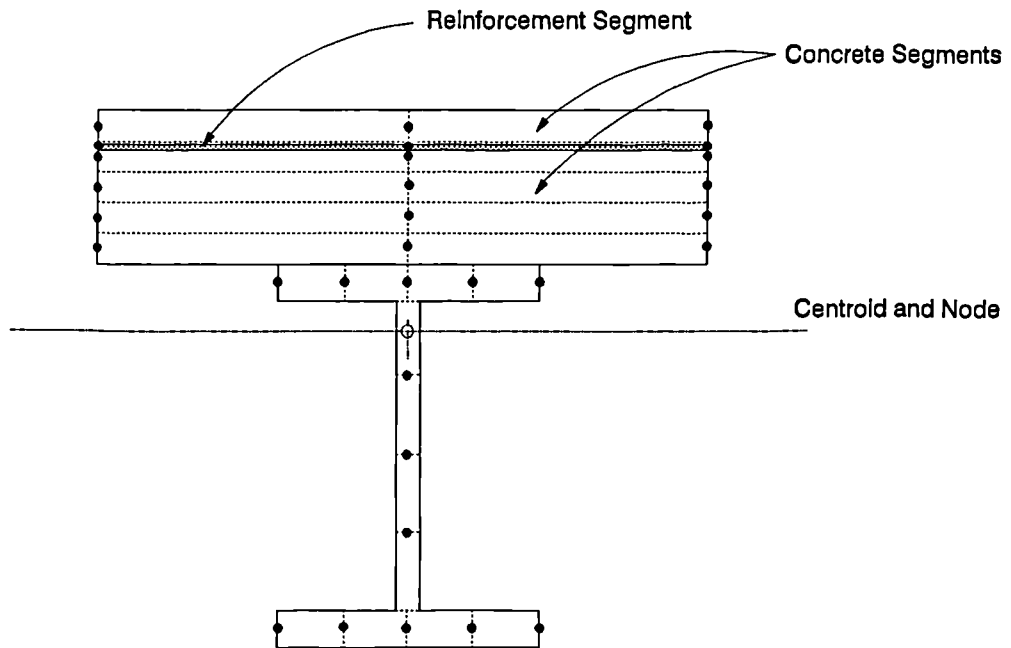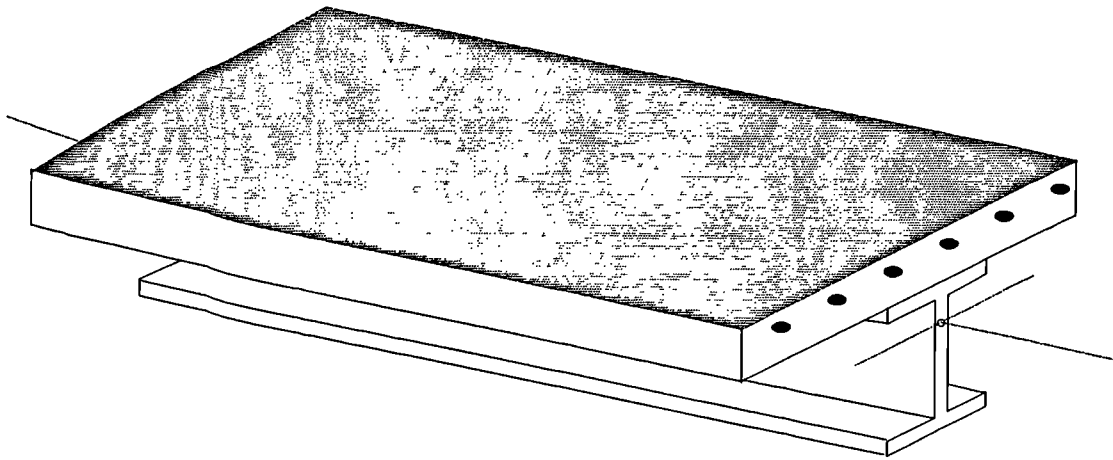
Fig. A.1 Composite Element Model

M = 50 KN.m

L = 6 m

u=1.74 mm

v=30.27mm

W = 1500 mm

y = 125.4 mm

T = 130 mm

ε = 0.49E-3

σ = 0

0.29E-3

60.75

-0.29E-3

-60.75

UB 356 X 171 X 51
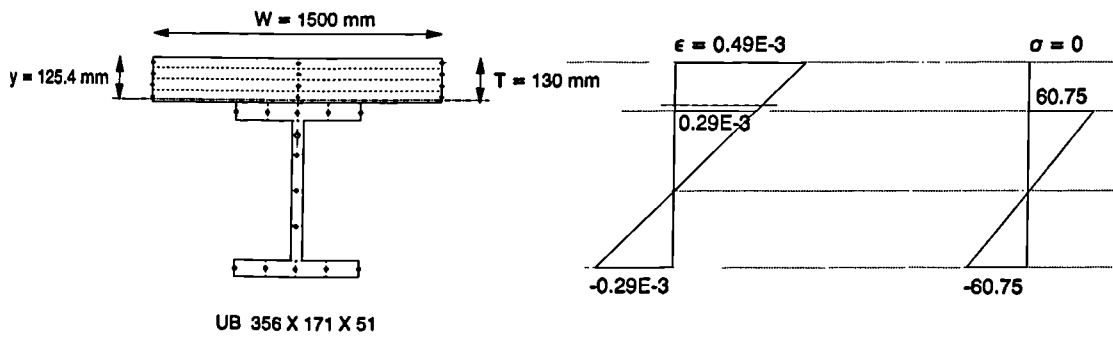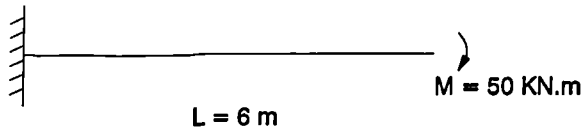
Fig. A.2 Composite Cantilever Beam with End Moment
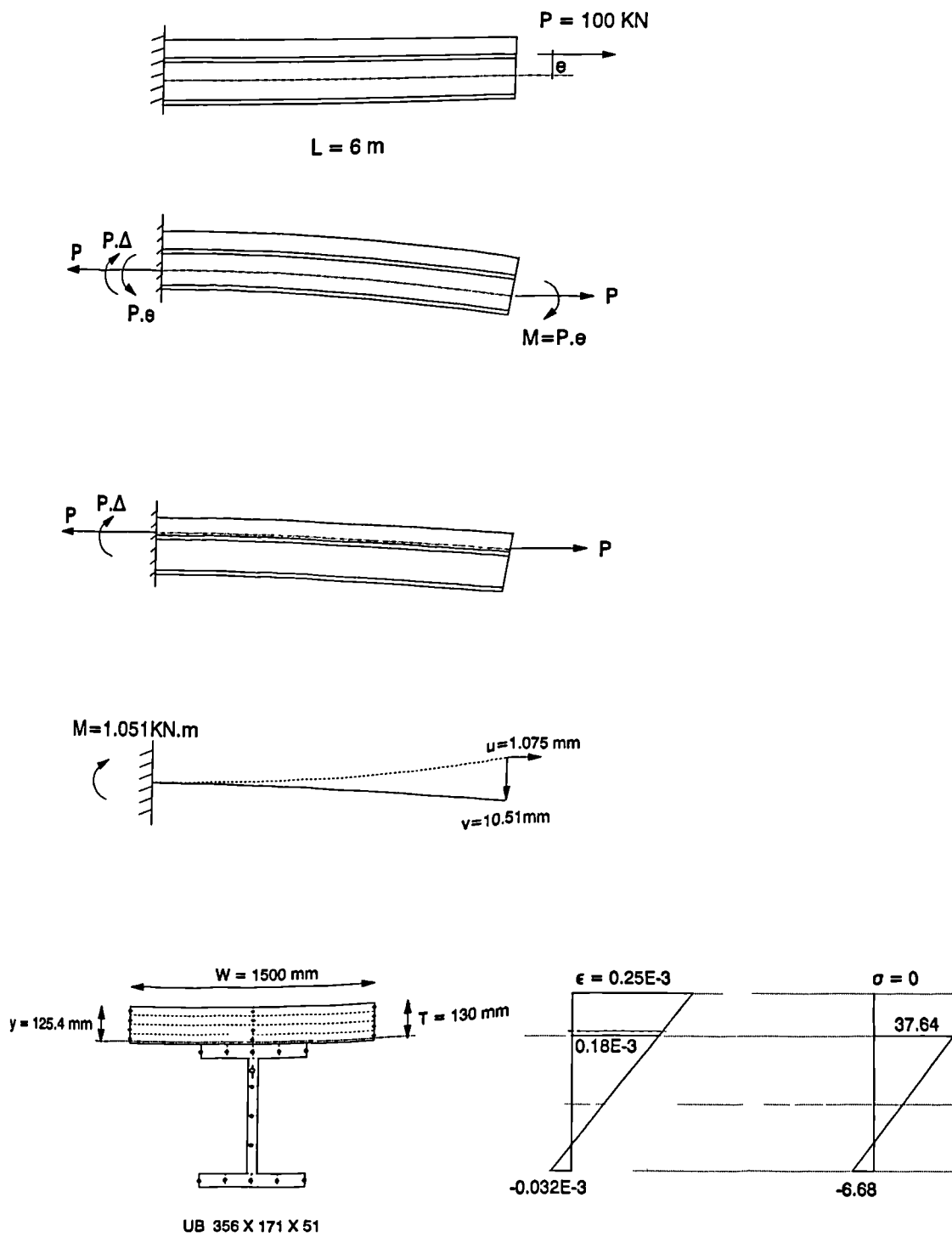
Fig. A.3 Composite Cantilever Beam with Axial Force

Model 1   Model 2   Model 3   Model 4

P = 297 KN

L= 6 m

1500mm

T6 @ 200mm,
As = 141mm/m²   130mm

UB 356 X 171 X 51

1.2m   3.6m   1.2m

T1   T2   T1

Temp. Distribution

0.2 T
0.7 T
T1   0.8 T
0.9 T

0.2 T
0.8 T
T2   1.0 T
1.0 T
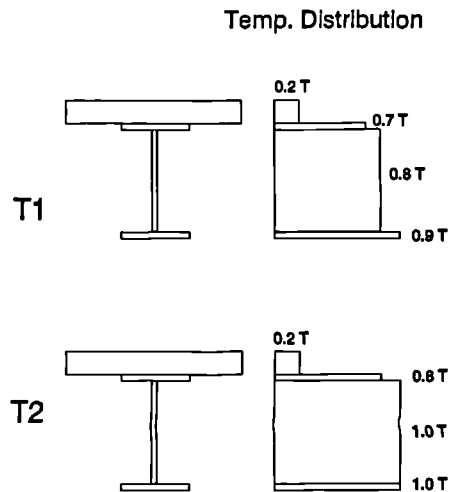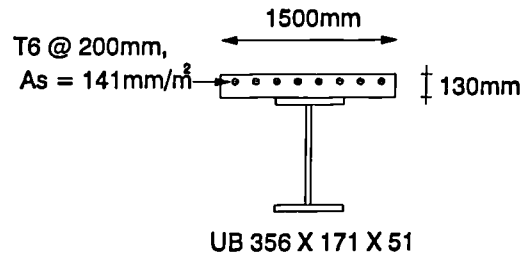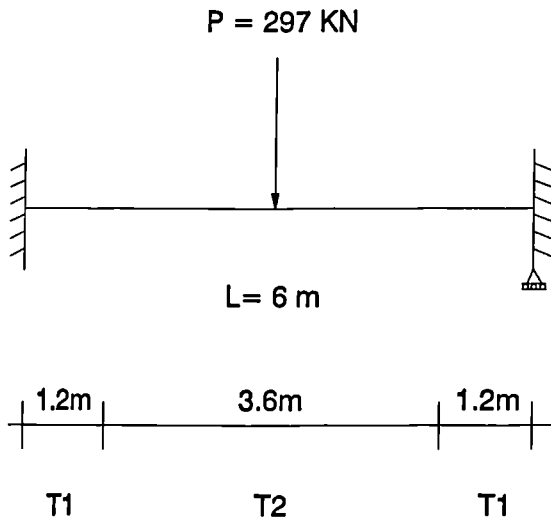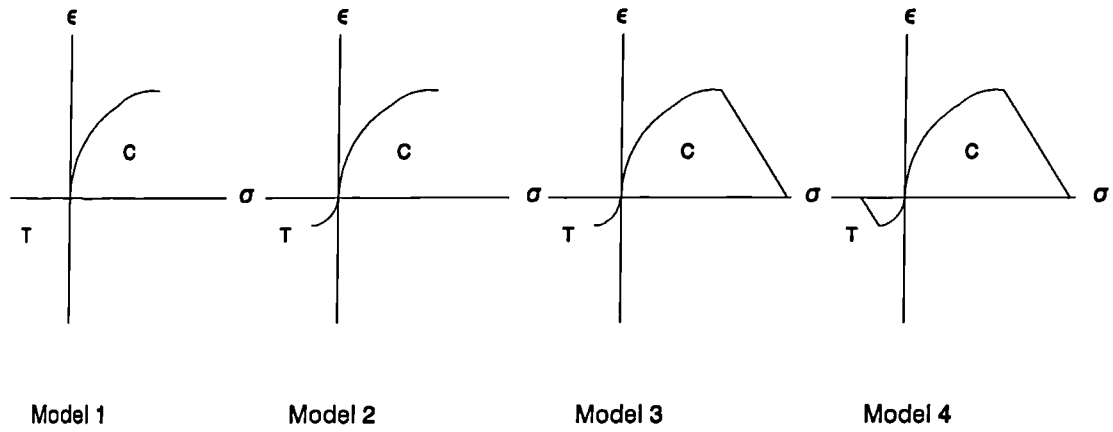
Fig. A.4 Stress-Strain Concrete Models and Beam Data
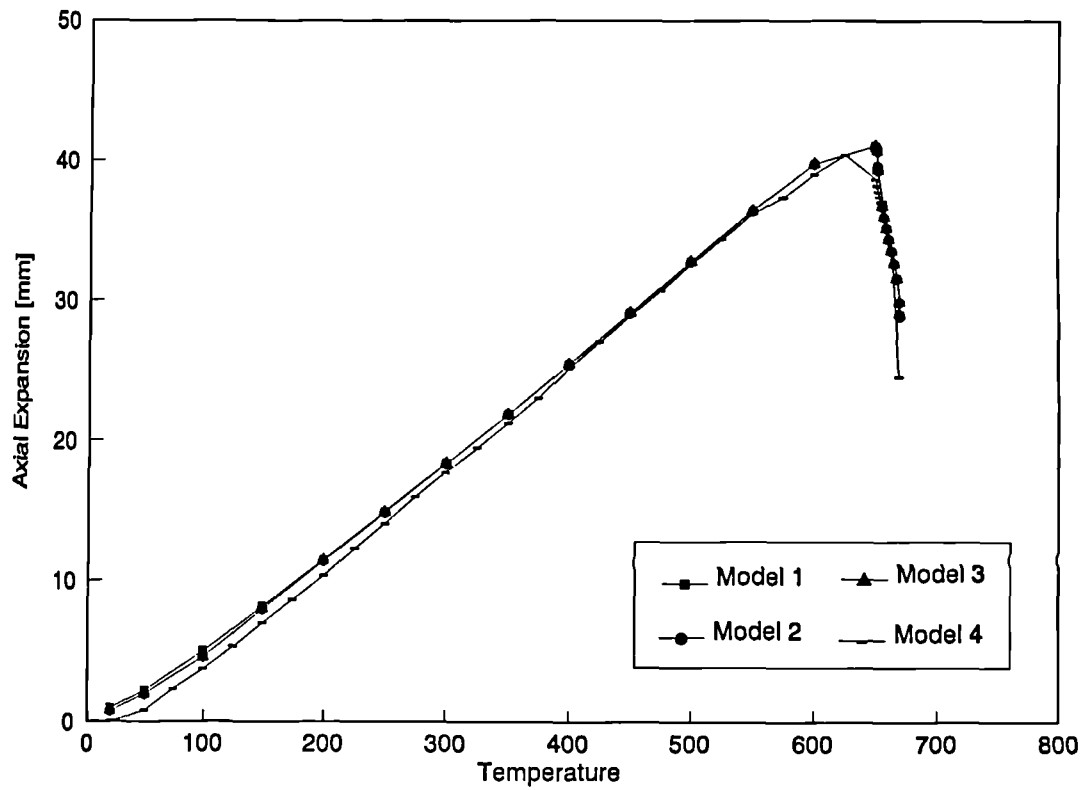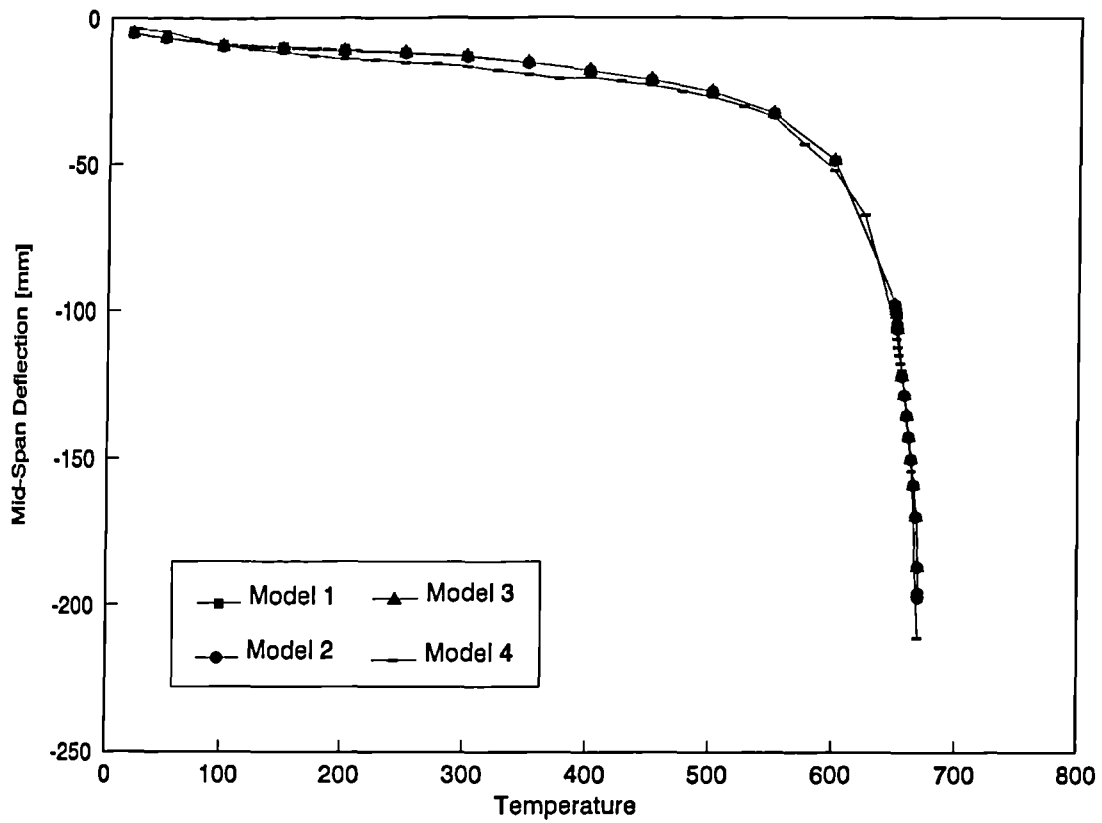
Fig. A.5 Displacements for Fixed-Ended Beam (Four Models)
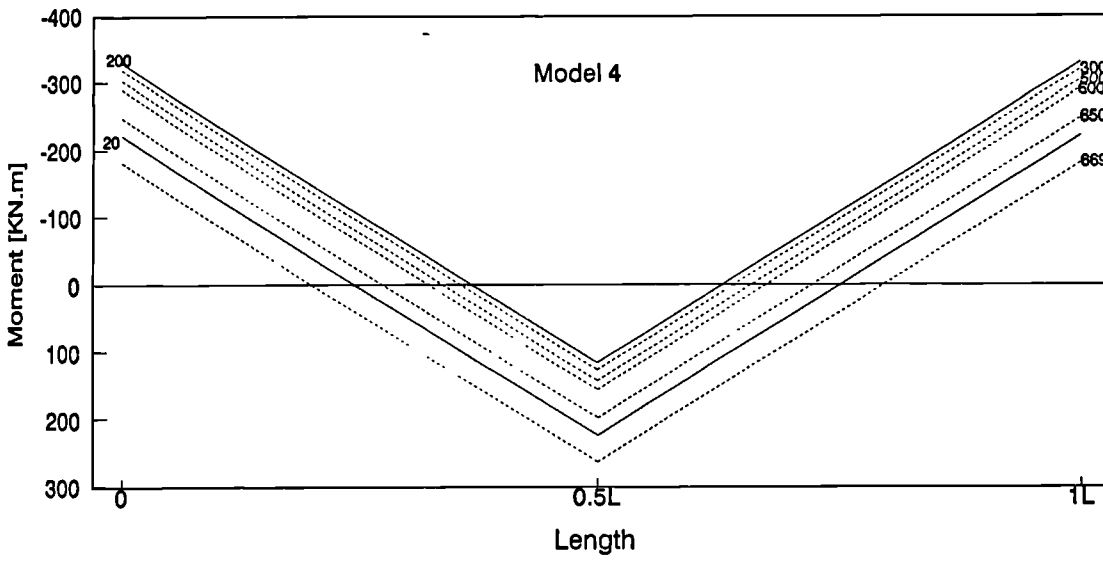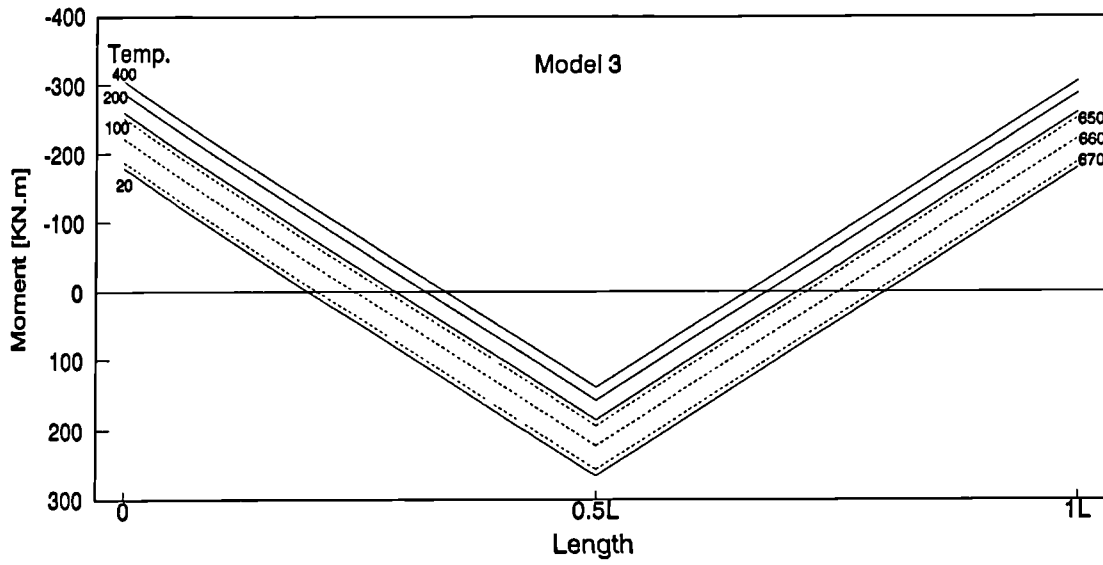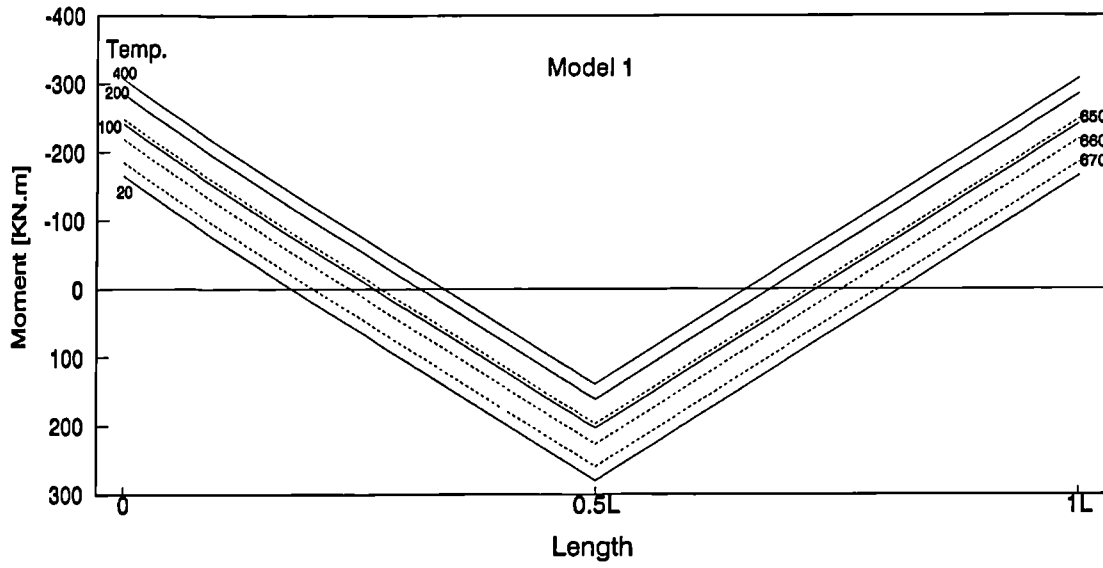
Fig. A.6 Moment Redistribution in Fixed-Ended Beam -Models 1, 3 and 4
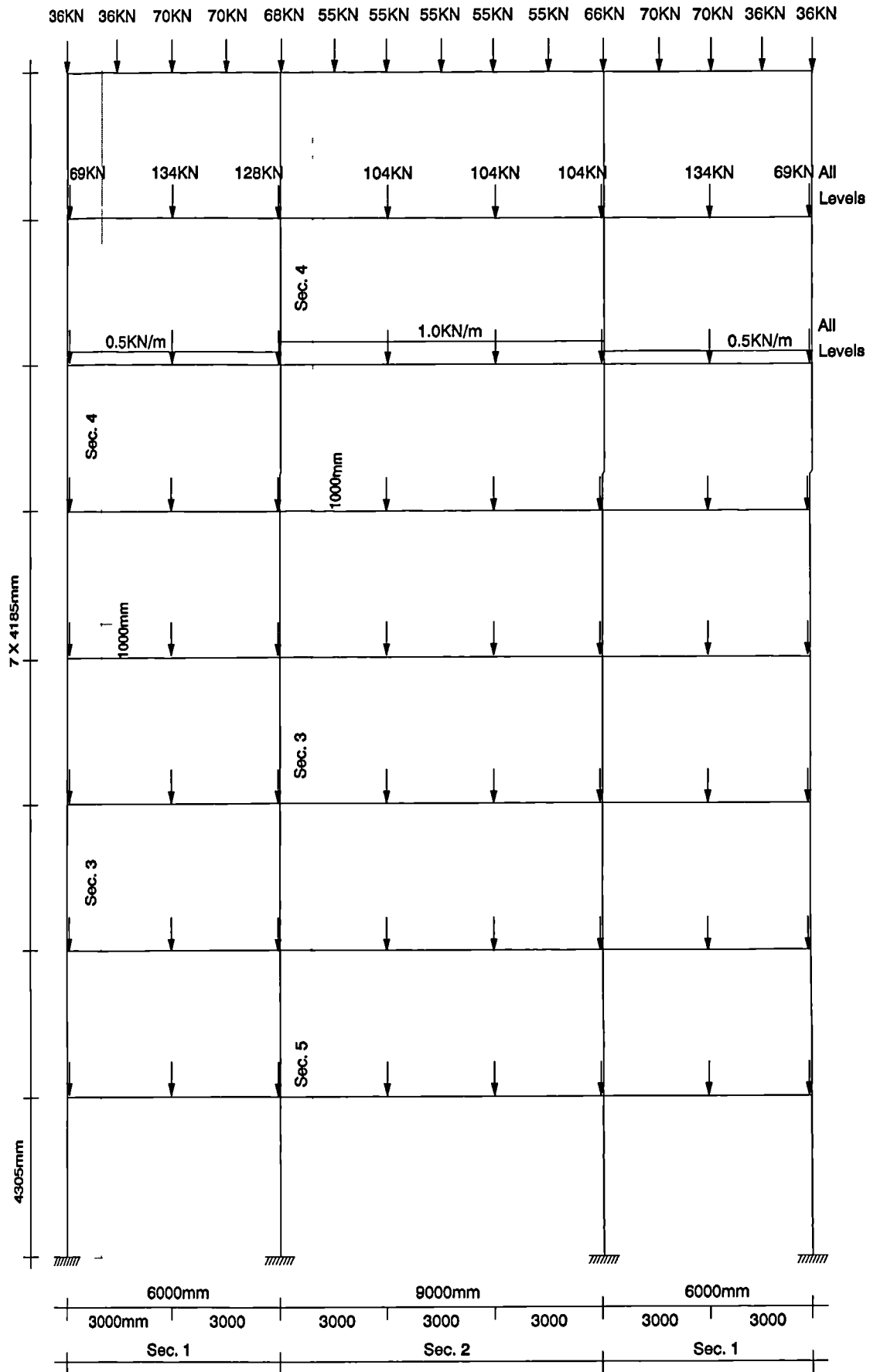
Fig. A.7 Cardington Frame -Dimensions and Loads

Top dimension labels (left to right):
1200mm | 3600mm | 1200mm | 1800mm | 5400mm | 1800mm | 1200mm | 3600mm | 1200mm

Left vertical labels: 3348mm, 637mm

Heating scheme values (top row of each bay):

0.2	0.2	0.2	0.2	0.2	0.2	0.2	0.2	0.2
0.7	0.8	0.7	0.6	0.7	0.6	0.7	0.8	0.7
0.8	1.0	0.8	0.7	0.9	0.7	0.8	1.0	0.8
0.9	1.0	0.9	0.8	0.9	0.8	0.9	1.0	0.9

Middle column values (vertical): 0.8 0.8 1.0 ... 1.0 1.0 1.0 ... 1.0 1.0 1.0 ... 0.5 0.8 1.0

Lower column values (vertical): 0.3 0.4 0.5 ... 0.5 0.5 0.5 ... 0.5 0.5 0.5 ... 0.5 0.4 0.3

T6 @ 200mm,
As = 141mm/m² → 1500mm ‖ 130mm

UB 356 X 171 X 51

Sec. 1

T6 @ 200mm,
As = 141mm/m² → 2250mm ‖ 130mm

UB 610 X 229 X 101

Sec. 2

UC 305 X 305 X 137

Sec. 3

UC 254 X 254 X 89

Sec. 4

UC 305 X 305 X 198

Sec. 5

Fig. A.8 Cardington Frame -Sections and Heating Schemes
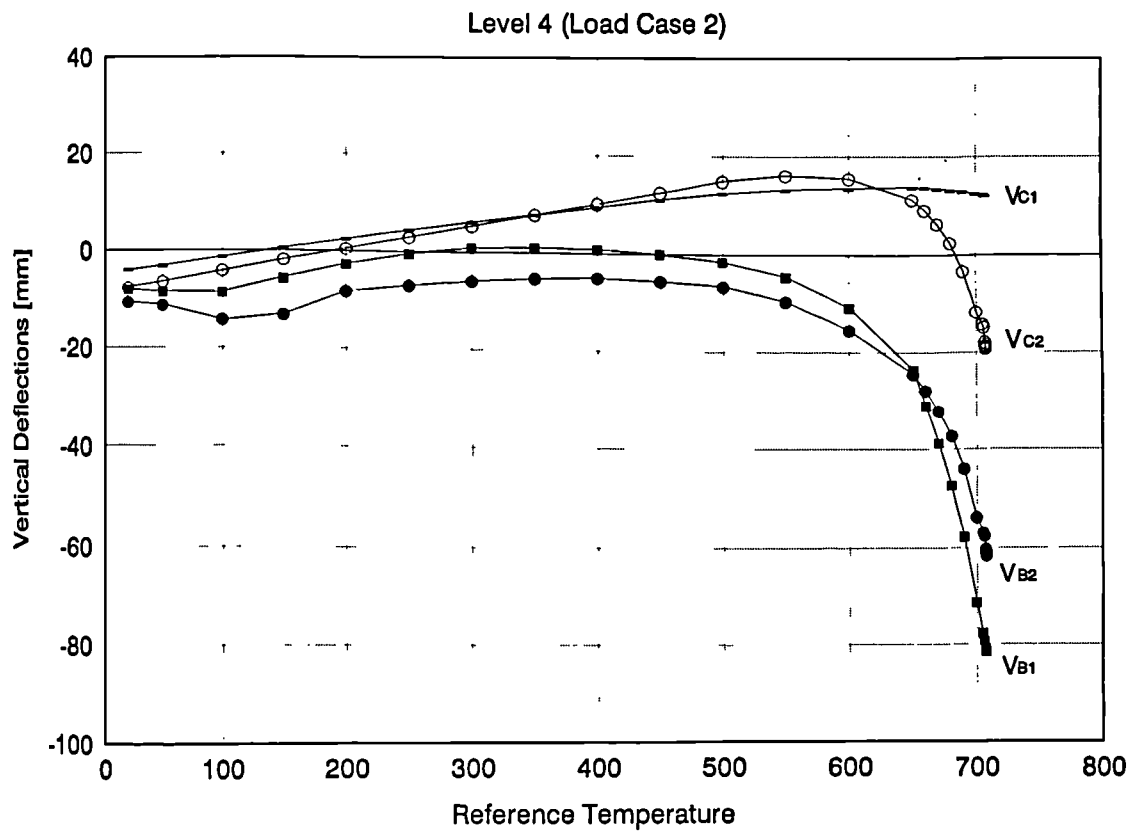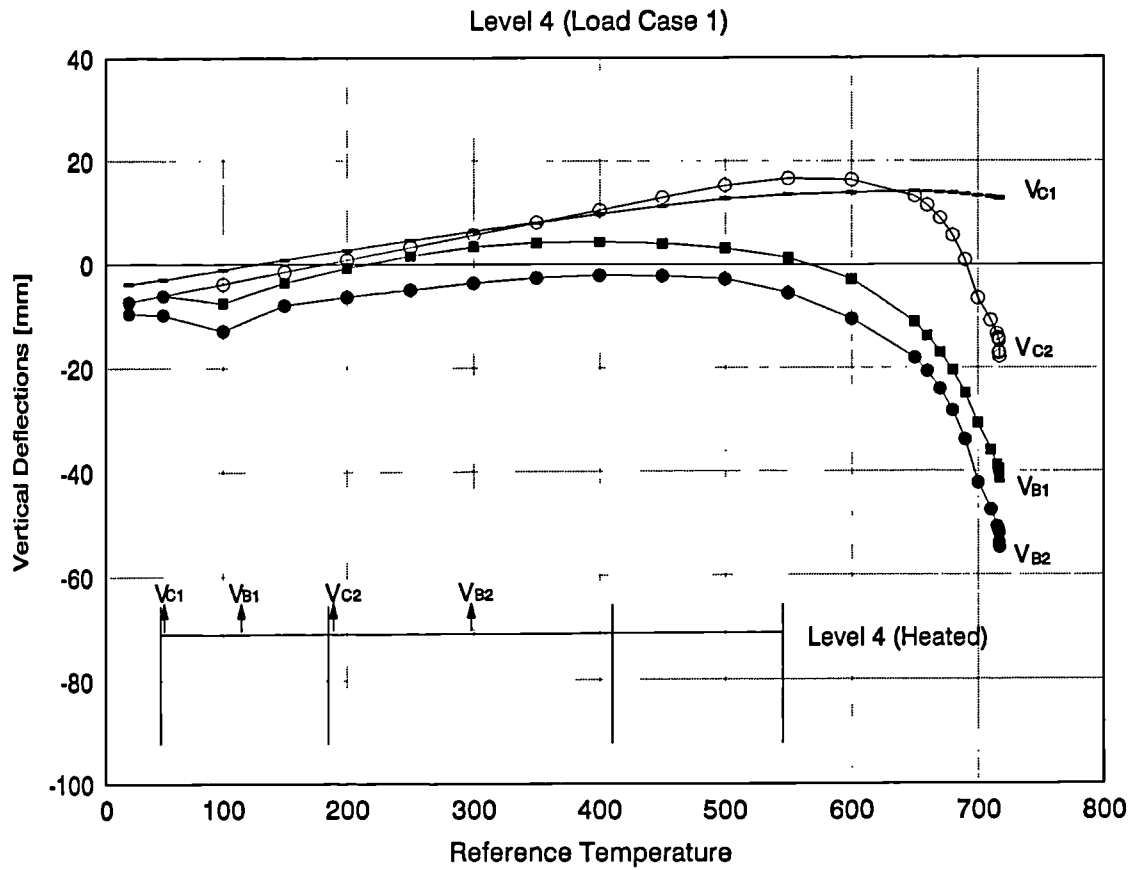
Fig. A.9 Vertical Deflections -Level 4
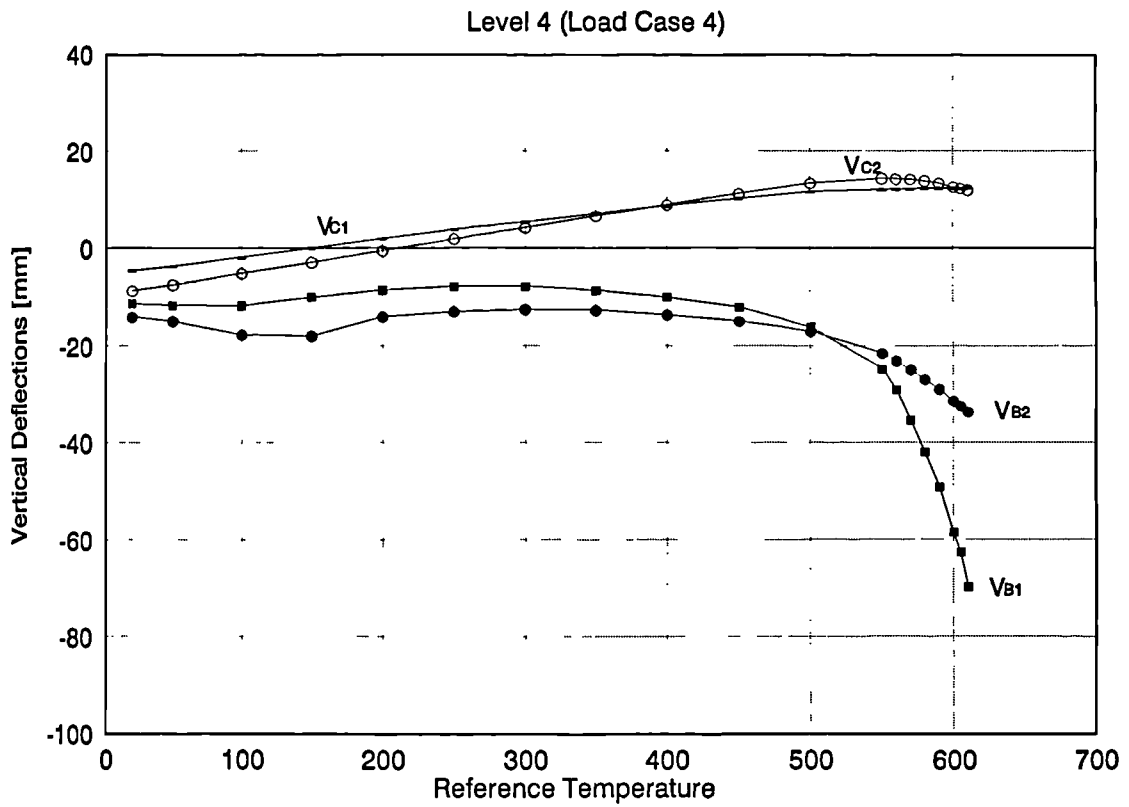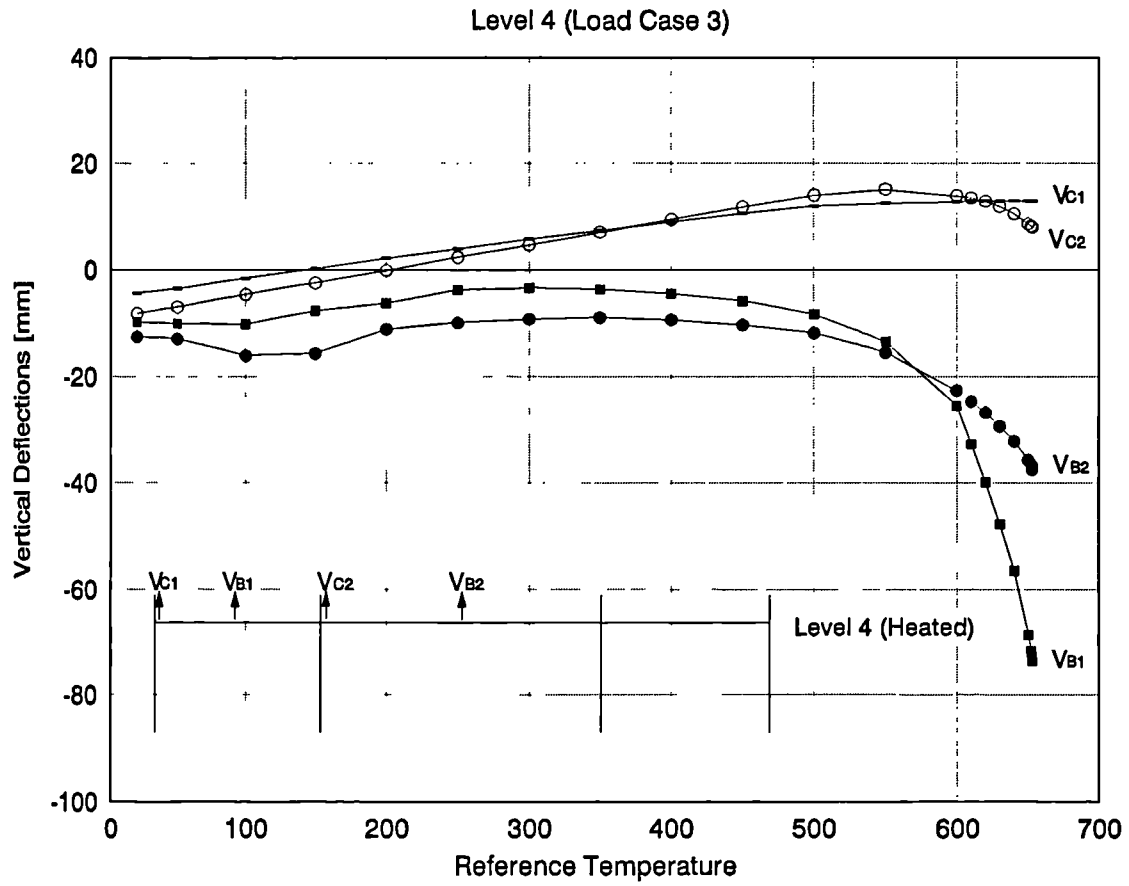
Fig. A.10 Vertical Deflections -Level 4
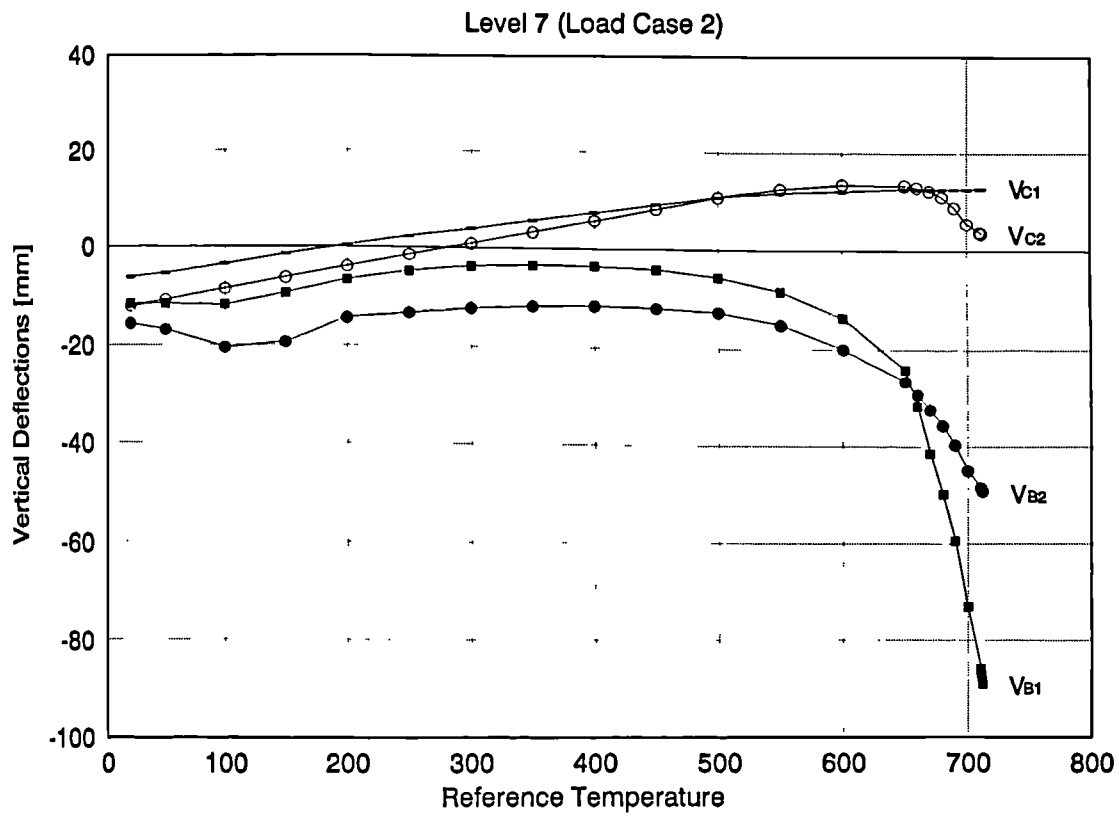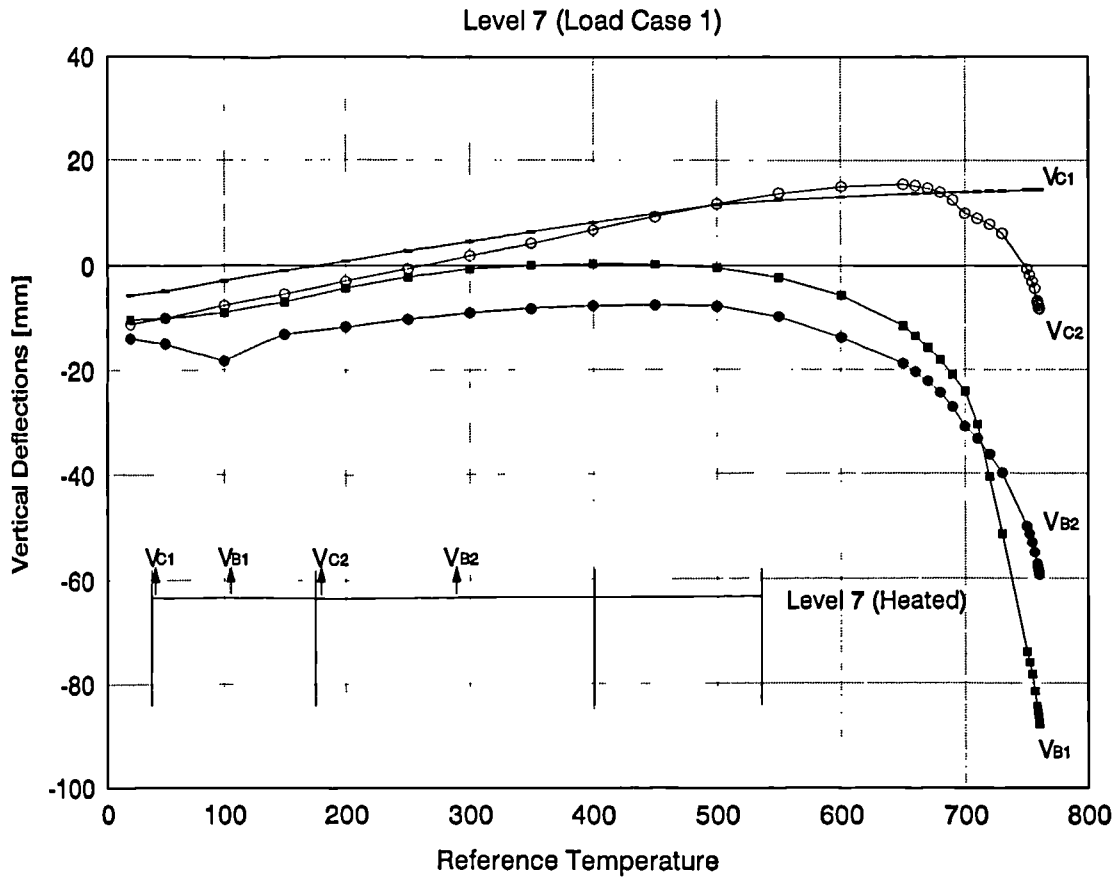
Fig. A.11 Vertical Deflections -Level 7
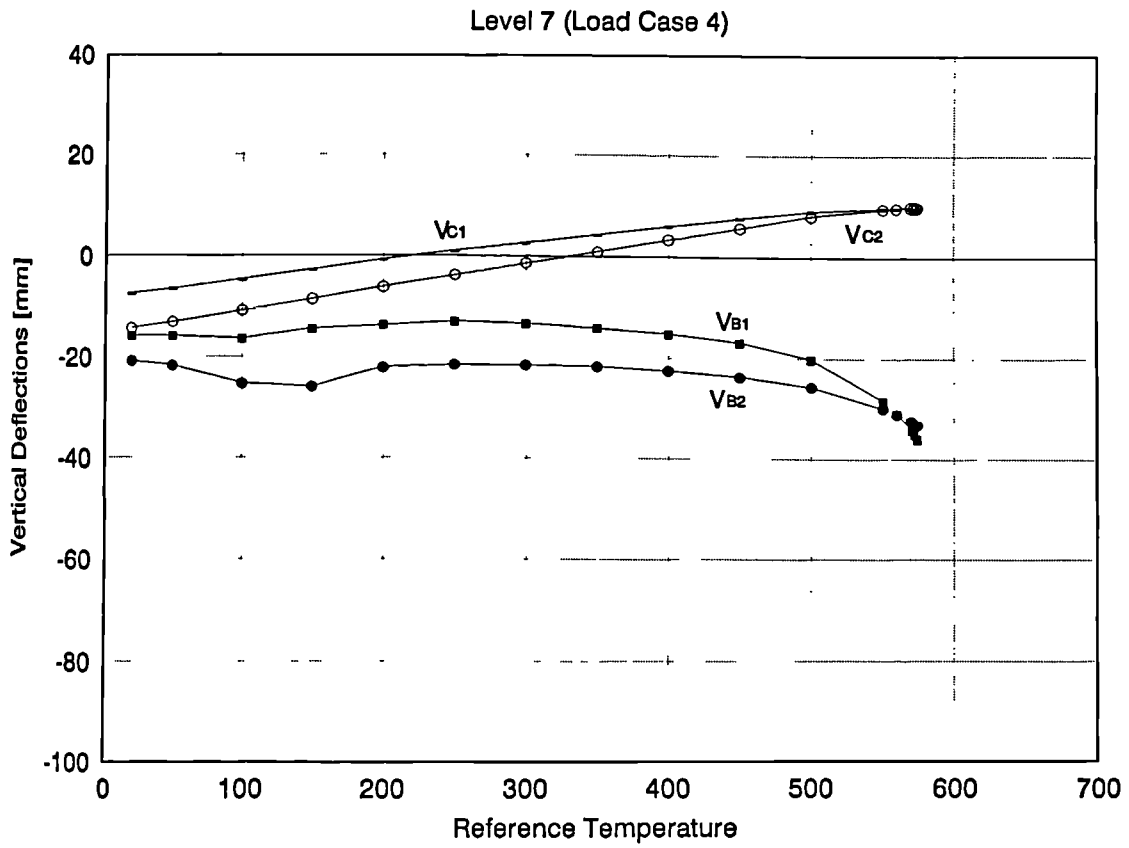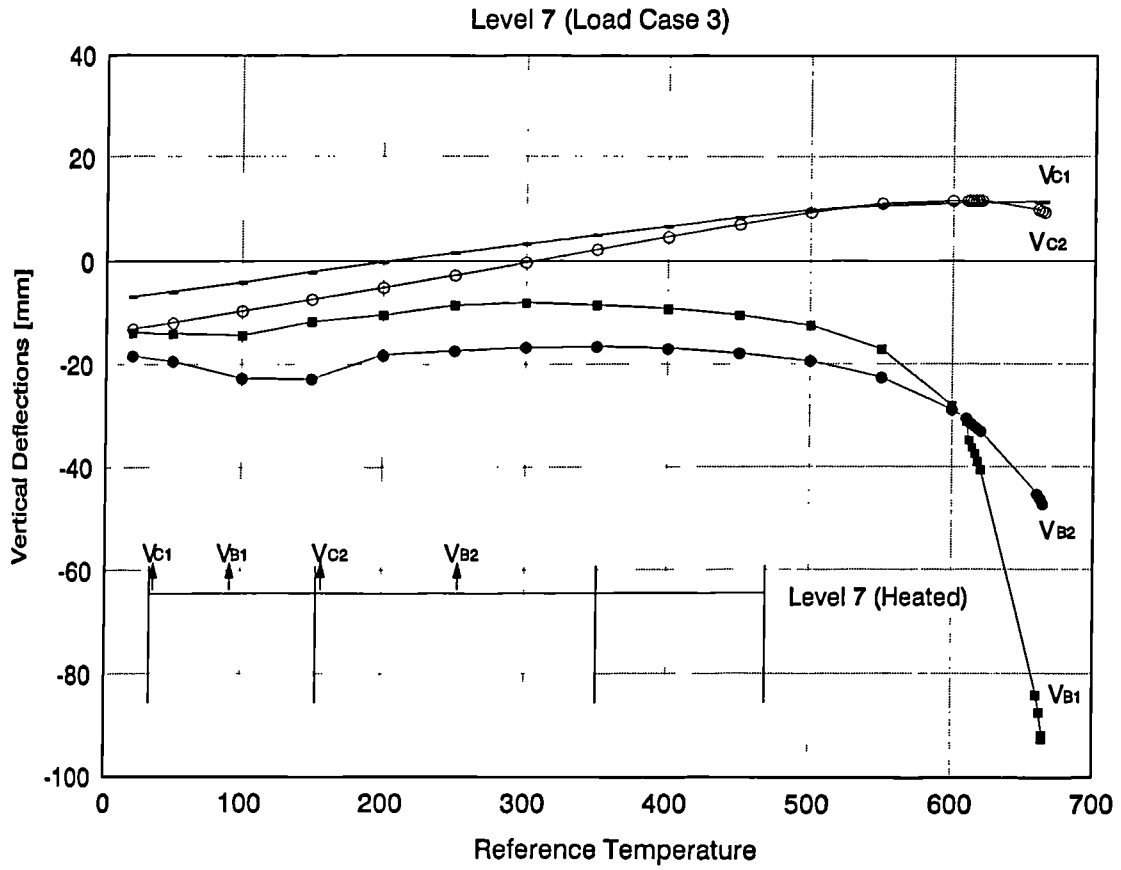
Fig. A.12 Vertical Deflections -Level 7
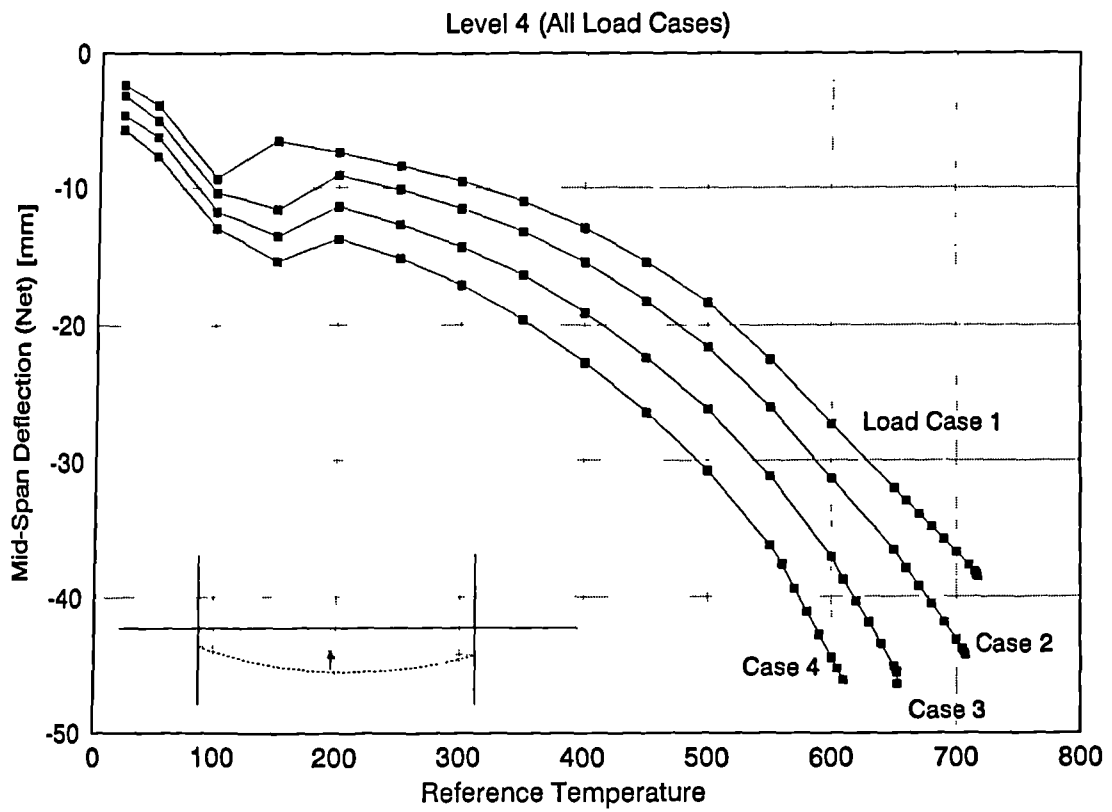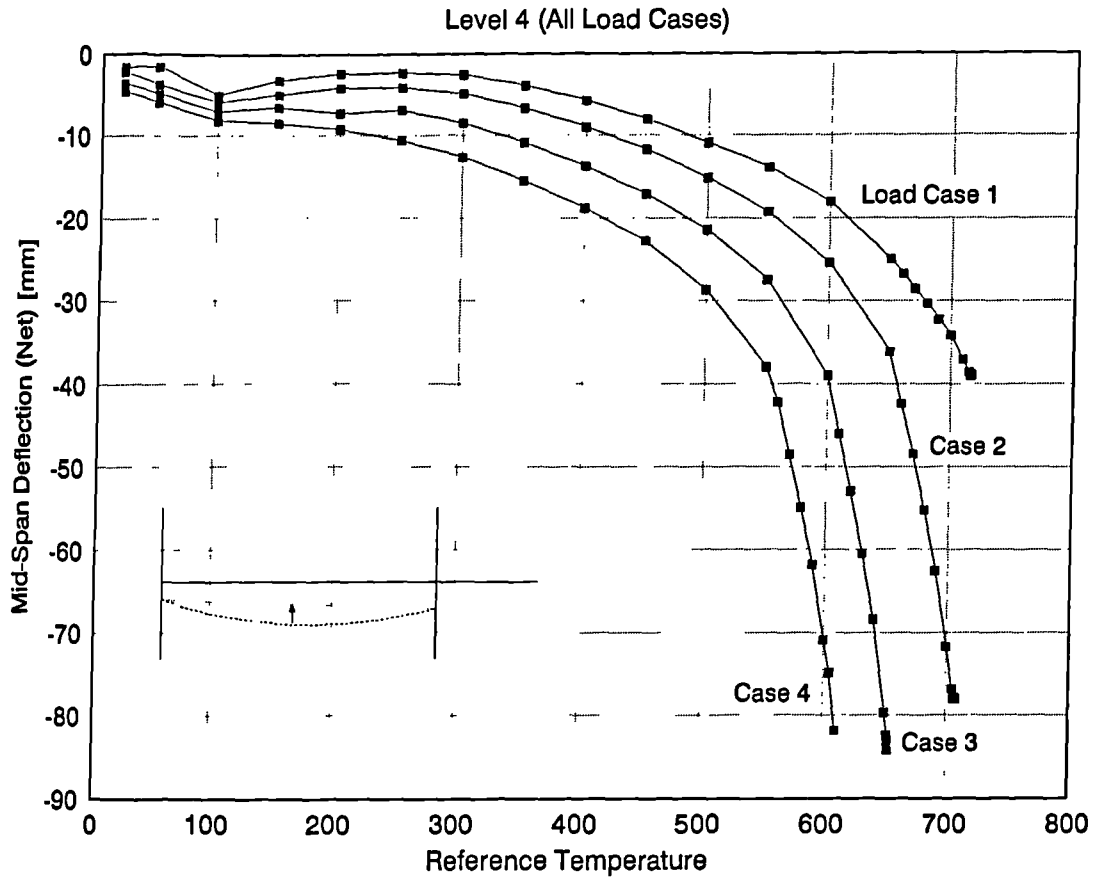
Fig. A.13 Net Vertical Deflections (Outer and Inner Beams) -Level 4

Level 7 (All Load Cases)

Mid-Span Deflection (Net) [mm] vs Reference Temperature. Curves labeled Load Case 1, Case 2, Case 3, Case 4.

Level 7 (All Load Cases)

Mid-Span Deflection (Net) [mm] vs Reference Temperature. Curves labeled Load Case 1, Case 2, Case 3, Case 4.
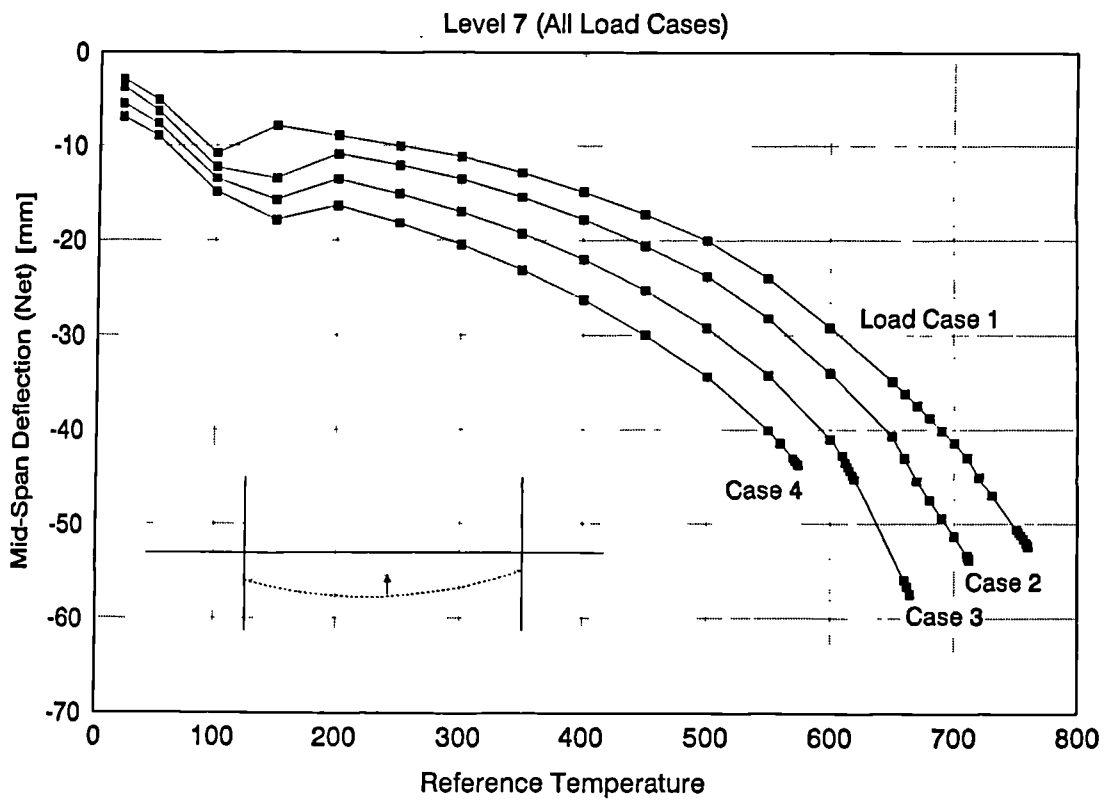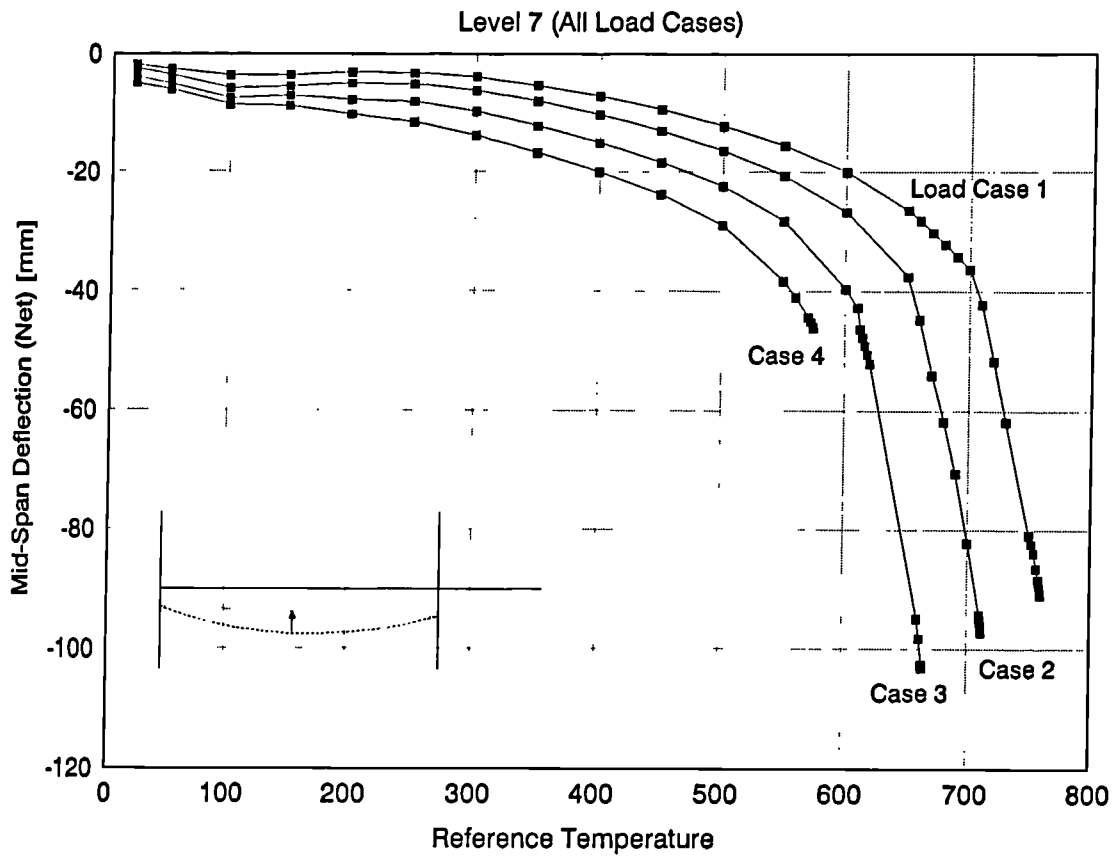
Fig. A.14 Net Vertical Deflections (Outer and Inner Beams) -Level 7
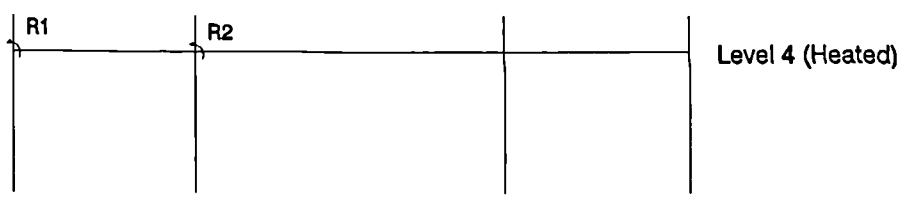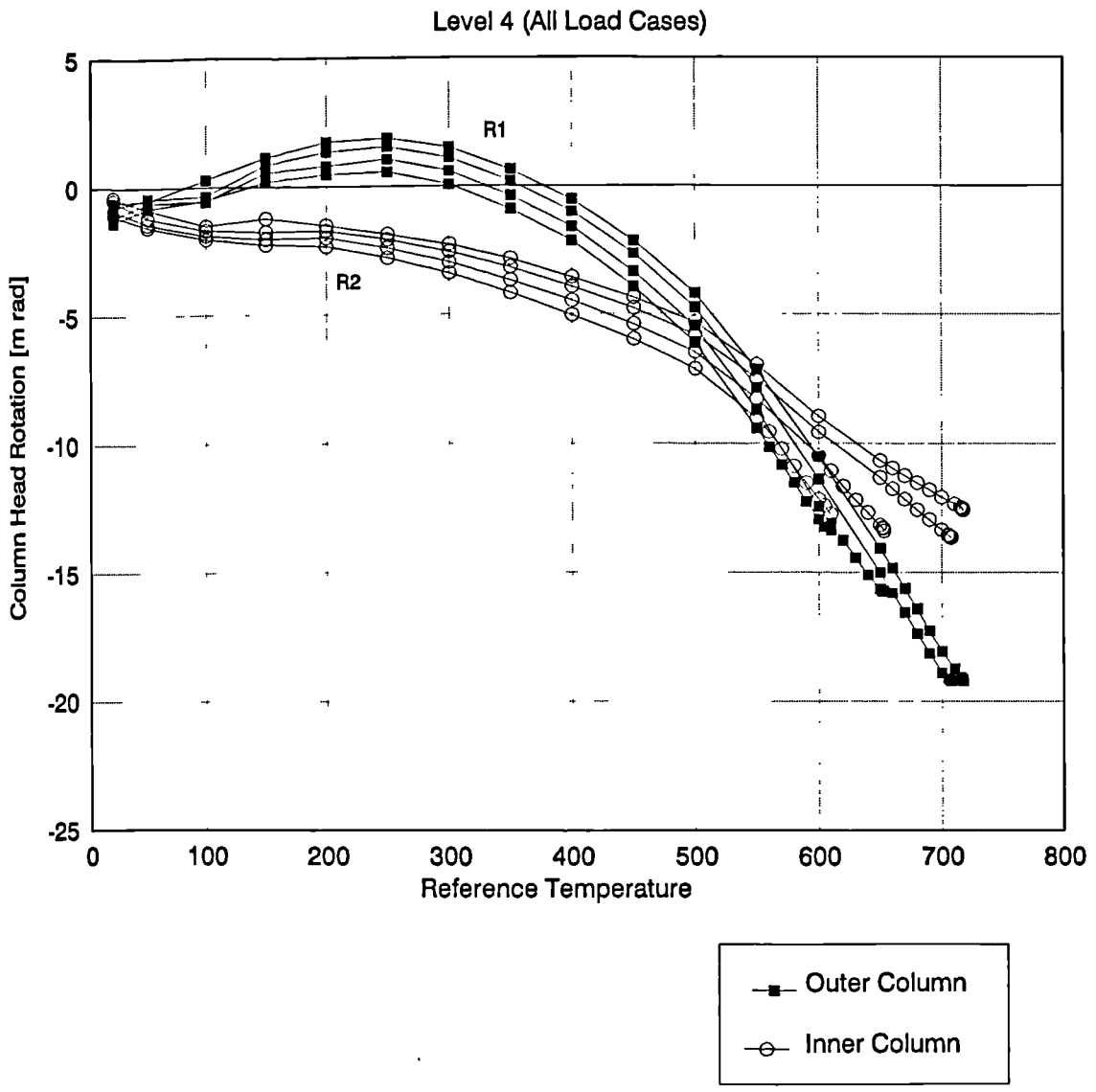
Fig. A.15 Column Rotations -Level 4
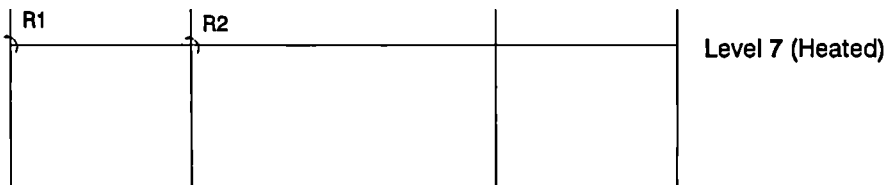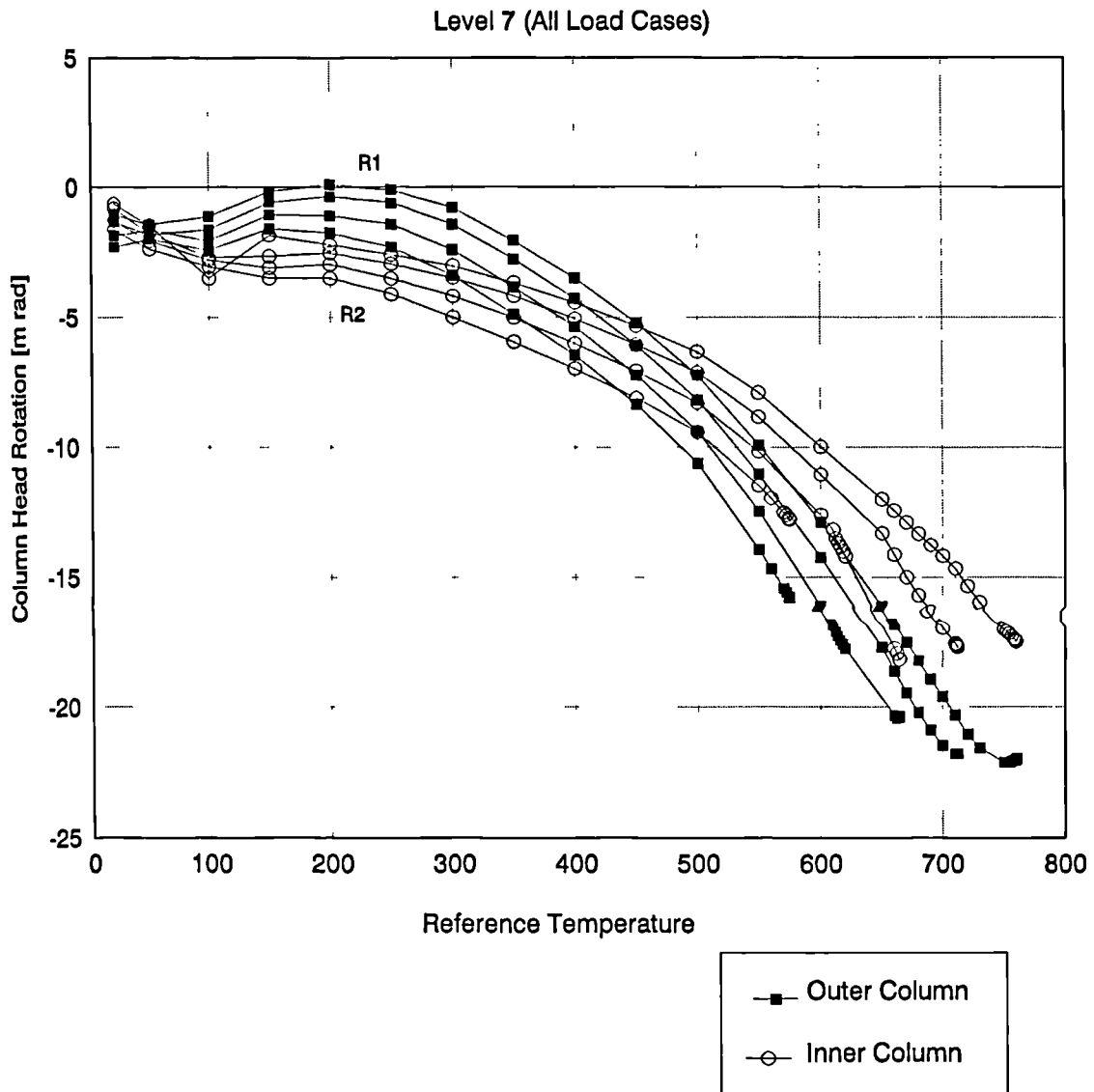
Fig. A.16 Column Rotations -Level 7

Level 4 (All Load Cases)
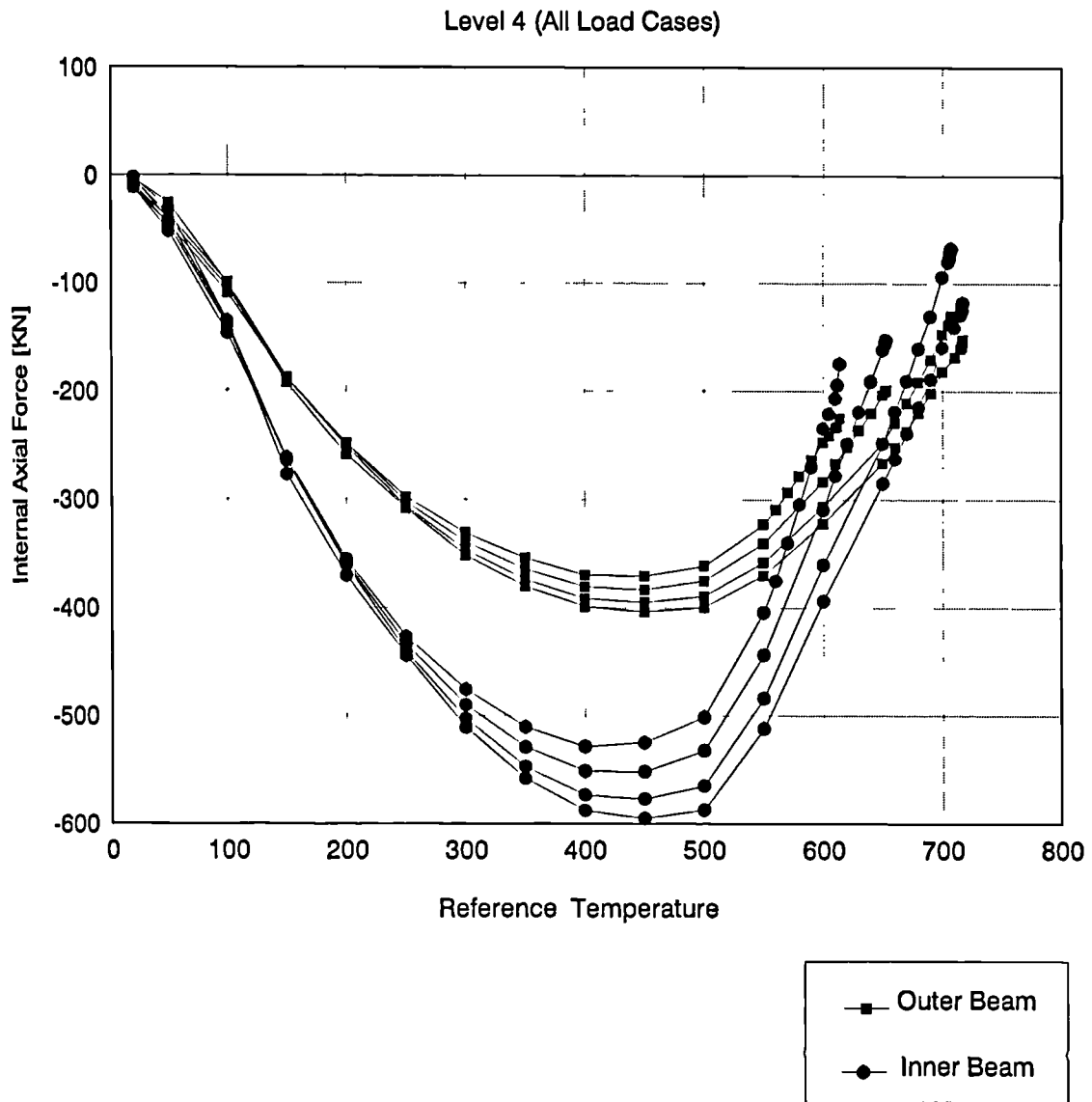
Fig. A.17 Beam Axial Forces -Level 4

Level 7 (All Load Cases)
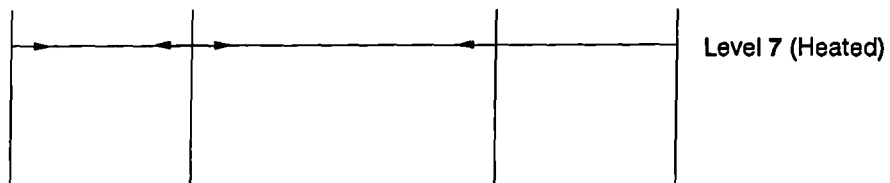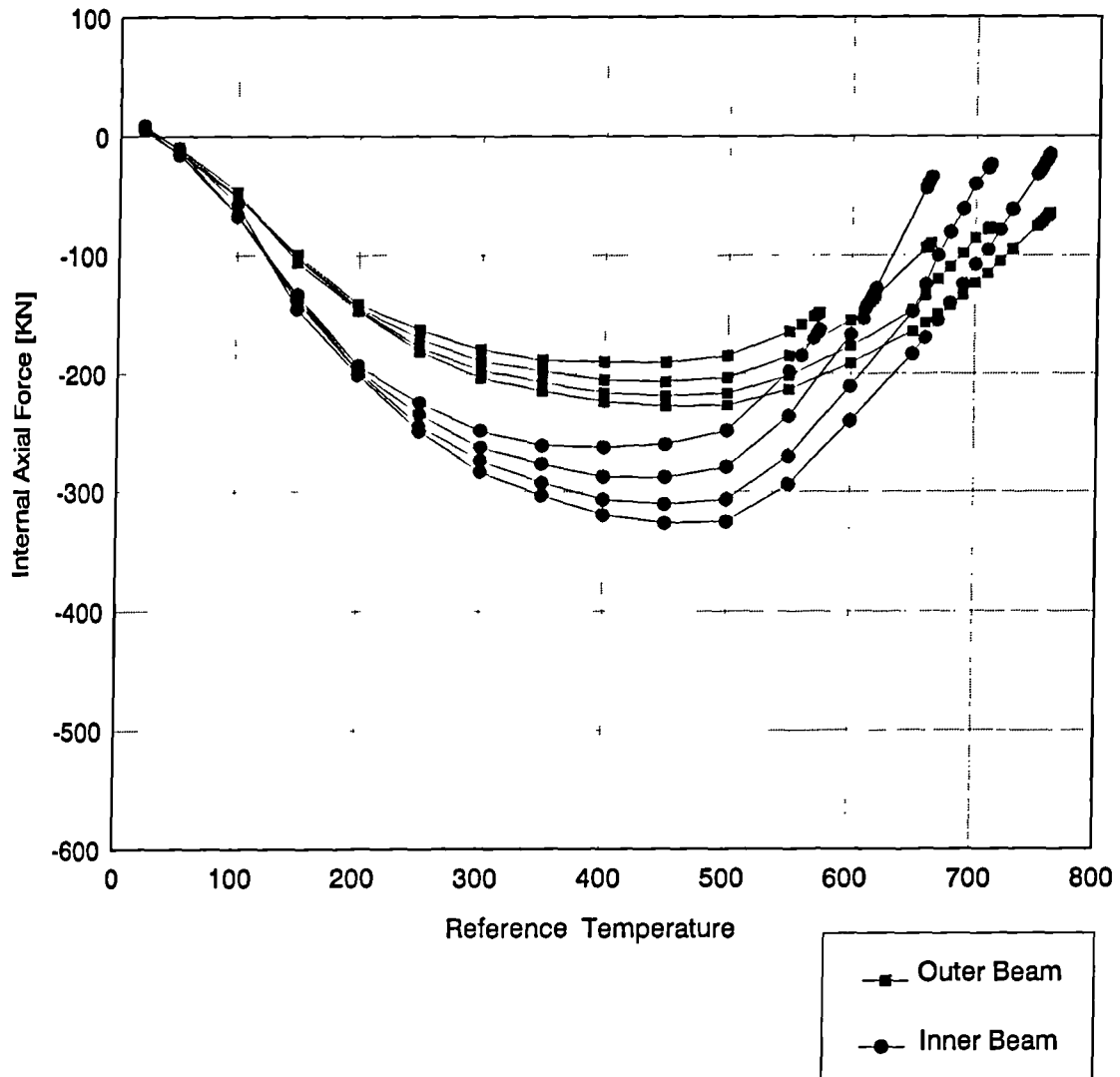
Fig. A.18 Beam Axial Forces -Level 7
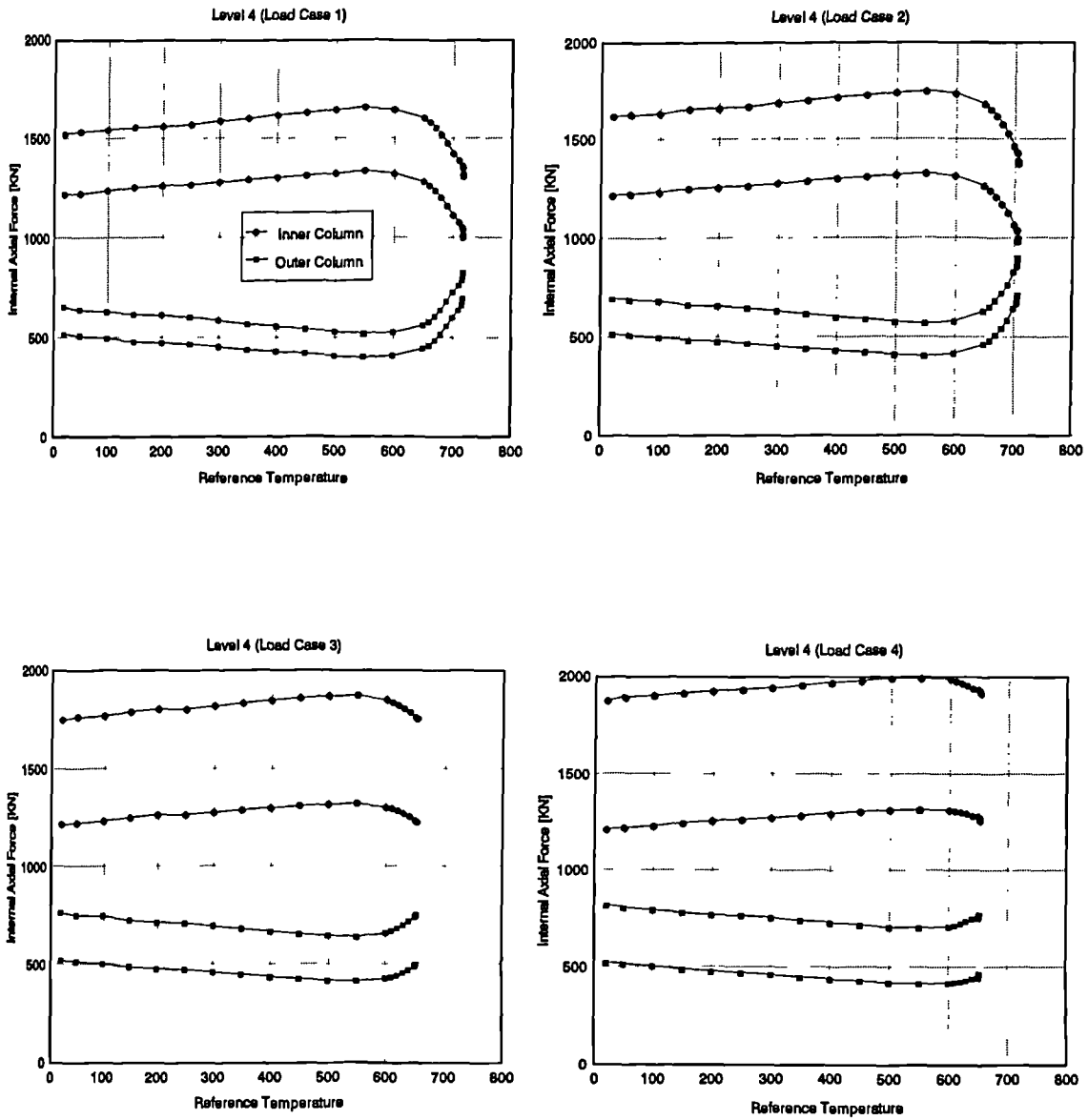
Fig. A.19 Column Axial Forces -Level 4
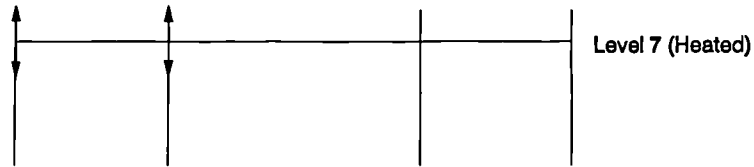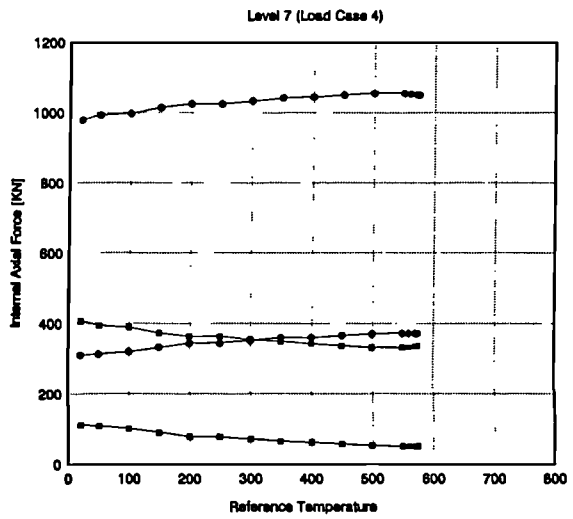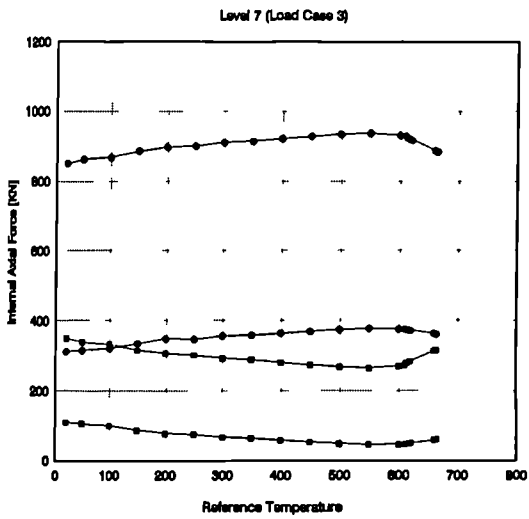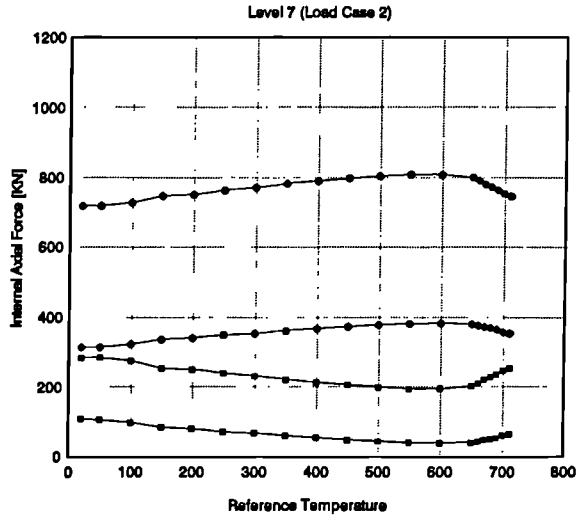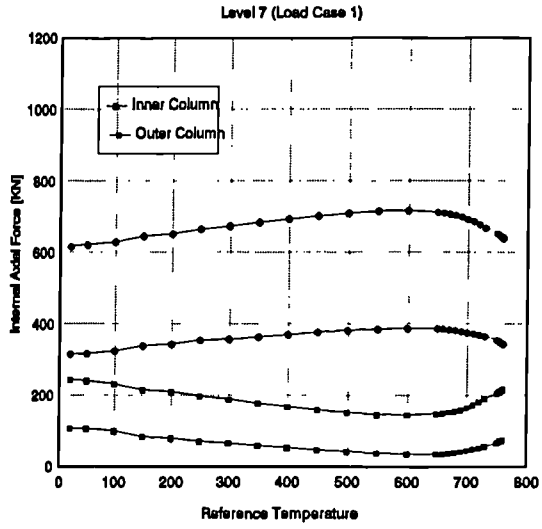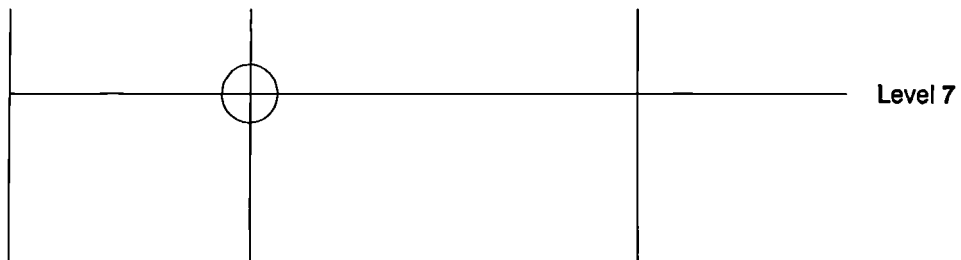
Fig. A.20 Column Axial Forces -Level 7

Level 4 (All Load Cases)
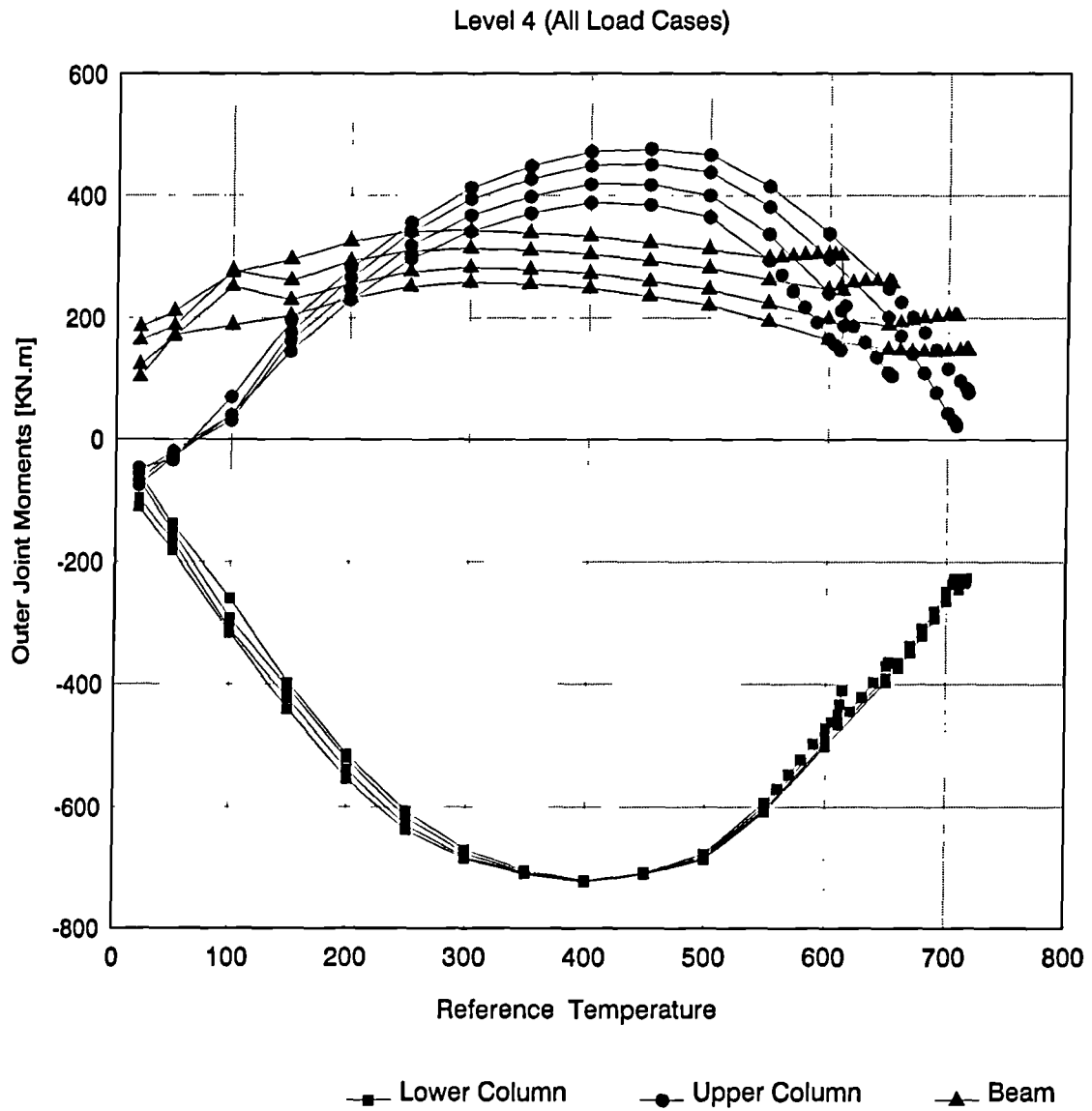
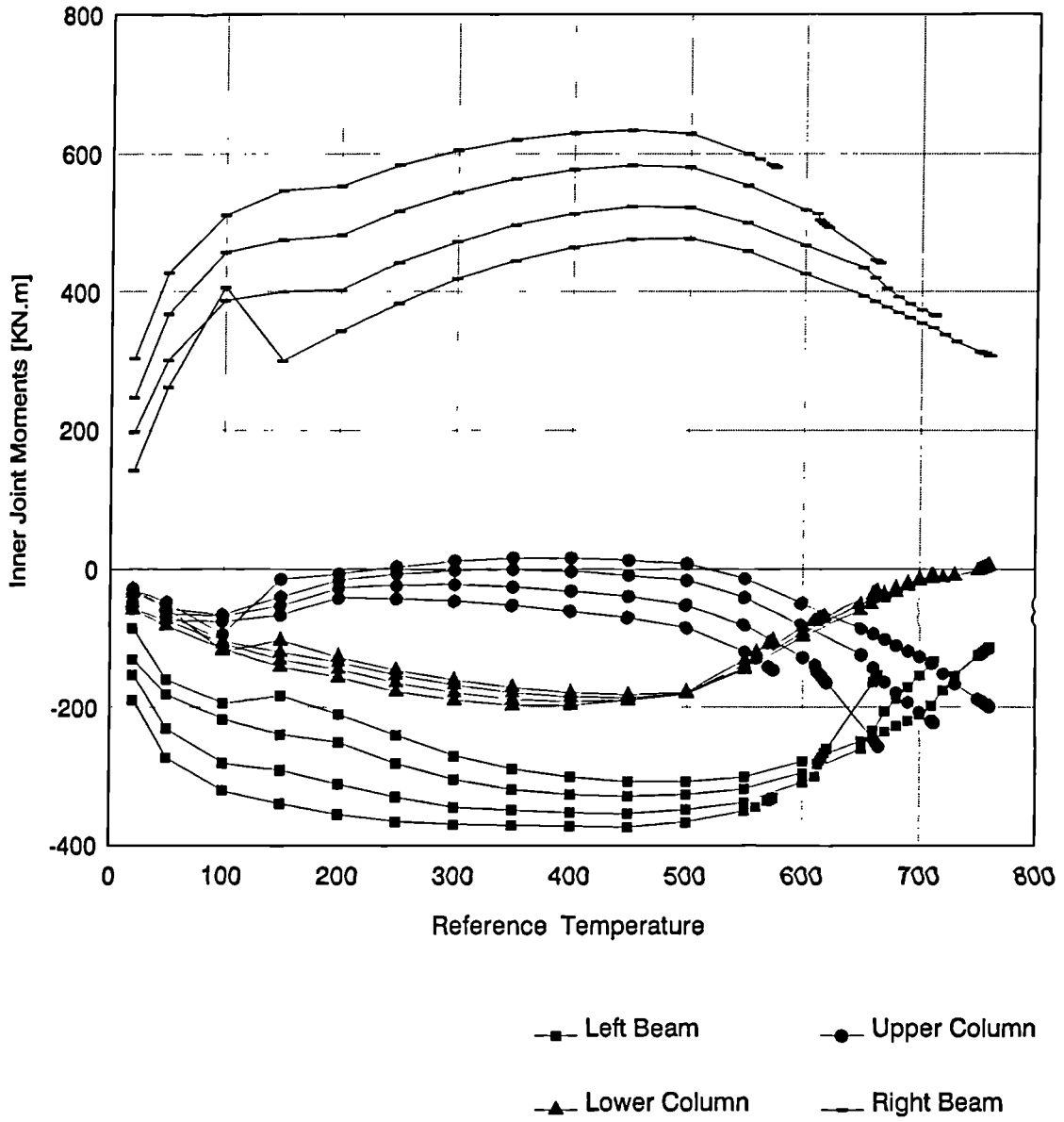Fig. A.21 Moments at Outer Joint -Level 4

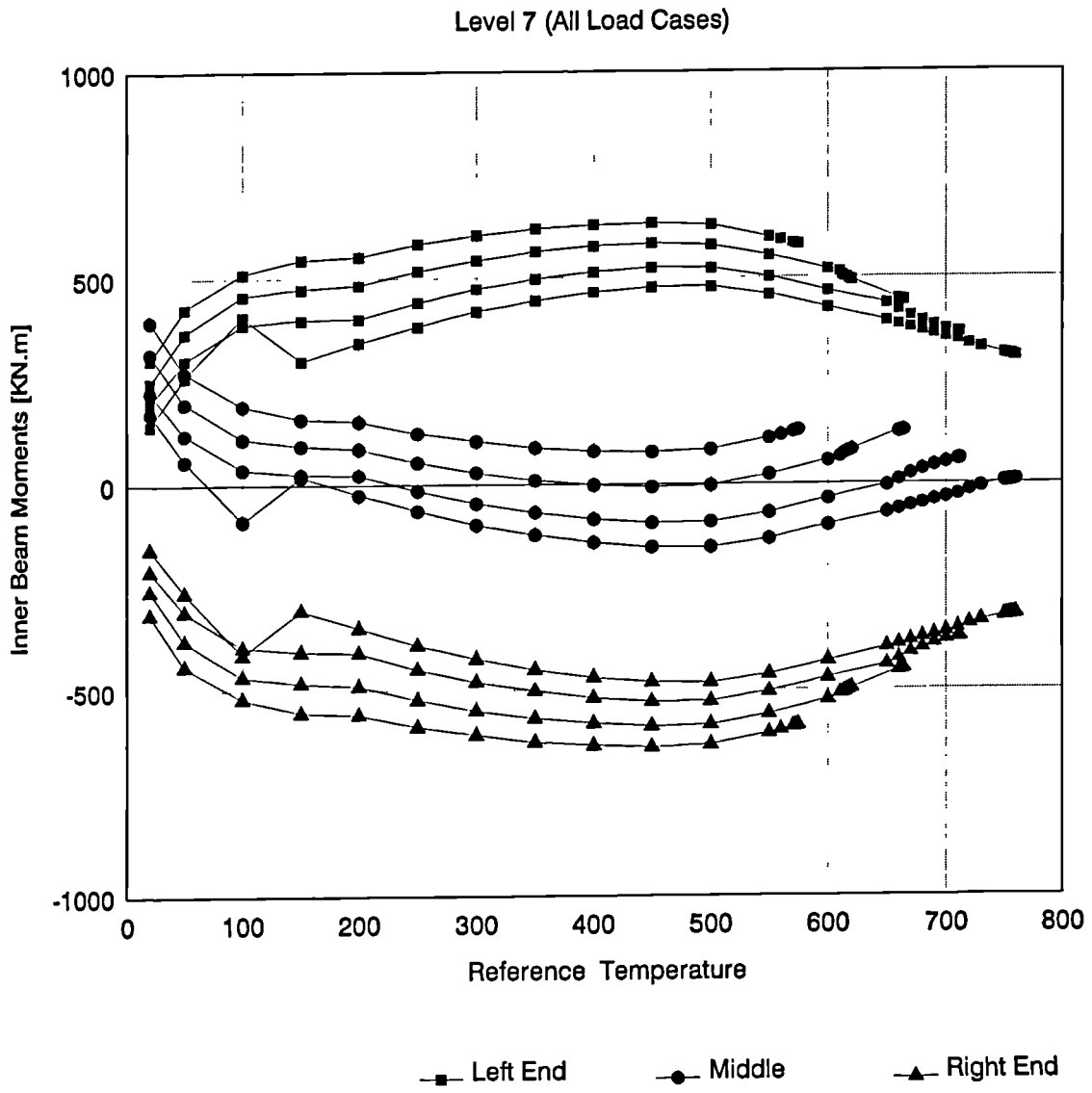Level 4 (All Load Cases)
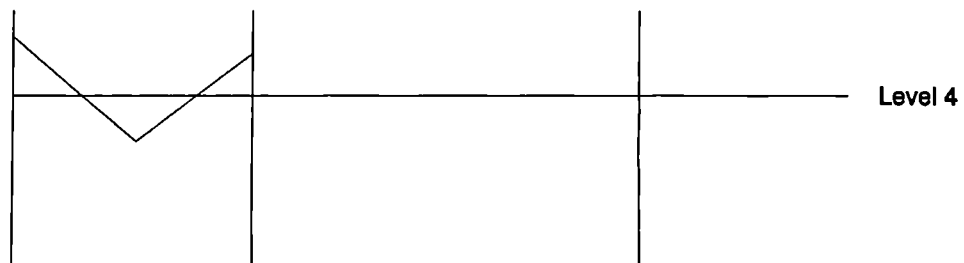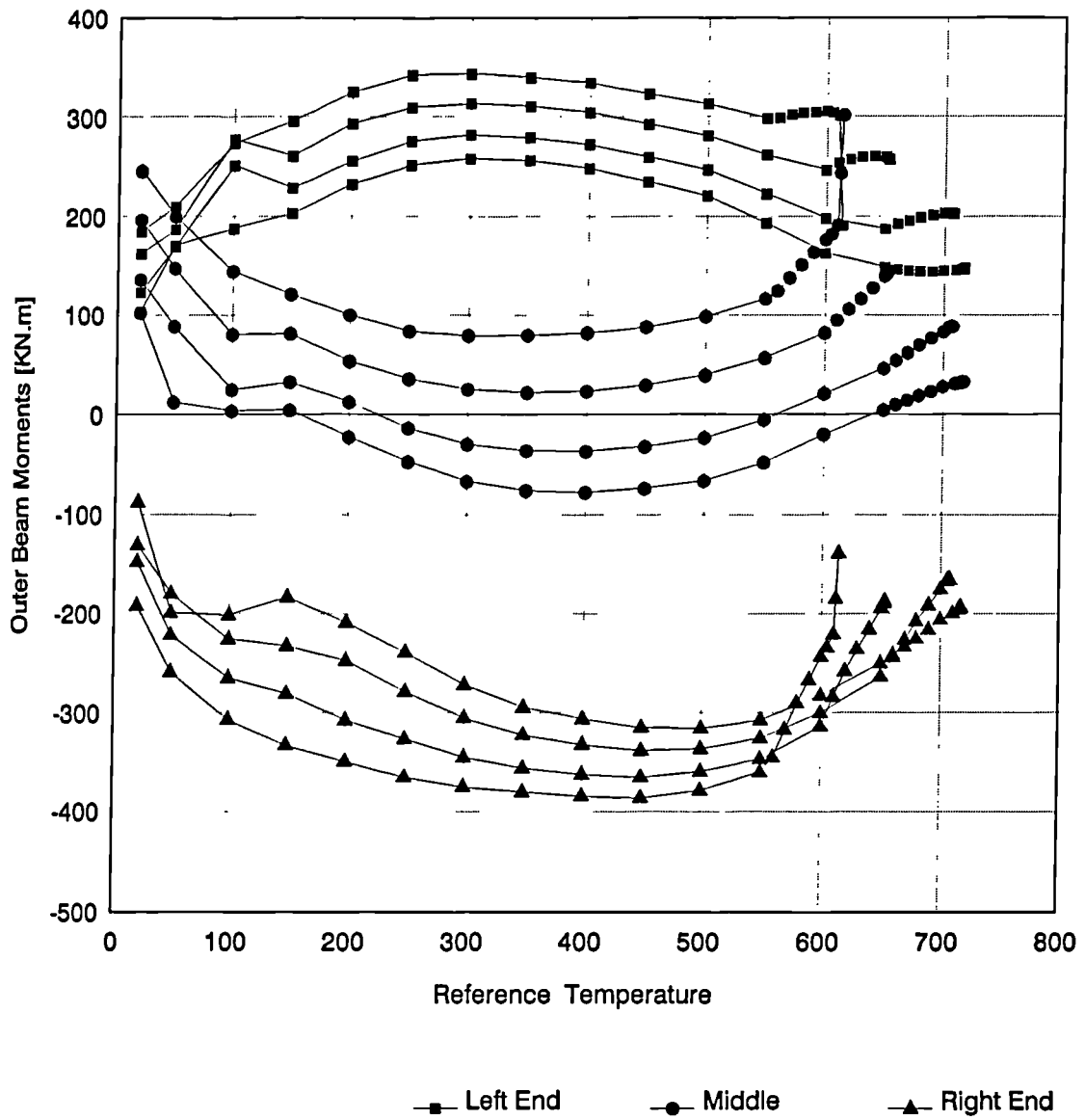
Fig. A.22 Moments at Outer Beam -Level 4
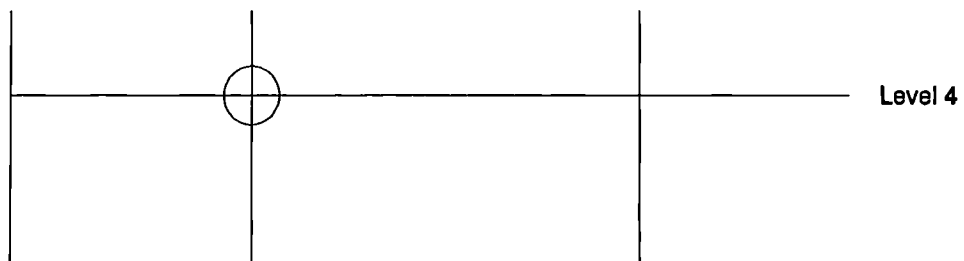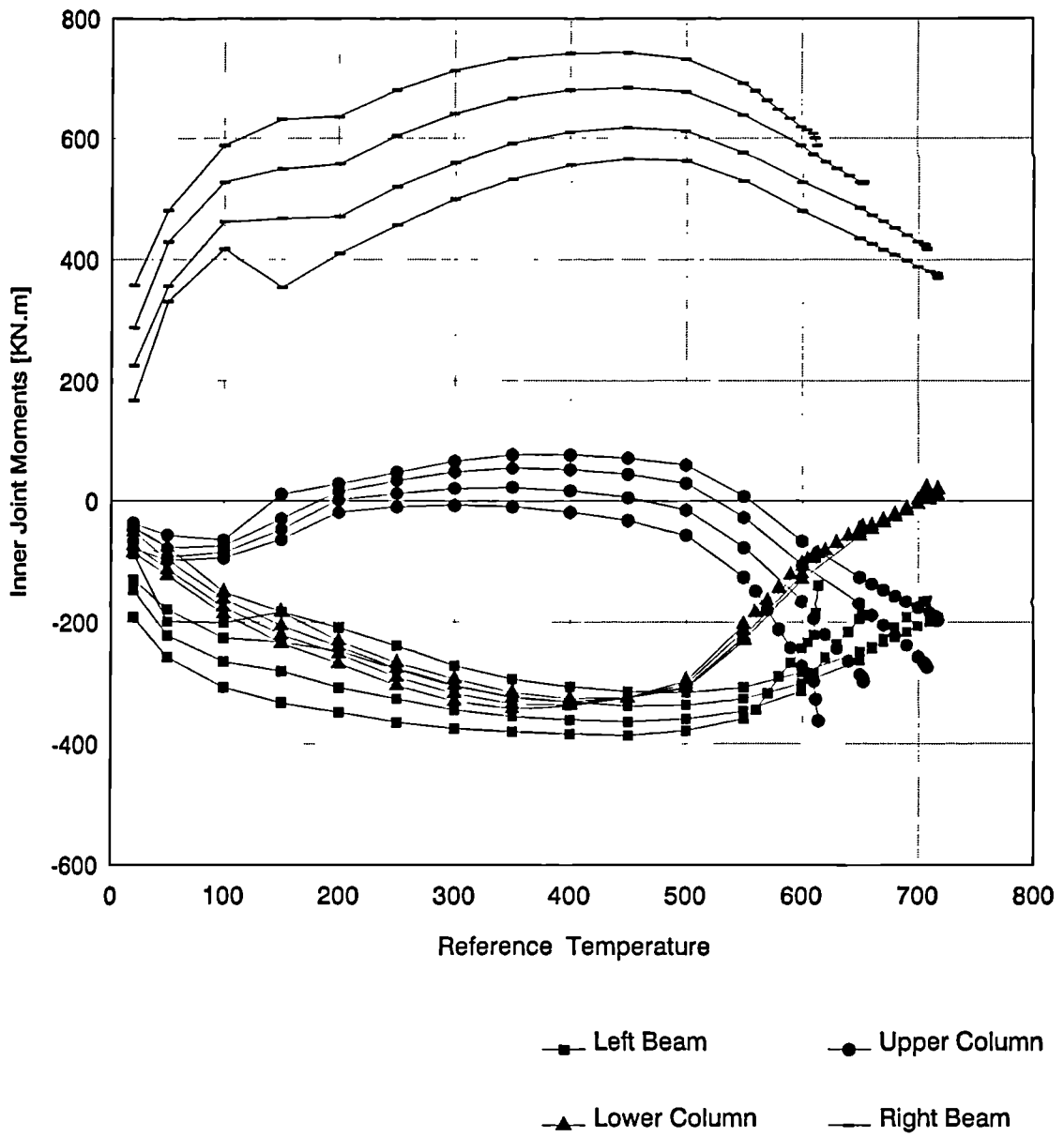
Fig. A.23 Moments at Inner Joint -Level 4
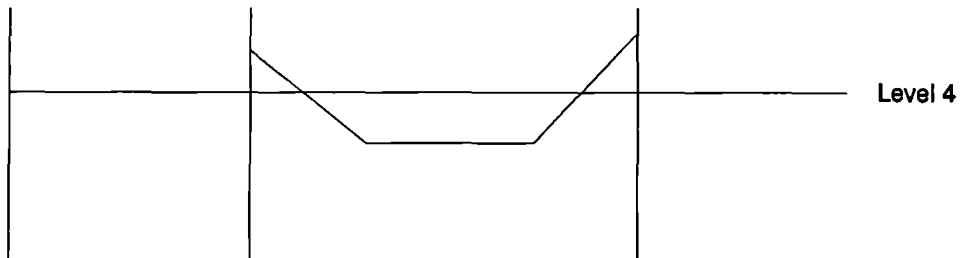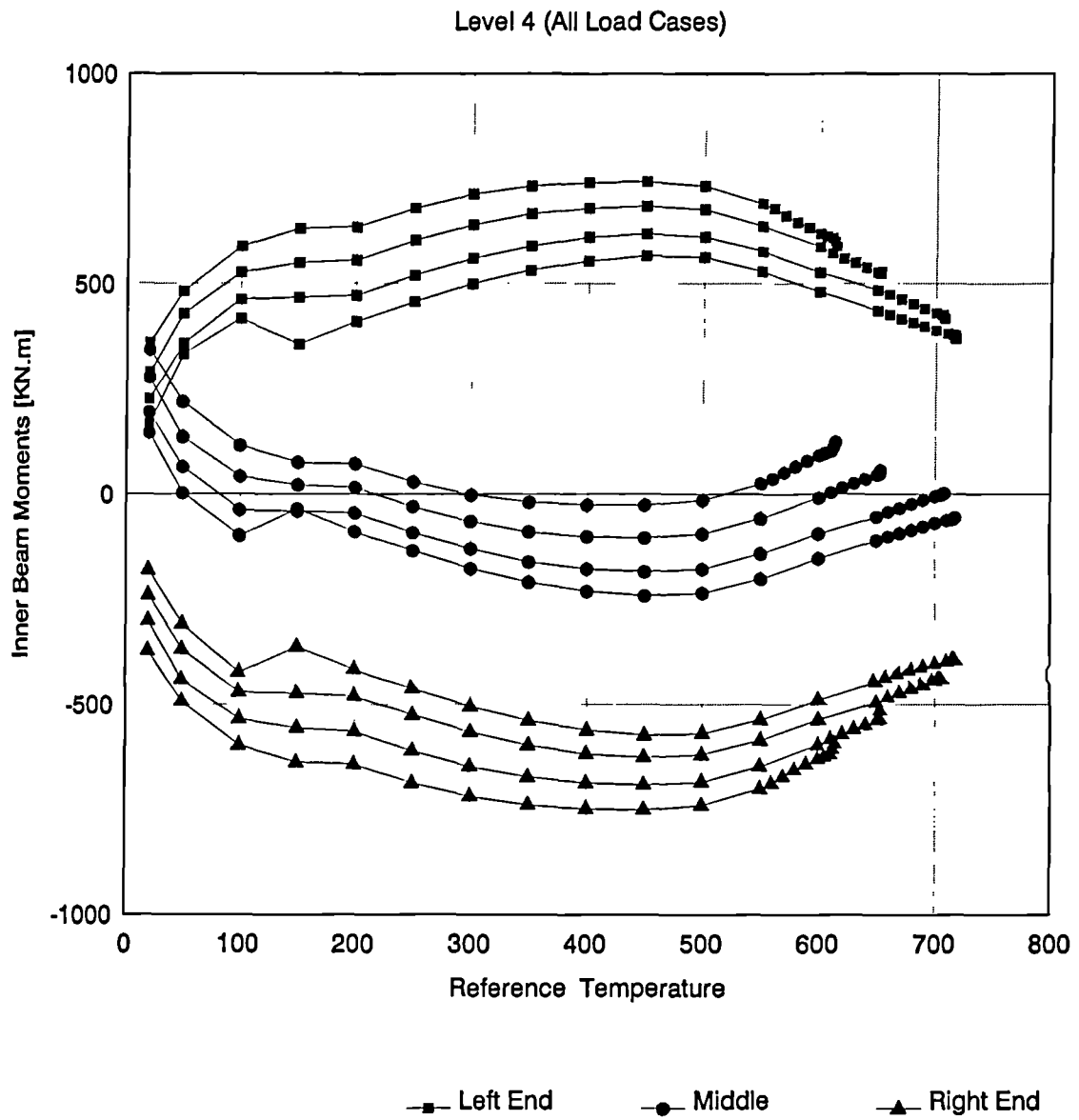
Fig. A.24 Moments at Inner Beam -Level 4

Level 7 (All Load Cases)
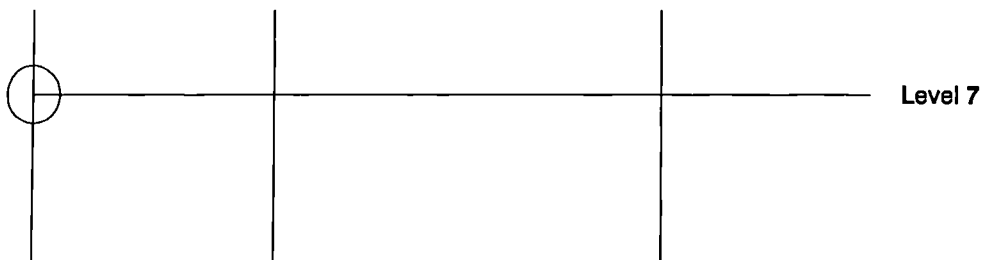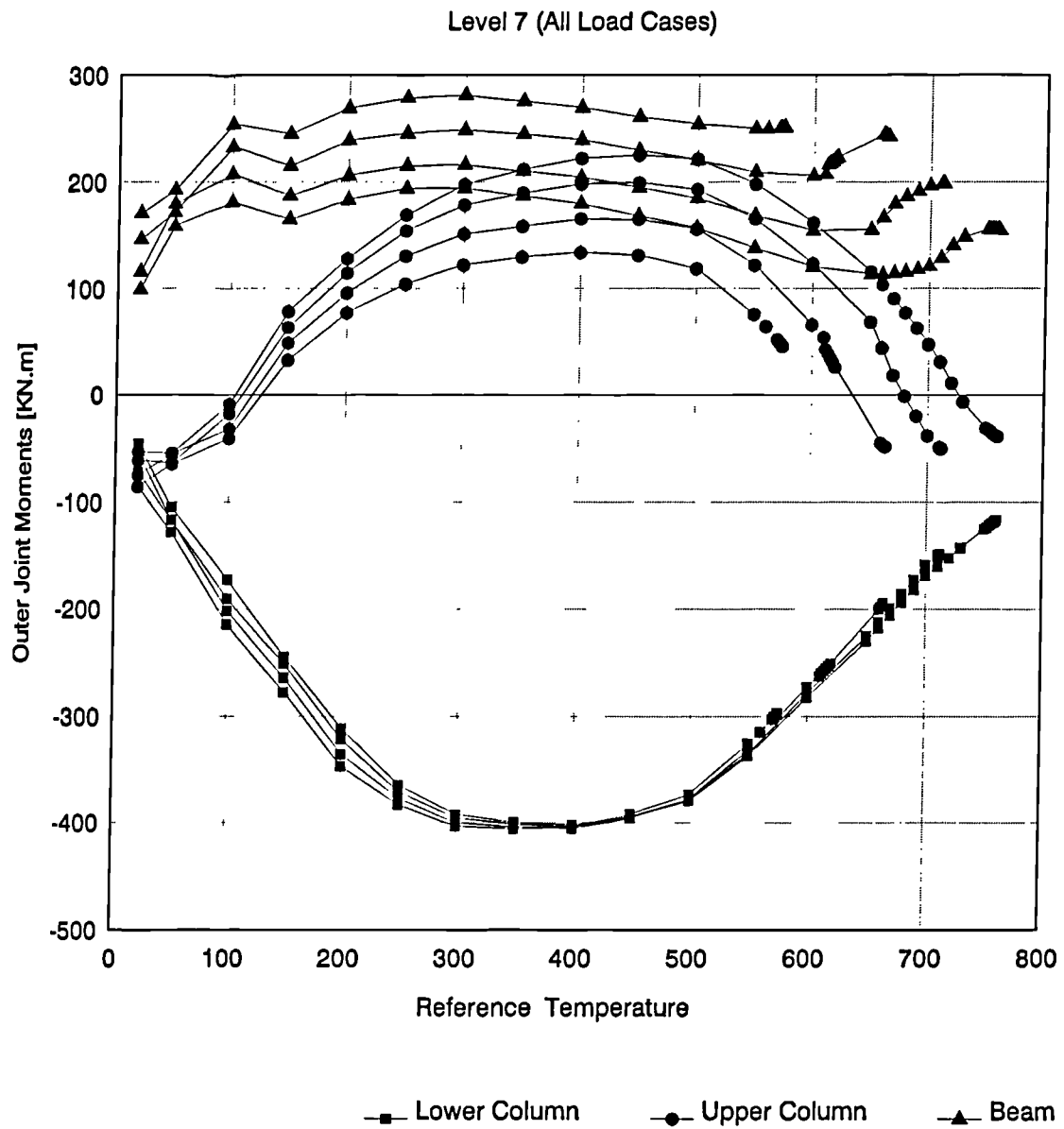
Fig. A.25 Moments at Outer Joint -Level 7

Level 7 (All Load Cases)
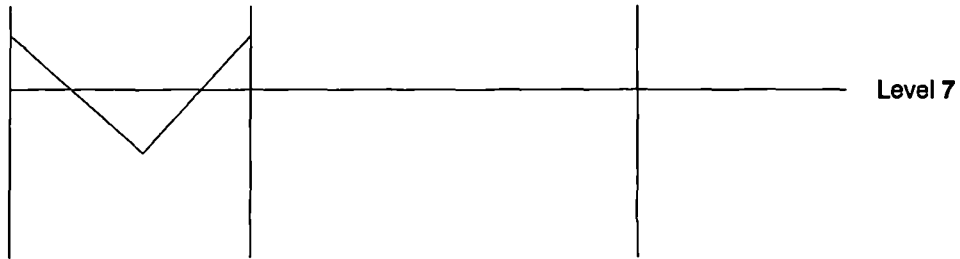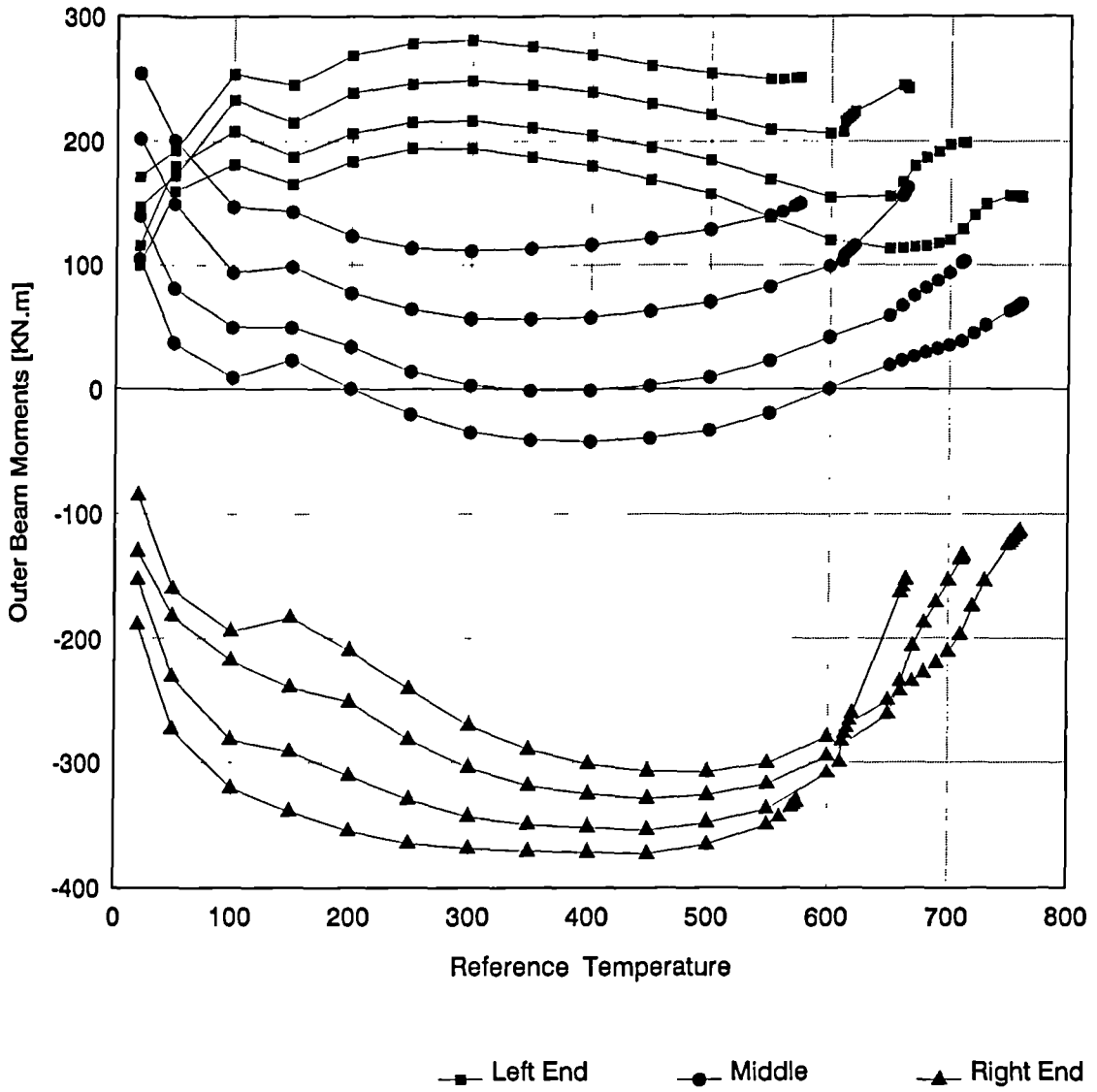
Fig. A.26 Moments at Outer Beam -Level 7

Level 7 (All Load Cases)

Fig. A.27 Moments at Inner Joint -Level 7
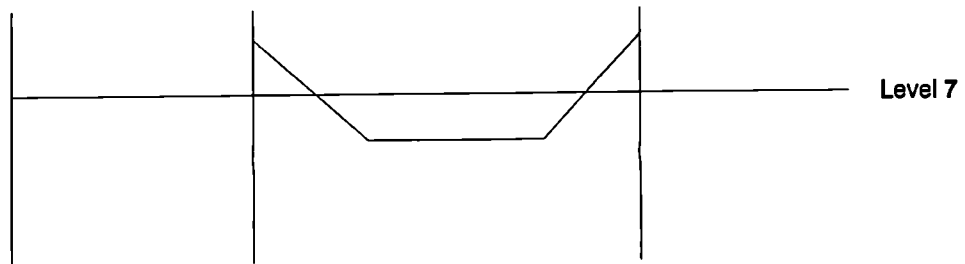
Fig. A.28 Moments at Inner Beam -Level 7

530KN

1175KN

1149KN

144.5KN

530KN

288.9KN

288.9KN

288.9KN

288.9KN

288.9KN

288.9KN

144.5KN
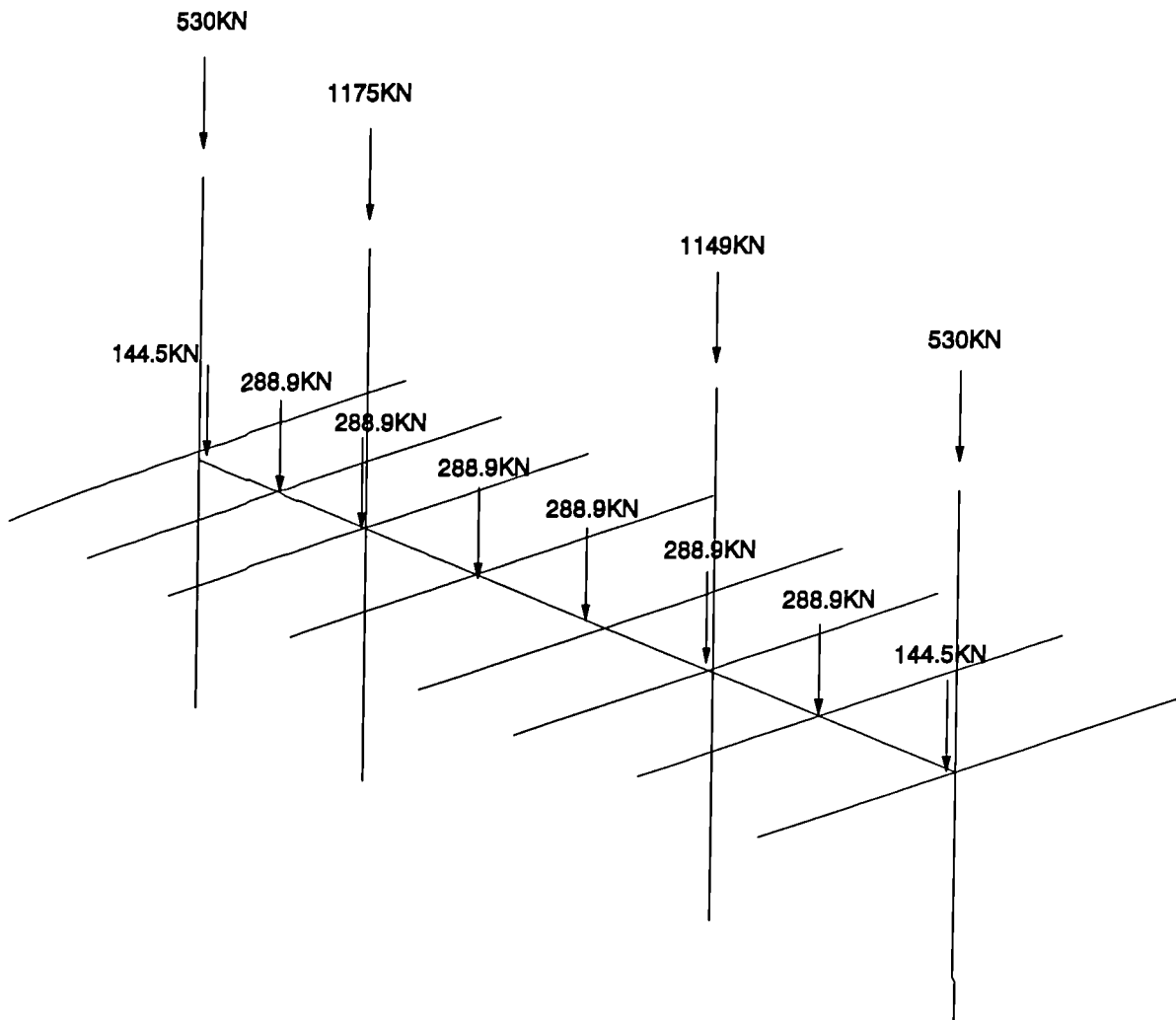
- Heating scheme similar to that of Fig. A.8.
- 2m of the secondary beams are heated as the adjacent main beam.
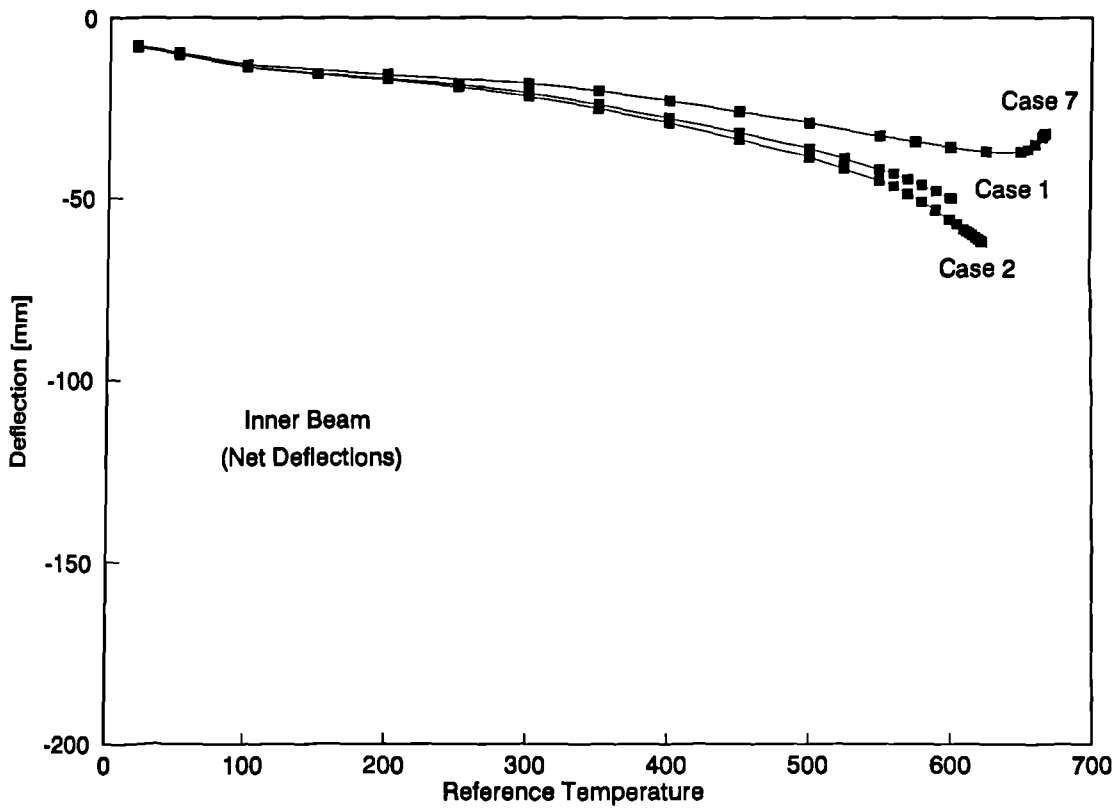
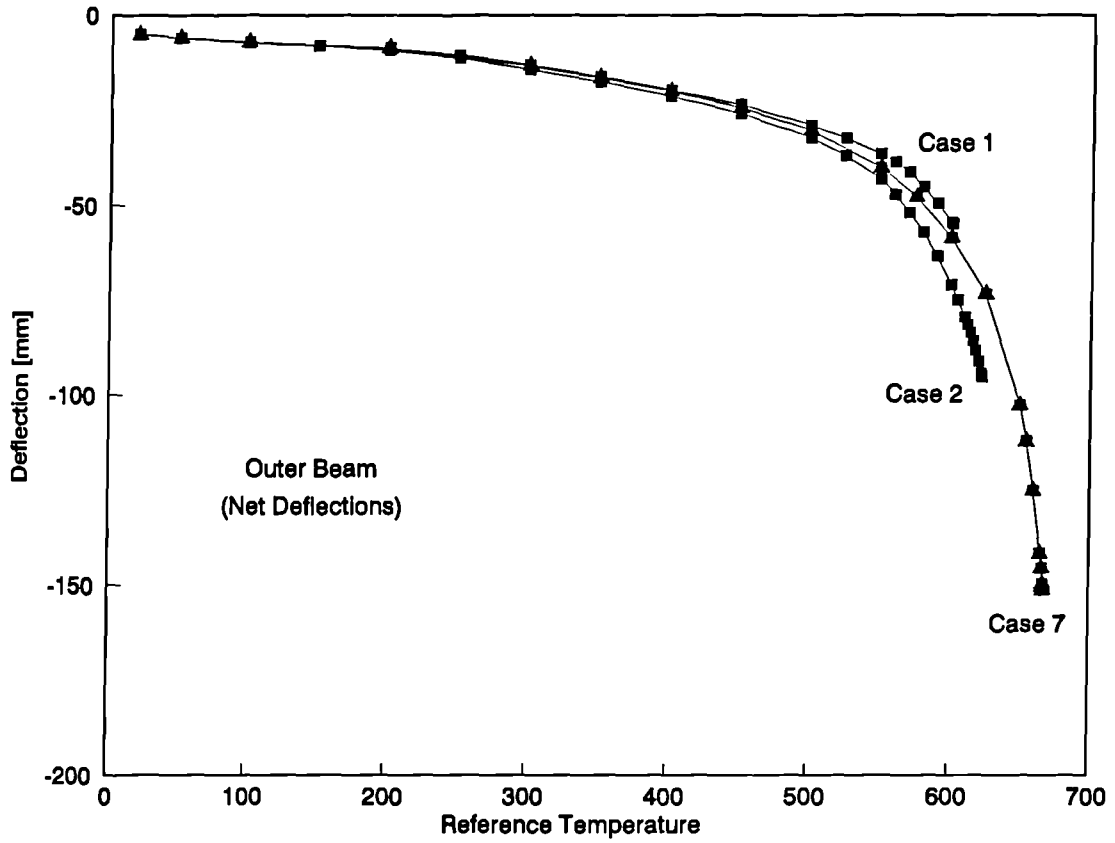**Fig. A.29 Loading of 3D Subassembly.**

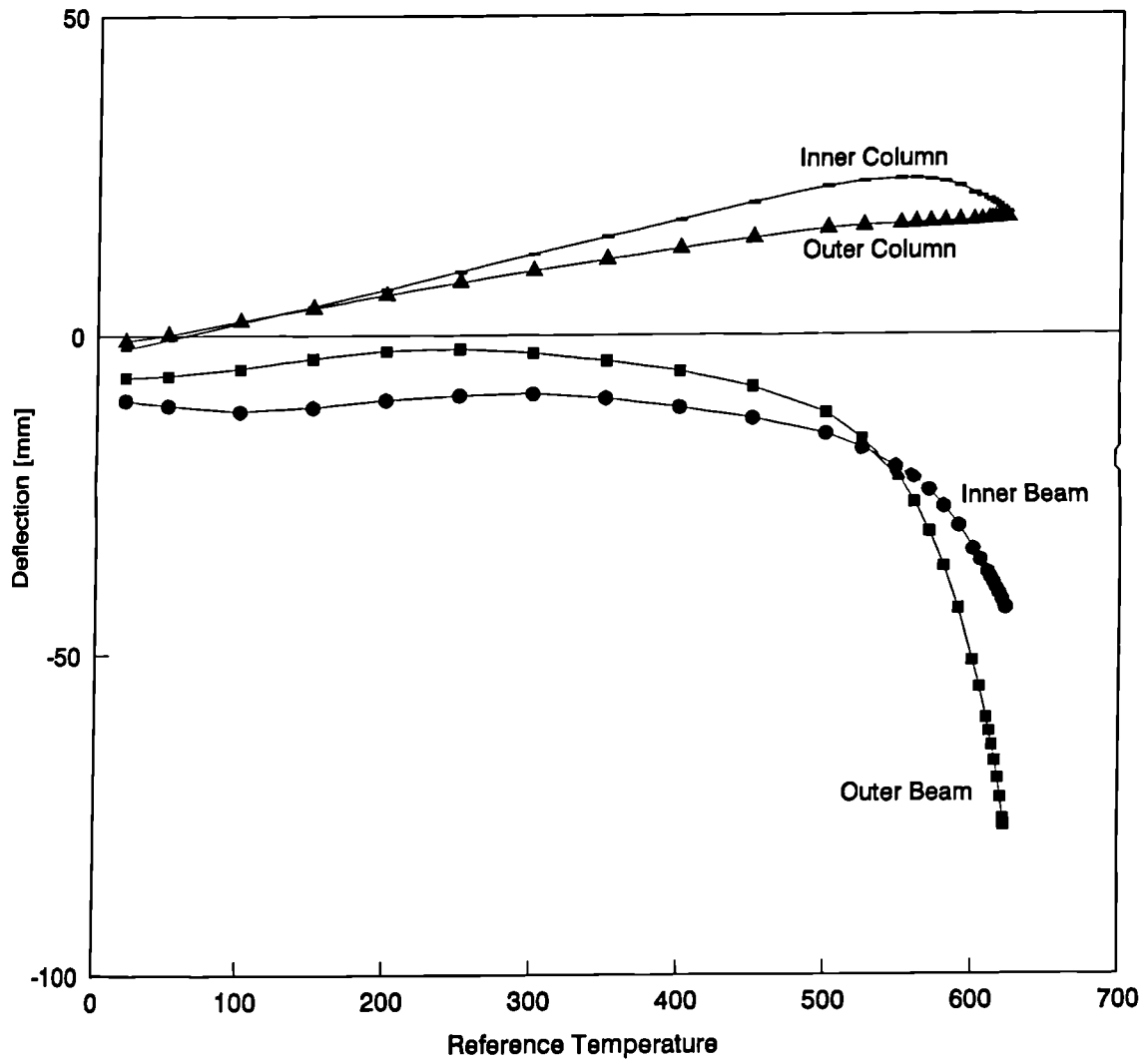**Fig. A.30 Temperature-Deflection of 3D subframe (Cases 1, 2 and 7)**

Fig. A.31 Temperature-Vertical Deflections for 3D Subframe -Case 2